Analysis of the Zebrafish Segmentation Clock

Thesis

ANALYSIS OF THE ZEBRAFISH SEGMENTATION CLOCK

Rachna Narayanan

Open University

and

The Francis Crick Institute

PhD Supervisors: Prof. Andrew C. Oates and Dr. James Briscoe

A thesis submitted for the degree of

Doctor of Philosophy

Open University

December 2017

Summary

In vertebrates, the repeating vertebrae in the vertebral column are the clearest indicators of the segmented body plan. The embryonic precursors of the vertebral column and skeletal musculature are bilaterally symmetric blocks of tissue flanking the notochord called somites. Somites are generated sequentially and periodically from an unsegmented tissue called the presomitic mesoderm (PSM) by a process called somitogenesis.

Underlying the periodicity of somitogenesis are transcriptional oscillations of cyclic genes in the cells of the PSM. On a tissue level, these oscillations manifest as travelling waves, departing from the posterior and arresting in the anterior. The position of arrest prefigures the position of the new somite boundary. The molecular network that comprises the cyclic genes and their regulation in the PSM is termed the segmentation clock.

Retinoic acid (RA) has been previously proposed to be a differentiation signal that acts to arrest the oscillations at the anterior of the PSM. This thesis shows the zebrafish RA catabolism mutant *giraffe* has an altered cyclic gene wave pattern, an observation that suggests that rather than stop their oscillations, cells tune their frequencies in response to RA signalling, introducing a novel function for RA in the zebrafish segmentation clock.

In amniotes, the segmentation clock instructs the metamery of the vertebral column, but in zebrafish, the relationship is not established. This thesis demonstrates that the segmentation clock is not required in zebrafish for the development of a periodic vertebral column by using a novel segmentation clock mutant, thereby supporting a role for the notochord in the development of vertebral column metamery. Therefore, two periodic patterning processes establish zebrafish body pattern – one segments the somites and musculature, and the second segments the vertebral column.

This thesis advances the understanding of the mechanisms of body pattern establishment by way of these novel insights.

Acknowledgement

I would, first and foremost, like to express my immense gratitude to Andy Oates, for his expert supervision and for all his guidance and support. I would also like to thank my friends and colleagues in the Oates lab for a great work and scientific environment.

Thank you to current and past members of the lab who have directly contributed to this work - Daniele Soroldoni, Guillaume Valentin and Leah Herrgen. Thank you to Daniele, who was my bench supervisor, and Klaire Neale for all her technical help. Thank you to Marko Storch for critical reading of (multiple) drafts of this thesis.

I am grateful to my collaborators – Stefan Schulte-Merker, Luis Morelli and Laura Lleras Forero. I would like to thank my thesis committee – James Briscoe, Greg Elgar, Justin Molloy, the fish labs at UCL, the UCL fish facility, the MPI-Dresden fish facility and the Knust lab for hosting me while I was there. I am also thankful to the Crick PhD office – Caroline Ransom and Jirina Markova – for excellent administrative support.

And finally, I would like to thank my family for all their love and encouragement, my friends Jamie, Sandra and Anni for providing emotional support. And to Marko, for saving the day, as always!

Table of Contents

Table of figures

List of tables

Abbreviations

Aldh1a2	aldehyde dehydrogenase family 1 member a2
bHLH	basic helix loop helix
ºC	degree Celsius
cad	*caudal*
Cyp26a1	cytochrome P450 family 26 subfamily a member 1
DMSO	dimethyl sulphoxide
DNA	deoxyribonucleic acid
dpf	days post fertilization
ECM	extra-cellular matrix
EMT	epithelial to mesenchymal transition
Entpd5	ectonucleoside triphosphate/diphosphohydrolase 5
eve	*even-skipped*
FGF	Fibroblast growth factor
fss	*fused somites / tbx6*
g	gram
GFP	green fluorescent protein
gir	*giraffe / cyp26a1*
her	Hairy / enhancer of split related
hes	Hairy / enhancer of split
hpf	hours post fertilization
l	litre
m	metre
M	Molar
MAB	maleic acid buffer
Mesp	Mesoderm posterior
MET	Mesenchymal to epithelial transition
NBT/BCIP	nitro blue tetrazolium chloride/5-brom-4-chlor-3-indoxyphosphate
nls	*neckless / aldh1a2*
nof	*nofin / aldh1a2*

PBS	phosphate buffered saline
PCR	polymerase chain reaction
PFA	paraformaldehyde
PSM	presomitic mesoderm
PTU	phenylthiourea
RA	retinoic acid
RARa/b	Retinoic acid receptor a/b
RARE	retinoic acid response elements
run	*runt*
SD	standard deviation
Tbx	T-box
TCF	T-cell factor
Wnt	Wingless / Int-1
YFP	yellow fluorescent protein
yot	*you too*
Xirp2a	Xin actin binding repeat containing protein 2a

Chapter 1. Introduction

1.1 Segmented bodies of vertebrates

Segmentation, in which a basic unit (a segment) is repeated along the anterior-posterior body axis, is a fundamental feature of the body plan in many invertebrate phyla and throughout the chordates. The prevalence and evolutionary success of this type of body architecture are attributed to the ability of segmentation to simultaneously confer rigidity for containment of the internal organs, and flexibility by allowing mobility at segment boundaries (Stern and Vasiliauskas 2000). The adult body of all vertebrates is composed of repeating segments of bone and muscle. The vertebral column is composed of repeating segments – the vertebrae, and consecutive vertebrae are connected by segments of muscle. This results in a segmented anatomy such that the vertebrae and the musculature are both periodic, but are half a segment out of register with each other. This arrangement of bone and muscle is crucial for locomotion.

The periodic pattern of body architecture is evident at multiple stages of vertebrate development. Segmented body pattern is first discerned when the organism is still an embryo during a process called somitogenesis. Somitogenesis segments the paraxial mesoderm, the tissue that is thought to ultimately give rise to the segmented skeletal musculature and the vertebral column, into blocks of tissue called somites. They can be observed as bilaterally symmetric blocks along the embryonic axis, bracketing the notochord (Gilbert and Raunio, 1997). Somites later differentiate into the precursors of the vertebral column - the sclerotome, and the precursors of the skeletal musculature of the adult body - the myotome.

The currently accepted model for the establishment of body pattern in amniotes (birds and mammals) is that somitogenesis, the earliest segmentation event, is the source of the subsequent periodic pattern that is developed by the musculature and the skeletal system. However, this remains an open question in zebrafish. This thesis aims to improve our understanding of the emergence of segmental pattern in zebrafish by studying the molecular regulation of somitogenesis itself and by assessing how much of the periodic pattern observed in the adult body is templated by somitogenesis.

This introduction provides an overview of the establishment of segmental pattern in the zebrafish body during development. The first section will focus on how segmental pattern is initially generated in the embryo. Somitogenesis and our current understanding of its molecular regulation are described here. The second section describes the development of segmented pattern in the body, covering the maturation of somites and their differentiation into muscle and bone tissue.

1.2 Generating segmental pattern in the embryonic axis

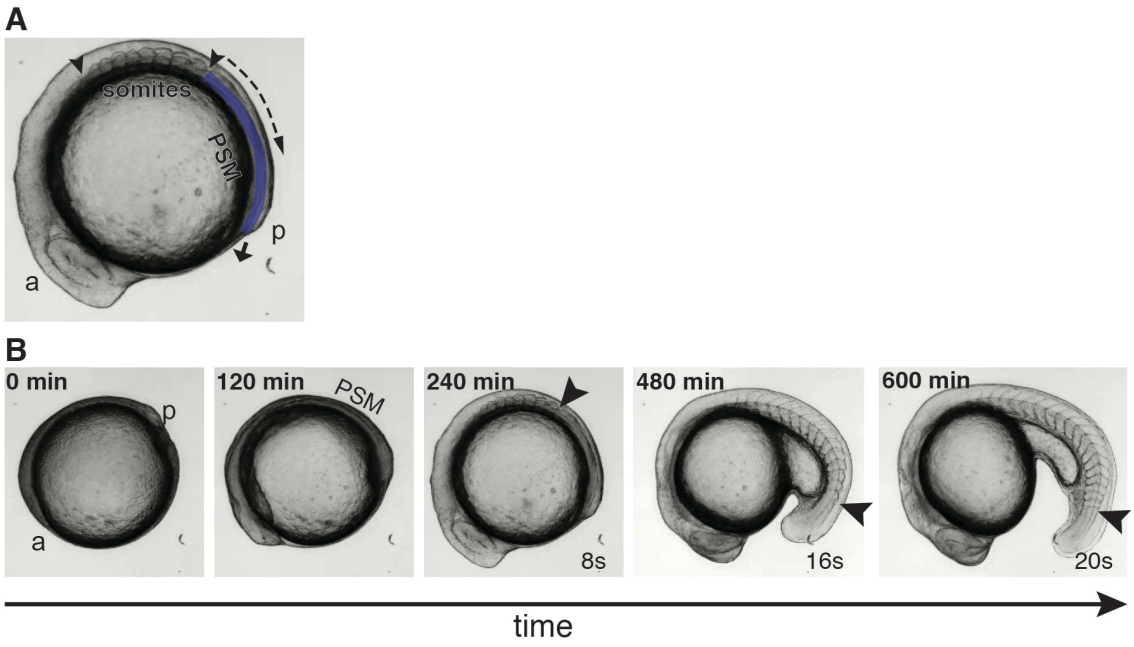

Figure 1.1 Somitogenesis proceeds sequentially and periodically.

Snap shot of a wild type zebrafish embryo undergoing somitogenesis **(A)** and advancing stages of zebrafish embryo somitogenesis **(B)**.
(A) The posterior unsegmented tissue, the presomitic mesoderm – PSM (blue line) is subdivided into somites sequentially (direction indicated with a dashed arrow) as the body axis elongates posteriorly (arrow). a – anterior, p – posterior, area within the arrowheads – somites. **(B)** Somites are generated periodically and somitogenesis is co-ordinated with embryonic growth. a – anterior, p – posterior, arrowhead points to the most recently formed somite, number of somites formed indicated in the bottom right.

Somitogenesis is the process by which the embryonic body axis is segmented into somites (Fig 1.1). It is a morphogenetic process that is conserved in vertebrate species and results in the formation of a species-specific number of somites at a rate that is also species-dependent (Gomez et al., 2008). In zebrafish, 34 somite pairs form with a period of ~25 mins at 28°C (Schröter et al., 2008). Somite pairs bud off sequentially in

an anterior-to-posterior order from an unsegmented tissue in the posterior of the embryo called the presomitic mesoderm (PSM), as the embryo grows and elongates its body axis. Gastrulation supplies cells to the PSM by adding them to the posterior of the tissue, while somitogenesis consumes cells at the anterior (Kimmel et al., 1995). Thus, somitogenesis coordinates the patterning of the tissue with its growth.

1.2.1 The segmentation clock is a multi-tier pattern generator

The rhythmicity of somitogenesis suggests the existence of a biological oscillator. Indeed, a group of genes that show oscillatory gene expression – called the cyclic genes – has been identified in the PSM of vertebrate embryos (Bessho et al., 2001; Krol et al., 2011; Oates and Ho, 2002; Palmeirim et al., 1997). Their dynamic gene expression manifests as waves that originate in the posterior and arrest in the anterior of the PSM. These waves shorten and slow down just before they arrest completely. The position of arrest prefigures the new somite boundary, and the wave pattern approximately repeats with the formation of each new somite pair. The observation of a wave pattern implies that the oscillations in the cells of the PSM are not in phase along the tissue, but that a phase profile is present in the tissue.

The cyclic genes and the molecules that regulate their wave patterns in the PSM are jointly defined as the segmentation clock (Fig 1.2). It can be thought of as a multi-scale rhythmic pattern generator whose processes can be conceptually organised in a three-tier hierarchy:

1. In the lowest tier is the activity of the cyclic genes within the PSM. Individual cells of the PSM are referred to as cellular oscillators by virtue of this activity. The cyclic genes are members of the Hes/her family of transcriptional repressors. Their mRNA and protein products are short-lived, and the protein products repress their own transcription, thus forming a negative feedback loop that leads to oscillatory gene expression (Bessho et al., 2003; Holley et al., 2002; Oates and Ho, 2002). The combined time delays from the processes of gene transcription, protein translation and protein degradation have been proposed to determine the intrinsic period of this genetic oscillator (Lewis, 2003).

2. The middle tier considers the local synchronisation of the cellular oscillators by means of Delta-Notch signalling. Travelling waves of expression of Notch pathway genes and receptor activation (Huppert et al., 2005; Maroto et al., 2005) indicate that oscillators are locally coupled to each other in every segmentation clock oscillation observed at the tissue level and neighbouring oscillators are in sync with each other in the PSM.
3. The top tier is concerned with the global control of the cellular oscillators in the PSM and ultimately, the arrest of the oscillations at the position of somite boundary formation. The travelling waves of cyclic gene expression are placed in this tier. The phase profile of the tissue is thought to emerge due to the gradual slowing of the frequency of cellular oscillators towards the anterior (Giudicelli et al., 2007; Morelli et al., 2009; Palmeirim et al., 1997). While the slowing of oscillators in this manner has been confirmed *in vivo* (Shih et al., 2015) and *in vitro* (Tsiairis and Aulehla, 2016), how the slowing of frequency is regulated is not currently understood. The currently accepted model is that opposing signalling gradients expressed across the PSM regulates oscillator frequency. Posterior to anterior Wnt and FGF gradients are postulated to be permissive for on-going oscillations. The frequency of the oscillators slow down as the level of FGF and Wnt signalling they experience decreases (Aulehla et al., 2007; Sawada et al., 2001). On the other hand, an anterior to posterior retinoic acid gradient is postulated to arrest the oscillators and promote their differentiation (Aulehla and Pourquie, 2010).

The processes described in each of these conceptual tiers are essential for segmentation clock activity – perturbations at any of these levels result in disrupted somitogenesis and an altered segmentation of the body axis.

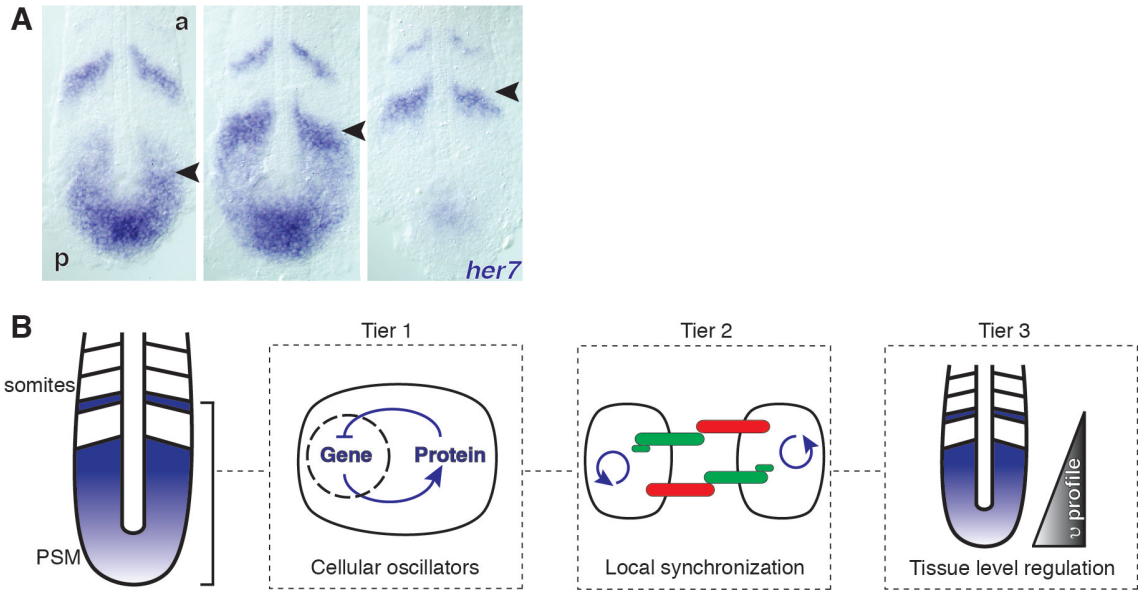

Figure 1.2 The segmentation clock is a tissue level segmental pattern generator.

In situ hybridisation for cyclic gene *her7* in dorsal view flatmount preparations of the PSM **(A)**. Schematic of the organisation of the segmentation clock into 3 tiers of activity **(B)**.
(A) Patterns of cyclic gene *her7* mRNA expression in one cycle of the segmentation clock show waves of gene expression travelling from the posterior to the anterior PSM, becoming progressively thinner (arrowheads). a – anterior, p – posterior. **(B)** The segmentation clock comprises the single cells of the PSM (cellular oscillators) that exhibit oscillating cyclic gene expression (Tier 1), the local synchronization of oscillation between cells by Delta-Notch signalling (Tier 2) and the regulation of frequency across the tissue (Tier 3). ***υ*** – frequency.
Panel A – courtesy of Andrew Oates.

1.2.2 The segmentation clock as a universal design principle

Overt body segmentation is prevalent in 3 major animal phyla – annelids, arthropods and chordates. Despite these segmented clades being evolutionarily more distant from each other than other unsegmented taxa, the majority present sequential segmentation where segments are generated rhythmically and serially from a posterior unsegmented tissue and the activity of a genetic oscillator circuit has been detected in the posterior tissue (Pais-de-Azevedo et al., 2018). *Drosophila* segmentation and the segmentation of long-germ arthropods stands out as an exception as they generate their body segments almost simultaneously along their axes by means of a hierarchical gene cascade (Wolpert et al., 2015).

The question of whether segmentation is an inherited trait originating from a common ancestor is still greatly debated. Evidence to conclusively rule out either hypothesis –

that the segmented body plan has evolved independently and is an example of convergent evolution, or that it is homologous across all the segmented phyla – is yet to be found.

The main argument in favour of homology rests on the observation that some of the molecules involved in the regulation of segmentation have been found to be well-conserved across all the segmented species studied so far. The *Hes/her* genes of the vertebrate cellular oscillator are orthologous to *Drosophila* pair-rule gene *hairy*. Further, the *Drosophila* pair-rule gene orthologs of *hairy*, *eve (even-skipped)*, *odd (odd-skipped)* and *run* (*runt*) are candidates of the core oscillator network in the sequentially segmenting arthropods that have been studied so far, giving traction to the homology hypothesis with *Drosophila* representing a highly specialised mode of segmentation (Pais-de-Azevedo et al., 2018). Similarly, the Wnt and Delta-Notch molecular pathways have been observed to be part of the gene regulatory network underlying sequential segmentation in arthropods (McGregor et al., 2009). However, the pleiotropic nature of these pathways has been used as a counter-argument against homology and their conserved role in tissue growth has made functional studies probing their role in the regulation of segmentation difficult, as this approach results in the loss of posterior body structures. In light of this, an additional hypothesis has been put forward – the posterior growth mechanism of *Urbilateria*, the common ancestor of all bilaterally symmetric animals, has been independently co-opted by multiple lineages to generate segmentation (De Robertis and Sasai, 1996).

By far the most challenging aspect of determining homology directly from the molecules involved is the diversity in the genetic details of the segmentation process across arthropods and chordates. The cache of oscillating genes is not well-conserved even across the vertebrate model organisms (Krol et al., 2011). However, the similarity of the morphogenetic process offers an opportunity to describe the design principles of a sequential segmentation mechanism (Richmond and Oates, 2012). The processes attributed to the three tiers of the segmentation clock i.e. cellular oscillations, the local synchronisation of the oscillations and the global control of oscillation arrest, emerge as

being key to generating serial anatomy, while the genetic players in each of these conceptual tiers can vary.

In the annelids that have been studied, such as leeches and sandworms, the cell cycle provides the oscillator activity. In the sequentially segmenting arthropods studied so far wave-like striped expression of *eve*, *odd*, *run*, *hairy* and *delta* have been observed. The genetic oscillator circuit proposed for the flour beetle *Tribolium castaneum* is a hierarchical repressor loop, comprising *Tc-eve*, *Tc-odd* and *Tc-run* (Choe and Brown, 2007; Choe et al., 2006), that oscillates with a 2-segment periodicity i.e. 1 stripe of gene expression leads to the formation of 2 morphological segments, unlike the vertebrate auto-repressor circuit that oscillates with single segment periodicity (Sarrazin et al., 2012). However, the spider oscillator has single segment periodicity while the centipede oscillator shows both single and 2-segment periodicity depending on the axial position (Liao and Oates, 2017).

How local synchrony of the cellular oscillators is achieved in arthropods is not clear yet (Liao and Oates, 2017). In silkworms, cockroaches, centipedes and spiders, Delta-Notch signalling is involved in body segmentation; however, the explicit role in synchrony has not yet been explored. There is no requirement for Delta and Notch in honeybee and cricket segmentation. In the spiders, a deficiency of Notch or Delta leads to a disturbed *hairy* expression pattern (Stollewerk et al., 2003), suggesting that similar to vertebrates, Delta-Notch signalling might indeed provide the mechanism by which cellular oscillators are synchronised. However, this possibility is yet to be tested. Local synchrony might be dispensable as pattern coherence could be built into either the lower-most or upper-most tier of the segmentation clock. For example, in *Hellobdella* (leeches), where the oscillator is the cell cycle, pattern coherence is maintained by virtue of cell lineage (Weisblat and Kuo, 2014).

Finally, the Wnt pathway provides the global control of oscillator arrest. In the flour beetle *Tribolium castaneum*, the Wnt dependent *caudal* (*Tc-cad*) gradient is expressed in the posterior to anterior direction, with the anterior limit coinciding with the anterior-most *Tc-eve* stripe (El-Sherif et al., 2014). Manipulation of the *Tc-cad* gradient leads to

corresponding changes in the position of the *Tc-eve* stripe (El-Sherif et al., 2014), suggesting that the Wnt pathway plays a similar role in the global control of oscillators in *Tribolium* as in vertebrates. Thus, although the molecular details vary, arthropod segmentation can be organised into the conceptual framework of the 3-tier hierarchy of the segmentation clock and demonstrates how it can be considered a universal design principle for generating sequential segmentation.

1.2.3 The core pace-keeping circuit of the zebrafish segmentation clock

The core pace-keeping circuit of the zebrafish genetic oscillator consists of two negative feedback loops comprising Hes/her proteins. Hes/her proteins are members of the basic-helix-loop-helix (bHLH) superfamily which are characterized by four domains: a basic DNA-binding domain, a helix-loop-helix (HLH) dimerisation domain, the orange domain and the C-terminally localized WRPW motif (Kageyama et al., 2007). Hes proteins dimerise to bring about their transcriptional repressor activity – they either form homodimers (Leimeister et al., 2000) or heterodimerise with other bHLH proteins (Sasai et al., 1992). However, only certain dimer combinations can bind DNA (Schröter et al., 2012; Trofka et al., 2012).

The two negative feedback loops of the core pace-keeping circuit are – one based on Her1 homodimers and a second on Her7:Hes6 heterodimers, operating in parallel to repress the expression of *her1* and *her7* (Schröter et al., 2012). *her1* and *her7* have cyclic expression in the PSM (Fig 1.2A). These oscillations have been imaged in zebrafish embryos by means of transgenic fluorescent reporters. *hes6* does not oscillate on the mRNA level, but its protein product Hes6 participates in the core circuit by way of dimerization with the other Her proteins (Hanisch et al., 2013; Kawamura et al., 2005b; Schröter and Oates, 2010).

These two parallel negative feedback loops have overlapping and partially redundant activity. This was elucidated from the segmentation defects that resulted when *her1*, *her7* and *hes6* genes were mutated or knocked down with morpholinos – complimentary oligomers that can prevent the translation or splicing of their target mRNA by steric blocking. Loss of *her1* by mutation or by morpholino knockdown has a mild effect on

segmentation – only the anterior-most somites are affected. Loss of *her7*, however, is more severe, causing segmentation defects posterior to the 9th somite. Mutation of the *hes6* gene affects the period of somitogenesis, slowing down somite formation. This results in the mutant having fewer, but longer somites (Schröter and Oates, 2010). Combined morpholino knockdown of *her1* and *her7* or *her1* and *hes6* causes segmentation defects all along the body axis (Choorapoikayil et al., 2012; Gajewski, 2003; Henry et al., 2002; Oates and Ho, 2002) whereas the simultaneous loss of *her7* and *hes6* results in a normally segmented embryo (Schröter et al., 2012).

There are other *Hes/her* genes, in addition to *her1* and *her7,* whose expression has been reported to oscillate (Krol et al., 2011; Shankaran et al., 2007; Sieger et al., 2004). It is unclear what their exact role in the genetic oscillator is – the loss of these genes either by mutation or morpholino knockdown does not affect segmentation, but they are able to interfere with normal segmentation when overexpressed in the PSM (Shankaran et al., 2007). It has been postulated that these genes participate in the genetic oscillator, along with *her*1, *her7* and *hes6*, by means of a "dimer cloud" in the PSM. All possible Hes/her dimeric combinations are made in the dimer cloud, including combinations that don't bind DNA, and this dimer cloud regulates the availability and effective stability of the dimers that have DNA binding ability (Schröter et al., 2012; Schwendinger-Schreck et al., 2014; Trofka et al., 2012).

1.2.4 Synchronization of the genetic oscillators

The genetic oscillator described above functions autonomously within the cells of the PSM (Masamizu et al., 2006; Webb et al., 2016). However, the oscillations of single cells, as determined by an *in vitro* study of isolated zebrafish PSM cells, are noisy due to stochastic gene expression and degradation of mRNA and protein (Webb et al., 2016). Therefore, mechanisms are necessary to ensure that the genetic oscillators in the single cells are co-ordinated across the tissue. This tissue level synchrony of the cellular oscillators is achieved by cell-cell communication between neighbouring cells by Delta-Notch signalling (Maroto et al., 2005). The role of the Delta-Notch signalling pathway in zebrafish somitogenesis was elucidated from the somitogenesis phenotypes of mutants of members of the Delta-Notch family (Itoh et al., 2003; Jülich et al., 2005b;

van Eeden et al., 1996). Delta-Notch mutants have defective somitogenesis posterior to the 5^{th} – 10^{th} somite. Kinematic waves of *her1* and *her7* mRNA expression are not observed in these mutants, but individual cells are seen to remain oscillating, leading to a salt-and-pepper expression pattern in the tissue (Jiang et al., 2000). This was interpreted to be a result of a loss of synchrony between the cellular oscillators. These out of sync cyclic gene oscillations in Delta-Notch mutants have now been directly visualised *in vivo* (Delaune et al., 2012).

A number of members of the Delta-Notch family are expressed in the zebrafish PSM during somitogenesis (Holley et al., 2002; Jiang et al., 2000; Oates et al., 2005a). Of these factors, only *deltaC* has cyclic expression. Cyclic expression of *deltaC* is lost when *her1* and *her7* function is simultaneously knocked down with morpholinos (Riedel-Kruse et al., 2007). Sustained expression of *deltaC* is observed in this case, indicating that the rhythmic transcriptional repression of *deltaC* is lost.

From these observations, the following genetic network has been proposed: genes of the Hes/her family oscillate autonomously via transcriptional auto-repression; hes/her repressors also target one or more genes in the Delta-Notch pathway bringing their expression into the feedback-loop and rhythmic Delta-Notch signaling between the PSM cells modulates the timing of Hes/her oscillations. Thus, the oscillations between neighbours are synchronized (Liao and Oates, 2017).

1.2.5 The Clock and Wavefront Model

Insight into how the temporal information of a biological oscillator might be converted into a segmented pattern in space was provided by the Clock and Wavefront model that was put forward by Cooke and Zeeman (Cooke and Zeeman, 1976). They proposed the existence of a ‘clock’ – a collection of cellular oscillators in the unsegmented PSM that oscillate in sync – and postulated that temporal information in this clock would be converted into a spatial pattern by a ‘wavefront’. The wavefront was described as a wave of cellular differentiation that moves across the PSM from the anterior towards the posterior. They proposed that the activity of the oscillators would be arrested as they encountered the wavefront. Therefore, the wavefront would leave behind a record of the

oscillation state of the cells at the time of their arrest, thereby generating a repetitive pattern. Thus, the combined activity of the clock and wavefront would periodically segment the unsegmented body axis.

The distance travelled by the wavefront in one oscillation cycle of the clock, i.e. its period, would determine the length of segments generated. The Clock and Wavefront model formalises this dependency of segment length (S) on the velocity (v) with which the wavefront sweeps through the PSM and the period of the clock (T_c) as $S = vT_c$, at steady state. Thus, as per the Clock and Wavefront mechanism, altering v or T_c will alter segment length S.

The biological counterpart that can provide the temporal activity ascribed to the "clock" in the Clock and Wavefront mechanism is the segmentation clock that has been described earlier. The kinematic waves are not formalised in the mechanism, but the observation of the repetition of the wave pattern with the formation of every new somite was interpreted to mean that the time taken for the wave pattern to repeat matched the period of somite formation. Therefore, the relationship of segment length, wavefront velocity and clock period *in vivo* was considered to be consistent with the Clock and Wavefront model (Oates et al., 2012).

1.2.6 Molecules providing wavefront activity

The activity of the wavefront is thought to be achieved by the signalling gradients across the PSM, by providing a system of positional information. These gradients are FGFs and Wnts expressed in a posterior to anterior gradient and retinoic acid (RA) present in an anterior to posterior gradient. The dynamics of axis elongation extending the PSM posteriorly, and somite formation shortening the tissue anteriorly results in the sources of signaling being in motion with respect to the formed somites, thereby producing a wavefront velocity.

FGFs, Wnts and their downstream targets are expressed most highly in the tailbud with tapering expression in the anterior PSM (Aulehla and Pourquie, 2010). An RA gradient was inferred to be present in the anterior to posterior direction on the basis of the

expression of the RA biosynthesis enzymes - the RA biosynthetic enzyme *aldh1a2* (*Raldh2* in mice) is expressed in the anterior PSM and formed somites (Begemann et al., 2001; Grandel et al., 2002; Niederreither et al., 1999), and the RA specific catabolic enzyme *cyp26a1* is expressed in the tailbud of vertebrate embryos (Dobbs-McAuliffe et al., 2004; Sakai et al., 2001). The RA gradient has been demonstrated to be restricted to the anterior PSM and the somites in mouse embryos, by means of a fluorescent RA signalling reporter (Vermot, 2005). The RA gradient was also recently directly demonstrated to be present as an anterior-to-posterior gradient in zebrafish embryos with a FRET based RA bio-sensor (Shimozono et al., 2013).

The RA and Wnt – FGF counter gradients mutually inhibit each other's activity (del Corral and Storey, 2004; Diez del Corral et al., 2002; 2003; Moreno and Kintner, 2004; Vermot, 2005). The position in the PSM where their activity overlaps is thought to specify the position of the wavefront. Evidence in support of this idea comes from experiments based on gradient perturbations. FGF, Wnt and RA inhibition or overexpression typically interfere with axial outgrowth (Emoto et al., 2005; Sakai et al., 2001; Shimizu et al., 2006; Wilson et al., 2009); therefore the gradients have been perturbed in transience. A change in somite length was interpreted as affecting the wavefront velocity, following from the prediction of the Clock and Wavefront mechanism $S = vT_c$

Transient inhibition of FGF signalling in chick and zebrafish increases somite length (Dubrulle et al., 2001; Sawada et al., 2001). Transient inhibition of Wnt in mouse and zebrafish embryos also increases somite length and a transient activation of Wnt signalling correspondingly decreases somite length locally (Aulehla et al., 2007; Bajard et al., 2014). However, of these studies, only Bajard et al. explicitly measured somitogenesis period T_c. They found that it was unaffected, and thus concluded that the Wnt perturbation specifically affected the velocity (v) of the wavefront.

1.2.7 Zebrafish somitogenesis is not at steady state

The Clock and Wavefront mechanism was formulated for a system that is in steady state. At steady state, the rate of addition of cells to the PSM in posterior matches the rate at

which they are removed from the anterior by somitogenesis. The number of kinematic waves in the PSM stays constant and the wave pattern repeats perfectly every time a new somite is formed. Thus, as per the Clock and Wavefront mechanism, the time taken for this pattern to repeat would define the period of somitogenesis, *T* which would be the same as T_c, the period of the clock (Ares et al., 2012; Morelli et al., 2009). However, recent evidence demonstrates that the zebrafish PSM is not at steady state during somitogenesis and so the predictions of the Clock and Wavefront model need to be reconsidered (Fig1.3).

In vivo time-lapse imaging of somitogenesis and the kinematic waves of expression of a transgenic reporter for cyclic gene *her1* showed that the PSM continually shortens and the number of kinematic waves decreases with the progression of somitogenesis. In other words, the wave pattern never perfectly repeats. The observable rate of somite formation (the somitogenesis period, *T*), instead of depending only on the period of the "clock", T_c, emerges at the tissue level as a function of (1) the timescale of genetic oscillations in the posterior of the tissue, (2) the rate of PSM shortening, and (3) the dynamic changes in the wavelength of the wave patterns (termed the dynamic wavelength effect) (Soroldoni et al., 2014). In this formalisation, the period of somitogenesis is related to the local frequency of the oscillations in the anterior PSM as $T = \frac{\Omega_A}{2\pi}$, where $\Omega_A = \Omega_p + \Omega_D + \Omega_w$. Ω_p is the frequency of the oscillations in the posterior PSM, Ω_D is the contribution of PSM shortening and Ω_w is the dynamic wavelength contribution (Jörg et al., 2015). The shortening of the PSM contributes to the somitogenesis period by means of an embryonic Doppler effect. The motion of cellular differentiation (the wavefront, in the Clock and Wavefront model) into the kinematic waves at the anterior end of the PSM, relative to the motion of the growing posterior end, leads to an increase of the frequency of oscillations seen by an observer at the anterior end (Fig 1.3B(a)).

Central to the original Clock and Wavefront mechanism is the idea that wavefront velocity *v* and somitogenesis period *T* are independent parameters that do not affect each other. However, in reality, *T* and *v* are not independent in zebrafish somitogenesis and *v* contributes to *T* by means of the embryonic Doppler effect. Therefore, when

testing a candidate “wavefront” molecule, it is not sufficient to measure just somite length and the somitogenesis period. The analysis needs to include a characterisation of the rate of PSM shortening and the wave patterns of cyclic gene expression.

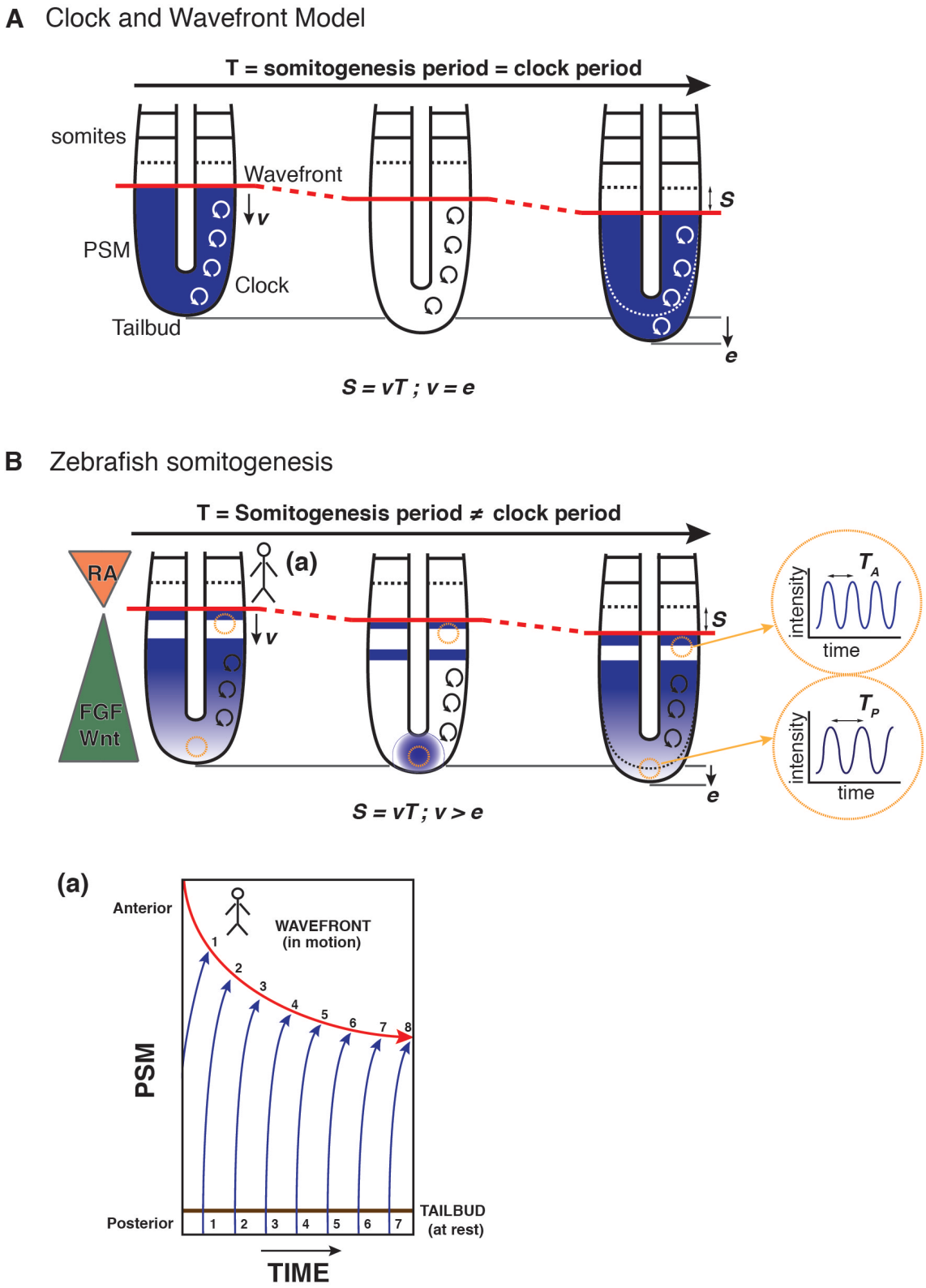

Figure 1.3 Zebrafish somitogenesis is not at steady state.

Schematic description of the Clock and Wavefront Model **(A)**. Schematic description of zebrafish somitogenesis **(B)**.

(A) The Clock and Wavefront model proposes that the presomitic mesoderm (PSM) comprises a Clock made of cellular oscillators that cycle between on/off states (blue – on white – off) whose activity is arrested when a wave of cellular differentiation, the Wavefront (red line), is encountered, resulting in the formation of a somite (dotted line - nascent somite boundary). The somitogenesis period (*T*) is measured as the time taken for each somite to form. As the new somite forms and the axis elongates (with an elongation rate *e*), the wavefront moves posteriorly in concert. In this steady state condition, the somite length (*S*) is determined by the wavefront velocity (*v*) and the period of the clock, which is the period of somitogenesis (*T*).
(B) In zebrafish, the wavefront (red line) is influenced by FGF and Wnt signalling gradients from the posterior end and a counter-gradient of RA from the somites. As the new somite forms and the axis elongates, the wavefront sweeps posteriorly in concert. When the kinematic waves of *hes/her* genes (blue in the PSM) move across the wavefront, the oscillations arrest and a new segment boundary is determined. The wavefront sweeps posteriorly faster (*v*) than the rate of axis elongation (*e*) and the system is out of steady state. In this situation, the somitogenesis period *T* is not given by clock period, but by T_A – the oscillation period in the anterior end of the PSM. Measurement of *hes/her* expression in real-time at the anterior or posterior ends of the PSM over time (yellow dotted circles in the PSM) reveals that the oscillations in the anterior have a faster period (T_A) than the oscillations in the posterior (T_P, yellow dotted inset at the right of the panel).
(a) The anterior end (wavefront, red) acts as an observer that is moving towards the posterior, relative to the *her*/*hes* kinematic waves and perceives an increased oscillation frequency as compared to the posterior end (tailbud, brown), the observer at rest. Therefore, the observer in motion experiences more waves (blue arrows) than the observer at rest in the same time interval.
blue – cellular oscillator/kinematic wave, red line – wavefront, *v* – wavefront velocity, *e* – axis elongation rate, *S* – somite length, *T* – somitogenesis period, T_A – anterior period, T_P – posterior period, black dotted line – nascent somite boundary.

1.2.8 Role of retinoic acid in the wavefront

A role in setting wavefront velocity has been attributed to RA from observed somite length changes in experiments that perturbed the level of RA in embryos. The best evidence comes from a single study – Moreno and Kintner (2004) found that treating *Xenopus* embryos with exogenous RA (1 μM for 5 hours) led to an increase in somite length. However, the treatment also interfered with normal somite formation and the general development of the embryos. RA is a pleiotropic molecule that is essential for other contemporary developmental processes, including outgrowth of the body axis. Therefore, from these experiments, it is difficult to interpret the observed PSM defects. In a further example, Vitamin A deficient (VAD) quails and *Raldh2*$^{-/-}$ mice, systems that lack RA biosynthesis, show smaller-sized somites when compared to wild type embryos (Maden et al., 2000; Niederreither et al., 1999). However, these embryos also show a general reduction in size.

It is still unclear if RA plays a role in zebrafish segmentation. Zebrafish mutants for RA biosynthesis enzyme *aldh1a2 – necklesss* (Begemann et al., 2004) and *nofin* (Grandel et al., 2002) – that correspond to the VAD quails and mice *Raldh2* mutants, show defects

in heart, hindbrain and fin formation and suffer early mortality. These *aldh1a2* zebrafish mutants have nonetheless been described as having normal somites in a normal body at the end of somitogenesis. Moreover, the somitogenesis period during trunk somite formation of the RA deficient *aldh1a2 (nofin)* embryos has been reported to be comparable to wild type (Herrgen et al., 2010). Therefore, seemingly, zebrafish somitogenesis is unaffected by the abrogation of RA biosynthesis.

However, preliminary data from our lab indicates that RA inhibits genetic oscillations *in vitro* in single cells extracted from the posterior PSM (unpublished data from Alexis Webb) and it can induce the formation of longer somites *in vivo* when transiently applied (unpublished data from Lola Bajard). Therefore, a systematic characterisation of somitogenesis and the wave pattern in perturbed RA signalling conditions is necessary before any conclusions can be made regarding the effect of RA on zebrafish somitogenesis and the segmentation clock.

1.3 The development of the segmented body

The dynamic signal from the segmentation clock is converted into permanent segmental output. Segmental expression of *Mesp2* (*Mesp2* in mice, *mespb* in zebrafish) is considered to be the first indication of somite determination (Saga et al., 1997; Sawada et al., 2000). In zebrafish, 2 stripes of *mespb* are visible in the anterior PSM prior to somite boundary formation (Sawada et al., 2000). Downstream of this segmental output of the segmentation clock are the molecular events that lead to the formation of somites that are morphologically distinct from the PSM. Shortly after their formation, somites begin to differentiate into muscle precursors (myotome) and bone precursors (sclerotome).

1.3.1 Somite maturation

The segmental output of the segmentation clock appears to be binary – the presumptive somite is regionalised into anterior and posterior compartments (Fig 1.4). This anterior-posterior polarity is thought to be necessary for the formation of morphologically distinct somites (Dahmann et al., 2011; Durbin et al., 2000; Oates et al., 2005b; Stickney et al., 2000). Initially, *mespb* occupies the entire width of the somite. It is then

restricted to the presumptive anterior half of the somite. T-box gene *tbx6* is vital to the establishment of the anterior-posterior polarity in the presumptive somite, by regulating *mespb* and the posterior identity factor *ripply1* (Durbin et al., 2000; Kawamura et al., 2005a; Sawada et al., 2000; Wanglar et al., 2014; Windner et al., 2015; Yabe et al., 2016). The anterior and posterior halves of somites can be distinguished from each other by their differential expression of molecular markers, including *mespb* and *ripply1*.

On the tissue level, progressive mesenchymal to epithelial transitions (MET) of the cells at the borders of the tissue accompanies this segmental gene expression (Fig 1.4). These cells develop apicobasal polarity, such that the apical side is oriented towards the interior and the basal side towards the exterior of the somite (Henry et al., 2000; Jülich et al., 2005a; Sawada et al., 2000). An intersomitic furrow develops between consecutive somites, separating them. This intersomitic furrow accumulates extracellular matrix to form the somite boundary (Jülich et al., 2005a; 2009). Each somite develops an outer epithelial monolayer around an inner core of loosely packed mesenchymal cells, ultimately resulting in the formation of a three-dimensional block of cells that is distinct from the PSM.

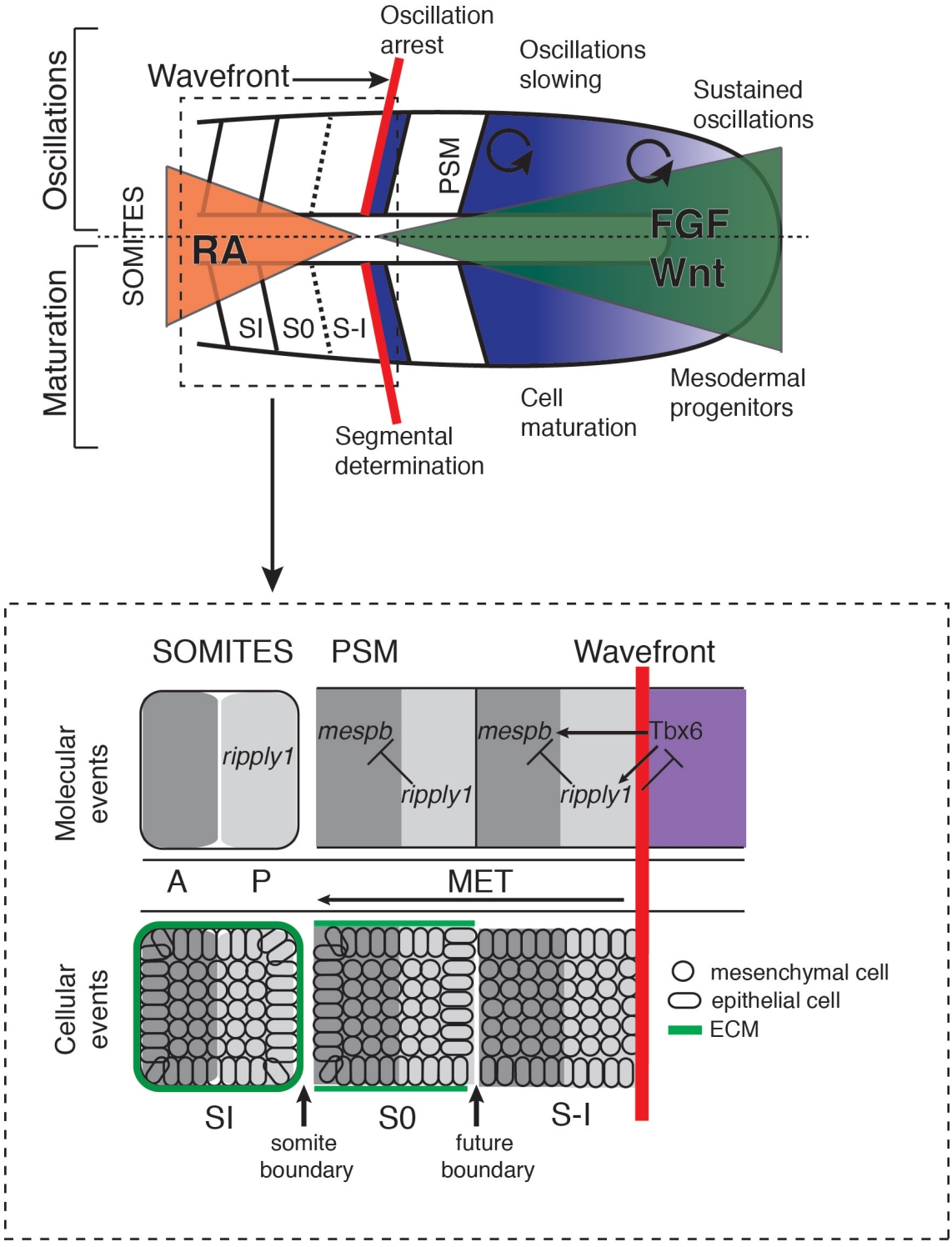

Figure 1.4 Steps to somite formation.

Schematic representation of the oscillation state and cellular events during the activity of the segmentation clock (**Top panel**). Schematic representation of molecular and cellular events in somite maturation (**Bottom panel**).
Top panel: FGF/Wnt and RA gradients control slowing and arrest of the cellular oscillators. **Top half, from right to left:** Sustained high-frequency oscillations are observed in the posterior region of the tissue. The frequency of the oscillators gradually reduces as they approach the wavefront (red line).

Bottom half, from right to left: The mesenchymal mesodermal progenitors undergo their maturation programme as they traverse the presomitic mesoderm.
Bottom panel, top half, from right to left: At the wavefront (red line), defined by the anterior limit of the Tbx6 protein domain (purple), segmental determination is triggered by the expression of *mespb* and *ripply1*. *mespb* is cleared from the presumptive posterior compartment (light grey) of the somite by *ripply1* and is restricted to the presumptive anterior compartment (dark grey), thus establishing the anterior-posterior polarity of the somite.
Bottom panel, bottom half, from right to left: The presumptive somite (S-I) becomes regionalised into anterior and posterior compartments. Progressive cellular epithelialisation of the border cells accompanies this (S0). The epithelialisation is associated with the accumulation of extracellular matrix (ECM) on the surface of the tissue and at the boundary, ultimately resulting in the formation of a new somite (SI).
PSM – presomitic mesoderm A – anterior somite compartment, P – posterior somite compartment, MET – mesenchymal to epithelial transition, SI – newly formed somite, S0 – forming somite, S-I – next somite to form, nomenclature as per (Pourquie and Tam, 2001). Dashed line in top panel – nascent somite boundary.

1.3.2 Somite differentiation

Shortly after the somite forms, the cells of the somite differentiate into the muscle and bone precursors, myotome and sclerotome respectively, from distinct locations in the somites. As they differentiate, these precursors begin to migrate from their embryonic locations and occupy the positions where the future musculature and axial skeleton will develop.

1.3.2.1 Myotome differentiation

Adult zebrafish muscle can be broadly categorised into 2 types – slow muscle fibres and fast muscle fibres. As the somite differentiates into myotome, embryonic muscle fibres can be identified. Much like their adult counterparts, the embryonic fast twitch fibres are located medially in the deeper layers of the myotome and the embryonic slow twitch fibres are present as a layer superficial to the fast fibres, on the lateral sides of the embryo (Bryson-Richardson and Currie, 2008; Jackson and Ingham, 2013; Stickney et al., 2000).

The slow twitch fibres originate from paraxial mesoderm cells located adjacent to the notochord (Thisse et al., 1993). These cells are called the adaxial cells and are the earliest developing muscle progenitors (Devoto et al., 1996). Their differentiation is accompanied by cell shape changes. The initially cuboidal adaxial cells begin to elongate to span the length of the somite along the anterior-posterior axis and stack to form a monolayer along the notochord, shortly after somite formation (Daggett et al.,

2007; Nguyen-Chi et al., 2012). The first slow muscle progenitors that migrate are called the muscle pioneers. They are identified by their expression of *engrailed2a* (*en2a*) (Felsenfeld et al., 1991; Hatta et al., 1991). They migrate dorsally and ventrally, while remaining medial in the somite, to form the horizontal myoseptum. In a second migration, non-pioneer slow muscle precursors migrate radially towards the lateral surface of the somite (Devoto et al., 1996).

Fast muscle precursors are specified shortly after the somite forms. They arise from the dermamyotome, located in the anterior of the somite (Stellabotte et al., 2007; Stellabotte and Devoto, 2007; Windner et al., 2015), and the myotome, located in the posterior compartment of the somite. Coincident with the migration of the slow muscle precursors, the fast fibre precursors begin to differentiate from the somites and remain medial to the slow fibre population (Devoto et al., 1996). The migration of the slow muscle precursors has been demonstrated to be necessary and sufficient to induce the morphogenesis of rounded fast fibre precursor cells into elongated fast fibres (Henry and Amacher, 2004).

Elongating muscle progenitors attach to the cytoskeletal elements of the somite boundaries immediately anterior and posterior to them. The somite boundaries now take on a chevron shape, with the apex pointing anteriorly (Rost et al., 2014; van Eeden et al., 1996) and this shape is maintained by the slow fibre population (Rost et al., 2014). As the muscle progenitors differentiate into elongated muscle fibres, the boundaries become enriched with cytoskeleton and adhesion proteins to differentiate into myotome boundary junctions that retain the chevron shape.

Myotome boundary junctions are homologous to the mammalian tendon as they transmit muscle force to the skeleton (Long et al., 2002). They are variously referred to as transverse myosepta, myotendinous junctions, myoseptal tendons (Charvet et al., 2011), but in this thesis, they will be referred to as the myotome boundary junctions or simply myotome boundaries. Structurally, they comprise actin filaments and actin binding proteins, in addition to collagen, focal adhesion and dystroglycan complexes (Charvet et al., 2011; Crawford et al., 2003; Henry and Amacher, 2004). The chevron-

shaped myotome boundary junctions can be identified by their accumulation of actin and by the accumulation of Xirp2a, on both mRNA (Deniziak et al., 2007) and protein levels (Otten et al., 2012).

1.3.2.2 Myotome boundary junctions as readout for the segmentation clock

In situ hybridisation for *xirp2a* to visualise the myotome boundary junctions is a simple, high contrast and high throughput methodology that has been utilised to assess functionality of the segmentation clock (Liao et al., 2016; Oates and Ho, 2002; Riedel-Kruse et al., 2007; Schröter et al., 2012; Soroldoni et al., 2014;) as perturbations of the clock – such as the progressive desynchronisation of cellular oscillations in the PSM, have resulted in corresponding myotome boundary defects (Riedel-Kruse et al., 2007). Consequently, in this thesis too, disruption of the segmentation clock has been interpreted from the loss of integrity of the myotome boundaries. The boundary characterisation method that has been utilised is binary, scoring boundaries as either normal or defective (Liao et al., 2016).

Although visualising *xirp2a* expression can capture the defects arising as early as during the activity of the segmentation clock, the multiple processes that occur between the segmentation clock output and the formation of the myotome boundary that have been described above also impact the expression. The observation of defective boundaries could be due to defects in any of the process leading up to myotome boundary morphogenesis (Richter et al., 2017). Segment boundary formation has been described as occurring in 3 stages – the initial formation of a somite boundary, the transition during which the somite boundary begins to accumulate ECM and rounded muscle precursor cells elongate, and the final development of the myotome boundary that is rich in ECM and is the attachment site of the elongated muscle fibres (Henry et al., 2005). While it has been assumed that a defective segment remains defective and vice-versa in the scoring of myotome boundaries, it is still unclear if there is a 1:1 correspondence between somites and myotome boundary junctions. Furthermore, there are examples in the literature that contradict this assumption – fibronectin and integrin mutants, *natter* and *before eight* respectively, have normal somite boundaries but have

defective myotome boundaries in their anterior trunk (Jülich et al., 2005a; Koshida et al., 2005; Schröter et al., 2008). More surprisingly, *deltaC* mutants (*beamter*) that fail to make anterior somite boundaries have myotome boundaries that appear normal (Herrgen et al., 2010; van Eeden et al., 1996). It has been proposed that the "recovery" of myotome boundaries in the absence of initial somite boundary formation is slow muscle dependent (Henry et al., 2005).

1.3.2.3 Sclerotome differentiation

As the muscle pioneers migrate away from the notochord, the sclerotome differentiates by undergoing epithelial to mesenchymal transition (EMT) and migrating to surround the notochord and the neural tube. Sclerotome arises from a cluster of cells in the ventromedial region of the somite. However, there are qualitative differences between the cells located anteriorly and posteriorly in this region (Morin-Kensicki and Eisen, 1997). All of the anterior cells of the ventromedial cluster undergo EMT, express sclerotomal marker *twist2* (previously *twist*) (Germanguz et al., 2007; Morin-Kensicki et al., 2002) and begin to migrate dorsally towards the anterior end of the future vertebra. Only some of the cells of the posterior compartment undergo EMT and these cells migrate after the anterior cells, over a broader region, but with a tendency to remain ventral to the notochord (Morin-Kensicki and Eisen, 1997).

Somites and myotomes are in segmental register. In contrast, the segmental register of the somites and vertebral column is offset – the original boundary between somites is near the midline of the adjacent vertebra. This offset of register between myotome and vertebrae is necessary for movement and is thought to be brought about by a process termed resegmentation by Remack in 1855 (Aoyama and Asamoto, 2000; Fleming et al., 2015). In this model, a somite is proposed to contribute to 2 consecutive vertebrae. Sclerotome from the anterior compartment of a somite contributes to the posterior end of the first vertebra and sclerotome from the posterior compartment of the somite contributes to the anterior end of the 2nd vertebra. This model seems to hold for amniotes, but not for zebrafish. In zebrafish, the sclerotome contribution to the vertebral column is not strictly dependent on the anterior or posterior somite domain of its origin. Lineage tracing studies have shown that cells from either anterior or posterior

sclerotome are capable of contributing to all positions of the adjacent vertebra. Therefore, in zebrafish, resegmentation is proposed to be 'leaky' (Morin-Kensicki et al., 2002).

1.3.3 Postembryonic development of the vertebral column

By the first 24 hours of development, somitogenesis is almost complete and therefore, the segmented body plan can be considered to be established within the first day of development. However, the vertebral column – the organ in which segmentation is most clearly seen in adults – is yet to start developing. Vertebral development is first observed by staining fry with calcein (a fluorescent chromophore that specifically binds to calcium) at a week post birth as small, ossified rings around the notochord (Du et al., 2001). These rings are called the chordacentra (Fleming et al., 2015). Within each chordacentrum, the calcification process is initiated at the boundary and then expanded both anteriorly and posteriorly to finally form the centrum (Du et al., 2001). The chordacentra are added in a sequential order over a period of several days, the formation of all chordacentra completing by three weeks of development. At this stage, the periodically re-iterated vertebral column can be observed and axial structures have their adult morphology. The segments of the vertebral column – the vertebrae comprise an ossified barrel, called the centrum and protruding arches. The vertebrae of the anterior body bear ribs and have protruding neural arches. The vertebrae of the posterior body are not rib-bearing and have protruding hemal and neural arches. Ribs and hemal arches protect the internal organs and the neural arches enclose the spinal cord (Fig 1.5) (Bird and Mabee, 2003).

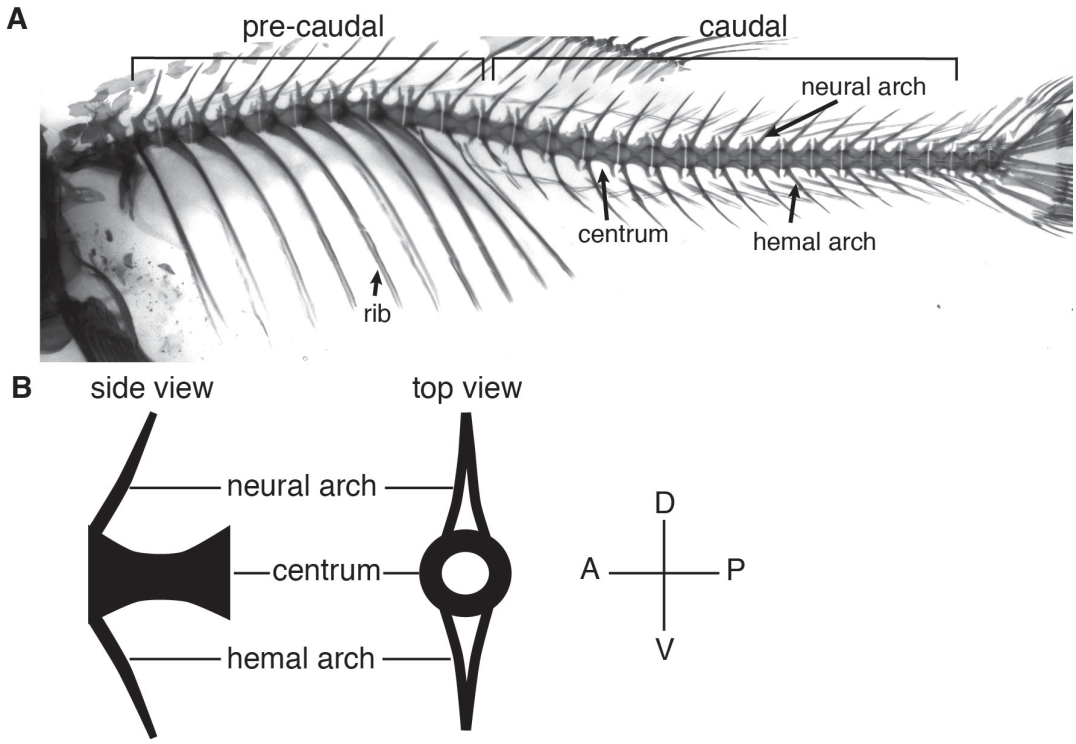

Figure 1.5 The adult vertebral column of zebrafish.

Skeleton of an adult zebrafish **(A)** and schematic representations of a caudal vertebra **(B)**.
(A) The vertebral column comprises periodic vertebrae. Vertebrae comprise a bony centrum and associated ribs or arches. Precaudal vertebrae are rib-bearing and have neural arches; caudal vertebrae have hemal and neural arches. **(B)** Arches are positioned on the anterior end of the centrum. Neural arches are dorsal and hemal arches ventral (side view). Arches fuse medially (top view).

Therefore, although the embryo has a segmented axis by the first day of life, it takes weeks for the segmented body to complete development (Fig 1.6).

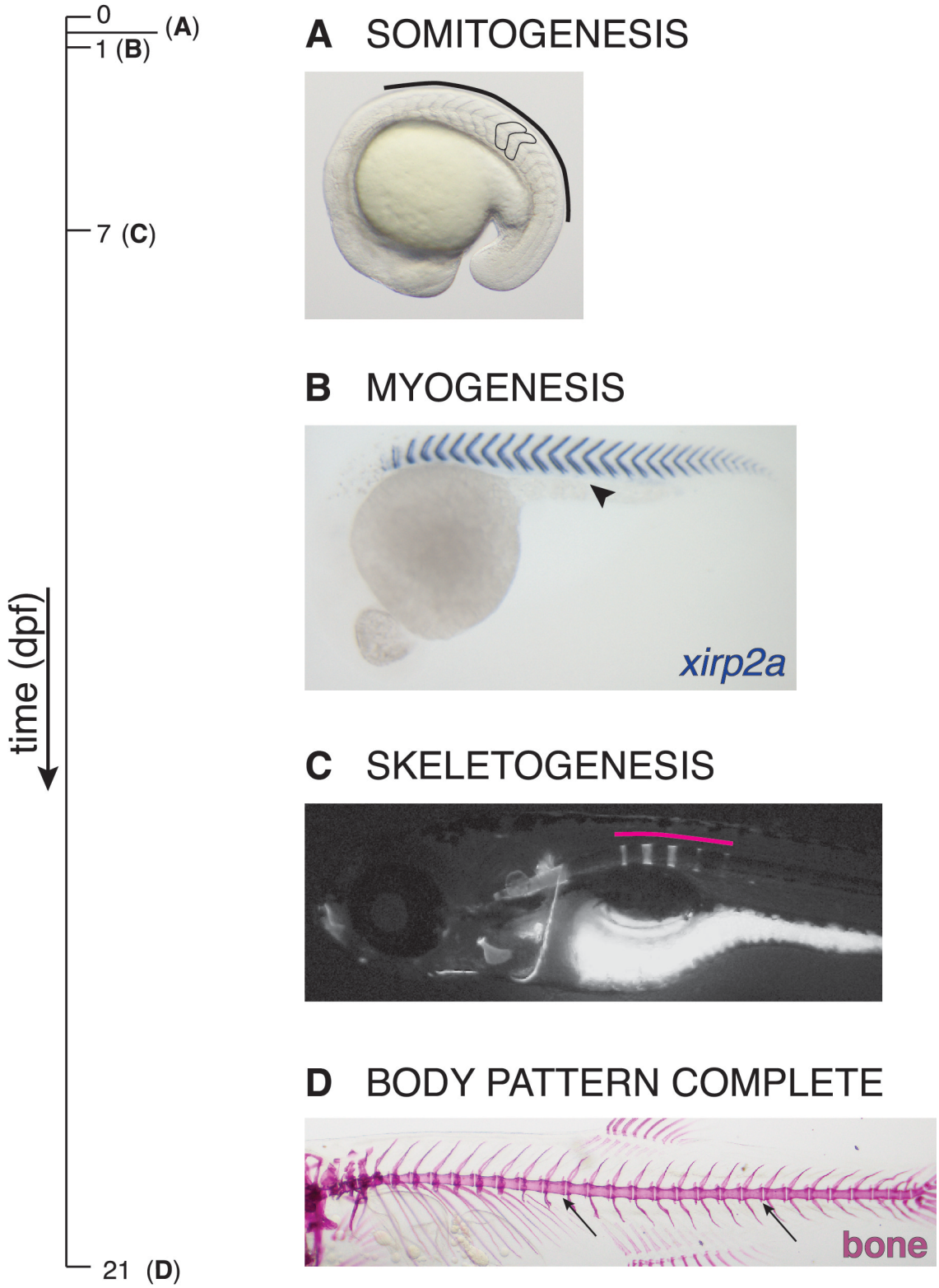

Figure 1.6 The developmental timeline of establishing segmental body pattern.

Development of segmentation in zebrafish indicated in a timeline in days post fertilization (dpf). Bright field image of embryo undergoing somitogenesis **(A)**, *in situ* hybridisation for myotome boundary junction marker *xirp2a* **(B)**, chordacentra development in the notochord visualised with calcein **(C)** and an alizarin red skeletal preparation **(D)**.

(A) Segmentation of the embryonic axis (black line – somites) and **(B)** periodic myotomes (arrowhead) are visible by 1 dpf. **(C)** Rings of ossification (pink line), indicating the onset of skeletogenesis, are visible at 7 dpf. **(D)** Periodic centra (arrows) in the vertebral column are fully developed by 21 dpf.

1.3.4 Pattern in the absence of somitogenesis

The observation of segmentally patterned somites resulting in the formation of correspondingly segmented skeletal and muscle elements in biomechanical register makes it tempting to conclude that the segmentation clock is the key developmental process that lays down the framework for the metameric vertebrate body. There is wide consensus that amniotes (birds and mammals) pattern their musculature and vertebral column at the same time in development by using the pre-pattern established by the segmentation clock (Pourquié, 2009). That is to say, the segmentation clock creates segmental somites and this segmental information is inherited by the myotome and sclerotome, thus giving rise to the metameric musculoskeletal system that is in biomechanical register. Correspondingly, perturbations that disrupt the segmentation clock lead to defects in the centra and arches of the vertebral column. For example, in mouse embryos, the loss of cyclic gene *Hes7* leads to the formation of fused vertebrae (Bessho et al., 2001), while an engineered *Hes7* that shortens somitogenesis period and therefore produces more somites, results in the formation of more vertebrae (Harima et al., 2013). Similarly, surgically perturbing somites in chick embryos produces defects in the centra and arches (Aoyama and Asamoto, 1988; Stern and Keynes, 1987).

However, in zebrafish, it is not clear if the segmentation clock is the master periodic pattern generator. The skeletal phenotypes of 2 somitogenesis mutants simultaneously support and refute this hypothesis. The zebrafish *hes6* mutant forms somites more slowly than wild type and makes correspondingly fewer centra (Schröter and Oates, 2010), therefore suggesting that the segmentation clock can influence vertebral patterning. However, the zebrafish *tbx6 (fused somites)* mutant, which fails to make somites (Barrios et al., 2003; Nikaido et al., 2002) and differentiate a segmental sclerotome, still has a strikingly periodic vertebral column (Fleming et al., 2004; van Eeden et al., 1998), suggesting that a segmented sclerotome is not necessary for the development of periodic centra in the vertebral column (Fig 1.7).

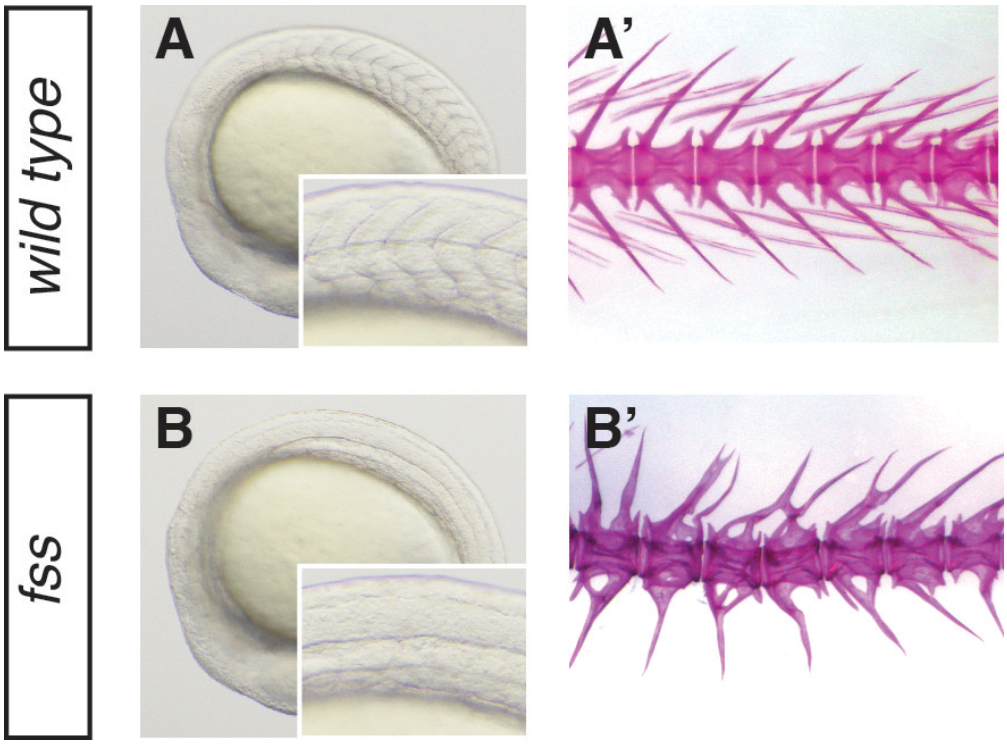

Figure 1.7 Axial segmentation in the absence of paraxial segmentation.

Bright field images of somites **(A)** and caudal vertebrae from alizarin red skeletal preparations **(A')** in wild type embryos and adults respectively. Somites in *fused somites (fss)* embryos **(B)** and caudal vertebrae of *fss* adults **(B')**.
(A, A') Wild type embryos have periodic somites and adults have correspondingly periodic vertebrae.
(B, B') *fss* embryos fail to make somites, yet adults have periodic vertebrae.
Panel B' – courtesy of Laura Lleras Forero.

The following hypotheses have been put forward to explain the segmented *fused somites* (*fss)* skeleton:

1. The segmentation clock is responsible for the patterned vertebral column – The *fss* mutant retains a dynamic segmentation clock in the posterior of the PSM. The kinematic waves are lost in the anterior PSM and there is no output of the clock's information in the anterior PSM – *mespb* is not expressed (Nikaido et al., 2002; Sawada et al., 2001) and morphologically distinct somites fail to form (Barrios et al., 2003; Durbin et al., 2000; Oates et al., 2005b). It can be argued that an active clock in the posterior PSM of the *fss* mutant is sufficient to correctly pattern the chordacentra, even in the absence of morphological somitogenesis.
2. The muscle pioneers are a source of segmental pattern – Although the myotome of *fss* mutants is not organised as chevrons, the muscle fibres themselves do not differ greatly in length from wild type (van Eeden et al., 1998). Myotome boundary

junctions can be seen as short fragments scattered in the trunk (van Eeden et al., 1996). The myotome boundary junction fragments are lost when muscle pioneer formation is inhibited in *fss*. From this observation, van Eeden et al.,1998 have proposed that "order" can be imposed on the paraxial mesoderm by the elongation and stacking of the muscle pioneers and that this is sufficient to rescue the segmentation of the paraxial mesoderm derivatives.

3. Segmental pattern of the vertebral column does not arise from the segmentation clock – Fleming et al., 2004 have asserted that the notochord is the primary source of segmental information for the centra, and not the somite-derived sclerotome. They tested this assertion by laser ablating cells in the notochord and observing the loss of centra in the location of ablation. This idea also explains the formation of segmented centra in *fss* where somites are not made. However, it cannot explain the correspondence between the number of somites and the number of vertebrae in the *hes6* mutant.

Therefore, in zebrafish, there is no clear answer to the fundamental question of whether an early developmental segmentation event is giving rise to the periodicity observed in later development. The direct approach to test the first hypothesis is to develop a somitogenesis mutant in which the dynamics of the segmentation clock is lost and then assess if any pattern is present in the later developing vertebral column.

1.4 Aims of the thesis

In this thesis, it was aimed to

1. Investigate the role RA plays in the zebrafish segmentation clock
2. Investigate the developmental mechanisms by which periodic pattern is established in the zebrafish body.

The approaches adopted to achieve these aims were:

- The development of a novel RA signalling reporter to visualise RA signalling events in the PSM during somitogenesis
- A spatiotemporal description of somitogenesis in the RA biosynthesis mutants
- The establishment of a mutant that does not have a segmentation clock

- The assessment of the notochord as a source of segmental body pattern

Chapter 2. Materials & Methods

2.1 Zebrafish methods

2.1.1 Fish maintenance

Wild type, mutant and transgenic zebrafish (*Danio rerio*) were raised and maintained according to standard laboratory procedures (Westerfield, 2000; Nusslein-Volhard and Dahm, 2002). Wild type AB (ZDB-GENO-960809-7) and wild type TL (ZDB-GENO-990623-2) zebrafish were used in this work. Zebrafish (*Danio Rerio*) mutant and transgenic strains used in this work are listed below:

Fish strain	allele
hes6	*ZM00283007*
fss	*te314a*
gullum (her1;her7)	novel TALEN induced *her1* mutation in *her7*^{hu2526}
giraffe	*rw716*
Looping1	*Tg(her1::YFP)*

Table 2.1 Mutant and transgenic fish strains used

hes6, *fss* and *gullum* (*her1;her7)* double homozygous mutant are fertile and viable. *giraffe (gir)* were maintained as heterozygotes as homozygotes suffer early mortality.

Embryos for experiments were obtained by natural spawning and staged according to Kimmel et al. (Kimmel et al., 1995). They were of AB or ABxTL hybrid wild type backgrounds. Parental fish of the desired genotype were mated pairwise in 1.5 l breeding containers and allowed to produce embryos for 20 min before harvesting. A mesh inlet separated newly produced embryos and parental fish. Harvested embryos were directly put into E3 embryo medium (E3). Sibling embryos were evenly distributed into petri dishes (Ø 9 cm) and incubated at 28.5°C and clutches with identical developmental progression were selected for further experimentation. When late somitogenesis stages (19 – 20 somites) were desired, embryos were moved to 23°C at 50% epiboly for 14 hours and returned to 28°C till the embryos achieved the desired stage of somitogenesis.

For *in situ* hybridisation and antibody staining of embryos older than 24 hpf, embryos were treated with 0.003% Propylthiouracil (PTU) diluted into the embryo medium at ~24 hpf to suppress natural pigmentation.

2.1.1.1 Buffers and solutions for embryo handling

Embryo medium E3:

5 mM NaCl

0.17 mM KCl

0.33 mM $CaCl_2$

0.33 mM $MgSO_4$

Buffered with: 0.458 mM Na_2HPO_4, 0.042 mM KH_2PO_4 for pH 7.3 – 7.5

0.3x Danieau's solution

0.4 mM $MgSO_4$

0.6 mM $CaCl_2$

0.7 mM KCl

58 mM NaCl

5 mM Hepes, pH 7.6

PTU 100x stock:

Phenylthiouracil (Sigma)

0.3% solution in distilled water

2.1.2 Genotyping of mutant zebrafish lines

All PCR-based genotyping protocols were carried out according to standard procedures of handling genomic DNA. DNA samples of zebrafish were extracted by alkaline lysis (Meeker et al., 2007) or with a Blood and Tissue DNA extraction kit (Qiagen). Caudal fin tissue derived from adult zebrafish, whole embryos or explants from processed embryos served as genomic DNA sources. An appropriate volume of 1X Base solution (25 mM KOH, 25 μM EDTA) was added to the tissue (50 μl for adult fins, 15 μl for embryonic explants) and heated to 95°C for 30 mins. The samples were cooled to room temperature and then an equal volume of 1X Neutralization solution (40 mM Tris HCl) was added. Samples were stored at 4°C in the short-term and at -20°C for long-term use.

1:5 dilutions of fin genomic DNA extracts were used for PCR. Extracts of embryonic genomic DNA were diluted up to 1:4. DNA extracts were further purified if a multiplex PCR was to be performed. DNA extracts were precipitated with 0.7 volumes of isopropanol by centrifugation (21,000 x g, 20 mins, 4°C). Subsequent washing with 70% ethanol was followed by another centrifugation step. The DNA pellet was air-dried and resuspended in nuclease free water, pH 7.5. DNA was extracted as per the manufacturer's instructions when the DNA extraction kit was utilized. PCR cleanup, where required, was performed with SV Wizard PCR and Gel Purification kit (Promega) as per the manufacturer's instructions, except for the final centrifugation step required for elution – a 20 min centrifugation at 17,000 x g was implemented to remove ethanol contamination.

1 to 2 µl of DNA preparation (25 ng – 50 ng of genomic DNA) was used as template in 10 µl PCR reactions. PCR reactions were carried out using 200 nM of allele specific primers (see below), 200 µM dNTP mix, 1 x GC buffer, 3% DMSO and 0.02 U/µl Phusion DNA polymerase (NEB) or 200 nM allele specific primers, 1X HF-Hotstart Phusion Mastermix (Thermoscientific) and genomic sample DNA in a 10 µL volume. The reaction was performed on an Eppendorf Mastercycler (Eppendorf) with the following program for all genotyping PCRs:

98°C	3 min	
98°C	15 sec	30 x
X °C	15 - 20 sec	
72°C	20 sec	
72°C	5 min	
10°C	hold	

Annealing temperature and annealing and extension time were adapted to the specific primers used and to the length of the expected reaction product, respectively.
gir heterozygote adults and homozygote embryos were identified by PCR for a 252 bp fragment of *cyp26a1* followed by digestion of the amplicon with *Xba*I (Fast digest, ThermoScientific), which cleaves the mutant *cyp26a1* allele, but not the wild type allele (Emoto et al., 2005).

The retroviral insertion in the *hes6* gene was detected with a multiplex PCR reaction, using hes6-701-for, hes6-1522-rev and 5'LTR-600 together. The two gene-specific primers amplify an 840 bp gene product on the wild type allele. Alleles with retroviral insertion amplify a 560 bp PCR product with one gene-specific primer and the viral primer. According to the band pattern in an agarose gel electrophoresis, wild type (840 bp band), heterozygous (840 bp & 560 bp bands) and homozygous carriers (560 bp band) can be identified (Schröter and Oates, 2010).

gullum was identified by PCR for a 606 bp fragment of *her1* and subsequent digestion with restriction enzyme *Age*I/*BshT*I (Fast digest, Thermoscientific) that yielded 2 fragments of sizes 339 bp and 267 bp. The mutant allele is resistant to digestion. Therefore, wild type, heterozygous and homozygous individuals can be identified by the presence of 2, 3 or 1 band(s) respectively by agarose gel electrophoresis.

fss was identified by PCR amplification of 532 bp fragment of *tbx6* and subsequent sequencing (Eurofins).

2.1.2.1 Solutions and reagents for genotyping

Stock solutions for genomic DNA extraction*:*

Base solution (50X)
1.25 M potassium hydroxide
10 mM EDTA
in distilled water

Neutralisation solution (50X)
2 M Tris HCl
in distilled water

Primer name	Sequence (5' - 3')	Tm (°C)	Digest
gir ID R	CAGGGTTTGAGGGCACGCAATTT	58.3	XbaI
gir ID L	GCTGCTTCTTTCATCGCCTAAGC	58.3	
gui_ID F	TCGAAGACCAACCAAACGAGT	63.7	BshT1
gui_ID R 606	GCCTTGATCTCTCGCAGTCG	63.7	
fssID_F	ATGGGCTTGCTAATTTTCCATTCT	61	
fssID_R 532	CTGAGCTCTGCGTTGAGGAC	61	
hes6-701-for	AGCAACACTCACGACGAGGATTA	55	
hes6-1522-rev	CAGAACAAATGTCGTCGCTGGAG	55	
5'LTR-600	AAGTCGGATGCAACTGCAAGAAGG	57	

Table 2.2 Primer sequences used for genotyping

Reagents:

Phusion high-fidelity PCR kit	NEB (E0553)
Phusion green hot start II high-fidelity PCR master mix	Thermoscientific (F-566S)
Blood and Tissue DNA extraction kit	Qiagen (69506)
Wizard SV Gel and PCR Clean up system	Promega (A9282)

2.2 BAC recombineering

The BAC recombineering protocol used is based on (Sarov et al., 2006) and was optimized for zebrafish by Daniele Soroldoni (Soroldoni et al., 2014). The BAC (CH211-215I2), which contains a ~49 kb genomic DNA fragment of *Danio rerio* (TU line) spanning the *cyp26a1* locus and the last exon and terminal UTR of *exoc6*, just upstream of *cyp26a1*, was obtained from the BACPAC Resources Center. The BAC was purified from its host cells (DH10B) (using Promega SV Wizard Gel miniprep kit) and electroporated (Eppendorf Electroporator 2510) into HS996 cells containing the pRedFlp4 plasmid that has the red operon, which includes all necessary elements to perform homologous recombination in *E. coli*. The HS996 cells were inoculated in 1.5 ml LB with Hygromycin at 30°C to a final OD_{600} of 0.3. 30°C is the permissive temperature for the thermosensitive pSC101 origin. After washing the cells twice with ice-cold distilled H_2O/10 % Glycerol, 1 µl of the BAC miniprep was added and cells were electroporated at 2.5 kV. A 60-min recovery was performed in pre-warmed SOC

at 37°C and a fresh overnight (ON) culture was made by inoculating 100 µl of the recovery culture in 1.5 ml LB with chloramphenicol and hygromycin at 30°C.

2.2.1 Generation of the tagging and subcloning cassettes

Tagging and subcloning cassettes were generated by PCR from plasmid templates. Primers consisting of 50 bp homology arms and 22-24 bp template specific sequence were used in 100 µl PCR reactions. The reaction was set up as 1x GC buffer, 200 nM specific primers, 200 µM dNTPs, 3% DMSO, 0.02 U/µl Phusion DNA polymerase and 15 – 30 ng of plasmid DNA as template. The PCR program was as following:

98°C	1min	
98°C	5 sec	30 x
X °C	10 sec	
72°C	45 sec	
72°C	5 min	
10°C	hold	

The tagging cassette carried a kanamycin-resistance gene flanked by loxP or FRT sites. The homology arms on either side of the tagging cassettes allowed for specific integration of the reporter protein and for the deletion of the stop codon of the *cyp26a1* gene. The product of the first recombination event was a fusion of *venus* at the C-terminus of the *cyp26a1* gene. The kanamycin resistance gene allowed for the selection of positive clones. The homology arms flanking the subcloning cassette had a reverse orientation and lead to integration of the tagged *cyp26a1* gene into the plasmid backbone (pNCP2 Plasmid). This plasmid has a low-copy origin, *I-SceI* sites, a CloNAT resistance gene and is counter-selectable via its *ccdB* gene. PCR products were purified with the Wizard SV Gel and PCR Clean-up System (Promega) and their purity was checked on a 1% agarose gel.

	Primer name	Sequence (5' - 3')	Tm (°C)
Subcloning *cyp26a1* locus	cyp26a1_HAL	CTTTAAACCTTAACCTGAATAGTATTTAGAAATACAA AGCTCTTGTTAAGCCGTAGGGATAACAGGGTAATTT	61
	cyp26a1_20K_HAR	TGTGGAAGGGACTTGTCCTTGTGTGACACGGTGA GATGCTGGCAGATGCTAGGGATAACAGGGTAATTG CACTGAAATCTAGA	61
cyp26a1 tagging	cyp26a1_venus_TAGL	TTTACCCAGTGGACAATCTCCCTACCAAATTCACTA GTTATGTCAGAAATAGCTCAGGAGGTAGCGGC	68
	cyp26a1_venus_TAGR	ACATCACAGTTCATCTAAAATAAAAACATATGTACAA AGCTCCGGTTAGGGGCAGATCGTCAGTCAG	68

Table 2.3 Primers for generation of tagging and subcloning cassettes

2.2.2 Recombineering events: tagging the gene of interest and subcloning the region of interest

HS996 cells were grown to an OD_{600} = 0.2 in LB with chloramphenicol and hygromycin. 600 µl of 10 % L-Rhamnose was added to induce the red operon in the pRedFlp4 and the culture was shifted from 30°C to 37°C till a final OD_{600} = 0.4. A second culture without L-rhamnose induction served as a negative control. OD measurements were taken on a NanoDrop 1000 (Thermo Scientific). Bacteria were collected by centrifugation and washed twice with ice-cold, sterile distilled H_2O/10% Glycerol. Centrifugation steps were carried out at 12,800 x g and 4°C for 30 seconds. After the second wash, the supernatant was carefully decanted to retain the pellet and approximately 50-60 µl of liquid. 500 ng of the tagging or subcloning cassette was quickly added and the mixture was transferred into pre-cooled 0.2 cm disposal cuvettes (Gene Pulser, Bio-Rad). The cells were electroporated at 2.5 kV and a time constant of 5-6 ms. Cells were recovered for 60 mins in 1 ml of pre-warmed SOC medium at 37°C. Subsequently, 1.5 ml LB medium containing the appropriate antibiotics was inoculated using 100 µl of the recovery culture and grown overnight at 30°C, if the red operon was still required for further recombineering events. A backup culture was plated for positive clones. To identify positive recombination events, plasmid DNA of single colonies picked from the plate of positive clones was obtained by miniprep without column purification and subjected to restriction digest analysis.

The region of interest (~20 kb) was subcloned into the pNCP2 backbone. The kanamycin resistance gene flanked with loxP or FRT sites was removed after the subcloning step. Flp4 is present in the plasmid with the red operon and is induced by anhydrotetracyclin. A plasmid carrying the pCre under the control of a heat inducible promoter was electroporated into the HS996 cells carrying the plasmid. The *E. coli* strain carrying the pCre or Flp4 plasmid was plated on LB_CN/anhydrotetracyclin agar (to induce Flipase expression) and grown overnight at 37°C (to induce Cre) expression. Both Cre and Flp4 plasmids are lost during culturing at 37°C. Subsequently, single colonies were screened for removal of the kanamycin resistance gene by restriction digest. Plasmid DNA of the chosen single colony bearing the desired tagged and subcloned BAC construct was isolated by a midi preparation and used for meganuclease-mediated transgenesis. The sequence of the construct was confirmed by primer walk (Sequencing Facility, MPI-CBG, Dresden).

2.3 Live embryo manipulations

2.3.1 *I-SceI* meganuclease mediated transgenesis in zebrafish

BAC constructs were injected into the single cell of one-cell stage embryos along with *I-SceI* meganuclease as per (Soroldoni et al., 2009). Pairwise mating crosses of AB wild type fish were set up as described before. Eggs were collected in E3 medium as soon as the fish spawned (5 -10 mins after dividers have been removed) to ensure that injections could be performed at the one-cell stage of embryonic development. Embryos were transferred into a 1-2% agarose injection mould and the injection was performed in 0.3x Danieau's solution. The injection needles (Borosilicate glass capillaries 0.1 mm O.D. x 0.58 m I.D., Harvard Apparatus) were pulled using a micropipette puller (Sutter Instruments). The needles were opened by breaking the tip using watchmaker's forceps and the bolus size was adjusted before and after each injection by injecting into mineral oil (Sigma) covering a stage micrometer. Eject pressure of 40 psi was used for boluses of 100 – 120 μm diameter. The hold pressure was adjusted to inhibit unwanted in- or outflow. The gating time varied between 300 and 400 ms. The injection pre-mix was prepared as:

DNA [50 ng/µl] – 1 µl,
10X Buffer (Roche) – 2 µl,
$MgCl_2$ (50 mM) – 2 µl,
Water – up to 18 µl,

and kept on ice till the time of injection. Meganuclease (2 µl, Roche) was added directly before injecting. After injection, the Danieau's solution was exchanged with E3 medium and embryos were incubated at 28.5°C until 50% of epiboly was reached and shifted to 20°C. Transient expression of the construct was checked at mid-somitogenesis the following day.

2.3.2 Small molecule treatments of embryos

Embryos were treated 20 at a time in 24-well plates. Desired concentration of small molecule stock solutions in DMSO – retinoic acid (Sigma) and cyclopamine-KAAD (Calbiochem) – were applied in 1 ml of E3 medium per well, supplemented with a final volume of 0.5% DMSO. Small molecule concentrations used for retinoic acid treatments were 1 nM, 10 nM and 100 nM, and concentrations of cyclopamine used were 10 µM and 25 µM. Embryos were incubated in the small molecule solutions in darkness at 28°C till the desired developmental stage. The small molecule treatment was subsequently stopped by several washing steps in E3 medium and prepared for *in situ* hybridisation.

2.3.2.1 Stock solutions of small molecules

RA
1 mM stock in DMSO

cyclopamine KAAD
5 mM stock in DMSO

Reagents

Retinoic Acid	Sigma (R2625)
cyclopamine KAAD	Calbiochem (239804)

2.4 Molecular and Histological techniques

2.4.1 *In situ* hybridisation

2.4.1.1 Riboprobe Synthesis

For riboprobe synthesis, the appropriate vector was linearized by standard restriction digest (ThermoScientific fast digest enzymes) and purified with a PCR purification kit (Qiagen). Riboprobes were transcribed *in vitro* from the DNA template using the appropriate RNA polymerase with digoxigenin-labelled rNTPs (Roche). Antisense riboprobes were purified using the RNeasy kit (Qiagen) and eluted with RNase-free water. To check for quality and correct size of the riboprobe, agarose gel electrophorese was performed using 1-2 µl of the transcript. The remaining riboprobe was taken up in 5 ml of hybridisation buffer and stored at -20°C.

Probe	Plasmid source/Template
mespb	(Sawada et al., 2000)
myoD	(Weinberg et al., 1996)
her7	(Oates and Ho, 2002)
her1	(Müller et al., 1996)
deltaC	(Oates and Ho, 2002)
tbx16/spt	(Ruvinsky et al., 1998)
tbx6/fss	(Nikaido et al., 2002)
ta/ntl	(Schulte-Merker et al., 1994)
venus/ eGFP	
cyp26a1	cloned by Leah Herrgen, Oates lab
her11	cloned by Christian Schroeter, Oates lab
papc	(Yamamoto et al., 1998a)
ripply1	Primers: Rip1 F (CGTGGCTTGTGACCAGAAAAG) and Rip1 R T7 325 (TAATACGACTCACTATAGGCTGTGAAGTGACTGTTGTGT)
ripply2	Primers: Rip2 F (ACGCGAATCAACCCTGGAGA) and Rip2 R T7 281 (AATACGACTCACTATAGGGAGAGAGCTCTTTCTCGTCCTCT TCAT)
xirp2a/ cb1045	(Deniziak et al., 2007)
twist2	Gift from Stefan Schulte-Merker
en2a deltaC intron4	(Erickson et al., 2007) (Oates et al., 2005a)

Table 2.4 Templates for riboprobes

2.4.1.2 Whole-mount in situ hybridisation

Whole-mount *in situ* hybridisation was performed as previously described (Hauptmann and Gerster, 1994). Embryos were fixed for at least 1 hour in 4% PFA in PBS-T, manually dechorionated in PBS-T and dehydrated by an alcoholic series and left in 100% methanol for at least 12 hours at -20°C. Embryos were rehydrated through a decreasing alcohol series and digested with Proteinase K depending on the stage, rinsed in PBS-T and re-fixed for 20 mins to inactivate Proteinase-K. Embryos were pre-hybridized at 60°C, the temperature of riboprobe hybridisation, for 30 mins to 3 hours. Embryos were incubated in riboprobe in hybridisation mix. Excess riboprobe and non-

specific binding were removed by a series of washes of decreasing salt concentration performed at the hybridisation temperature (2 times for 30 min in Wash I, 15 min in Wash II and two times for 30 min in Wash III). Embryos were then incubated in 2% blocking reagent in MAB-T at room temperature for 30 minutes before incubation in anti-DIG label antibody for 2 hours at room temperature. Unbound antibody was washed using MAB-T over 2 hours with multiple exchanges at room temperature or overnight at 4°C. Embryos were then equilibrated (2 times for 5 mins) in staining buffer. Specific binding was visualised using a chromogenic solution based on NBT/BCIP chemistry prepared in staining buffer according to the manufacturer's instructions. The reaction was stopped by rinsing several times with PBS-T, followed by washes in methanol to clear the embryo. The samples were briefly re-fixed, rinsed in PBS-T and stored in 87% glycerol/ 13% dH_2O for further analysis or documentation.

2.4.1.3 Buffers, solutions and reagents for in situ hybridisation

PBS 1x solutions:
PBS, pH 7.4
137 mM NaCl
2.7 mM KCl
10 mM Na_2HPO_4
2 mM KH_2PO_4

PBS-T
PBS + 0.1% (v/v) Tween20

Fixing solution:
4% PFA
4 g paraformaldehyde powder
100 ml PBS
Incubation at 68°C to completely dissolve
or
10 ml 16% paraformaldehyde solution
30 ml PBS-T

Proteinase K stock solution:
200x stock
1 mg/ml Proteinase K
in distilled water

Proteinase K solution:
5 µl/ml (1:200)
10 µl/ml (1:100)
in PBS-T

20x SSC buffer
3 M NaCl
300 mM tri-sodium citrate
in distilled water

Hybridisation solutions:
Pre-hybridisation mix
50% Formamide ultrapure
5x SSC buffer
50 µg/ml Heparin
0.5 mg/ml Torula-RNA solid
0.1% Tween20
in distilled water

Hybridisation mix
5 ml pre-hybridisation mix
30 µl riboprobe

Wash I
50% Formamide ultrapure
10% of 20x SSC buffer
0.1% Tween20
in distilled water

Wash II

10% of 20x SSC buffer

0.1% Tween20

in distilled water

Wash III

1% of 20x SSC buffer

0.1% Tween20

in distilled water

Maleic Acid Buffer x1 solutions

1x Maleic Acid Buffer (MAB), pH 7.5

100 mM Maleic Acid,

150 mM NaCl

MAB-T

1x MAB-T + 0.1% Tween20

Blocking solution stock

10% blocking reagent in MAB

Blocking solution

2% blocking reagent in MAB-T

Antibody solution

2% Roche Block in MAB-T

1:2000 Anti-Digoxigenin-AP

Staining buffer

100 mM TrisCl pH 9.5

100 mM NaCl

50 mM $MgCl_2$

0.1% Tween20

in distilled water

NBT/BCIP solution

Staining buffer

+ 3.5 µl/ml BCIP (5-Bromo-4-Chloro-3-indolyl phosphate)

+ 4.5 µl/ml NBT (Nitro blue tetrazolium)

Reagents:

Restriction enzymes	Thermoscientific, Fast Digest
rNTP – DIG	Roche (11277073910)
RNA polymerases	Roche
RNase-OUT	Invitrogen (100000840)
QIAquick PCR purification kit	Qiagen (28106)
RNeasy MinElute clean up kit	Qiagen (74204)
16% PFA	Thermoscientific (28908)
Proteinase K	Merck (1.24568.0100)
Heparin	Sigma (H 3400)
Formamide	Roche (1814320)
Torula RNA	Sigma (R6875)
Blocking Reagent	Roche (1109676001)
NBT	Roche (11383213001)
BCIP	Roche (11282221001)
Anti-Digoxigenin – AP F'ab fragments	Roche (11093274910)

2.4.2 Immunohistochemistry

Embryos at the desired stage were fixed in 4% PFA for 1.5 hours, then washed 4 x 15 min in PBSDTr. Fibronectin localization in embryos during somitogenesis was performed as previously described (Jülich et al., 2005a) using rabbit anti-Fibronectin Antibody (1:200) in 2% blocking reagent and incubated over night at 4°C. Embryos were washed 4 x 15 min in 1% blocking reagent. Alexa-Fluor488 goat anti-rabbit IgG F'ab fragments were used as secondary antibody (1:200) in 1% blocking reagent. Slow muscle myosin was localized with mouse S58 antibody (1:10) in 2% blocking reagent in 36 hpf embryos. It was visualised with 1:20 Alexa-Flour488 goat anti-mouse IgG

F'ab fragments as secondary antibody, incubated for 2 hours at room temperature. For co-staining of the actin cytoskeleton Alexa-Flour568 phalloidin was added with the secondary antibody, 1:500 for somitogenesis stages and 1:20 for 36 hpf embryos. Samples were washed 4 x 15 mins before being imaged.

2.4.2.1 Solutions and reagents for immunohistochemistry

PBS 1x solutions

PBSDTr

PBS + 1% DMSO + 0.1% Triton X 100

Reagents

rabbit anti-Fibronectin antibody	Sigma (F3648)
mouse S58 antibody	Developmental Studies Hybridoma Bank
Alexa-Flour488 F(ab')2 fragment of goat anti-rabbit IgG	Life technologies (A11070)
Alexa-Flour488 F(ab')2 fragment goat anti-mouse IgG	Life technologies (A11017)
Alexa-Flour568 Phalloidin	Life technologies (A12380)

2.4.3 Skeletal stains

2.4.3.1 Alizarin red stainings

Skeletal stains of adults were performed according to Potthoff 1984, with minor modifications as per the Parichy lab protocol at www.zfin.org. Adult fish were euthanized in 2% phenoxyethanol in aquarium water at 3 months and fixed in 4% PFA for at least a week. Specimens were dehydrated for several days in 100% ethanol, soaked in saturated sodium borate solution overnight and then bleached in 0.45% H_2O_2/0.85% KOH for 1.5 hours. Muscle tissue was cleared by trypsin digestion (1%/ 35% saturated $NaBO_4$) overnight, until the body achieved 60% clarity. Bones were stained by incubation in a 0.1% alizarin red/1% KOH for 24 hours. Trypsin digestion was performed to de-stain the fish over several days, followed by incubation in a graded

glycerol series (1% KOH/30% glycerol, 1%KOH/60% glycerol) for 24 hours each. Fish were then transferred to 100% glycerol for long-term storage.

Skeletal stains of 21 dpf larvae were performed as per a modified protocol from Walker and Kimmel (Walker and Kimmel, 2007; protocol at www.zfin.org). Larvae were euthanized in 2% phenoxyethanol in aquarium water. They were fixed in 2% PFA for 3 hours at room temperature. They were then transferred to 80% ethanol in distilled water for at least 30 minutes or stored at 4°C if the protocol needed to be stopped. Samples were rehydrated in an alcohol series (50% ethanol for 30 min, 25% ethanol for 30 min and 0.5% KOH for 30 min). The specimens were bleached in 3% H_2O_2/ 0.1% KOH for 30 min exactly and subsequently rinsed with 35% saturated $NaBO_4$; 30 min or more on a rotator, before clearing the body with 1% Trypsin in 35% Saturated $NaBO_4$ for 30 min. Samples were rinsed with 10% glycerol/0.5% KOH for 30 min and stained with 0.01% Alizarin Red overnight at room temperature. Specimens were de-stained by washing in 50% glycerol/0.1% KOH with 1 quick wash for 30 min and then transferred into a second 50% glycerol/0.1% KOH wash overnight at room temperature. Samples were stored in 100% glycerol at room temperature.

2.4.3.2 Solutions and reagents for skeletal staining

Fixing solutions:
4% PFA
1:4 16% PFA in PBS

2%PFA:
1:8 16% PFA in PBS

0.5% Alizarin Red S stock solution:
0.25 g Alizarin Red S
50 ml distilled water

Saturated solutions of sodium borate
Saturated solution of sodium borate ($NaBO_4$)
24 g sodium borate decahydrate

in 500 ml distilled water.

35% saturated sodium borate ($NaBO_4$)
8.3 g sodium borate decahydrate
in 500 ml distilled water

Digestion solution
1% Trypsin/35% saturated sodium borate
0.01 g/ml Trypsin
in 35% saturated $NaBO_4$

Reagents

Alizarin Red S	Sigma (A5533)
Porcine Trypsin (1:250)	SAFC (85450C)
H_2O_2	Sigma (216763)

2.4.3.3 Calcein stainings

Larvae were euthanized in 2% phenoxyethanol in aquarium water. Larvae were rinsed in aquarium water and then transferred, 10 at a time, into 35 ml of a 0.2% calcein solution in petri dishes for 5 min. Calcein was removed by several water exchanges (5 - 6). Larvae were then washed 2 X 5 min with aquarium water and 1 X 10 min before imaging. The protocol was adapted from the published vital calcein staining protocols (Du et al., 2001).

2.4.3.4 Solutions and reagents for calcein staining

Calcein solution, pH 7
1 g calcein
500 ml aquarium water
5 ml 1 N NaOH
filtered through 0.22 µm membrane

Reagents

Calcein	Sigma (C0875)

2.5 Imaging

2.5.1 Whole embryo time-lapse (WET)

For time-lapse imaging experiments embryos of adult pairings of the desired genotype were collected within 20 min after spawning, to minimize asynchronous clutches/siblings and incubated in E3. They were incubated at 33°C till bud stage, dechorionated and allowed to equilibrate at room temperature. Prior to imaging, 20 – 25 embryos were laterally aligned in conical depressions in a pad of agarose (Sigma, low-melting, 2% in E3) that was cast in a glass-bottom dish (Matek, 35 mm), as described previously (Soroldoni et al., 2014). The size of these conical depressions was chosen to fit only the yolk of an embryo so that embryos could grow without physical restrictions on top of the agarose pad, but were stabilized in the z-direction. The imaging dish contained E3 with 0.014% Tricaine to prevent muscle twitching and was equilibrated for 100 minutes in the thermal insert of the time-lapse set-up before imaging was started.

A wide-field microscope (Zeiss, Observer Z1) equipped with a 10X objective (Zeiss, NA 0.5), an automated stage (Prior), a LED-based light source (CoolLED pE-100), an EM-CCD camera (Andor, iXon 888), a thermal insert and an environmental cage (Okolab) were used to record zebrafish segmentation in 6 z-slices (range: 100 µm in 20 µm steps) for 20 – 25 xy-positions at time intervals of 5 min for at least 12 hours at an experimental temperature of 23.5°C in the insert and 28°C in the cage. The software driving microscope operations is Andor iQ2. The thermal insert is water bath controlled and capable of heating and cooling to maintain a set temperature to within 0.1°C. The environmental cage is heated by hot air within 1°C.

giraffe;Looping1 time-lapses were performed on a wide-field microscope (Zeiss, Axiovert 200M) equipped with a 10X objective (Zeiss, NA 0.5), an automated stage (Maerzhaeuser), a LED-based light source (Lumencor, SpectraX7), an EM-CCD camera (Andor, iXon 888) and a thermal insert (Harvard apparatus). During each experiment, the temperature was controlled by the closed thermal insert and monitored by an independent external thermometer that was used to log temperatures throughout recordings, which typically ranged between 23.3°C to 23.6°C. To compare

measurements from different experiments/days at slightly different temperatures, 6-7 wild type embryos were used in each experiment that were used to normalize the measured somitogenesis period. The random distribution of wild type and transgenic siblings in the imaging dish avoided any bias due to temperature gradients within the imaging dish.

2.5.2 Documentation of *in situ* hybridisation

Wholemount *in situ* hybridisations were documented with a stereomicroscope (Olympus SZX10 or Olympus SZX12) equipped with an appropriate CCD camera (Qimaging, Micropublisher). Flatmounted embryos were photographed using an Olympus MVX10 equipped with an RGB camera (Olympus DP22).

2.5.3 Documentation of skeletal stains

Alizarin red and calcein preparations were photographed on an Olympus MVX10 stereomicroscope equipped with an Olympus DP22 camera and a metal halide lamp (Lumen200, Prior) for fluorescent imaging. Vertebrae were counted from the first rib-bearing vertebra to the tail vertebra that supports the dorsal part of the tail fin. This counting procedure omits the most anterior, highly modified vertebra that form the Webberian apparatus as well as the posterior-most vertebrae that support the medial and dorsal parts of the caudal fin. Post-embryonic developmental stages were determined from bright field photographs of calcein stained larvae or photographs of fixed larvae that had been made prior to clearing and staining. Developmental staging was performed as per Parichy et al., 2009.

.

2.5.4 Confocal imaging of immunostains

Confocal images of whole mount immunostains were performed on a Nikon A1R confocal with a 16x/0.8 NA water dipping lens (Nikon) and a *galvano* scanner.

2.6 Image processing and analysis

Image processing was carried out using Fiji. Brightness levels of some images were adjusted in Adobe Photoshop.
Data analysis was performed using Graphpad Prism.

2.6.1 Image processing, measurements and analyses of whole embryos time-lapses

Image processing was carried out using Fiji and all tools used were those developed for Soroldoni et al. 2014. They are available at http://fiji.sc/Fiji. The stack focusing technique used extracts in-focus single layer images from the bright field z-stacks ("Gaussian StackFocusing"). Venus signals were subjected to maximum projections. All measurements were performed on these z-projections without any further image processing.

2.6.1.1 Somitogenesis period determination

All period measurements were restricted to trunk segmentation because the segmentation period is constant over this developmental interval (Schröter et al., 2008). The formation of segments was scored visually as described previously (Schröter et al., 2008). The first visible sign of each somite boundary was determined and each successive time point was noted. The average segmentation period of an embryo was calculated from a linear regression through the data points of a plot of the number of somites over time. These individual period measurements were pooled according to genotype and used to calculate the mean segmentation period for a given experiment. The average segmentation period of wild type embryos or control siblings was set to 100% and used to normalize all other period measurements for a given experiment. Individual period measurements were then normalized by dividing by the mean period value of all wild type embryos in the experiment, which allowed pooling of data from independent experiments.

2.6.1.2 Instantaneous somite, PSM and axial length measurements

Somite length was measured as soon as a boundary could be visualised (Bajard et al., 2014; Schröter et al., 2008). Axial and PSM length measurements were made by measuring the length of lines-of-interest (LOI) generated by the "LOI Interpolator" whose width was set to 20 pixels.

2.6.1.3 Posterior period determination

The periods of genetic oscillations were determined locally using the ROI interpolator tool available in Fiji. The obtained raw traces (mean grey values over time) were exported to Prism 6 and analyzed using the standard function for the second derivative. The average period per embryo was calculated from the inter-peak distance of the resulting curves. The individual periods obtained were normalised to the mean somitogenesis period of the control siblings and pooled to obtain an average period for oscillations in the posterior for a given experiment.

Chapter 3. Retinoic acid in the zebrafish segmentation clock

3.1 Background

A role in the wavefront has previously been attributed to RA on the basis of the following observations:

1. The formed somites can act as a source for RA, as RA biosynthesis enzyme *aldh1a2* expression is detected in the formed somites, and a potential sink for RA is present in the tissue, as the RA catabolism enzyme *cyp26a1* expression is detected in the tailbud (Dobbs-McAuliffe et al., 2004; Sakai et al., 2001) in the paraxial mesoderm of vertebrates. Therefore, the existence of an anterior-posterior gradient of RA in the PSM can be postulated. This gradient was recently visualised in zebrafish embryos (Shimozono et al., 2013).
2. Chronic loss of RA in *Raldh2*$^{-/-}$ mice (Niederreither et al., 1999) and VAD quails (Diez del Corral et al., 2003) results in the formation of shorter somites, albeit in a shortened body axis. However, although the VAD quails show a growth deficit, during trunk somitogenesis the total length of the trunk paraxial mesoderm is comparable to that of wild type quails. At this developmental stage, the 3 last formed somites are smaller and the PSM longer in VAD quails compared to wild type.
3. Treatment of *Xenopus* embryos with exogenous all-trans RA for 5 hours caused an increase in somite length (Moreno and Kintner 2004). *Thy2,* the *Xenopus mespb,* stripe width also increased. However, the treatment interfered with normal somite formation and embryonic development. Additionally, the somitogenesis period was not reported.

There has been no good evidence to date to support a role for RA in the zebrafish wavefront. The zebrafish *aldh1a2* mutant, *neckless*, has been reported as having normal somites in a normal body during somitogenesis (Begemann et al., 2001), and in the *aldh1a2* mutant, *nofin*, somitogenesis period is wild type (Herrgen et al. 2010). The somitogenesis of zebrafish *cyp26a1* mutant, *giraffe* (Emoto et al., 2005), has not been

described, but it shows an axial growth defect by 3 days of development. Elevated RA in the PSM of these mutants has been confirmed by use of the RA biosensor (Shimozono et al., 2013). The segmentation clock gene that has been put forward as a candidate RA target in the anterior PSM is *mespb*. However, the zebrafish *mespb* gene does not positively respond to exogenous RA (Moreno and Kintner 2004) and the loss of the 4 *mesp* genes in zebrafish has no effect on somite length (Yabe et al., 2016).

The study of RA in somitogenesis has been complicated by its pleiotropy and also due to a lack of tools to visualise the RA signalling pathway and signalling events. Although immunohistochemistry remains a relatively simple way to gauge the timing and location of protein expression in developing embryos, no immunohistochemical stains for RA signalling proteins in zebrafish have been published. Moreover, the dynamics of RA signalling in the PSM have been difficult to visualise due to a lack of suitable fluorescent reporters and microscopic techniques. Published RA reporters are not suitable for reporting RA signalling in the PSM – the zebrafish transgenic RARE (retinoic acid response element) reporter line driving GFP (Perz-Edwards et al., 2001) that has been used to report RA signalling in most of the published literature has expression in the neural tube and retina from 18 hpf onwards (about 20-somite stage), a time beyond our developmental window of interest. A newer transgenic reporter (Mandal et al., 2013) does not express during somitogenesis either (J. Waxman – personal communication). These transgenes are also inducible only at supra-physiological RA levels. Moreover, as the protein product is the relatively stable GFP, it does not provide useful information on the dynamics of signalling in somitogenesis, as the half-life of GFP might be different from that of the RA targets. Recent advances have made it possible to directly observe the RA gradient through the development of a FRET bio-sensor (Shimozono et al. 2013). However, this approach does not visualise signalling events either.

I, therefore, set out to develop a transgenic reporter fish to visualise RA signalling in the PSM with the aim of generating a description of the spatiotemporal dynamics of RA signalling by time-lapse microscopy. To develop an RA signalling reporter, I decided to generate a fluorescently tagged version of an endogenous gene that is expressed in the

PSM and that is a known direct target of RA. Since it is still unclear which factors in the segmentation clock are directly responsive to RA, I looked in the RA biosynthetic pathway for a suitable RA signalling reporter candidate. RA regulates its own activity by changing its synthesis and catabolism via control of its key regulating enzymes (Schilling et al., 2012). *aldh1a2* and *cyp26a1* are direct targets of RA signalling. The expression of *aldh1a2,* which is responsible for RA biosynthesis, is downregulated by RA. In contrast, *cyp26a1*, the protein product of which catabolises RA, is upregulated by RA.

Of the two, *cyp26a1* was a more suitable candidate for an RA signalling reporter as it is under positive regulation by RA and it is expressed in the tailbud throughout somitogenesis. Establishment of the tailbud domain is RA independent (Martin and Kimelman, 2010) and is achieved by the T-box transcription factor *ta*, a crucial player in mesoderm development (Morley et al., 2009; Schulte-Merker et al., 1994) and a necessary factor for the maintenance of a mesodermal progenitor niche in the tailbud (Griffin et al., 1998; Martin and Kimelman, 2010; Morley et al., 2009). *cyp26a1* is RA sensitive and can be rapidly upregulated by exogenous RA. The 2.5 kb sequence upstream of the ATG of *cyp26a1* bears *t-box* binding sites and RARE sequences. The fragment has been demonstrated to be RA inducible both *in vitro* and *in vivo* (Hu et al., 2008). GFP expression driven by the fragment could be observed in the tailbud and in the PSM in somitogenesis stages, suggesting that the 2.5 kb sequence is sufficient to recapitulate *cyp26a1* expression.

The second factor that has hindered the study of the role of RA in somitogenesis is the strong effect it has on axial growth. However, the observation that the PSM of VAD quails is comparable to wild type during somitogenesis suggests that growth might be uncoupled from somitogenesis and the axial truncation observed might be due to RA induced growth deficits at a later time point. Indeed, the observation that *neckless* and *nofin* embryos are indistinguishable from their wild type siblings during somitogenesis is further support for this hypothesis.

Therefore, to determine if RA has a role in the wavefront the somitogenesis of the zebrafish RA biosynthesis mutants was investigated. An initial analysis of *nofin* and *giraffe* embryo somitogenesis on the morphological level was performed, determining somite lengths at their time of formation and the period with which they formed. Given our current understanding that zebrafish somitogenesis is out of steady state and somitogenesis period (*T*) is not strictly independent of the velocity of the wavefront (*v)*, the question was expanded to ask what role RA might play in the segmentation clock. Thus, a characterisation of the *her1::YFP (Looping1)* cyclic gene reporter expression in *giraffe* was undertaken to include a systematic characterisation of the posterior period of the oscillator, the phase profile and the rate of PSM shortening, the factors that affect somitogenesis period.

3.2 Developing a novel transgenic reporter for RA signalling events in the PSM

3.2.1 *cyp26a1* is expressed in the tailbud and expression in the PSM can be induced by retinoic acid

An RA signalling reporter for somitogenesis firstly needs to be expressed in the PSM during somitogenesis and secondly be sensitive to retinoic acid (RA) signalling. As a first step to assess the suitability of *cyp26a1* as an RA signalling candidate *in situ* hybridisation was performed to visualise expression of *cyp26a1* in wild type zebrafish embryos at mid-somitogenesis stages (Fig 3.1). As per published reports (Dobbs-McAuliffe et al., 2004; Emoto et al., 2005; Thisse *et al.,* www.zfin.org), strong staining was detected in the tailbud. On prolonged colour development weaker staining was detected in the formed somites.

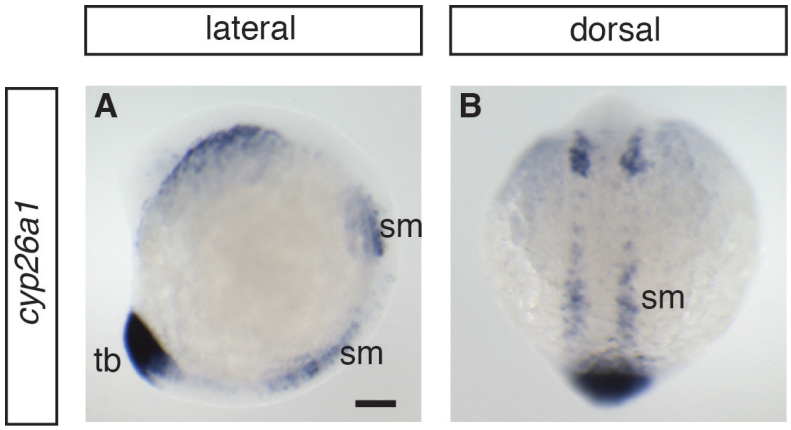

Figure 3.1 *cyp26a1* is expressed in the tailbud during somitogenesis.

In situ hybridisation for *cyp26a1* in a 12-somite stage wild type embryo **(A, B)**. Views are as indicated, anterior to the top.
(A) *cyp26a1* is expressed strongly in the tailbud and **(B)** has weak expression in the somites (40/40). tb – tailbud, sm – somites. Scale bar 100 µm.

While *cyp26a1* expression during embryonic development has been characterised, nothing is known about Cyp26a1 protein expression. To this end, an anti-Cyp26a1 antibody was tested for suitability to characterise Cyp26a1 expression in the zebrafish PSM. Use of the antibody had been previously reported in *Xenopus* (Thomas and Henry, 2014), but it was found to be unsuitable for use in zebrafish (data not shown).

To assess the sensitivity of *cyp26a1* to RA during somitogenesis wild type embryos were treated with RA (Fig 3.2). 15 sibling wild type embryos were exposed to 3 concentrations of RA – 1 nM, 10 nM and 100 nM in the embryo medium for 1 hour or 2.5 hours at 28°C beginning at the 10-somite stage and 15-somite stage. At the 1 nM concentration, *cyp26a1* expression did change considerably from the wild type expression in either the short or the long treatment conditions (Fig 3.2B – B', F – F'). Strong expression of *cyp26a1* was seen in the tailbud and PSM of both 10-somite and 15-somite stage embryos treated with 10 nM and 100 nM concentration (Fig 3.2C – D', G – H'). Upregulation of *cyp26a1* was also noted in the head, eyes, somites and the anterior spinal cord. The higher concentration resulted in a stronger upregulation of *cyp26a1* in the PSM (Fig 3.2 C – C', D – D' and G – G', H – H'); however, a higher response was elicited in the 1-hour treatment when compared to the 2.5-hour treatment (Fig 3.2C – C', G – G' and D – D', H – H'). The results were the same for both somite stages tested. Therefore, *cyp26a1* is RA sensitive during somitogenesis and the strength

of its expression increases with the exogenous RA concentration applied. However, it shows an adaptive response as its sensitivity decreases when the time of exposure to exogenous RA increases, likely through the catabolic activity of the Cyp26a1 enzyme itself.

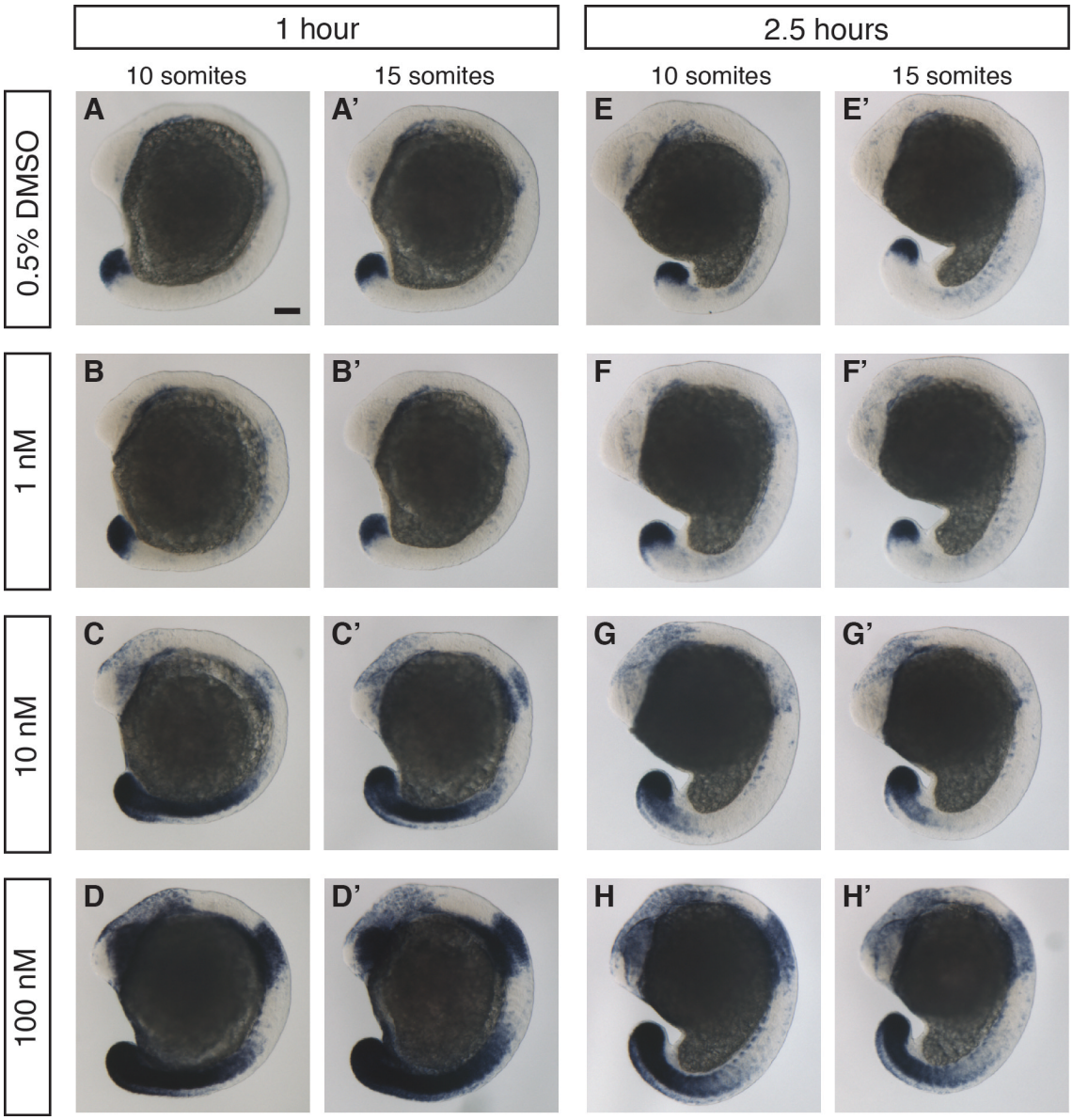

Figure 3.2 RA upregulates *cyp26a1* expression in the PSM.

In situ hybridisation for *cyp26a1* in control wild type embryos treated with 0.5% DMSO for 1 hour at the 10-somite stage **(A)** and 15-somite stage **(A')**, and in wild type embryos treated with exogenous RA – 1nM **(B, B')**, 10 nM **(C, C')** and 100 nM **(D, D')**. *In situ* hybridisation for *cyp26a1* for wild type embryos treated for 2.5 hours with 0.5% DMSO at the 10-somite stage **(E)** and 15-somite stage **(E')** and RA treated wild type embryos – 1 nM **(F, F')**, 10 nM **(G, G')** and 100 nM **(H, H')**. Lateral views, PSM oriented to the bottom left. Concentration of RA, starting somite stage of treatment and exposure times are as indicated. 15 sibling embryos were used per treatment condition.

1-hour treatment – **(A)** *cyp26a1* expression is detected in the tailbud. **(B, B')** No expression change is detected. **(C, C', D, D')** Upregulation of *cyp2*6a1 in the PSM is detected, independent of the somite stage.
2.5-hour treatment – **(G, G', H, H')** Longer treatment times lead to a weaker *cyp26a1* upregulation response. Scale bar 100 µm.

3.2.2 Developing a transgenic *cyp26a1::venus* construct

Having established the suitability of *cyp26a1* as a candidate RA signalling gene, the strategy of fusing a fluorescent protein to the Cyp26a1 protein was chosen. A choice was also made to use the 2.5 kb upstream regulatory sequence to drive the transgene to be able to recapitulate endogenous *cyp26a1* expression and to mimic endogenous *cyp26a1* RA sensitivity. *cyp26a1::venus* was made by BAC recombineering (Sarov et al., 2006; Soroldoni et al., 2014). The tagging strategy is summarised in Fig 3.3. A bacterial artificial chromosome (BAC) that had a 49 kb insert spanning the *cyp26a1* locus was used. The stop codon of *cyp26a1* was deleted in the BAC backbone and replaced with the *venus* ORF to generate a Cyp26a1 C-terminally fused to Venus with a 6-amino acid linker. A 20 kb long sequence consisting of the *cyp26a1* fusion gene, all the intergenic sequence between *cyp26a1* and *exoc6*, the gene immediately upstream, and some of the downstream intergenic sequence, was subcloned into a subcloning vector. The subcloned sequence included the upstream region tested by Hu *et al.*, 2008 to be RA inducible and sufficient to drive GFP expression *in vivo*. The subcloning vector contained two restriction sites for meganuclease *I-SceI*. *I-SceI* facilitates transgenesis by insertion of low-copy concatemers of the transgenic construct at a single site in the genome by double-strand break repair (Thermes et al., 2002).

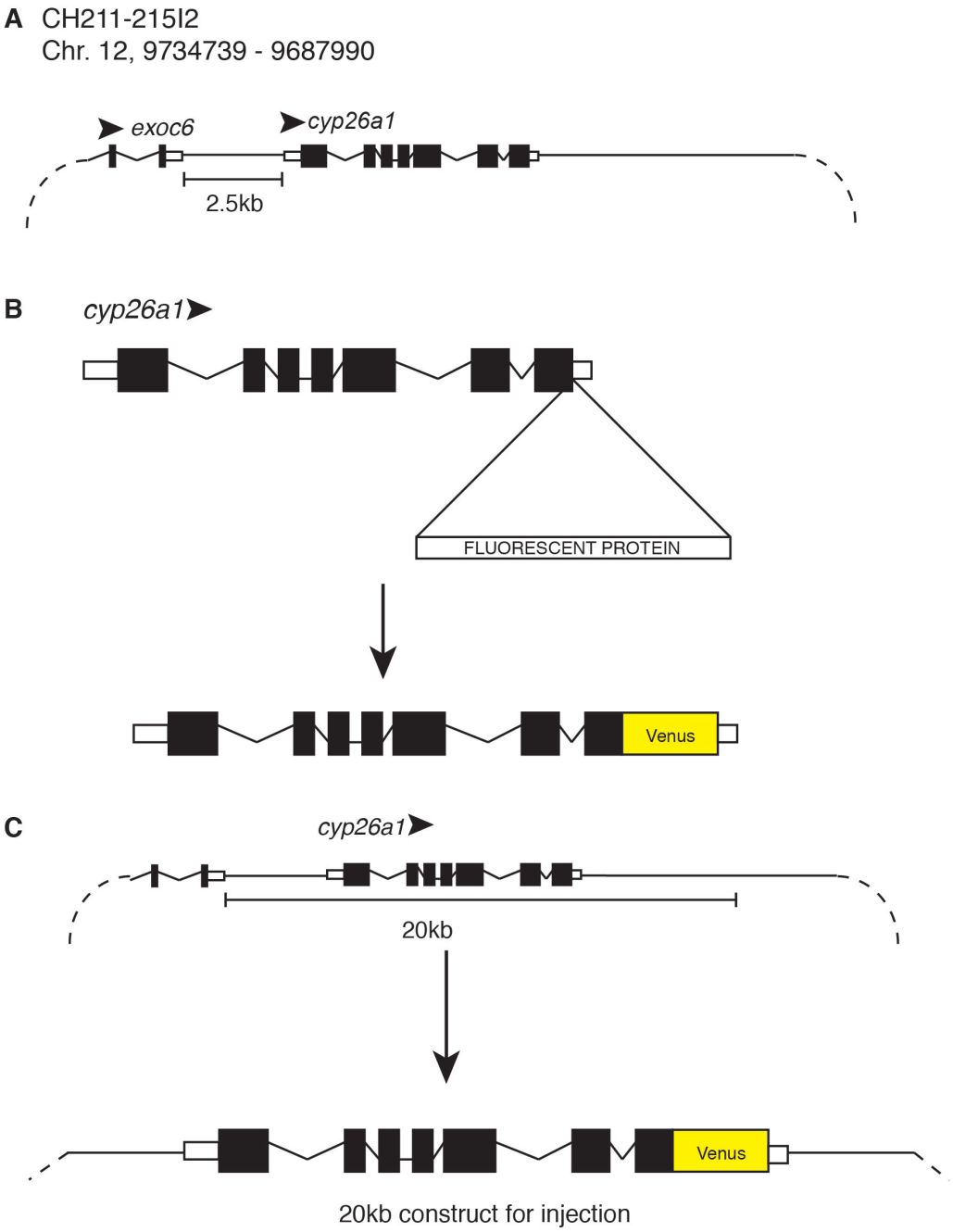

Figure 3.3 Workflow for developing the fluorescently tagged *cyp26a1* reporter construct.

Schematic of the BAC used for recombineering **(A)**, schematic of the tagging step **(B)** and schematic of the subcloning of the construct into a vector injection **(C)**.
(A) The BAC utilised has a 49 kb insert from zebrafish chromosome XII that spans the *cyp26a1* locus and the last exon and 3' UTR of the upstream gene *exoc6.* **(B)** Cyp26a1-Venus was generated by replacing the stop codon in frame with a tagging cassette. **(C)** 20 kb regions spanning the tagged gene and the 2.5 kb intergenic sequences were subcloned into a vector for injection into embryos.

25 ng to 50 ng of this 20 kb Venus fusion construct was microinjected into wild type AB embryos at the one-cell stage by Daniele Soroldoni at the MPI-CBG, Dresden, Germany. Transient expression of the Venus reporter construct was observed in the brain and the tail. Some developmental abnormalities were noted at 24 hours post fertilisation (hpf), such as yolk extension defects, somite defects and brain necrosis to varying degrees, the severity correlating with the amount of DNA injected. 74 injected embryos that showed no gross developmental deficits at 48 hpf were raised in the MPI-CBG fish facility. 59% of these survived to adulthood.

3.2.3 Transgenic *cyp26a1::venus* does not recapitulate endogenous *cyp26a1* expression but retains sensitivity to RA

Transgenic founders (F0) were identified by *in situ* hybridisation with a *venus* riboprobe for *cyp26a1::venus* in 30 F1 embryos from outcrosses of the F0 fish to wild type TL adults. 8 founders were identified, corresponding to a transgenesis frequency of 18%. 3% to 25% of embryos in clutches spawned by F0 fish gave a positive *venus* signal, indicating that the transmission rate (the percentage of the germline of the founder that is transgenic) was low. Additionally, long development times of the *in situ* were necessary to observe this signal, suggesting that the fluorescent signal of the reporter was faint. In fact, no fluorescent signal was observed on a screening fluorescent microscope using filters appropriate for YFP.

Expression patterns of *cyp26a1::venus* in the F1 embryos from four F0 fish are presented here (Fig 3.4B – E). Wild type expression of *cyp26a1* (Fig 3.4A) was not recapitulated in any of the screened embryos. There was weak *venus* signal in the tailbud in the F1 of only 2 F0 fish (F1 from 1 F0 shown here, Fig 3.4B). Most commonly, ectopic expression was noted in the anterior somites of the F1 embryos (Fig 3.4B – E). Hence, it was concluded that the transgenic construct is not expressed in the same domains as endogenous *cyp26a1*.

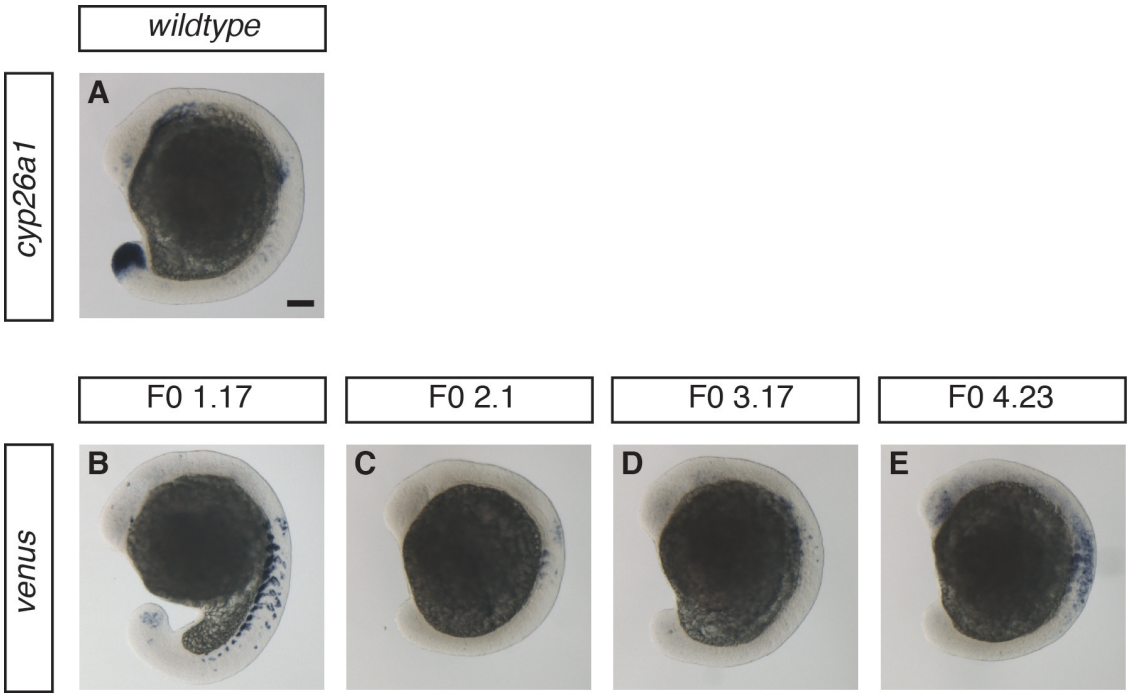

Figure 3.4 *cyp26a1::venus* does not mimic *cyp26a1* expression.

In situ hybridisation for *cyp26a1* in a wild type embryo **(A)** and for *venus* in embryos from pairings of transgenic founder fish (F0) to wild type. Representative transgenic F1 progeny from 4 founders: F0 1.17 **(B)**, F0 2.1 **(C)**, F0 3.17 **(D)** and F0 4.23 **(E)** during somitogenesis. Lateral views, tailbud to the bottom left.
(B) Signal for *venus* is detected weakly in the tailbud and in the somites (5/5). **(C)** No expression detected in the tailbud, weak expression is present in the somites (3/3). **(D)** No expression in the tailbud, weak expression in the somites (8/8). **(E)** No expression in the tailbud, expression is observed in the somites, anterior spinal cord and the head (2/2). Scale bar 100 µm.

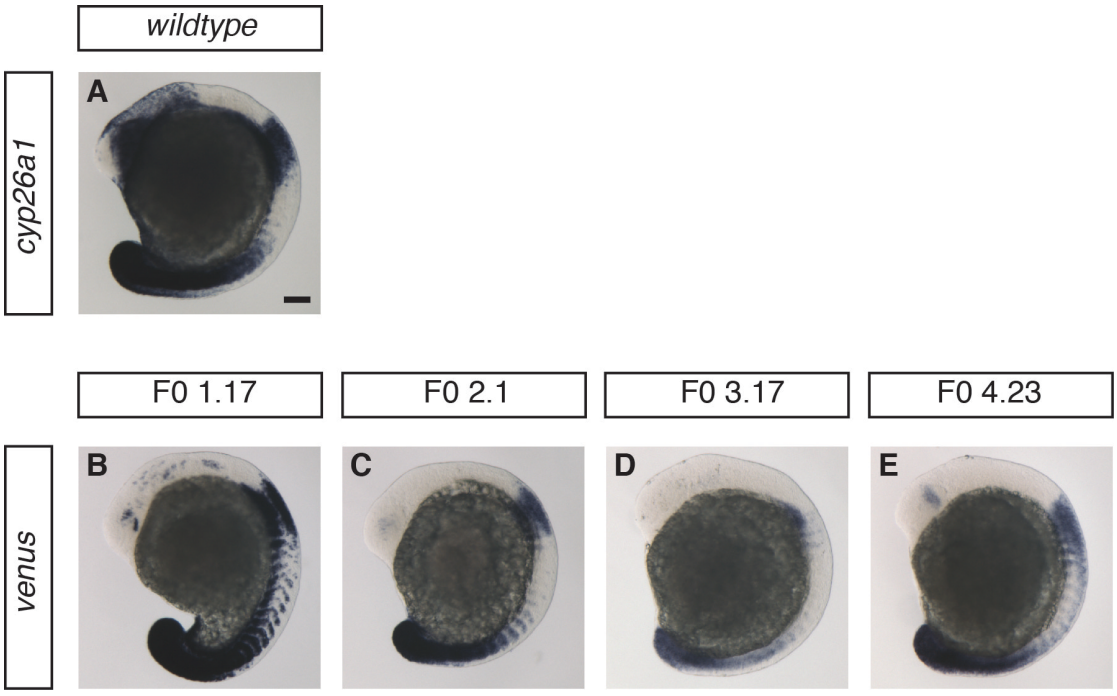

Figure 3.5 *cyp26a1::venus* expression in the PSM can be regulated by RA.

In situ hybridisation for *cyp26a1* in a wild type embryo treated with 100 nM RA for 1 hour **(A)** and for *venus* in representative transgenic progeny of 4 transgenic founder (F0) fish treated with 100 nM RA for 1 hour **(B – E)**. Lateral views, tailbud to the bottom left.
(A) Strong *cyp26a1* expression is detected in the PSM, anterior spinal cord and head (20/20). **(B)** *venus* expression is detected strongly in the PSM and weakly in the head (3/3). **(C)** *Venus* expression is detected strongly in the PSM**,** no expression is seen in the head (2/2)**. (D)** *Venus* expression is detected in the PSM (5/5) and **(E)** *venus* expression is detected in the PSM and weak expression is present in the head (1/1). Scale 100 µm.

To determine whether the transgenic construct was responsive to RA, F1 embryos were treated for an hour with 100 nM RA. Upregulation of c*yp26a1::venus* expression in the PSM was observed (Fig 3.5B – E). This upregulation was similar to that of endogenous *cyp26a1* in the wild type controls (Fig 3.5A). The time required for *in situ* development was also similar to wild type – 10 minutes. Ectopic upregulation was present in the somites, but no considerable upregulation was observed in the head. These observations indicated that the transgenic construct has comparable sensitivity to exogenous RA as endogenous *cyp26a1* in the tailbud and PSM, but not in the head regions.

In light of the low transmission rate and low levels of fluorescent protein mRNA detected by *in situ* hybridisation, coupled with the non-endogenous expression patterns, I chose not to characterise the transgenic founders any further and not establish stable transgenic lines from them.

3.3 *nofin* and *giraffe* RA biosynthesis mutants have somite phenotypes

3.3.1 *nofin* makes axially restricted short somites during somitogenesis

To characterise *nofin* (*nof*) somitogenesis time-lapse microscopy movies, made by Leah Herrgen and published in the study Herrgen *et al*., 2010, of siblings from heterozygous *nofin* breedings were analysed. Somitogenesis period was determined by calculating the average of the time taken per somite to form for somites 5 to 18. Time taken per somite to form was determined by tracking the onset of somite boundary formation, which can be seen as a high contrast notch on the lateral edge of the PSM tissue. A distinction between wild type and heterozygous siblings was not made for the analysis. The somitogenesis periods were normalised to the mean somitogenesis period determined

for the wild type group for the experiment. Somitogenesis period determined for wild type and *nofin* embryos did not significantly differ (n = 16 animals per genotype, N = 2, Welch corrected t (24) = 1.9, P = 0.07, two-tailed; Fig 3.6B). This finding is in agreement with previously published results (Herrgen et al., 2010). I next determined the instantaneous somite length for somites 7 to 20. This is the length of the somite at its time of formation. It was determined by measuring the length of the somite as soon as its posterior boundary formation was completed. The anterior-most somites typically increase in length and then the length stays constant from somites 6 to 14, before showing a decreasing trend till the end of somitogenesis (Schröter et al., 2008). In the wild type sibling embryos (n = 4, N = 1), lengths of somites 7 to 9 showed variability but then remained approximately constant from somites 10 to 14. The somite length then decreased from somites 15 to 20 (Fig 3.6A). The instantaneous lengths of somites 8 and 11 of *nofin* (n = 4), on average, were shorter than wild type. Somite 8 is 10% shorter than the wild type somite 8. The failure to synthesise RA in *nofin* results in the formation of shorter somites, but only in the anterior trunk of the embryo.

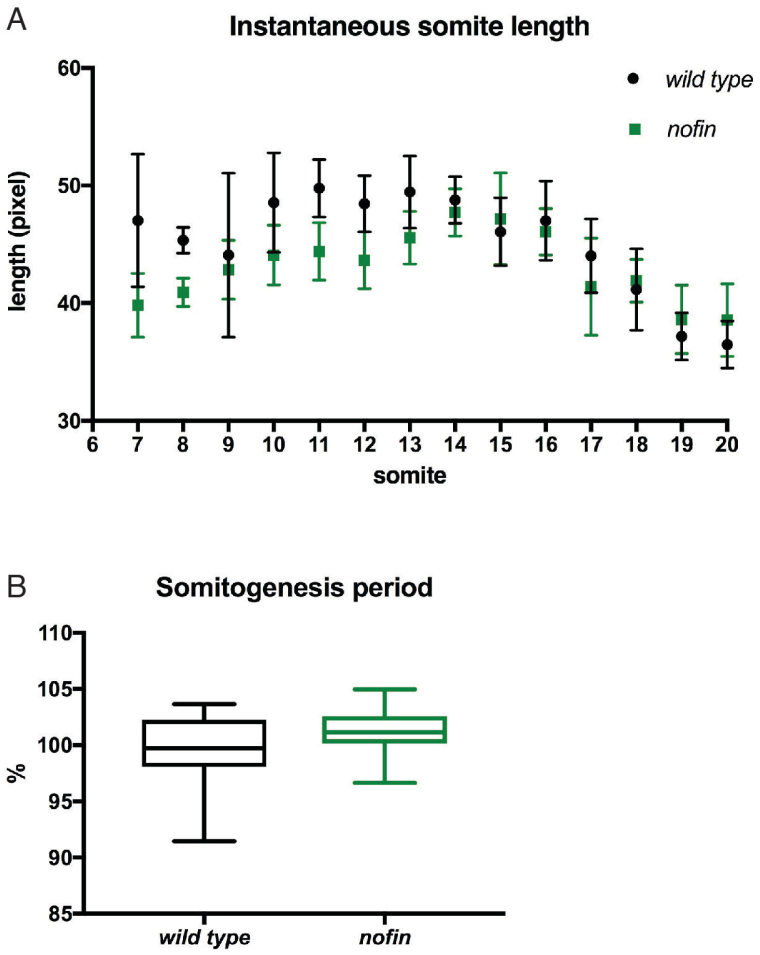

Figure 3.6 *nofin* makes a few shorter somites, but has wild type somitogenesis period.

Plot of Instantaneous somite lengths **(A)** and average trunk somitogenesis period **(B)** determined from time-lapse videos of siblings from heterozygous *nofin*+/- crosses. Somitogenesis period has been normalised to mean somitogenesis period of the control embryos.
(A) Rostral trunk somite 8 is smaller than wild type somite 8. Mean ± SD, measurements made for 4 embryos per genotype. **(B)** *nofin* somitogenesis period is unchanged from wild type (mean ± SD, wild type – 99.51 ± 3.3, *nofin* – 101.4 ± 2.1; Welch corrected t(24) = 1.9, P = 0.07, two-tailed) Boxes are 25^{th} – 75^{th} percentile, median indicated by the line, whiskers are max / min. Determined from 16 embryos per genotype, pooled from two experiments.

3.3.2 *giraffe* makes axially restricted long somites during somitogenesis

As the failure to synthesise RA results in the formation of smaller somites, I next asked how the failure to degrade RA would affect somite length. Therefore, to analyse trunk somitogenesis of *giraffe (gir)* time-lapse images of developing *gir* embryos at 23.5ºC were made and instantaneous somite lengths and the somitogenesis period of somites 5 to 18 were determined. For comparison of experiments, the somitogenesis period was

normalised to the mean somitogenesis period of the control cohort. The control group included both wild type and heterozygous *gir* embryos. The embryos were recovered at the end of the experiments and kept up to 72 hpf to identify the mutants on the basis of their phenotype of smaller eyes, heart edema and axial growth deficiency. Wild type embryos had instantaneous somite lengths that followed the published trend (n = 10, N = 2) (Schröter et al., 2008). The anterior trunk somites of *gir* (n = 6, N = 2) were longer than wild type (Fig 3.7B). Somite 8 of *gir* was 20% longer than wild type (Fig 3.7A, B). Over the duration of trunk segmentation, the somitogenesis period was approximately 7% slower in *gir* embryos when compared to wild type siblings (Fig 3.7C). Therefore, excessive RA in *gir* affects both somitogenesis period and the length of somites. The change in somite length was longer than the change in the somitogenesis period.

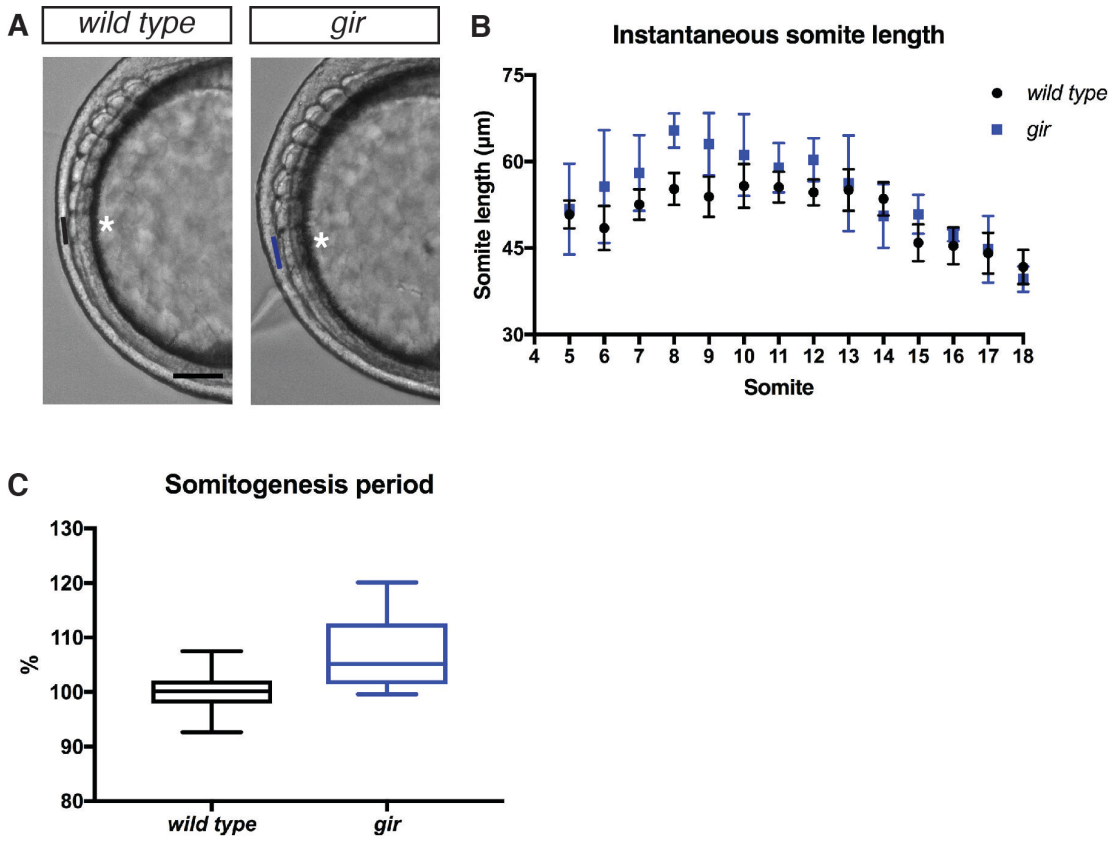

Figure 3.7 *giraffe* makes a few longer somites and has a longer somitogenesis period.

Snapshot of the forming 8th somite in a wild type and *gir* embryo during somitogenesis **(A)**. Plot of instantaneous somite lengths **(B)** and plot of average trunk somitogenesis periods **(C)** determined from time-lapse micrographs of siblings from heterozygous *gir* pairings. Somitogenesis period has been normalised to the mean period determined for the control embryos.

(A) *gir* somite 8 (asterisk) is longer than the wild type somite 8 (asterisk) at the time of formation (lengths indicated by lines – black line in wild type, blue line in *gir*). **(B)** Plot of instantaneous somite length, mean ± SD. *gir* somite 8 is longer. **(C)** Somitogenesis period of *gir* is slower than control siblings (mean ± SD, wild type – 100 ± 3.6; *gir* – 107.4 ± 7.1). Box is 25th to 75th percentile, line is the median, whiskers are max/min. Data from 10 wild type and 6 *gir* mutant embryos per genotype pooled from 2 experiments. Scale bar 100 µm.

3.4 The *gir* mutant has an altered pattern of kinematic waves of *her1*

The distance travelled by the wavefront in the time taken to form one somite (*T*) sets somite length. The observable rate of somite formation (the somitogenesis period*, T*) emerges at the tissue level as a function of (1) the timescale of genetic oscillations in the tailbud, (2) the rate of tissue shortening (Doppler), and (3) the slowly changing wave patterns (the dynamic wavelength effect) (Jörg et al., 2015; Soroldoni et al., 2014). As a step to understanding the formation of the longer somites in the *gir* trunk and the slower somitogenesis period, the expression of a *her1* cyclic gene fluorescent reporter, *Looping1*, was investigated in *gir* to determine the period of the genetic oscillations in the posterior of the embryo and the wave patterns over the course of *gir* somitogenesis. Synchronously laid embryos from a heterozygous *gir* in-cross, *Looping1* out-cross were used, so that every embryo was heterozygous for *Looping1* and were wild type, heterozygous or homozygous for *gir*. Synchronised development of embryos was ensured by allowing the parent pair to spawn for 20 minutes, a time interval that is less than the somitogenesis period at 28.5ºC. The experiment was conducted at 23.5ºC. Non-sibling, non-transgenic wild type embryos were included as additional controls for temperature. *gir* homozygous embryos were identified by *in situ* hybridisation for *cyp26a1* at the end of the experiment as *gir* embryos show elevated *cyp26a1* transcript in the PSM during somitogenesis stages (Emoto at al., 2005), resembling *cyp26a1* expression during the exogenous RA treatment described previously (Fig 3.2).

3.4.1 Somitogenesis period, somite length and axial outgrowth

The non-transgenic, non-sibling wild type embryos (n = 6) were determined to have an average somitogenesis period of 34 minutes. Somitogenesis periods determined for each of the genotypic groups were normalised to the somitogenesis period determined for the wild type embryos. The period of the wild type embryos did not differ significantly over

the 2 experiments (Fig 3.8A). The *Looping1* cohort (wild type or heterozygous for *giraffe,* n = 10) had significantly different mean somitogenesis periods in the 2 experiments (Fig 3.8B, Welch corrected t (15) = 3, P = 0.014, two-tailed). Therefore, the data have not been pooled. However, the trends in both experiments are consistent. *Looping1* embryos had a slower average somitogenesis period than non-sibling wild type embryos, consistent with the published characterisation of the transgene (Schröter et al., 2012; Soroldoni et al., 2014). *gir;Looping1* embryos had a slower period than both the non-sibling wild type and the sibling *Looping1* embryo cohorts (Fig 3.8C, D). In one experiment, the period was 9% slower than *Looping1* embryos (n = 6). In the second experiment, the mean period of *gir* was 6% slower than *Looping1* (n = 7), but there was high variability among the *gir* embryos. The instantaneous length of somite 8 was 20% longer in both experiments (Fig 3.9A, B**)**; additionally, somite 9 was 20% longer in the first experiment (Fig 3.9A). The slower somitogenesis period and the longer 8th somite are consistent with the initial analysis of *gir* somitogenesis.

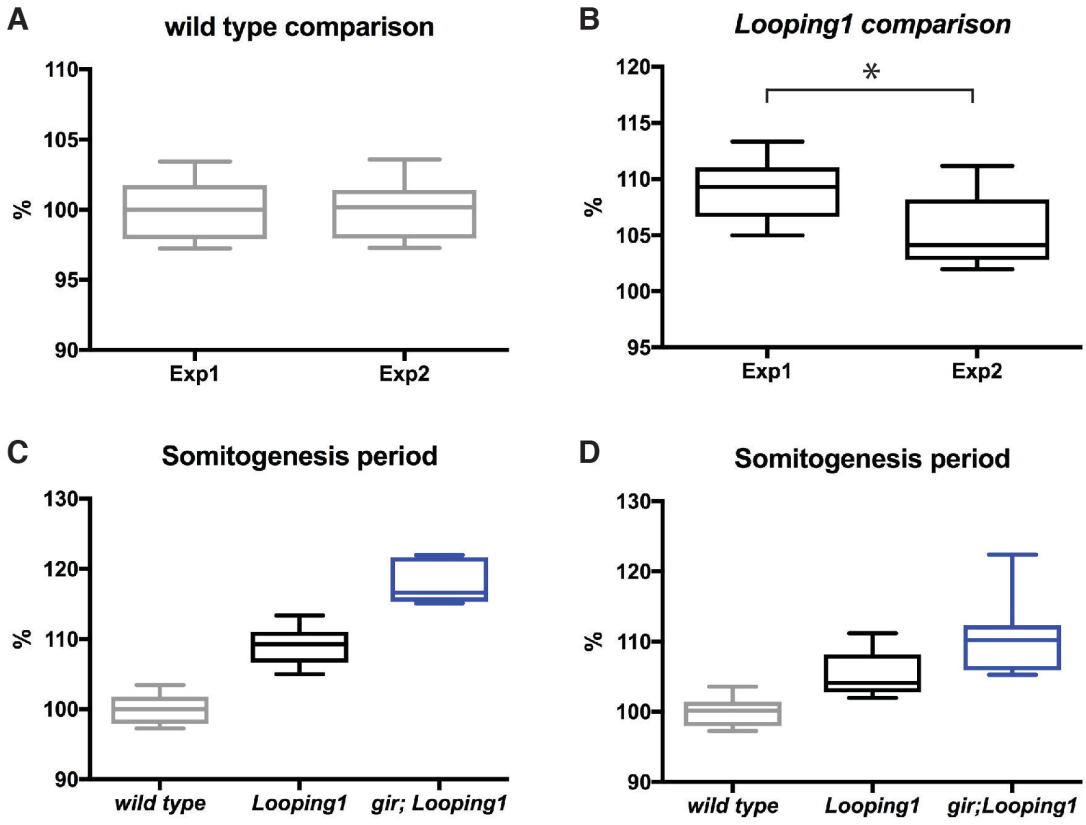

Figure 3.8 Trend for a slower somitogenesis period is observed in *gir* in a cyclic gene reporter background.

Plot of average trunk somitogenesis period of wild type embryos used as controls in 2 independent experiments **(A)**. Plot of trunk somitogenesis periods of *Looping1* embryos from heterozygous *gir;Looping1* to heterozygous *gir* pairings in the 2 experiments **(B)**. Plot of trunk somitogenesis periods of wild type controls and siblings from heterozygous *gir;Looping1* to heterozygous *gir* pairings **(C, D)**. Somitogenesis periods normalised to the mean period determined for the wild type embryos.
(A) Wild type control embryos had comparable somitogenesis periods across the 2 experiments. Period determined for 5 animals per experiment. **(B)** *Looping1* control embryos had significantly different periods (Welch corrected t (15) = 3, *P* = 0.014, two-tailed). Period determined for 10 embryos per experiment. Therefore, experimental data is not pooled. **(C)** Somitogenesis period of *gir;Looping1* is slower than that of *Looping1* (mean ± SD, *Looping1* – 108.9 ± 2.6, *gir;Looping1* – 105.5 ± 6.6). Period determined for 6 embryos per genotype. **(D)** Somitogenesis period of *gir;Looping1* is slower than that of *Looping1* (mean ± SD, *Looping1* – 105.3 ± 3.2, *gir;Looping1* – 111.1 ± 5.7), period determined for 7 embryos per genotype. Box and whisker plots – boxes are 25th to 75th percentile, line indicates the median; whiskers are max / min.

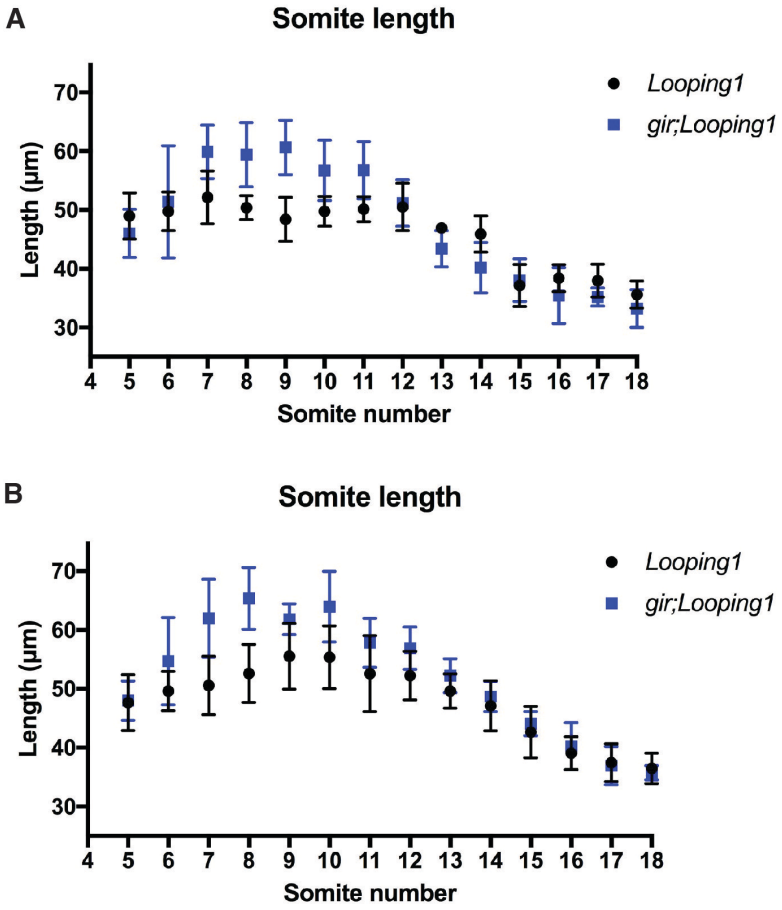

Figure 3.9 Axially restricted longer somites are observed in *gir;Looping1* embryos.

Plots of somite lengths determined at their time of formation from time-lapse videos of siblings from heterozygous *gir;Looping1* and heterozygous *gir* pairings. Data presented from 2 independent experiments **(A, B)**.

(A) Somites 8 and 9 are longer from their time of formation. Measurements made from 6 embryos per genotype. **(B)** Somite 8 is longer from its time of formation. Measurements made from 7 embryos per genotype. Points in plots are mean ± SD.

RA is known to affect axial outgrowth of developing vertebrate embryos and *gir* embryos show a growth deficit at 72 hpf compared to their wild type siblings (Emoto et al., 2005). Therefore, to test whether any growth deficits occur during somitogenesis and the possibility that the somite phenotype arises due to a growth phenotype, the axial elongation was determined. The axial elongation was determined by measuring the body length (Fig 3.10A) from the time-lapse videos at 30-minute time intervals. *gir* embryos (n = 5, Fig 3.10B and n = 7, Fig 3.10C) had slightly longer bodies than wild type during somitogenesis. However, elongation proceeded comparably in both *Looping1* and *gir;Looping1* embryos. Therefore, during somitogenesis *gir* does not show a growth deficit.

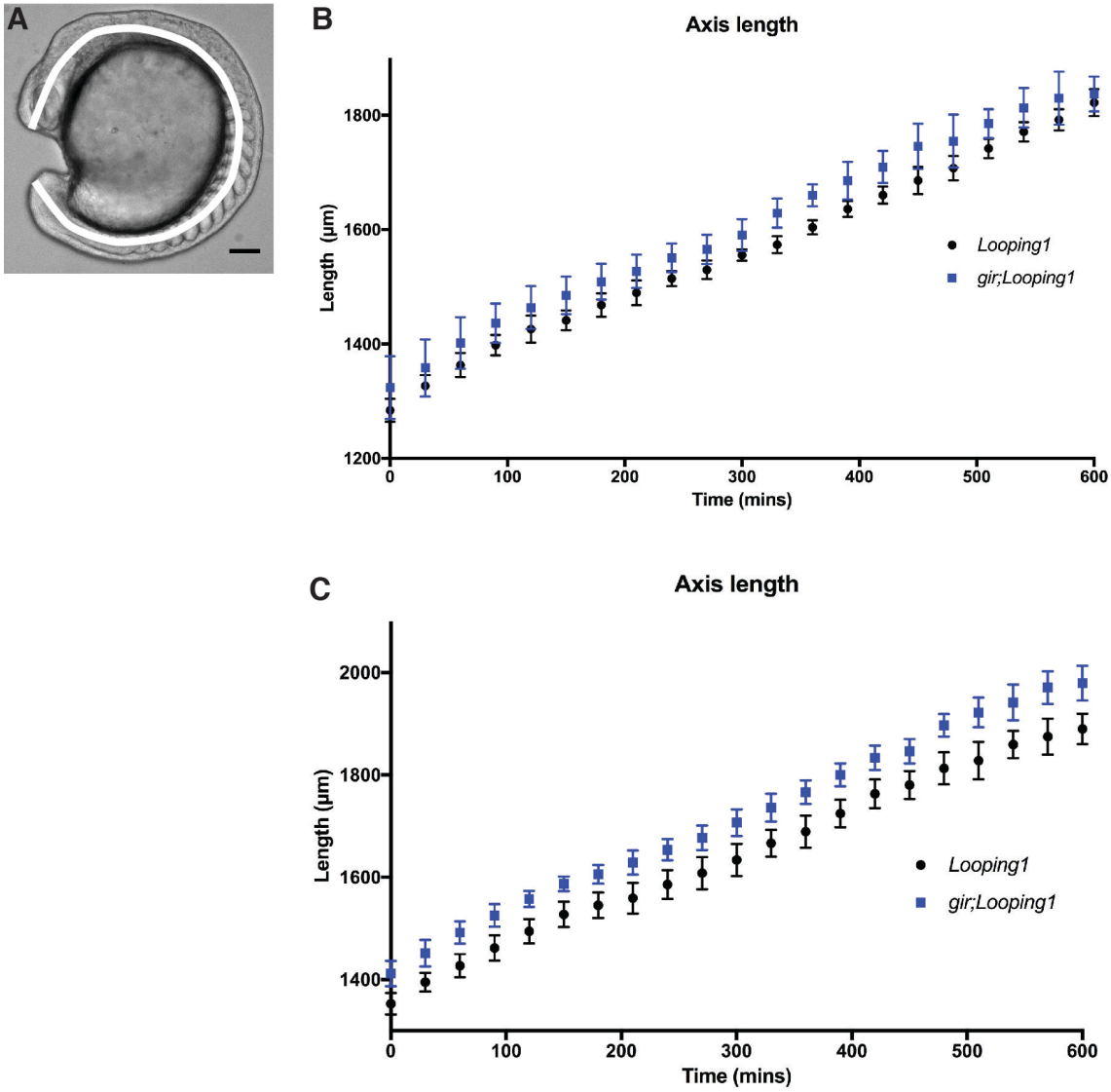

Figure 3.10 Axial growth is similar between *gir* mutant and wild type siblings.

Axial length determined by measurement from length from head to the tailbud (white line) **(A)**. Plots of axial length over time **(B, C)** determined from time-lapse videos of somitogenesis of siblings from heterozygous *gir;Looping1* to heterozygous *gir* pairings.
(B, C) *gir* embryos are longer from the start of the experiment, but grow at a rate comparable to wild type. **(B)** Axial length measurements made from 7 *Looping1* embryos and 5 *gir;Looping1* embryos. **(C)** Measurements made from 8 *Looping1* embryos and 7 *gir;Looping1* embryos. Points are mean ± SD. Scale bar 100 µm.

In summary, the effects of *gir* are the same in wild type and *Looping1* backgrounds, qualifying this live cyclic gene reporter approach.

3.4.2 Posterior period and PSM shortening

To describe the segmentation clock in *gir*, the period of the oscillators in the posterior PSM (referred to as posterior period from now on) was determined. The posterior period was determined by measuring the oscillations in the *her1::YFP* fluorescent signal of *her1::YFP* and determining the average inter-peak distance between maxima and minima of the oscillations in the second derivative of the raw data (Fig 3.11A). The second derivative was performed to increase the curvature of the raw data to enable easier peak finding. The posterior periods determined were normalized to the average somitogenesis period determined for the *Looping1* control group in each experiment. The posterior period has been reported to be 9% slower than the somitogenesis period (Soroldoni et al., 2014). The posterior period of *Looping1* embryos was slower than their somitogenesis period in both experiments, calculated as 11% in the first experiment (n = 7, Fig 3.11B) and 15% in the second (n = 4, Fig 3.11C). *gir* homozygous embryos had a mean posterior period that was 14% (n = 7, Fig 3.11B) and 15% (n = 6, Fig 3.11C) slower than the *Looping1* somitogenesis period. From these results there is no strong evidence that posterior period has been further slowed down in *gir* embryos than in wild type.

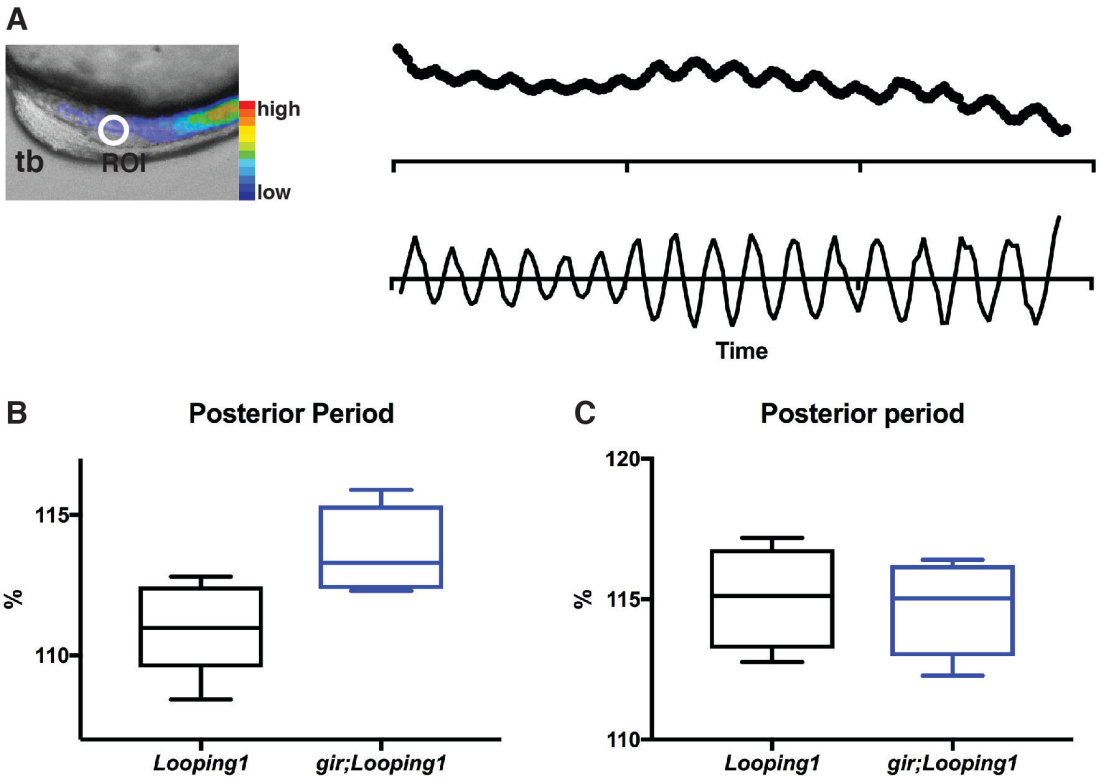

Figure 3.11 Posterior period of *gir;Looping1* is unchanged from *Looping1* embryos

Oscillations of reporter expression determined from a region of interest (ROI, white circle) in the posterior PSM (tb – tailbud). Reporter expression displayed with a lookup table – red high, blue low intensity. The raw data (top trace) and second derivative (bottom trace) of oscillations of *her1::YFP* in the ROI in the posterior PSM from which posterior period was determined **(A)**. Plots of the posterior period determined from the inter-peak intervals and normalised to the mean somitogenesis period determined for the *Looping1* embryos **(B, C)**. Measurements made from time-lapse videos of siblings from heterozygous *gir;Looping1* to heterozygous *gir* pairings.
(B, C) Posterior period of *gir;Looping1* embryos is not slower than that of *Looping1* embryos
(B) Mean ± SD, *Looping1* – 110.9 ± 1.6, *gir;Looping1* – 113.7 ± 1.6. Measurements from 7 *Looping1* and 7 *gir;Looping1* embryos. **(C)** Mean ± SD, *Looping1* – 115.2 ± 1.8, *gir;Looping1* – 114.7 ± 1.8. Posterior period determined for 4 *Looping1* embryos and 6 *gir;Looping1* embryos. Box and whisker plots – box is 25th to 75th percentile, line indicates the median and whiskers are max/min.

A second contributing factor to the somitogenesis period and therefore, somite length, is the rate of PSM shortening via the embryonic Doppler effect. PSM shortening, the rate of change of PSM length, was determined by measuring the length of the PSM in 30-minute intervals (Fig 3.12A) and then calculating the first derivative of PSM length over time as this determines the rate of change of position (i.e. the velocity). The PSM was seen to continuously shorten (Fig 3.12B, C), however, not at a constant rate (Fig 3.12B', C'). PSM shortening in the *Looping1* embryos was seen to initially rapidly increase for the first 200 minutes of analysis and then briefly proceed at a constant rate

before beginning to slow down till approximately the end of the analysis, giving a U-shaped profile of PSM shortening. The profile of PSM shortening of *gir* was different from the profile observed in the control cohort in both experiments, however, the profiles did not resemble each other. In the first experiment (Fig 3.12B'), the PSM rate was seen to constantly decrease, having approximately the reverse trend of the *Looping1* PSM shortening profile. In the second experiment, the rate of PSM shortening was U shaped (Fig 3.12C'), but the valley was shallow when compared to wild type. Taken together, these profiles suggest that the PSM shortening regime is altered in *gir*, with a more uniform velocity profile.

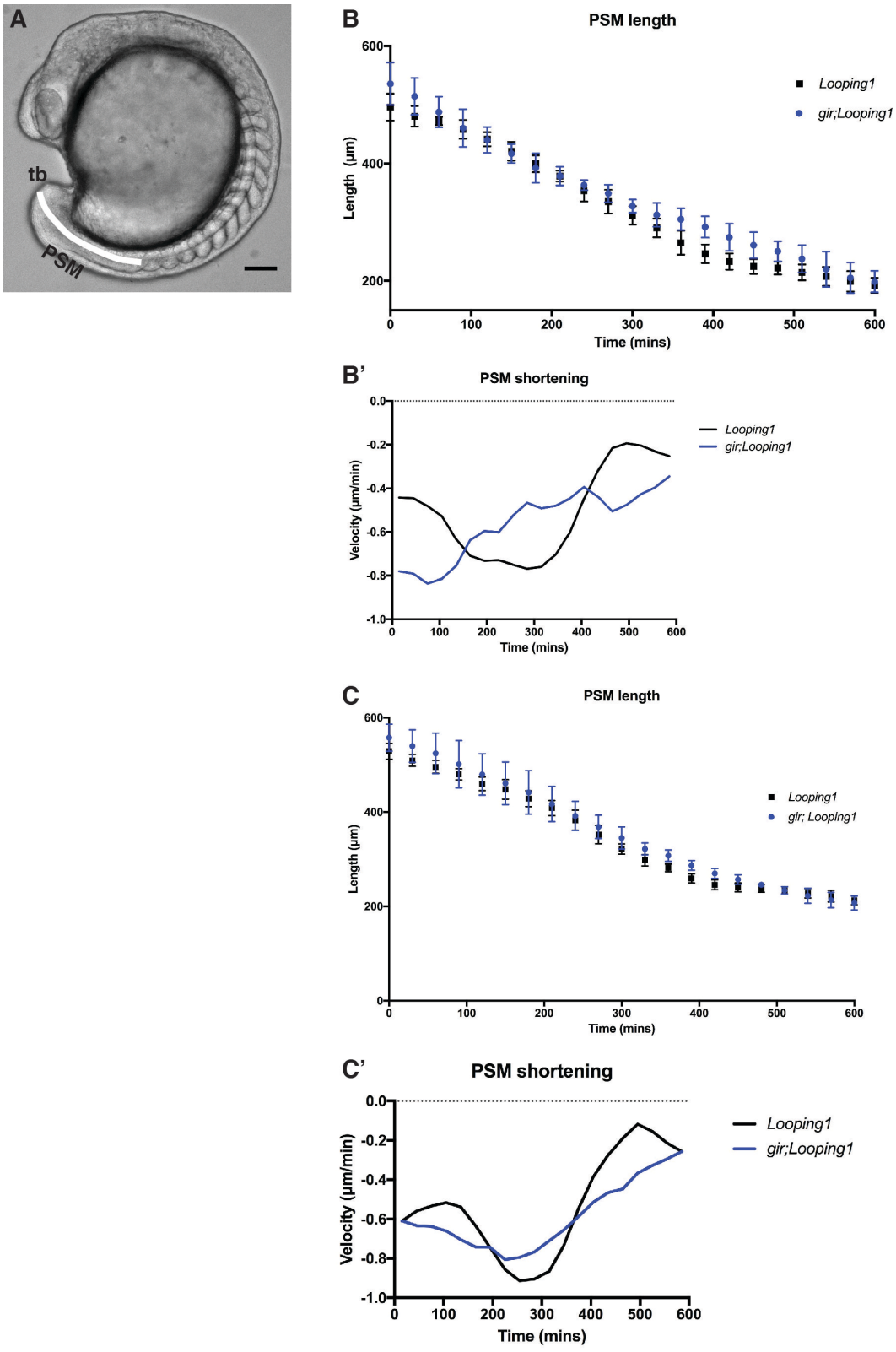

Figure 3.12 PSM shortening is altered in *gir;Looping1* embryos.

PSM length measured from the boundary of the most recently formed somite to the tip of the tailbud (white line) **(A)**. Plots of PSM length versus time **(B and C)** and PSM shortening (rate of change of

PSM length) over time **(B' and C')** in two independent experiments. Measurements made from time-lapse videos of sibling embryos from heterozygous *gir;Looping1* and *gir* pairings.
(B) The PSM of *Looping1* and *gir;Looping1* embryos continuously shortens (mean ± SD, measurements of 5 embryos per genotype). **(B')** The profile of PSM shortening of *gir;Looping1* has a reverse trend compared to the U-shaped profile of *Looping*1 (first derivative of the plotted means in B). **(C)** The PSM of *Looping1* and *gir;Looping1* embryos continuously shortens (mean ± SD, measurements of 7 embryos per genotype). **(C')** The profile of PSM shortening of *gir;Looping1* is more uniform compared to the U-shaped profile of *Looping*1 (first derivative of the plotted means in C). Scale bar 100 μm.

3.4.3 The phase pattern of *Looping1* is altered in *gir*

The third factor that contributes to the somitogenesis period is the changing pattern of the kinematic waves during somitogenesis. To investigate the wave pattern of reporter expression, kymographs of the *her1::YFP* fluorescent signal were generated. The phase of the oscillators across the tissue was determined from these kymographs. Phase profiles are agnostic to the amplitude of the fluorescent signal, therefore enabling the comparison of wave patterns of multiple embryos. Snapshots of the phase profile corresponding to the time of formation of the 10^{th} somite are presented in Fig 3.13A, B from one experiment. There was no phase difference between the oscillators in the tailbud and posterior PSM of *Looping1* embryos. The phase offset between tailbud and the anterior PSM was 4π, indicating that there were 2 waves in the tissue. The phase profile of reporter expression was exponential in shape, indicating that one wave had a longer wavelength than the other. The phase profile of the *her1::YFP* signal in *gir* was not exponential, appearing to be linear and a phase offset was present in the tailbud. The phase offset between tailbud and anterior PSM was almost 6π. Consistent observations were made in the second experiment. These observations suggest that the wave pattern in *gir;Looping1* differs from *Looping1* in that the waves have almost equal wavelength. The higher posterior to anterior offset suggests that *gir;Looping1* has more kinematic waves in the wave pattern than *Looping1*. These wave patterns are schematically represented in Fig 3.13C, D.

In situ hybridisation for endogenous *her1* was performed in mid-somitogenesis stage *gir* embryos and their wild type siblings (Fig 3.13E – F'). The wave pattern of the endogenous cyclic gene *her1* in *gir* also had a wave pattern where the waves were of similar wavelength (Fig 3.12F, F'). Hence, from these results, it can be concluded that *gir* has an altered wave pattern for cyclic gene *her1*.

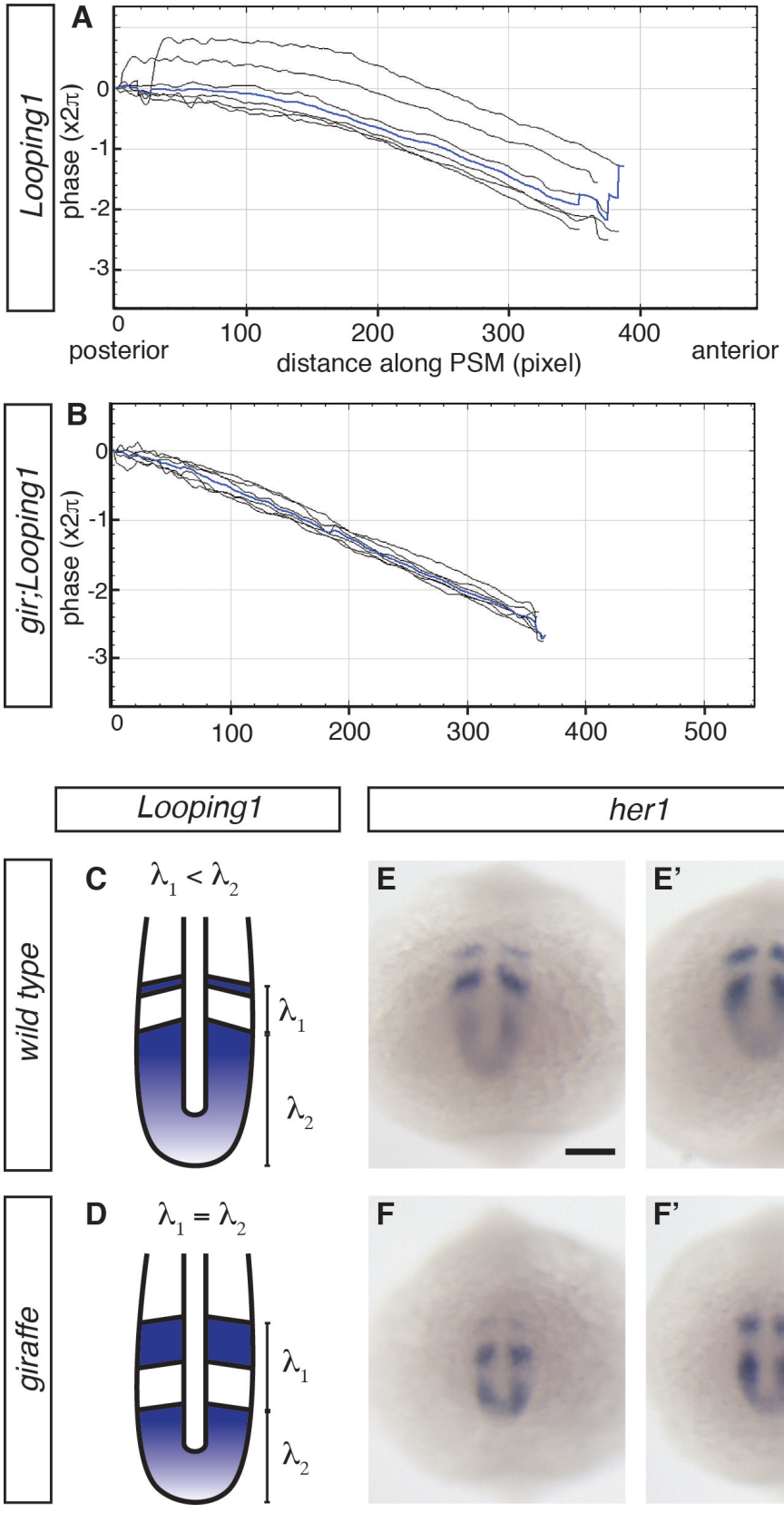
A
Looping1
phase (x2π)
0
-1
-2
-3
0
100
200
300
400
posterior
distance along PSM (pixel)
anterior
B
gir;Looping1
phase (x2π)
0
-1
-2
-3
0
100
200
300
400
500
Looping1
her1
wild type
C
λ1 < λ2
λ1
λ2
E
E'
giraffe
D
λ1 = λ2
λ1
λ2
F
F'

Figure 3.13 *giraffe* has an altered cyclic gene *her1* wave pattern in the PSM.

Phase profile of *her1::YFP* in *Looping1* and *gir;Looping1* embryos at the 10 somite stage **(A, B)** and schematic description of the same **(C, D)** determined from time-lapse videos of sibling embryos from heterozygous *gir;Looping1* and *gir* pairings. *In situ* hybridisation for cyclic gene *her1* in 13 somite stage embryos from heterozygous *gir* pairings **(E – F')**. Genotypes are as indicated.
(A, C) The phase profile of the *her1::YFP* in *Looping*1 embryos has an exponential profile. The wave in the posterior PSM has a longer wavelength than the waves in the anterior PSM. **(B, D)** The phase profile of *her1::YFP* in *gir;Looping1* has a linear profile – waves in the PSM are of equal wavelength. 1 wave = 2π of phase. **(E, E')** *her1* expression in wild type embryos shows a long posterior wave and shorter stripe-like anterior waves. **(F, F')** Endogenous *her1* expression in *gir* has a cyclic gene wave pattern where the waves have equal wavelength (6/6). Scale bar 100 µm.

To summarise this section of the thesis, I have described the generation of an RA-sensitive transgenic line. However, the low transmission rate and the weak *venus* signal in the transgenic embryos detected by *in situ* hybridisation require revisiting the design of the transgene. I have also presented data to support a role for RA in zebrafish somitogenesis. RA biosynthesis mutants have somites with altered length and these somites are axially restricted to the rostral trunk. The data generated so far suggest that *gir* also has a slower somitogenesis period and that the PSM shortens with a different rate profile than wild type. Furthermore, the wave pattern of cyclic gene *her1* is altered in *gir*, suggesting that RA affects the rate of slowing of the frequency of the oscillators across the PSM.

These preliminary results were not followed up during the course of this thesis as it was discovered that both *gir* and *Looping1* lines used contained an unknown number of unknown transgenic contaminations (Fig 7.1). At least 2 different transgenic contaminants were discovered in the wild type breeding stocks that had been used for experiments and to maintain the *gir* and *Looping1* lines. Future experiments will return to these promising leads with re-derived genetic lines.

Chapter 4. Embryo without a segmentation clock

Background

Somitogenesis is the process by which the embryonic body axis is sequentially and rhythmically subdivided into segments. Dynamic cyclic gene expression in the PSM is translated into a segmental pattern in the anterior PSM that specifies the position of the segment boundary and the anterior-posterior polarity of the segments. The segments that form as a result of somitogenesis are called somites. Somites have been defined as segmented blocks of mesodermal cells on either side of the notochord (Gilbert and Raunio, 1997; Wolpert et al., 2015) whose outer cells develop into a layer of epithelium while the inner cells remain mesenchymal. The epithelialization of each somite is stabilised by the synthesis of fibronectin (Gilbert and Raunio, 1997; Henry et al., 2000; Jülich et al., 2005a). Combining these, in this chapter, I define a somite as a block of mesenchymal cells surrounded by an epithelial layer, separated from consecutive somites by a boundary that accumulates fibronectin.

Somites differentiate into the sclerotome that contributes to the vertebral column and myotome that develops into the skeletal musculature. The sclerotome, myotome and the skeletomuscular system are segmented. In amniotes, it is believed that somitogenesis establishes the segmental pattern of the adult body (Pourquié, 2009). In zebrafish, however, this idea is controversial. There is evidence to support the idea that somitogenesis is the master periodic pattern generator, but there is also evidence that refutes this.

The *hes6* mutant has a 7% slower somitogenesis period when compared to wild type and makes longer but fewer somites (Schröter and Oates, 2010). The embryos have correspondingly, a lower total number of myotomes. The *hes6* mutant also has correspondingly fewer vertebrae than wild type. Therefore, altered segmentation during somitogenesis is reflected in the altered segmentation of the musculature and the vertebral column, supporting the idea that somitogenesis sets up the pre-pattern for the axial skeleton. In contrast, the zebrafish *fss* mutant that has defective somitogenesis and

fails to make somites (Nikaido et al., 2002; van Eeden et al., 1998), still has a strikingly periodic vertebral column, contradicting the notion that periodic somites are necessary for the formation a periodic vertebral column.

The periodic vertebral column of *fss* has been interpreted to indicate remnant periodicity in the paraxial mesoderm. The sources of periodicity that have been put forward are:

1. The segmentation clock – The kinematic waves of *her1*, *her7* and *deltaC* are still present in *fss*, but restricted to the posterior PSM (Holley et al., 2000; Sawada et al., 2001). This periodic activity is sufficient for the patterning of the vertebral column.
2. Slow muscle precursors – periodic patterning information is provided by the *en2a* positive adaxial cells, by virtue of sequential maturation along the A-P axis into elongating and stacking muscle pioneers and slow twitch fibres, in the *fss* paraxial mesoderm (van Eeden et al., 1998).

However, the *fss* sclerotome was demonstrated to lack segmental patterning by *in situ* hybridisations for sclerotome markers *pax9* and *smad1* at 24 hpf (Fleming et al., 2004) and an alternative hypothesis has been put forward:

3. Axial skeleton segmental patterning is somitogenesis independent. The source of segmental pattern is the notochord.

To enable testing of the first hypothesis i.e. that somitogenesis has an instructive role in the establishment of segmental body pattern, a segmentation clock mutant was made in the lab to incapacitate the core pace-keeping circuit of the genetic oscillator and thereby the segmentation clock. Previously, *her1* and *her7* had been jointly knocked down with morpholinos (Oates and Ho, 2002) and *her1;her7* double mutants had been generated by mutagenesis (Henry et al., 2002). Somitogenesis was found to be disrupted all along the axis in these embryos. However, it was not clear in the morpholino study if, and how much of, functionality was retained by the core circuit. More importantly, it was not possible to raise either the morphant or mutant embryos to be able to assess axial skeletal patterning.

her1 and *her7* are located ~12 kb apart on chromosome V. Given that 1 centiMorgan in zebrafish represents 740 kb (Shimoda et al., 1999), the chance of isolating a *her1;her7* double mutant by outcrossing *her1* and *her7* mutants is 0.016%, meaning ~10,000 recombinants would need to be screened to identify one double mutant. Thus, the analysis of a mutant combination was previously not feasible. Novel *her1*;*her7* double mutants were generated by Guillaume Valentin by injecting a TALEN construct (Dahlem et al., 2012) directed against exon2 of *her1* in the *her7* mutant background (Fig 4.1). Due to the linkage of *her1* and *her7*, the novel *her1* mutant allele and *her7* are inherited as a single linked pair. 2 novel *her1* mutant alleles were selected. The first allele had sequence inserted into the second exon resulting in the generation of 2 consecutive stop codons and is predicted to synthesise a truncated non-functional Her1 protein. The second allele had a 6 bp deletion corresponding to the loss of amino acids proline and valine in the basic DNA-binding domain. This proline has been proposed to confer unique sequence specificity to Hes/Her DNA binding (Kageyama et al., 2007). I chose to characterise the allele that has premature stop codons and this *her1;her7* combination was named *gullum* and will be referred to as such throughout the thesis.

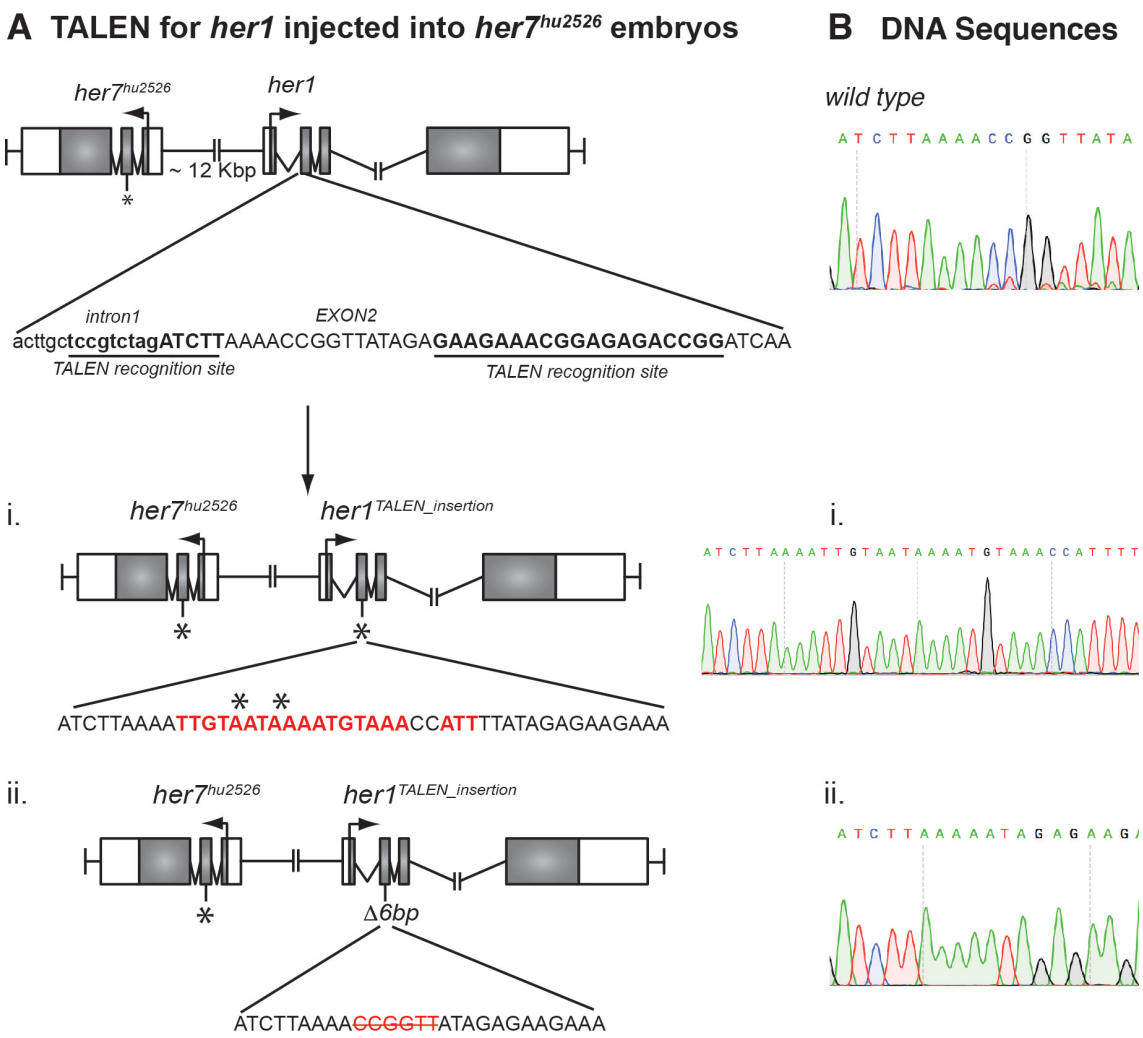

Figure 4.1 Generating a *novel her1;her7* mutants by TALEN.

Schematic of the TALEN strategy used to generate *her1;her7* mutants **(A)**. DNA sequencing traces of wild type *her1* and the two newly generated mutant *her1* alleles **(B)**. Predicted protein sequences of the same **(C)**.
(A – B) A TALEN construct directed against *her1* was injected into *her7* mutant embryos resulting in the creation of 2 mutant *her1;her7* alleles – **(Ai, Bi)** one with consecutive stop codons in exon2 of *her1* (inserted sequence indicated in red, asterisks – stop codons) and **(Aii, Bii)** a second with a 6 base pair (bp) deletion in exon2 (deleted sequence indicated in red). **(C)** *her1 TALEN i* is predicted to make a truncated protein that does not have the DNA binding basic domain or the Helix-Loop-Helix domain for dimerisation. *her1 TALEN ii* is missing conserved amino acids Pro and Val in the basic domain.

4.1 *gullum* has a disordered body segmentation phenotype that arises during somitogenesis

4.1.1 *gullum* has disrupted myotome boundary morphology

Before the newly generated *gullum* mutant could be utilized to probe the role of the segmentation clock in generating the adult metameric body pattern, it had to be confirmed if it had a segmentation phenotype. A quick and reliable method for doing this is assaying the expression of *xirp2a*. Disruption to myotome boundaries, as assayed with *in situ* hybridisation for *xirp2a* in fixed samples, can provide a readout for the dynamic state of the segmentation clock and somitogenesis (Riedel-Kruse et al., 2007; Schröter and Oates, 2010; Schröter et al., 2012). An *in situ* hybridisation strategy had been used previously to assay somitogenesis disruption caused by simultaneous injection of morpholinos for *her1* and *her7* (Oates and Ho, 2002). 25% of embryos per clutch from *gullum* heterozygous pairings had a segmentation phenotype, as visualised with *xirp2a* staining at 36 hours post fertilization (hpf). These embryos corresponded to *gullum*, confirming that the novel *her1;her7* mutation is inherited as a recessive allele in a Mendelian ratio.

Myotome boundaries were not present as periodic chevrons (Fig 4.2, 7.2). Instead, they were fragmented all along the body axis, a phenotype similar to that of embryos injected with morpholinos for both *her1* and *her7*. These fragments did not consistently span the body axis mediolaterally. Furthermore, they were not in register along the left and right sides of the body. Therefore, in contrast to wild type, the *gullum* myotome boundaries had lost their characteristic chevron shape and their left-right correspondence. However, the extent of disruption to the myotome boundaries was variable (Fig 4.2B, C) and occasional chevron-shaped boundaries were observed (Fig 4.2B,C, C'). 86% (42/49) of embryos analysed had a few chevron-shaped myotome boundaries, 4 on average (4 ± 2.9, mean ± SD), and these were predominantly located rostral or caudal in the body. Heterozygous *gullum* embryos were indistinguishable from their wild type clutch-mates with respect to the periodicity and shape of the myotome boundaries. On average, the boundary alignment to the proctodeum – a coarse-grain readout for somitogenesis period, was also comparable to wild type (Fig

4.3). Therefore the homozygous condition of the novel *gullum (her1;her7)* allele results in disrupted body segmentation at 36 hpf.

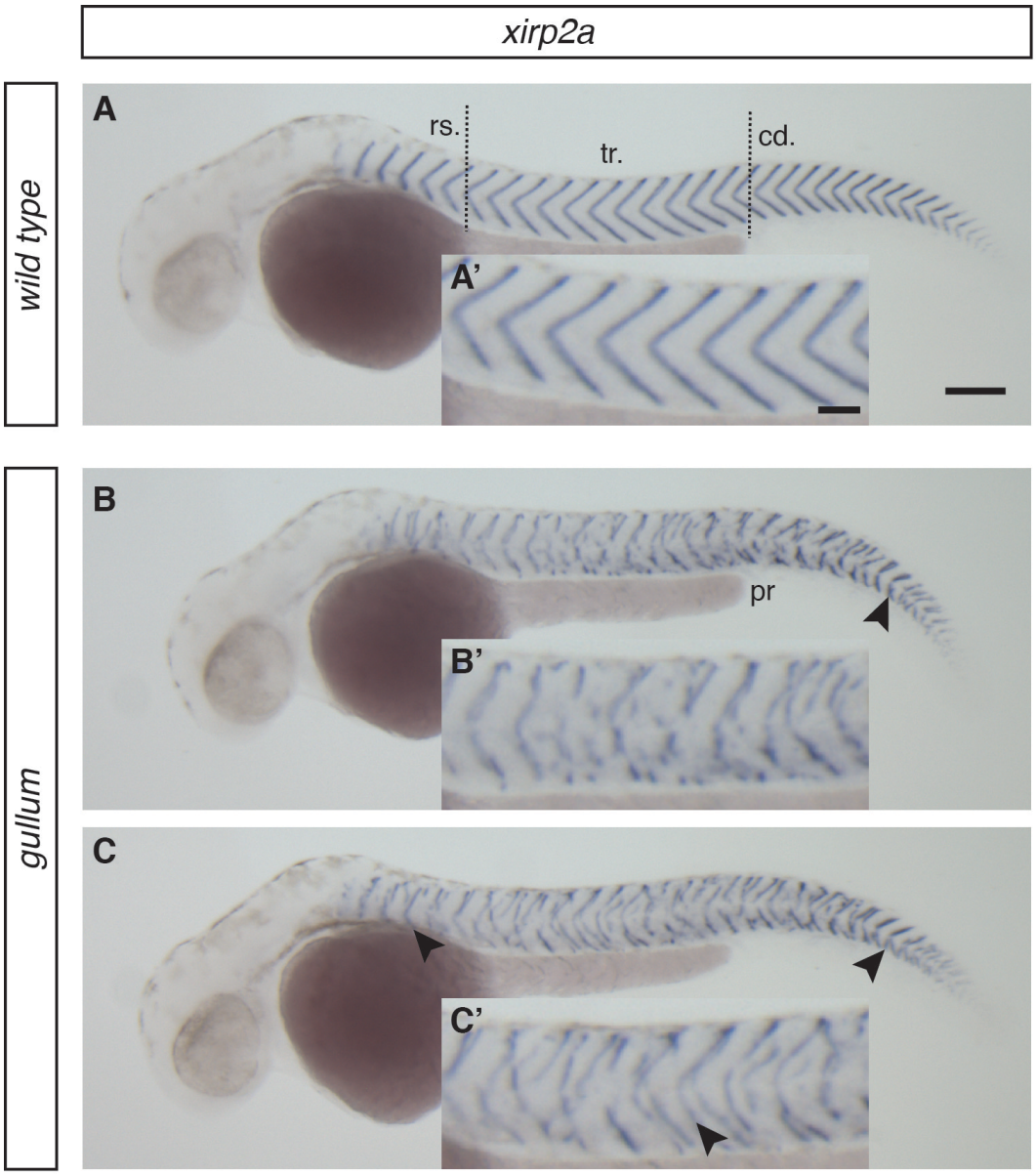

Figure 4.2 *gullum* mutants have a myotome segmentation phenotype.

In situ hybridisation for myotome boundary marker *xirp2a* **(A - C)** in 36 hours post fertilization (hpf) siblings from a heterozygous *gullum* +/- cross. Genotypes are as indicated, lateral views, head oriented to the left, insets are of the trunk.
(A, A') *xirp2a* staining delimits periodic, chevron-shaped boundaries in wild type embryos. **(B – C')** Boundary fragments are observed all along the body axis in *gullum* embryos. Occasional intact chevron-shaped boundaries are observed (4 ± 2.9, mean ± SD; arrowheads in B – C, determined from 49 *gullum* embryos pooled from 2 experiments). rs. - rostral, tr. – trunk, cd. – caudal, pr. – proctodeum. Scale bar 150 µm, scale bar A' – C' insets 50 µm.

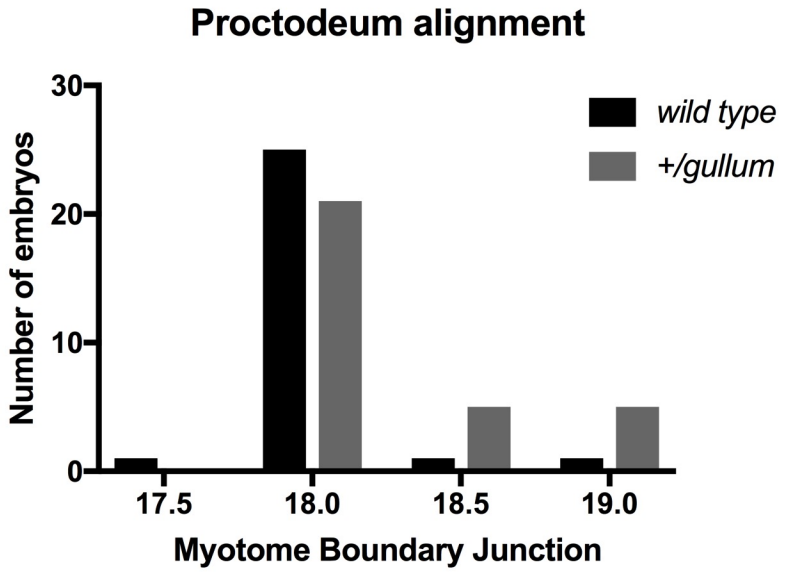

Figure 4.3 Wild type and heterozygous *gullum* siblings have comparable somitogenesis periods.

Distribution of the alignment between muscle boundary junction and the position of the proctodeum in wild type and heterozygous *gullum* 36 hpf embryos. Mode of the distributions of both wild type and *gullum* embryos is myotome boundary junction 18. Data from 30 embryos for each genotype.

4.1.2 *gullum* makes defective somite boundaries sequentially

Having established that myotome boundary morphology is disrupted in *gullum*, it had to be determined if this was due to defective somite boundary formation. Disruptions to processes downstream of the segmentation clock and somitogenesis, such as failure in somite boundary maintenance (Jülich et al., 2005a; Richter et al., 2017) or defective myogenesis (Richter et al., 2017; Rost et al., 2014), can also result in a myotome boundary phenotype. To determine if the somite boundaries in *gullum* were defective from their time of formation, time-lapse microscopy of *gullum* embryos undergoing somitogenesis at 23.5ºC was performed. As the heterozygous *gullum* condition was indistinguishable from wild type for myotome segmentation, synchronously laid *gullum* heterozygous siblings were used as controls for *gullum* mutants from a *gullum* homozygous to *gullum* heterozygous breeding. The time-lapse recordings made corresponded to somitogenesis from somite 5 to somite 18 in the controls. Analysis of these videos showed that somite boundaries of *gullum* are defective from their time of formation (Fig 4.4).

The formation of boundary fragments was not noticed to be ectopic i.e. boundary fragment formation was never observed in the undifferentiated PSM. Therefore, the PSM of *gullum* seems to still differentiate in a sequential manner, much like wild type. Explicit measurement of the time of formation of fragments was not made. This is for two reasons. Firstly, wild type somite boundary formation can consistently be observed initiating at the outer lateral edge of the PSM and this observation is used to score boundary formation. This is probably not always true in *gullum* as fragments rarely span mediolaterally and determining boundary formation at the lateral edge might lead to incomplete scoring of boundary fragments. Secondly, the fragments lacked sufficient contrast at their time of formation to be reliably scored. However, similar to the myotome boundaries, occasional somite boundaries that spanned the paraxial mesoderm mediolaterally were observed.

From the time-lapse microscopy videos it was also possible to investigate if the mutants showed any other deficiencies in embryonic growth or a general developmental delay. The mutant embryos were comparable to their heterozygous siblings in general body shape at every time point of the experiment. Axial outgrowth of the mutant and heterozygous embryos (measured from head to tailbud) was also similar (Fig 4.5).

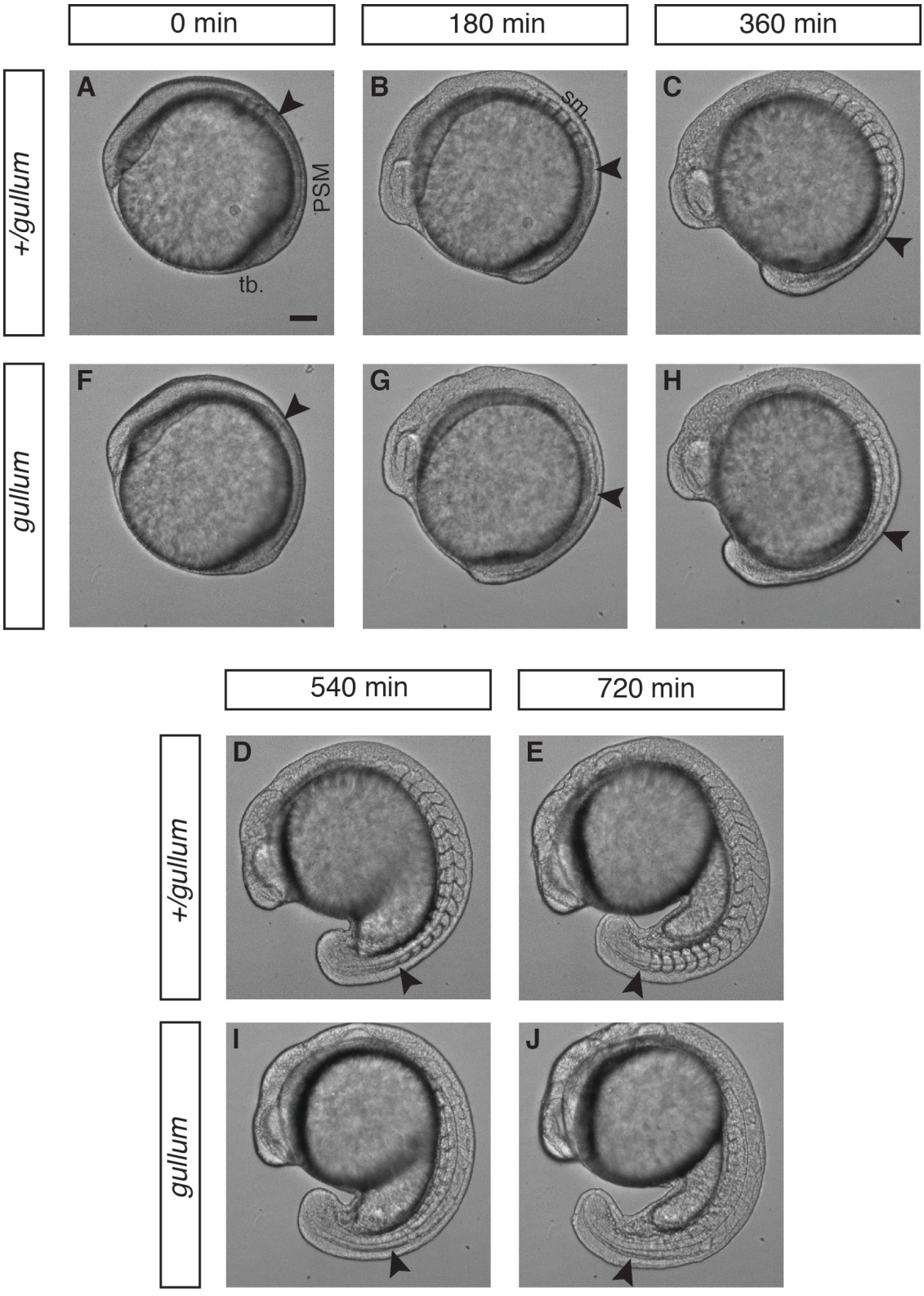

Figure 4.4 Defective somite boundaries form sequentially in *gullum.*

Time points from time-lapse micrographs of heterozygous *gullum* and homozygous *gullum* embryos undergoing somitogenesis **(A – J)**. Genotypes and time points are as indicated.

(A – E) Sequential and periodic formation of somites is observed in the *+/gullum* embryos. **(F – J)** Sequential differentiation of the PSM is observed in *gullum*, somite boundaries are defective. Arrows in panels indicate the forming somite boundary/boundary fragment. PSM – presomitic mesoderm, tb – tailbud, sm – somites. Scale bar 100 µm

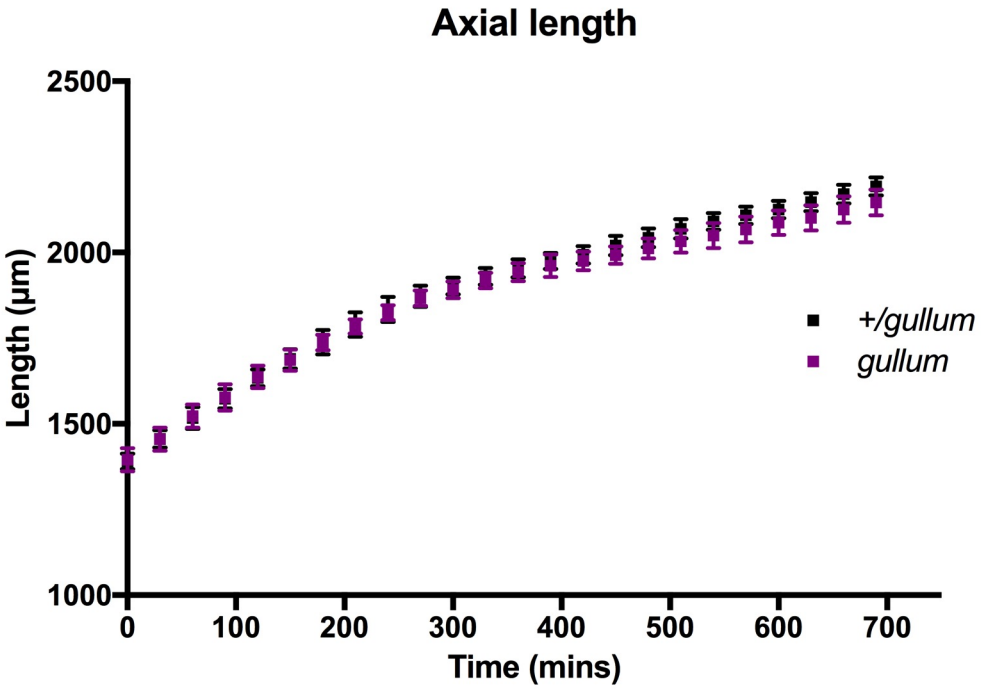

Figure 4.5 The axial elongation of heterozygous *gullum* and *gullum* embryos is comparable.

Plot of axial outgrowth over time. Axial outgrowth has been inferred from measurements of body length from head to tail from time-lapse videos of heterozygous *gullum* and homozygous *gullum* embryos undergoing somitogenesis. Axial outgrowth of *gullum* does not differ from that of its heterozygous *gullum* siblings. Points in graph - mean ± SD. Measurements made from 30 embryos for each genotype, pooled from 2 independent experiments.

Thus, from this analysis it can be concluded that during somitogenesis, *gullum* sequentially differentiates its PSM into boundary fragments. The *gullum* mutation does not affect general development and axial outgrowth of the homozygous condition is comparable to wild type. Therefore, a novel *her1;her7* mutant combination that shows a somitogenesis phenotype and no non-specific developmental deficits has been successfully generated.

4.2 The segmentation clock is disrupted in the *gullum* PSM

The sequential formation of defective boundaries in the paraxial mesoderm implied that one or more of the processes in the segmentation clock had been impeded by the loss of *her1* and *her7* in *gullum*. Therefore, as a next step to characterise the disruption of segmental pattern in *gullum*, an analysis of the segmentation clock was undertaken.

4.2.1 Presomitic mesoderm specification is not affected in *gullum*

The *t-box* genes are crucial factors in mesoderm specification. *t-box* gene *ta* maintains the mesodermal progenitor pool in the tailbud and is essential for the specification of axial mesoderm (Amacher et al., 2002; Schulte-Merker et al., 1994). *tbx16* promotes the differentiation of progenitors into presomitic mesodermal cells (Fior et al., 2012) and *tbx6* is required for segmentation clock function and segmentation clock output in the anterior PSM (Holley et al., 2000; Sawada et al., 2001). Their domains of expression are illustrated in the schematic in Fig 4.6A. The *t-box* genes are upstream regulators of the cyclic genes *her1* and *her7*. The *her1* and *her7* cyclic gene promoters have T-box binding sites and they are directly regulated by *tbx6* in the anterior PSM (Brend and Holley, 2009; Holley et al., 2000). The loss of *tbx6* in *fss* mutants results in the loss of *her1*, *her7* and *deltaC* expression in the anterior PSM. They also are downstream targets of Wnt signalling (Martin and Kimelman, 2008; 2010; Szeto and Kimelman, 2004; Thorpe et al., 2005).

To determine if the loss of *her1* and *her7* activity in *gullum* affected PSM specification, the expression of the *t-box* genes was assayed by *in situ* hybridisation in 10-somite stage siblings from synchronous clutches obtained from heterozygous *gullum* pairings. A distinction was not made between wild type and heterozygous embryos. Embryos of both genotypes have been presented as wild type. In wild type embryos, *ta* was expressed in a domain in the tailbud and in the notochord (Fig 4.6B), *tbx16* was present in the tailbud and the posterior PSM (Fig 4.6D) and *tbx6* was expressed in the anterior PSM (Fig 4.6F). In *gullum*, the expression domains of these three genes in the tailbud and PSM were comparable to wild type (Fig 4.6C, E, G). Therefore, differentiation of mesodermal progenitors into PSM is not affected in *gullum.*

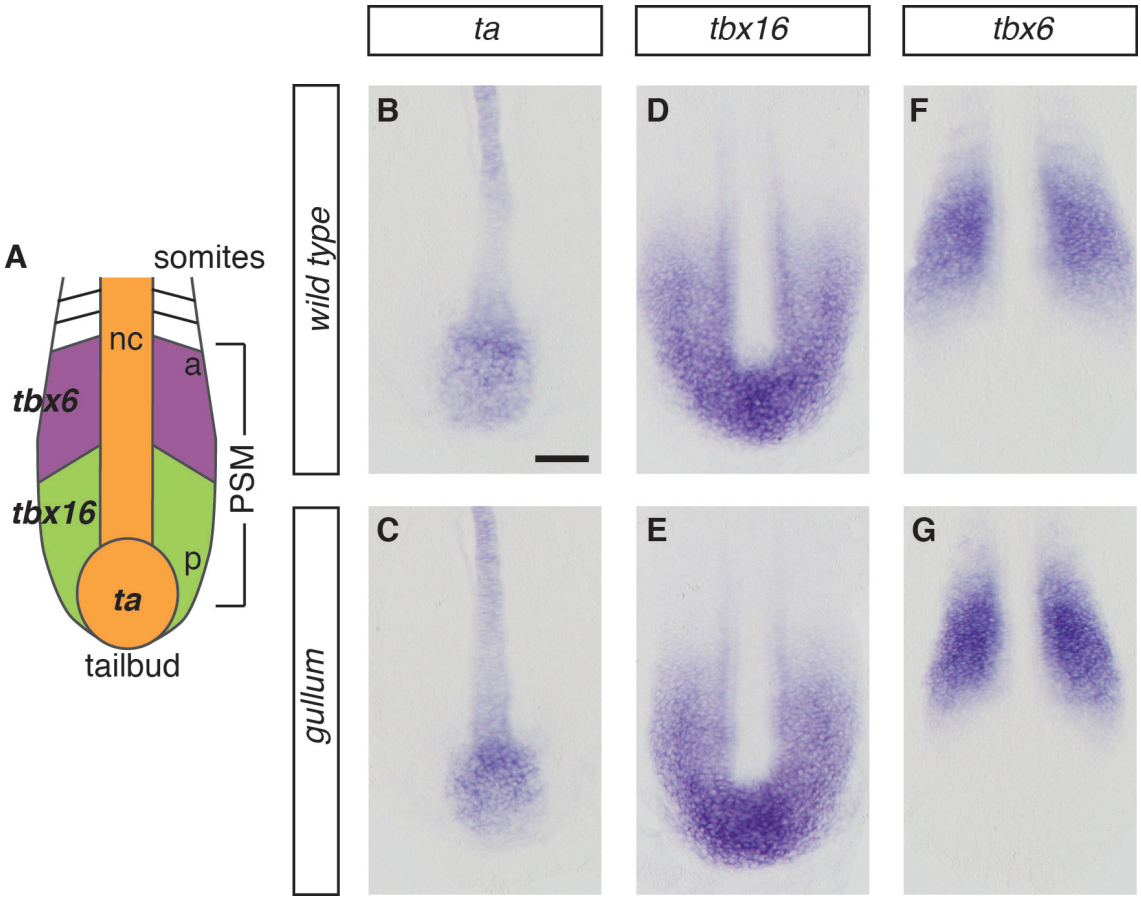

Figure 4.6 Sequential gene expression domains of the *t-box* genes are unaffected in the *gullum* PSM.

Schematic of the domains of gene expression of the *t-box* genes in the PSM **(A)**. *In situ* hybridisation for *ta* **(B, C)**, *tbx16* **(D, E)** and *tbx6* **(F, G)** in wild type and *gullum* homozygous 10-somite stage siblings derived from heterozygous *gullum* +/- pairings. Anterior to the top of the panels, genotypes are as indicated.
(B, C) Expression of *ta* is not different between wild type and *gullum* (30/30). **(D, E)** *tbx16* expression is identical in wild type and *gullum* (30/30). **(F, G)** *tbx6* expression is similar in wild type and *gullum* embryos (30/30). a – anterior, p - posterior, nc – notochord. Scale bar 100 µm.

4.2.2 The core pace-keeping circuit does not have dynamic mRNA expression in the *gullum* PSM

her1 and *her7* are thought to be integral to the genetic oscillator activity (in the bottom tier of the segmentation clock) and are 2 of 3 components of the core pace-keeping circuit. To determine if the observed somitogenesis and segmentation defects in *gullum* arose from a loss of this oscillator activity, I set out to determine if the transcriptional oscillations of *her1* and *her7* were affected in the mutant. *her1* and *her7* gene expressions were assayed by *in situ* hybridisation due to the unsuitability of the *her1::YFP looping1* transgenic reporter for this analysis. As the *Looping1* construct has

open reading frames for a functional chimeric Her1 protein and the wild type Her7, it can rescue the *gullum* phenotype. Although *in situ* hybridisation cannot report on the activity of the genetic oscillator within single cells, the kinematic waves of expression in the PSM can be observed. Wild type sibling embryos at the same somite stage show wave patterns of cyclic gene *her1* and *her7* expression that correspond to phases of the oscillation cycle (Fig 4.7A, A' and D, D'). The same somite stage can be achieved in a clutch by allowing a single male-female pair to spawn for 20 minutes, which is less than the somitogenesis period at 28.5°C – a technique termed synchronous spawning. 30 sibling embryos from synchronously spawned clutches of heterozygous *gullum* pairings were fixed at the 10-somite stage and *in situ* hybridisation for *her1* and *her7* was performed to investigate the wave patterns (N = 2). Wild type and heterozygous siblings were distinguished by genotyping.

Patterns of wave-like expression of *her1* and *her7* could be detected in wild type and heterozygous *gullum* siblings (Fig 4.7A – B' and D – E'), indicating that the expression of *her1* and *her7* was dynamic in the PSM on the tissue level in these embryos. In *gullum* embryos, *her1* and *her7* mRNA could be detected (Fig 4.7C, C', F, F'). However, the expression was seen throughout the PSM and not organised as spatial waves. Furthermore, the expression pattern was identical in all embryos and no phases of gene expression could be distinguished. *her1* had low expression in the tailbud and posterior PSM, and high expression in the anterior PSM. *her7* was expressed throughout the PSM, but had the highest expression in the tailbud. This pattern of staining intensity in *gullum* was comparable to that of the wild type and heterozygous *gullum* embryos. From these observations it can be concluded that in *gullum* the cyclic genes comprising the core pace-keeping circuit are no longer expressed as kinematic waves in the PSM.

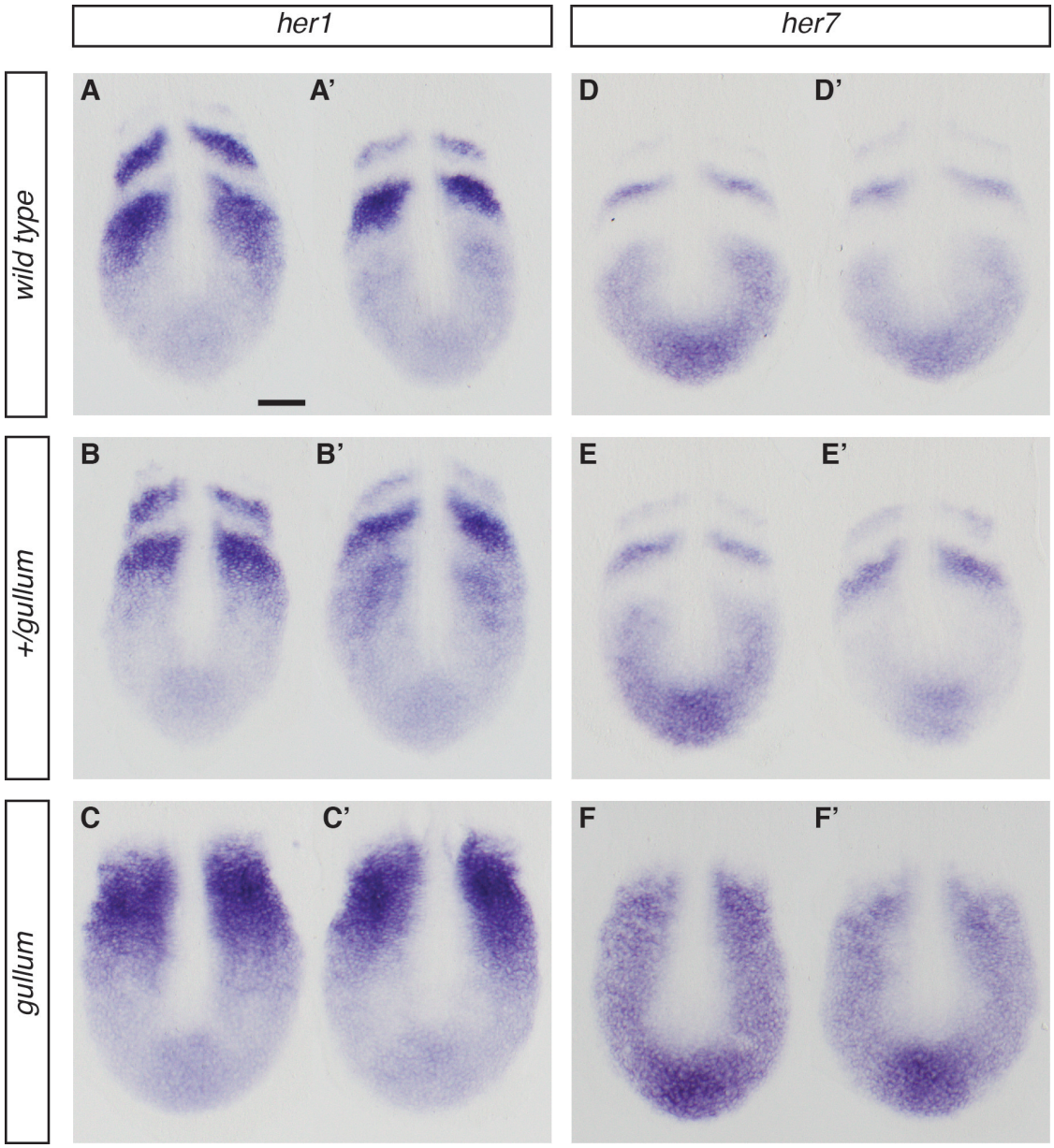

Figure 4.7 Cyclic expression of *her1* and *her7* is disrupted in the *gullum* PSM.

In situ hybridisations for cyclic genes *her1* **(A – C')** and *her7* **(D – F')** in 10-somite stage siblings from a heterozygous *gullum* +/- cross. Genotypes are as indicated. 2 flatmount preparations of the PSM, anterior to the top, are shown here per genotype for each probe.
(A – B') *her1* expression is seen as waves in wild type and heterozygous *gullum* siblings. **(C, C')** Static *her1* expression patterns are observed in *gullum* (30/30). **(D – E')** Wave patterns of *her7* are present in wild type and heterozygous *gullum* embryos. **(F, F')** *her7* expression is observed in the entire PSM and is invariant between *gullum* homozygous siblings (30/30). Scale bar 100 µm.

4.2.3 Notch ligand *deltaC* is expressed in a non-dynamic fashion in the *gullum* PSM

Notch receptors and Delta ligands play an essential role in the segmentation clock by providing the cell to cell communication by which cells in the PSM locally synchronise their genetic oscillations. The ligand *deltaC* is expressed in waves in the PSM, similar to *her1* and *her7* cyclic genes. This dynamic expression is thought to be dependent on the core pace-keeping circuit as the knockdown of *her1* and *her7* activity by morpholinos has been reported to affect the oscillatory expression of *deltaC* (Riedel-Kruse et al., 2007). In light of the loss of *her1* and *her7* wave patterns in *gullum* mutants, the expression pattern of *deltaC* was assessed to determine its dynamic state. 30 10-somite stage clutch-mates from synchronous heterozygous *gullum* pairings were fixed and *in situ* hybridisation for *deltaC* was performed (N = 2). Wave patterns of *deltaC* expression were observed in the wild type and heterozygous *gullum* siblings (Fig 4.8A – B', distinguished by genotyping). *deltaC* in *gullum* mutants was not expressed in waves (Fig 4.8C, C'). It was expressed throughout the PSM, with the highest expression in the anterior PSM. Differences in *deltaC* expression between different embryos that would correspond to dynamic expression in the PSM were not observed.

The observation that the mature transcript of *deltaC* was not present in the tissue as kinematic waves did not preclude the possibility that *deltaC* was still transcribed in an oscillatory fashion in the mutant. If this were the case, then nascent *deltaC* transcript would be present as travelling waves in the *gullum* PSM. To assess this possibility, *in situ* hybridisation analysis was undertaken in 30 10-somite clutch-mates from synchronous heterozygous *gullum* pairings with a riboprobe to detect an intron in *deltaC* (N = 2). Wild type and heterozygous siblings were not distinguished from each other and have been presented here as wild type. Nascent *deltaC* transcript was present in the wild type siblings as travelling waves in the PSM (Fig 4.8D, D'). In *gullum* (30/30), the nascent transcript was expressed throughout the PSM, with the highest expression in the anterior, like the processed *deltaC* transcript and the pattern of expression did not vary between embryos (Fig 4.8E, E'). From these results, it can be concluded that the loss of *her1* and *her7* causes the loss of dynamic *deltaC* transcription.

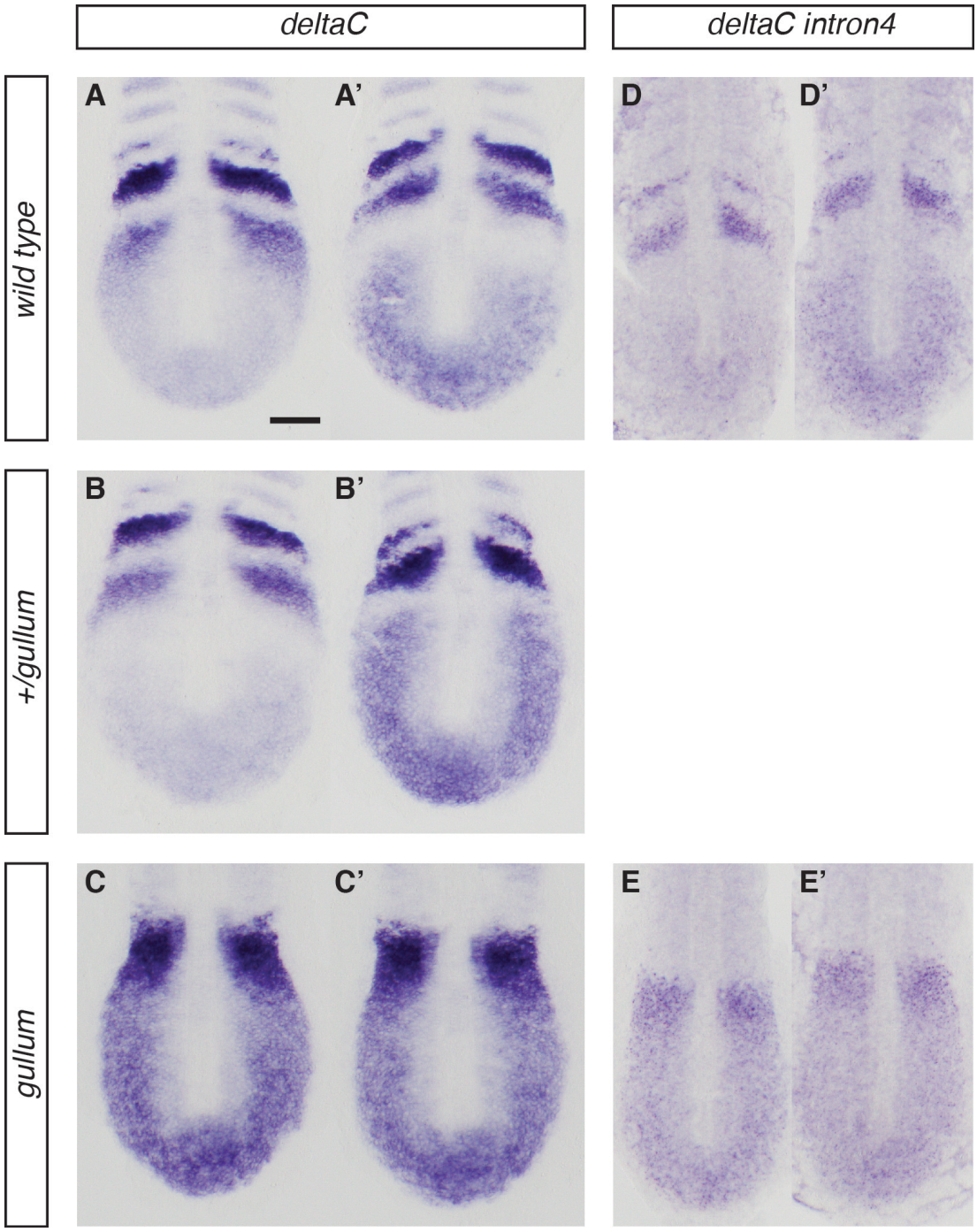

Figure 4.8 Cyclic *deltaC* expression is abolished in the *gullum* PSM.

In situ hybridisations for *deltaC* with a full coding sequence antisense riboprobe **(A – C')** and an antisense riboprobe for the 4th intron **(D – E')** in 10-somite stage siblings from a heterozygous *gullum* +/- cross. Genotypes are as indicated, panels are flatmount preparations of the PSM, anterior to the top. 2 representative embryos are shown per riboprobe per genotype.
(A – B') Cyclic *deltaC* expression is observed in the PSMs of wild type and heterozygous *gullum* siblings. **(C, C')** Static deltaC expression is observed in the entire *gullum* PSM (30/30). **(D, D')** Staining for *deltaC intron4* shows dynamic wave patterns in wild type siblings. **(E, E')** Staining for the intronic probe for *deltaC* is observed throughout the *gullum* PSM, with the highest intensity in the anterior PSM (30/30). Scale bar 100 µm.

4.2.4 Segmental output is not made in the anterior PSM of *gullum*.

Having determined that the core pace-keeping circuit comprising *her1* and *her7* and the downstream target *deltaC* no longer had dynamic expression in the PSM, I next queried if the segmentation clock output markers were expressed in the anterior PSM. The patterning output of the segmentation clock is observed as stripes of gene expression of *mespb* (Sawada et al., 2000) and its regulatory factors *ripply1* and *ripply2* (Kawamura et al., 2005a) in the anterior PSM. *papc* (Oates et al., 2005; Jiang et al., 2000) is also expressed as stripes in the anterior PSM. *In situ* hybridisations were performed for *mespb*, *papc*, *ripply1* and *ripply2* in 30 10-somite stage sibling embryos (per marker, per experiment) from synchronous spawning of pairwise heterozygous *gullum* matings (N = 2). For the *mespb* experiments, wild type and heterozygous siblings were identified by genotyping. For the remaining segmental output markers, a distinction was not made and both genotypes have been presented here as wild type. *mespb* was expressed in the anterior PSM of the wild type and heterozygous *gullum* siblings as 2 to 3 stripes (Fig 4.9A – D'). *mespb* was detected in the anterior PSM of *gullum* embryos in the anterior PSM, however the expression was not organised as segmental stripes (Fig 4.9E – H'). *papc*, which was organised as stripes in the anterior PSM of wild type embryos (Fig 4.10A, A'), also had disorganised expression in *gullum* (Fig 4.10B, B'). Small clusters and stripes of *papc* expressing cells were observed in the anterior expression domain, but these patterns were not stereotypical and varied among the mutant embryos analysed. *ripply1*, expressed as stripes in the anterior PSM and in the somites in wild type (Fig 4.10C, C'), also showed diffuse expression in the anterior PSM and the differentiated paraxial mesoderm (Fig 4.10D, D'). Similarly, stripes of *ripply2* (Fig 4.10E, E') were lost and the expression domain was disorganised in the *gullum* anterior PSM (Fig 4.10F, F'). Although it cannot be excluded that some cryptic segmental output remains in *gullum*, taken together, the expression patterns of these four key markers of segmentation suggest that the *gullum* segmentation clock does not generate segmental pattern in the anterior PSM.

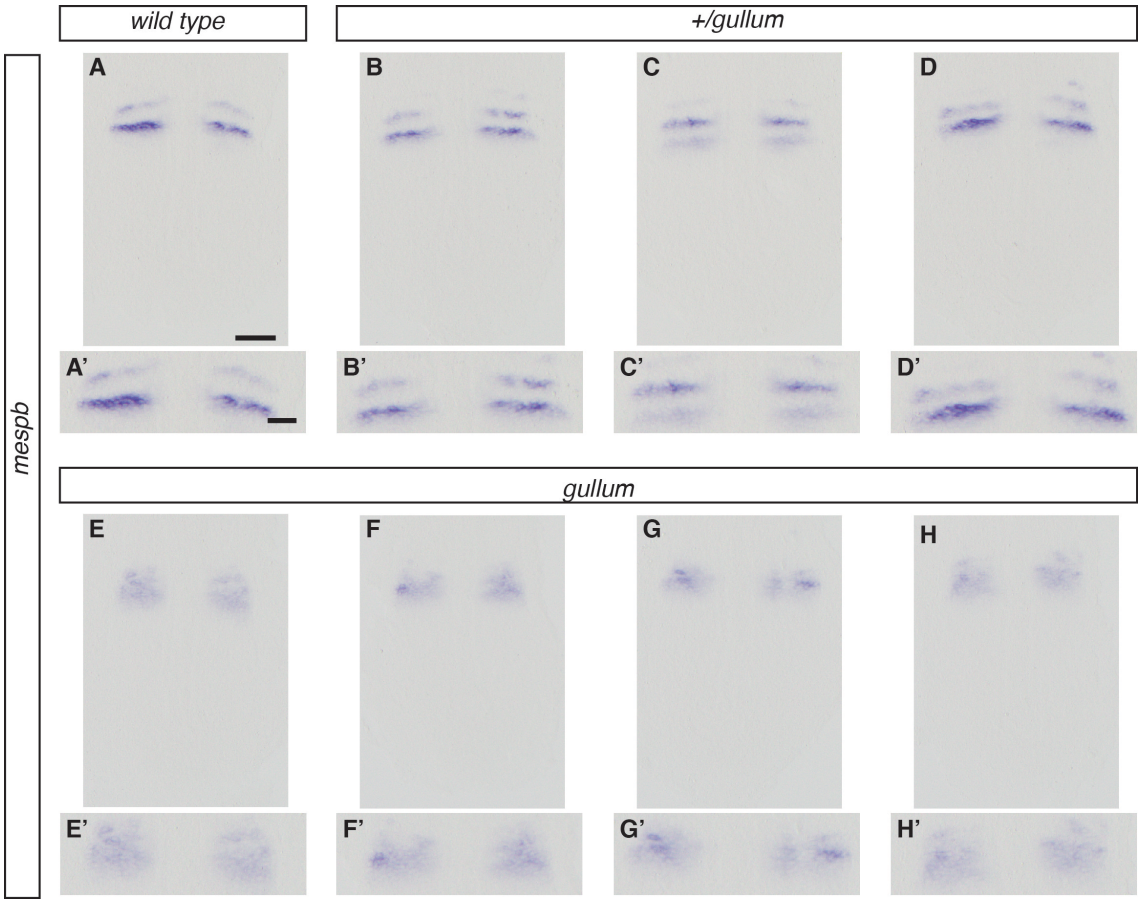

Figure 4.9 *mespb* is not expressed in stripes in the anterior PSM of *gullum*.

In situ hybridisation for clock output marker *mespb* **(A – H')** in siblings from a heterozygous *gullum* +/- cross at the 10-somite stage. Anterior to the top, genotypes are as indicated.
(A, A' – D, D') In wild type and heterozygous *gullum* embryos, *mespb* expression is organised as 2 – 3 stripes in the anterior PSM. **(E, E' – H, H')** In *gullum*, *mespb* is expressed in a diffuse domain in the anterior PSM. 30 mutant embryos analysed. 4 flatmount preparations presented to demonstrate variability in the expression pattern. Scale bar A – H 100 µm, scale bar A' – H' insets 50 µm.

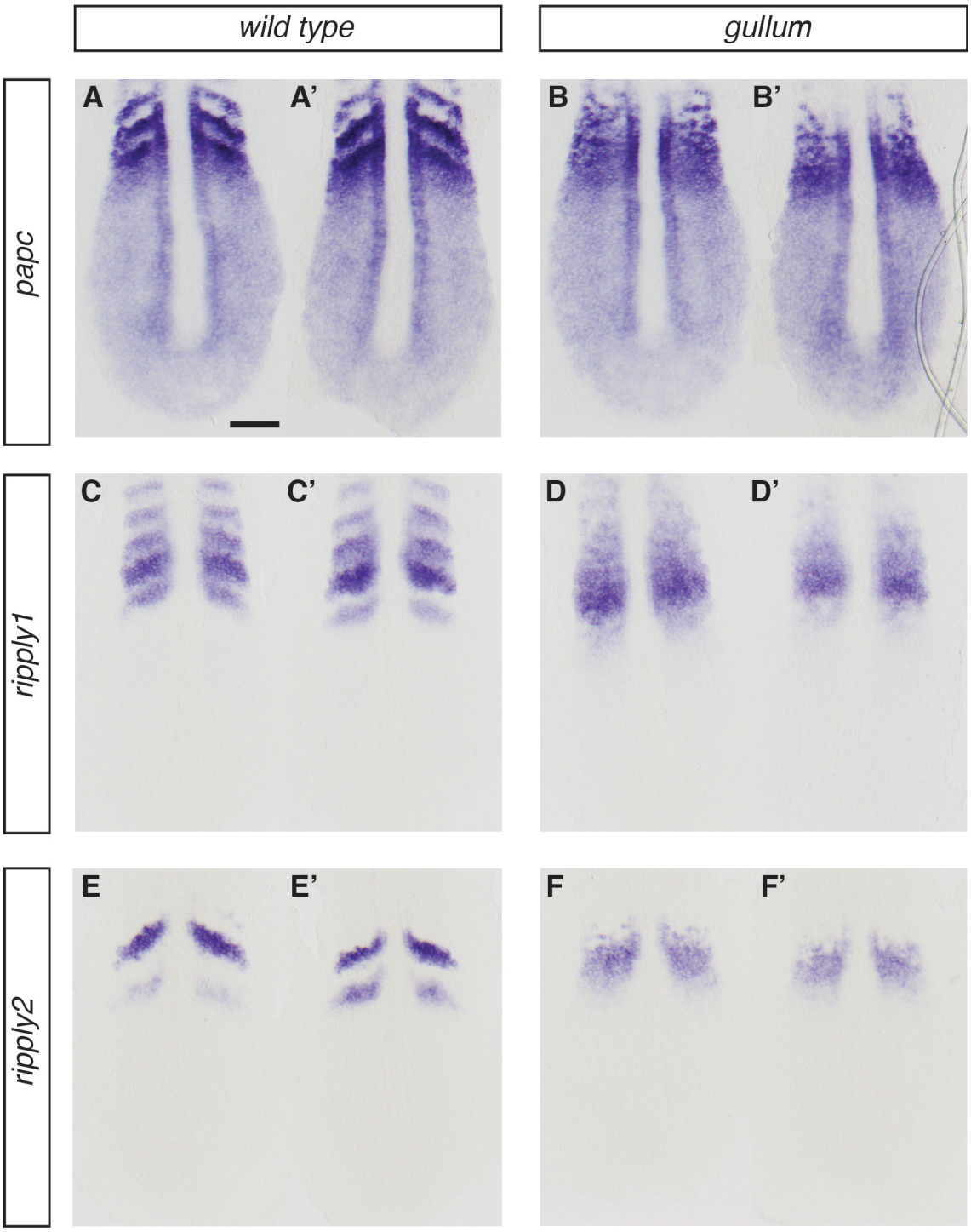

Figure 4.10 Segmental output markers have disorganised expression in the *gullum* anterior PSM.

In situ hybridisation for segmentation clock output markers *papc* **(A – B')**, *ripply1* **(C – D')** and *ripply2* **(E – F')** in siblings from a heterozygous *gullum* +/- cross at the 10-somite stage. Anterior to the top, genotypes are as indicated.
(A, A') In wild type, *papc* is organised as stripes in the anterior PSM. **(B, B')** The *papc* domain in *gullum* is disorganised. **(C, C')** *ripply1* is present as stripes in the anterior PSM and the paraxial

mesoderm. **(D, D')** *ripply1* expression is disorganised in the *gullum* anterior PSM and paraxial mesoderm. **(E, E')** *ripply2* is expressed as 2 – 3 stripes in the anterior PSM in wild type. **(F, F')** *ripply2* expression is disorganised in the anterior PSM of *gullum*. 30 mutant embryos analysed per marker, 2 flatmount preparations presented to show variability in the mutant expression patterns. Scale bar 100 μm, scale bar A'- C' insets 50 μm.

4.2.5 Complete loss of the core pace-keeping circuit is indistinguishable from *gullum*

The core pace-keeping circuit comprises 2 parallel feedback loops that operate redundantly – Her1 homodimers and Her7 and Hes6 heterodimers (Schröter et al., 2012). Therefore, I wanted to determine if the loss of *hes6* in the *gullum* background would further disrupt the segmentation clock. *In situ* hybridisations for *her1*, *her7*, *deltaC* and *mespb* were performed in 10-somite stage embryos obtained from heterozygous *gullum;hes6* pairings. 150 embryos were used per marker. The Mendelian expectation for the triple mutant from the pairing is 6 in a 100. The desired mutant genotypes couldn't be distinguished from each other on the basis of the expression patterns of the cyclic genes. Therefore, 10 – 20 flatmount preparations per marker were prepared and the *gullum (her1;her7)* double and *gullum;hes6 (her1;her7;hes6)* triple mutants were identified by genotyping. The *gullum;hes6* triple mutants did not have dynamic expression of *her1* (3/3), *her7* (3/3) and *deltaC* (3/3). *mespb* expression in the anterior PSM was not segmental (2/2). These observations suggest that double and triple mutants represent equivalent disruptions of the segmentation clock (Fig 4.11). Thus, the loss of *her1* and *her7* is sufficient for the loss of the dynamics of the core pace-keeping circuit in the PSM.

To summarise this section, *in situ* hybridisation analyses for components of the segmentation clock were conducted. These analyses indicate that the segmentation clock is perturbed in the *gullum* PSM and that it fails to generate segmental patterning output.

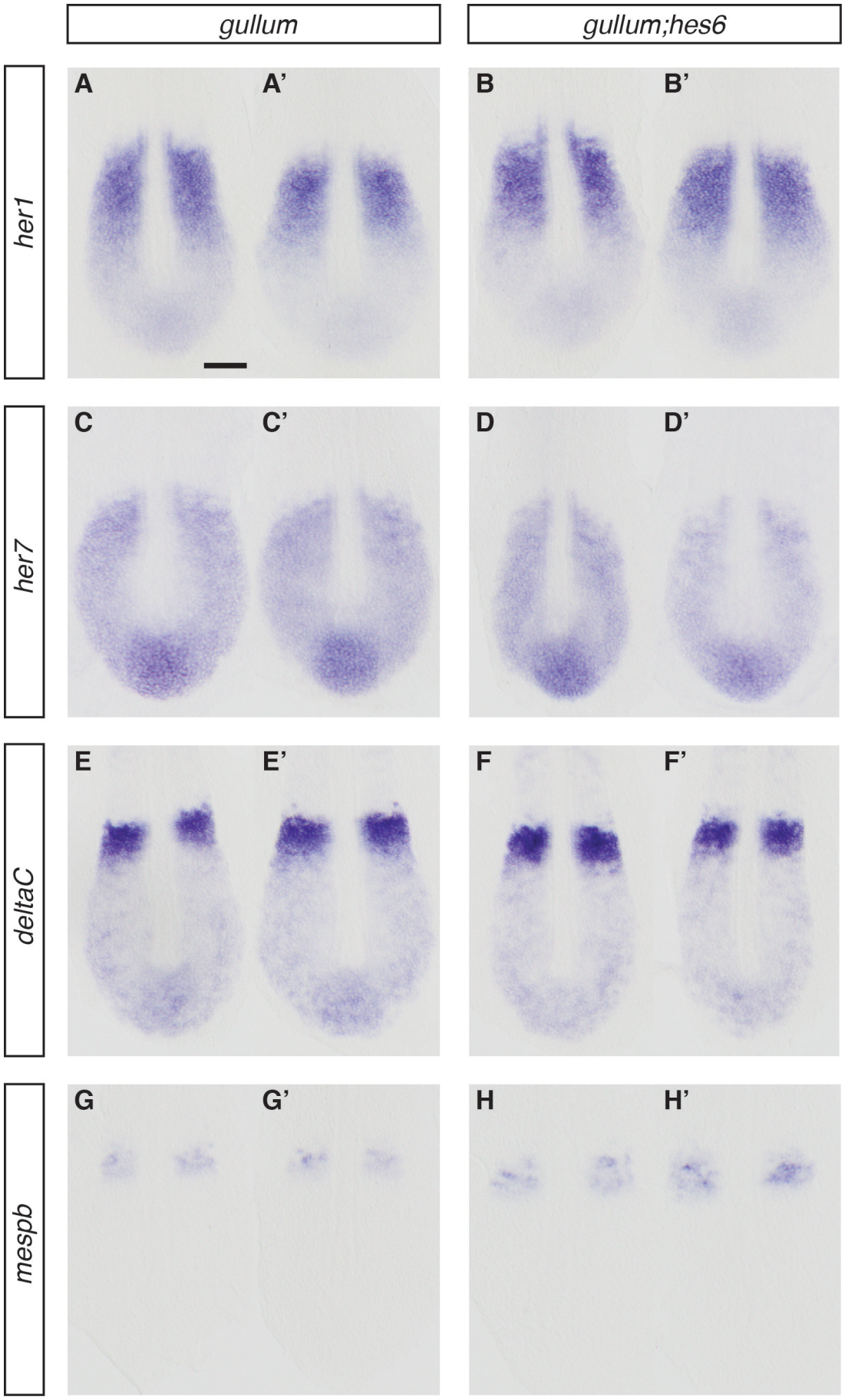
gullum
gullum;hes6
her1
her7
deltaC
mespb
A
A'
B
B'
C
C'
D
D'
E
E'
F
F'
G
G'
H
H'

Figure 4.11 Expression of PSM markers is similar between *gullum* and *gullum;hes6* mutants.

In situ hybridisation for *her1* **(A – B')**, *her7* **(C – D')**, *deltaC* **(E – F')** and *mespb* **(G – H')** in 10-somite stage *gullum* and *gullum;hes6* siblings from a heterozygous *gullum;hes6* cross. Mendelian expectation for the triple mutant from the cross is 0.06. Embryos are 13.5 hpf (10-somite stage). Anterior to the top, genotypes are as indicated.
(A, A') *her1* does not oscillate in *gullum* (3/3) or **(B, B')** in *gullum;hes6* embryos (3/3). **(C, C')** *her7* does not oscillate in the *gullum* PSM (2/2). **(D, D')** *her7* expression in *gullum;hes6* (3/3) is identical to *gullum*. **(E, E')** Expression of *deltaC* in *gullum* (2/2) and **(F, F')** in *gullum;hes6* (2/2) is identical. **(G, G')** Expression of *mespb* is disorganised in *gullum* (3/3) and **(H, H')** in *gullum;hes6* (2/2). Scale bars are 100 µm.

4.3 The differentiated paraxial mesoderm of *gullum* is not organised as periodic somites

Establishment of pre-segmental pattern is a requirement for the establishment of anterior-posterior polarity in the presumptive somites, subsequent boundary formation and ultimately, the formation of periodic somites in the paraxial mesoderm (Barrios et al., 2003; Krol et al., 2011; Oates et al., 2005b). Having determined that the *gullum* segmentation clock does not output wild type pre-segmental pattern and having observed the sequential formation of boundary fragments in the *gullum* paraxial mesoderm, I next asked if somites form in these mutants.

4.3.1 Anterior-posterior polarity markers are not segmentally expressed in the differentiated paraxial mesoderm of *gullum*

Anterior-posterior regionalisation of the presumptive somite is initiated by *tbx6* via *mespb* and *ripply1* expression (Barrios et al., 2003; Durbin et al., 2000; Oates et al., 2005b). *mespb* is initially expressed in all the cells of the presumptive somite and then becomes restricted to the future anterior compartment of the presumptive somite. This anterior restriction of *mespb* occurs when the *mespb* inhibitor *ripply1* is expressed in the future posterior compartment of the presumptive somite. *mespb* is cleared from the formed somites, while *ripply1* remains expressed in the posterior compartment and maintains the posterior identity. Both *mespb* and *ripply1* were expressed in the anterior PSM of *gullum*, but not in striped domains (Fig 4.9 and 4.10). This suggested that cells express markers of anterior and posterior identity. However, it was not clear if this gene expression was sufficient for the subsequent segmental expression of anterior and posterior compartments markers in the differentiated paraxial mesoderm of *gullum*.

To assay the anterior-posterior polarity of the paraxial mesoderm, I undertook an *in situ* hybridisation based analysis for anterior and posterior somite compartment markers. Anterior and posterior compartments of the somites can be reliably identified in the somites on the basis of metameric and bilaterally paired expression patterns of certain genes (Stickney et al., 2000). To assay for the anterior compartment, I used *deltaD* (Jiang et al., 2000), cyclic gene *her11* (Sieger et al., 2004) and *papc* (Kim et al., 2000; Oates et al., 2005b; Yamamoto et al., 1998b). To assay for the posterior compartment, I used *deltaC* (Jiang et al., 2000), *ripply1* (Kawamura et al., 2005a) and *myoD* (van Eeden et al., 1996). 30 siblings at the 10-somite stage from synchronous clutches obtained from pairwise heterozygous *gullum* crosses (N = 2) were used for the analysis.

In the wild type siblings, *deltaD*, *her11* and *papc* were expressed in the anterior half of the presumptive somites in the anterior PSM (Fig 4.12A, C, E). *deltaD* and *her11* were present in the anterior compartment of all somites while *papc* was present only in the most recently formed somites. In *gullum* siblings, *deltaD* and *her11* had a diffuse expression pattern in the differentiated paraxial mesoderm (Fig 4.12B – B'', D – D''). *papc* was expressed to a similar extent of the paraxial mesoderm as wild type, but this pattern lacked any discernible segmental organisation (Fig 4.12F – F''). *papc*+ cells were observed as small stripes and clusters, but this was variable in the mutant embryos analysed. Thus, the anterior compartment markers in *gullum* lack segmental organisation.

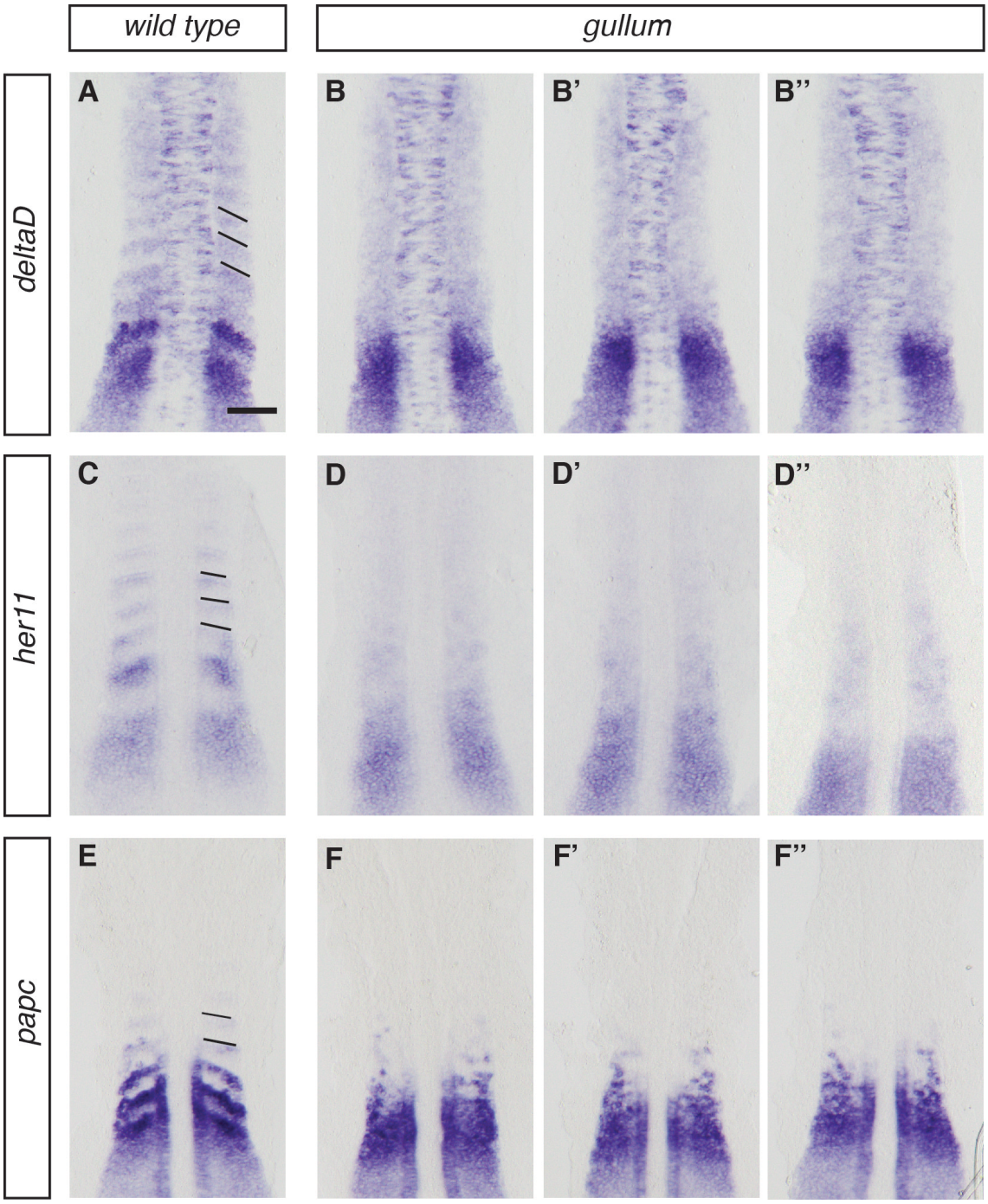

Figure 4.12 Differentiated paraxial mesoderm cells express anterior markers, but not as segmental stripes in *gullum*.

In situ hybridisations for anterior somite markers *deltaD* **(A – B'')**, *her11* **(C – D'')** and *papc* **(E – F'')** in 10-somite stage wild type and *gullum* siblings. Anterior PSM at the bottom of the panel, anterior to the top. Genotypes are as indicated.
(A, C, E) Somites of wild type embryos have anterior polarity. Black lines – anterior somite boundary. **(B – B'', D – D'', F – F'')** Anterior markers do not show segmental organisation in *gullum*. 30 mutant embryos per marker were analysed. 3 flatmount preparations presented here to demonstrate variability in the expression. Scale bars 100 µm.

The posterior compartment markers *deltaC*, *ripply1* and *myoD* were observed as stripes in the wild type paraxial mesoderm (Fig 4.13A, C, E). These markers lacked a similar segmental expression in the *gullum* siblings (Fig 4.13B – B'', D – D'', F – F''). They had disorganised and patchy expression in the paraxial mesoderm instead. Thus, posterior compartments are not established in *gullum*. Taken together, these results suggest that while cells of the differentiated paraxial mesoderm express anterior and posterior compartment markers, metameric anterior and posterior compartments are absent. Further analysis will need to be undertaken to determine if the expression of anterior and posterior markers confers anterior and posterior identity to the differentiated paraxial mesoderm cells in the mutant.

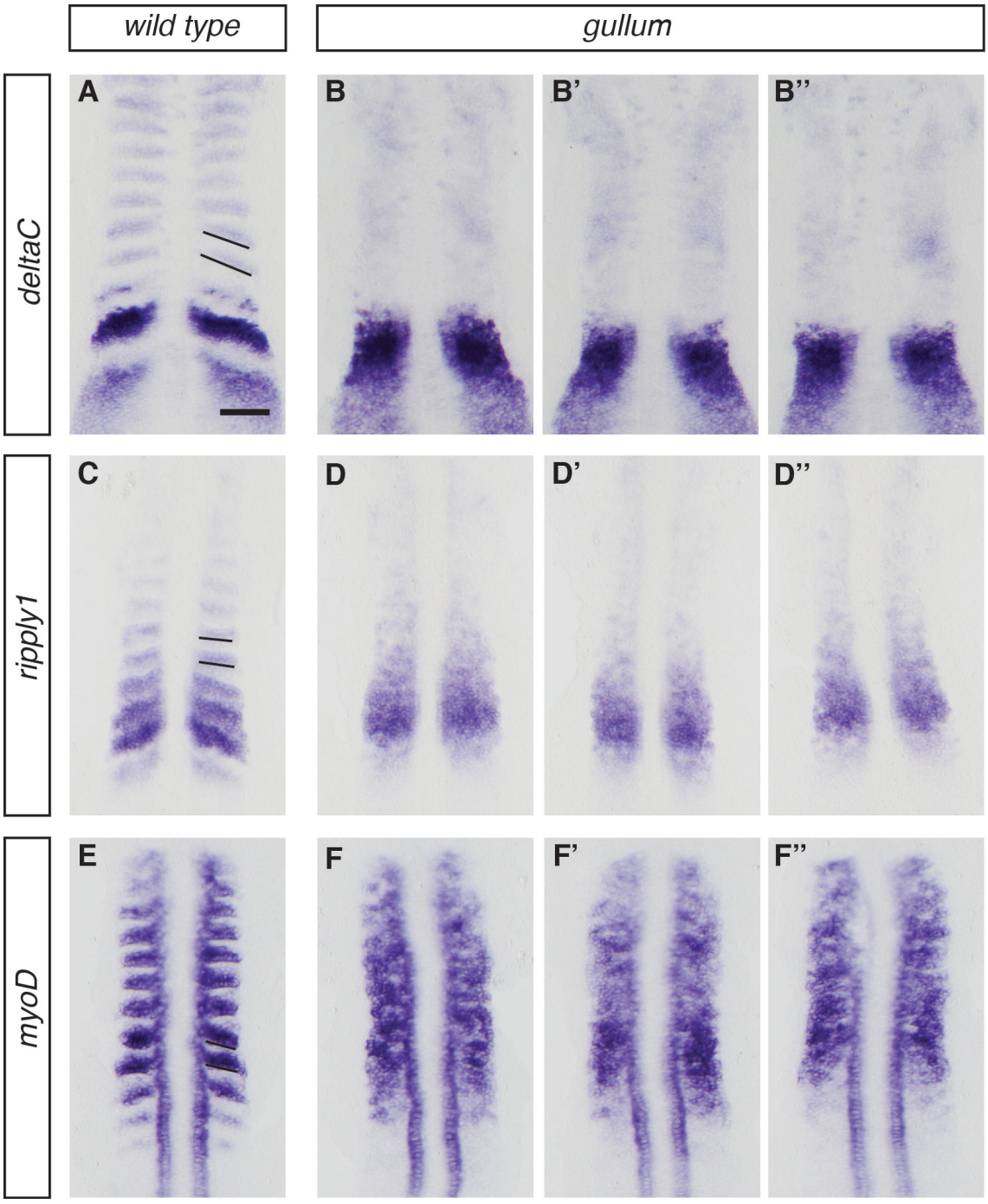

Figure 4.13 Differentiated paraxial mesoderm cells express posterior markers, but not segmentally in *gullum*.

In situ hybridisation for posterior somite markers *deltaC* **(A – B'')**, *ripply1* **(C – D'')** and *myoD* **(E – F'')** in 10-somite stage wild type and *gullum* siblings. Anterior PSM at the bottom of the panel, anterior to the top. Genotypes are as indicated.
(A, C, E) Somites of wild type embryos have posterior polarity. Black lines - anterior somite boundary. **(B – B'', D – D'', F – F'')** Posterior markers are not organised as stripes in *gullum* embryos. 30 mutant embryos were analysed. 3 flatmount preparations presented to show variability in the expression pattern of the posterior markers. Scale bars 100 µm.

4.3.2 Somite boundary fragments and mesenchymal to epithelial transition events are detected in the *gullum* paraxial mesoderm

Anterior-posterior polarity establishment is thought to be crucial for somite boundary formation and maintenance (Durbin et al., 2000; Oates et al., 2005b). Boundary formation is thought to trigger MET and the development of a mature somite comprising an outer columnar epithelial layer with an inner mesenchymal core (Barrios et al., 2003; Henry et al., 2000). Yet, in the absence of overt anterior-posterior polarity in the paraxial mesoderm, what appears to be boundary fragments form in the paraxial mesoderm. Therefore, I set out to determine whether the boundary fragments were rudimentary somite boundaries, if these were associated with MET and if groups of cells are organised in somite-like architecture in the *gullum* paraxial mesoderm. Cell shapes were assayed by phalloidin staining for F-actin and the formation of somite boundaries was determined by the accumulation of fibronectin, detected by antibody staining, in siblings from heterozygous *gullum* matings at mid-somitogenesis stages (10 embryos per genotype, pooled from 2 experiments).

In the wild type siblings, blocks of cells with stereotypical somite architecture were observed. These blocks were demarcated by a furrow that spanned the tissue mediolaterally (Fig 4.14A). Cells with columnar shape were observed on either side of the furrow and these cells formed a continuous layer around mesenchymal cells. Fibronectin was also observed to accumulate at the furrows and the accumulation was observed to be more extensive in the mature somites (Fig 4.14A', A''). Therefore, in wild type embryos, somites with intersomitic furrows that accumulate fibronectin with time are detected. In *gullum*, groups of cells organised in the stereotypical somite architecture couldn't be discerned (Fig 4.14B). However, cells with columnar shape could be observed. These cells were found to be accompanied by fragmented furrows that accumulated fibronectin (Fig 4.14B', B''). The fragments were of variable length and shape and did not extend over the full width of the tissue. Thus, in *gullum*, recognisable somites are not formed. However, somite boundary fragments that accumulate fibronectin and that are associated with columnar cells are present.

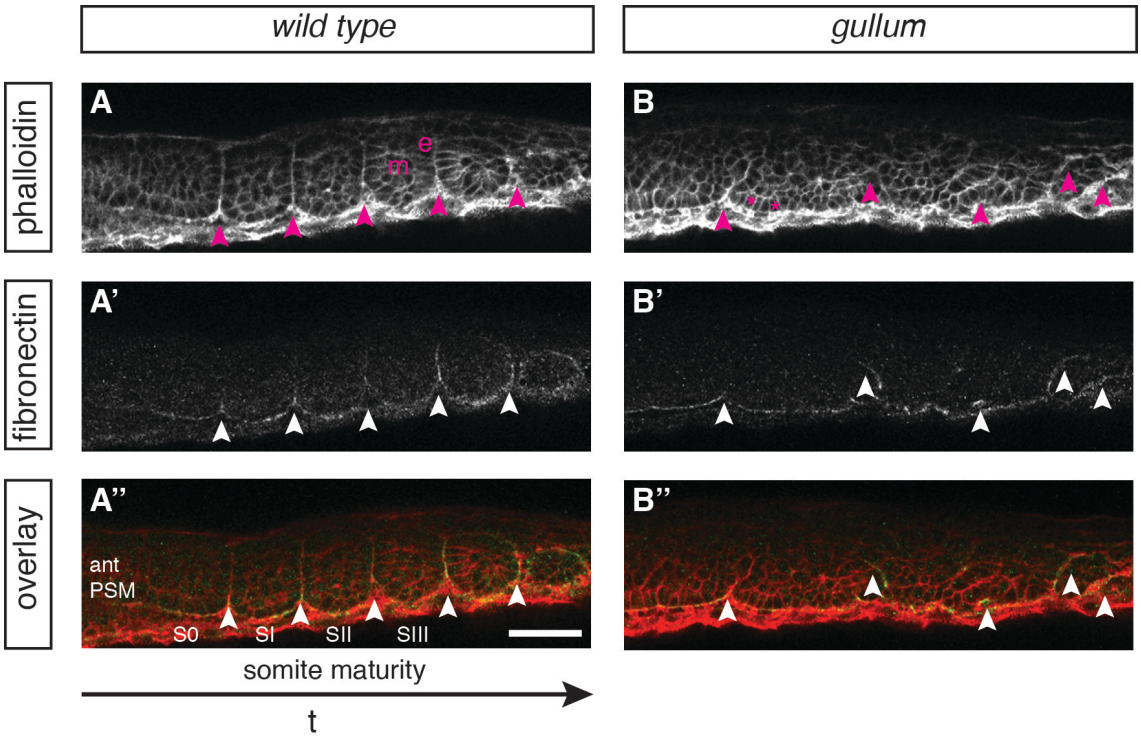

Figure 4.14 Fibronectin accumulation identifies the formation of fragmented somite boundaries in the *gullum* paraxial mesoderm.

Confocal slices from phalloidin and anti-fibronectin antibody co-stain performed to visualise cellular and boundary morphology of somites in 14-somite stage wild type and *gullum* siblings **(A – B")**. Anterior PSM to the left. Genotypes are as indicated.
(A) Wild type somites with an outer whorl of columnar cells (e) surrounding rounded cells (m) and separated by distinct boundaries (arrowheads) are observed. **(A' – A")** These boundaries accumulate fibronectin over time. S0 – forming somite, SI – most recently formed somite, SII, SIII – somites of increasing maturity. **(B)** Similar organisation of cells was not present in *gullum* (10/10). Columnar cells are observed in the paraxial mesoderm (asterisks), but lacking organisation reminiscent of somites. **(B' – B")** Boundary fragments (arrows) accumulate fibronectin. Scale bar 50 µm.

The results presented in this section suggest that the lack of segmental output from the segmentation clock leads to the disruption of segmental anterior-posterior polarity in the paraxial mesoderm. This likely results in the failure of *gullum* to differentiate periodic somites. However, the presence of groups of cells that express markers of anterior and posterior identity may lead to the formation of somite boundary fragments and the subsequent instigation of local MET events in the differentiated paraxial mesoderm.

4.4 Morphology of the embryonic musculature in *gullum* lacks wild type periodic organisation

Muscle precursors in zebrafish arise from two paraxial mesoderm cell populations – the adaxial cells and the posterior compartment of the somites. The adaxial cells are the earliest specified muscle precursors. These cells are initially columnar and are sandwiched between the notochord and somites. Hedgehog signalling from the notochord induces their differentiation into slow muscle precursors that elongate along the anterior-posterior axis and stack together, their length matching that of the somites (Barresi et al., 2001). This differentiation is sequential. As they migrate radially to the lateral edges of the body, they induce the elongation of rounded *myoD*+ precursors into fast muscle fibres (Henry and Amacher, 2004). In light of the disruption to the segmentation clock of *gullum*, the segmental organisation of the muscle precursors and the myotome that is derived from them was investigated.

4.4.1 Muscle precursors in *gullum* lack segmental organisation

Muscle precursors can be identified by their expression of *myoD* (Weinberg et al., 1996). *myoD* is expressed in the adaxial cells and segmentally in the somites. To determine if muscle precursors were specified and if they were periodically patterned in *gullum*, *in situ* hybridisation for *myoD* was performed in 30 10-somite stage *gullum* and wild type siblings (N = 2). *myoD* was expressed in the adaxial cells of both *gullum* and wild type (Fig 4.15A, B), but *myoD* positive cells in the *gullum* paraxial mesoderm lacked segmental organisation. Adaxial cells differentiate into slow muscle precursors that can be identified by the change in their cellular morphology from cuboidal to elongated. This cell shape change was observed by means of phalloidin staining for F-actin in mid-somitogenesis stage wild type and *gullum* embryos (Fig 4.15C, D; 10 per genotype, N = 2).

A subset of these elongating precursors express *engrailed2a* (*en2a*) and this group is the muscle pioneers (Hatta et al., 1991; Rost et al., 2014). *In situ* hybridisation for *en2a* in 30 19-somite stage wild type and *gullum* siblings (N = 2) revealed the presence of muscle pioneers in both (Fig 4.15E – F'). In wild type embryos, these muscle pioneers

were observed to be bilaterally metameric, whereas in *gullum* the bilaterally symmetric arrangement of the muscle pioneers was lost (Fig 4.15E', F'). These results suggest that while muscle precursor specification and their differentiation is unaffected in *gullum,* they are not periodically patterned.

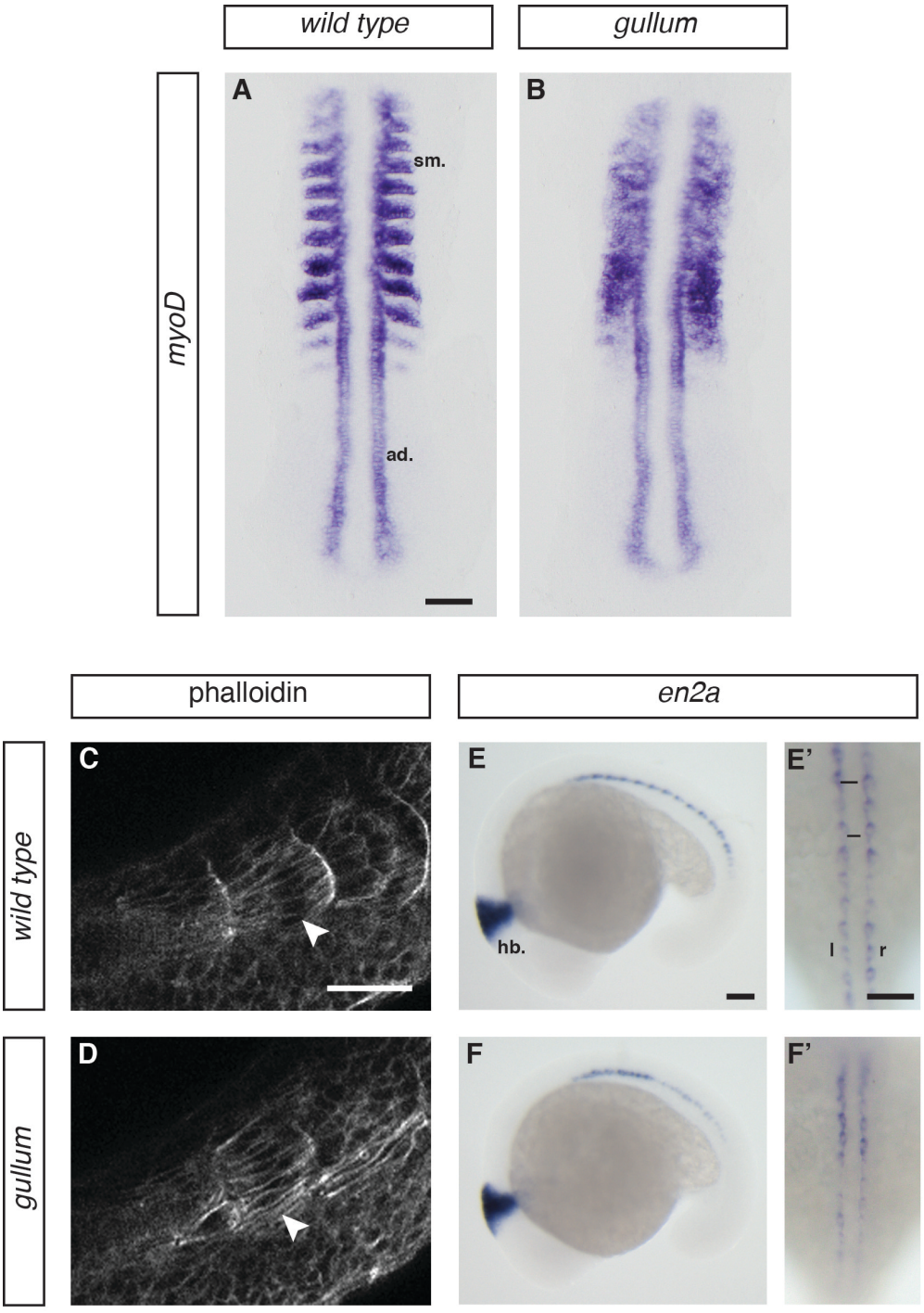

Figure 4.15 Muscle precursors are specified in *gullum*, but without segmental arrangement.

In situ hybridisation for muscle precursor marker *myoD* in 10-somite stage embryos **(A, B)**. Anterior to the top. Confocal slice of phalloidin staining showing slow muscle precursors in 14-somite stage embryos **(C, D)**. *In situ* hybridisation for muscle pioneer marker *en2a* **(E, F** lateral views; **E', F'** dorsal views**)** in 19-somite stage embryos. Embryos are wild type and *gullum* siblings, genotypes are as indicated.
(A) *myoD* is expressed by the adaxial (ad) cells and the posterior compartment of the somites (sm) in wild type. **(B)** *myoD*+ adaxial cells are also present in *gullum*. The differentiated paraxial mesoderm expresses *myoD*, but not segmentally (30/30). **(C)** Adaxial cells elongate and stack along the notochord in wild type. **(D)** This is observed in *gullum* as well (10/10). **(E, E')** *en2a* positive muscle pioneers have a bilaterally symmetric (indicated by the black lines) periodic arrangement in wild type. **(F, F')** Muscle pioneers are present in *gullum*, but pioneers on left and right sides are not in segmental register (30/30). hb – hindbrain, l – left, r- right. Scale bars 100 μm (A, B, E – F'), 50 μm (C, D).

4.4.2 The myotome of *gullum* has disrupted periodicity

Muscle precursors give rise to the muscle fibres of the myotome. The slow muscle precursors migrate and differentiate into a superficial layer of slow twitch fibres. The fast muscle precursors differentiate into the fast twitch fibres located medially (Devoto et al., 1996). These fibres are organised as parallel bundles in the myotome that are periodically re-iterated along the body axis. This arrangement was visualised by means of the muscle boundary junction marker *xirp2a*, described earlier in this chapter (Fig 4.2).

The morphology of the myotome boundary junctions indicated that myotome morphology in *gullum* is defective. This could be explained by the following possibilities: 1. fibres have wild type morphology and length scale, but are misaligned along the body axes 2. fibres have wild type morphology, but do not have a wild type length scale 3. fibres do not have wild type morphology. To explore these possibilities, phalloidin staining for F-actin and slow muscle myosin antibody staining was used to visualise fast fibres and slow fibres respectively in 36 hpf wild type and *gullum* embryos. In wild type, muscle fibres were arranged in the characteristic chevron shape of the myotome (Fig 4.16A, 4.17A**)**. In *gullum*, the myotome boundary junctions were disrupted (Fig 4.16B, 4.17B, B'**)**. However, the extent of disruption to the chevron-shaped morphology was variable. This might be due to a morphogenetic effect caused by the elongating slow muscle fibres (Henry et al., 2005; van Eeden et al., 1998).

The muscle fibres were comparable to wild type in that the bundles were straight and oriented parallel to each other, but the fibre length was variable (Fig 4.16C, D and 4.17C**)**. However, the length distributions along both the rostrocaudal and mediolateral axes did not differ from each other in a statistically significant manner (Mediolateral distribution of fast fibre length – Mann Whitney U = 230, n_1 = 28, n_2 = 24, P = 0.052, two-tailed. Rostrocaudal distribution of fast fibre lengths – Mann Whitney U = 5329, n_1 = 101, n_2 = 110, $P \sim 0.61$, two-tailed. Distribution of slow fibre lengths – 'Mann Whitney U = 1732, $n_1 = n_2 = 64$, P = 0.13, two-tailed). The alignment of fibres, interpreted from the muscle boundary junctions, was altered in the mediolateral.

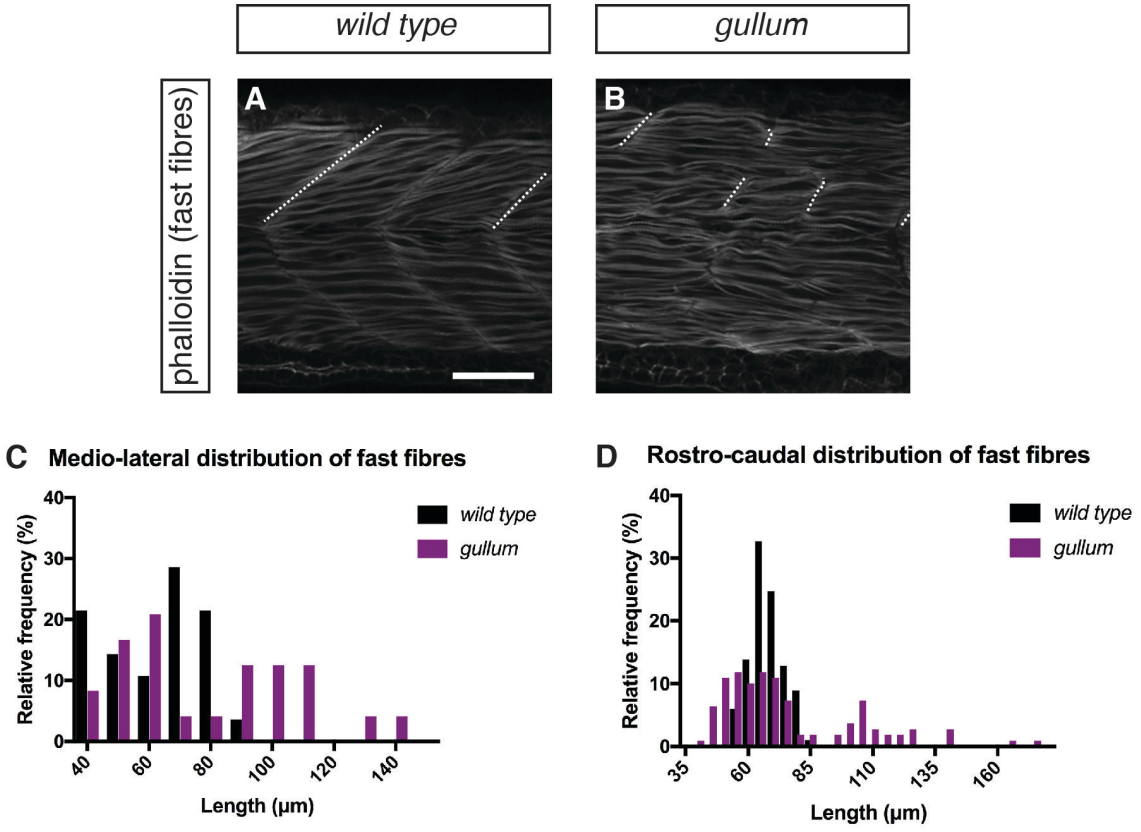

Figure 4.16 Fast fibres of the *gullum* myotome lack clear segmental organisation.

Confocal slices of phalloidin staining for F-actin in fast twitch fibres from the trunk **(A, B)** in 36 hpf sibling wild type and *gullum* embryos. Segments shown here correspond to 14 – 17 in wild type. Distribution of fast fibre lengths in a single segment along the mediolateral axis **(C).** Distribution of fast fibre lengths along the trunk at a single depth **(D)**. Measurements made from 4 embryos for each genotype.
(A) Wild type fast fibres are straight bundles, oriented parallel and connect to 2 consecutive myotome boundary junctions (dotted line). **(B)** Fast muscle fibres in the *gullum* myotome are similar

to wild type, but variable in length and connect between 2 boundary fragments (dotted line). **(C – D)** The distribution of fast fibre lengths in the trunk of the *gullum* embryos is wider than wild type along the mediolateral and rostrocaudal axes. There is no significant difference between the wild type and *gullum* fibre length distributions. Mediolateral distribution – Mann Whitney U =230, n_1 =28, n_2 = 24, P = 0.052, two-tailed. Rostrocaudal distribution – Mann Whitney U = 5329, n_1 = 101, n_2 = 110, P ~ 0.61, two-tailed. Scale bar 50 μm.

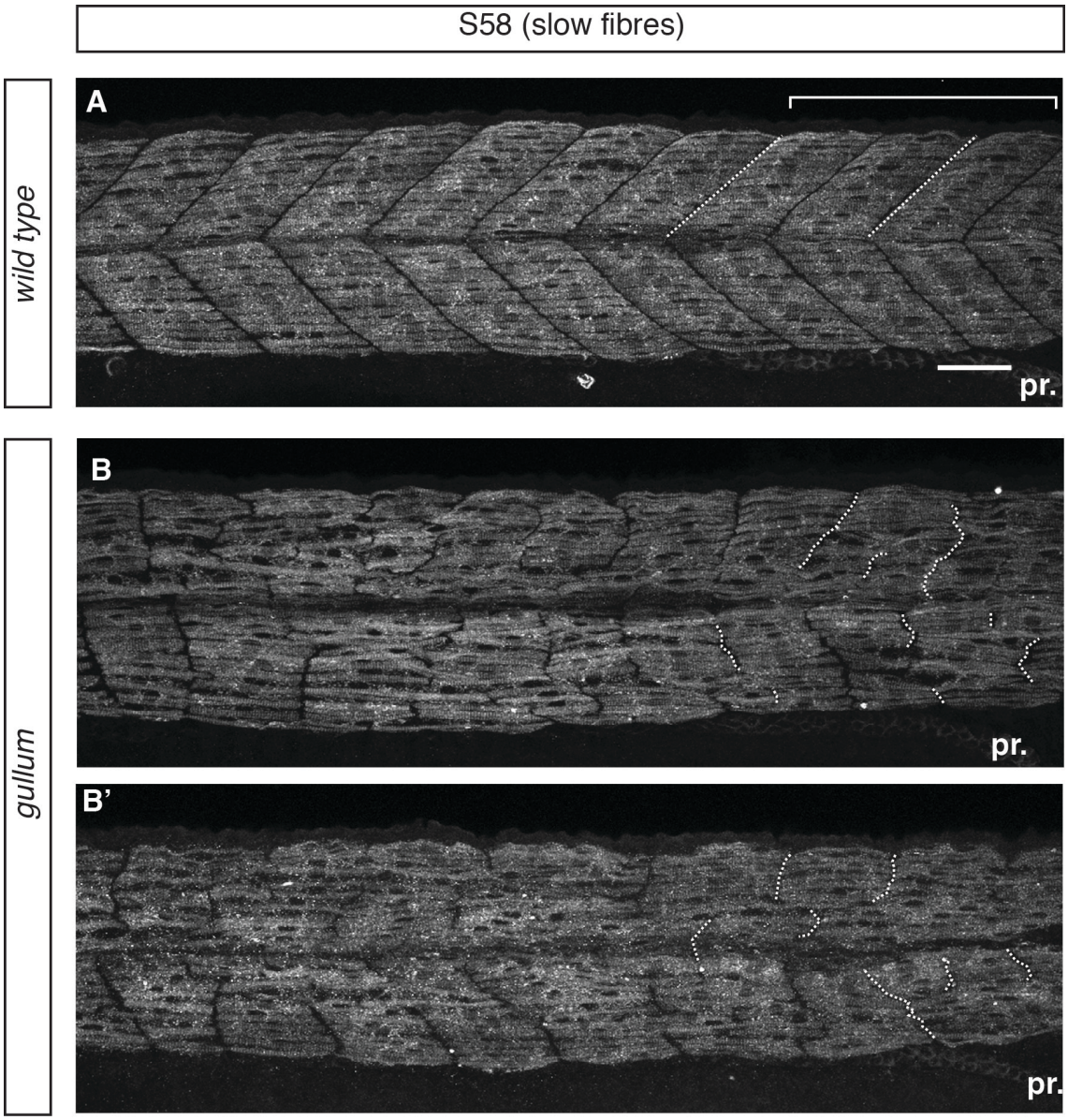
S58 (slow fibres)
wild type
gullum
A
B
B'
pr.
pr.
pr.
C
Distribution of slow fibres
wild type
gullum
Relative frequency (%)
60
40
20
0
35
60
85
110
135
Length (µm)

Figure 4.17 Segmental organisation of the slow fibres of the *gullum* myotome is disrupted.

Z-projection of confocal stacks of slow muscle myosin (S58) antibody stain for slow twitch fibres **(A – B')** in 36 hpf sibling wild type and *gullum* embryos. Segments from the trunk, corresponding to 8 – 17 in wild type, are shown, anterior to the left. Distribution of slow fibre lengths **(C)**. Measurements made from 4 embryos for each genotype in the area (corresponding to segments 14 – 17 of wildtype) indicated by the white bracket in (A).
(A) Wild type slow muscle fibres are straight and parallel to each other, and connect between 2 myotome boundaries (dotted line). **(B – B')** Slow fibres have variable length but retain their parallel orientation. Fragmented myotome boundaries indicated with dotted lines. **(C)** The distribution of slow fibres lengths is wider than wild type, but not in a statistically significant manner (Mann Whitney U = 1732, $n_1 = n_2 = 64$, $P = 0.13$, two-tailed). pr. – proctodeum. Scale bar 50 μm.

Therefore, the altered myotome morphology is not caused by a gross change in the morphology of the muscle fibres themselves. The misalignment of fibres along the body axes and the variable fibre length scale, along with the disrupted morphology of myotome boundary junction probably contribute to the final myotome morphology observed in *gullum*. The influence of the fibres on myotome boundary junction morphology and vice-versa in wild type and segmentation mutants remains unclear in the literature. Further analysis is necessary to determine how the two influence the myotome morphology observed in *gullum*.

In summary, *gullum* has been determined to have a disrupted segmentation clock and the segmental pattern of the *gullum* myotome is disrupted. A role for cryptic sources of pattern, such as the elongation of the muscle pioneers or the elongated morphology of the muscle fibres, cannot be ruled out. However, given the extent of disruption to myotome pattern in *gullum*, it can be concluded that the development of the segmental myotome is dependent on the patterning output of the segmentation clock.

Chapter 5. The segmentation clock does not instruct axial segmentation in zebrafish

5.1 Background

The current model of vertebral patterning in amniotes proposes that the segmentation clock is the major source of patterning information. The consensus is that sclerotomal derivatives form the individual centra and arches of the spinal column, via the formation of periodic somites. However, although somitogenesis is similar across vertebrate classes, whether the cellular lineages and mechanism of segmental patterning of the centra are homologous remains unclear (Fleming et al., 2015).

In all tetrapods and in some fish, centra arise initially as perichondral centrums i.e. ossifying external to and around the notochord. Osteoblasts, the cells that provide this mineralizing activity, are characterized by the expression of *osterix* (*osx*) and are of sclerotomal, and therefore, somitic origin (Fleming et al., 2015). In zebrafish and other teleost species of fish, however, centrum development begins as chordacentra – ossification begins directly within the notochord sheath cells, the perichondral centrum forming later in development. It has been proposed that in the teleosts zebrafish (Fleming et al., 2004) and salmon (Grotmol et al., 2003; Wang et al., 2013), the notochord, and not the sclerotome, is the initial source of bone matrix for chordacentra formation. In contrast, in medaka, sclerotome derived osteoblasts, that are located external to the notochord, have been suggested as the main drivers of chordacentrum formation (Inohaya et al., 2007; Renn et al., 2013).

Having established that *gullum* has a disrupted segmentation clock, it was investigated if disrupting somitogenesis also results in the failure to generate the serial anatomy of the vertebral column. The analyses presented in this chapter focuses on the development of the axial skeleton in *gullum*. The somitogenesis mutants *fss* and *fss;gullum* were included to explicitly test the hypothesis that the activity of the segmentation clock in the PSM, even when restricted to the posterior PSM, is sufficient to generate a periodic vertebral column. Fig 5.6J – M' presents data from collaborator Laura Lleras Forero.

5.2 *gullum* makes a periodic vertebral column

The bone precursors arising from the somites are called the sclerotome. These cells migrate from their ventromedial position in the somite to surround the notochord. Arches of the vertebrae are thought to have a sclerotomal origin (Fleming et al., 2015; Spoorendonk et al., 2008; Yasutake et al., 2004) in fish. However, their contribution to the centra is less clear. Centrum development in zebrafish begins as chordacentra – rings of ossification within the notochord sheath, the epithelium that surrounds the notochord (Fleming et al., 2015) and the embryonic origin of the cells that are responsible for the ossification of the chordacentrum is disputed in the literature (Fleming et al., 2004; Inohaya et al., 2007). To understand the consequence of a non-dynamic segmentation clock, analyses of the sclerotome, the vertebrae and the chordacentra of *gullum* were undertaken.

5.2.1 *gullum* does not have a segmentally patterned sclerotome, but its axial skeleton is periodically organised

Sclerotome can be identified by the expression of marker *twist2* (previously *zebrafish twist*) (Germanguz et al., 2007; Morin-Kensicki and Eisen, 1997; Oates et al., 2005a). To analyse the segmental pattern of the sclerotome, *in situ* hybridisation for *twist2* was performed in *gullum* mutant and wild type littermates at the 19-somite stage. To determine if the vertebral column had segmental architecture, 21 days post fertilization (dpf) wild type and *gullum* mutant fry were cleared and stained with alizarin red. Wild type embryos showed bilaterally symmetric segmental stripes of *twist2* staining (Fig 5.1A, A'), but similar organisation was not observed in *gullum* (Fig 5.1B, B'), suggesting that the sclerotome that differentiates in *gullum* has not been segmentally patterned. Strikingly, the vertebral column of *gullum* was organised as periodic and distinct vertebrae, like wild type (Fig 5.1C, D).

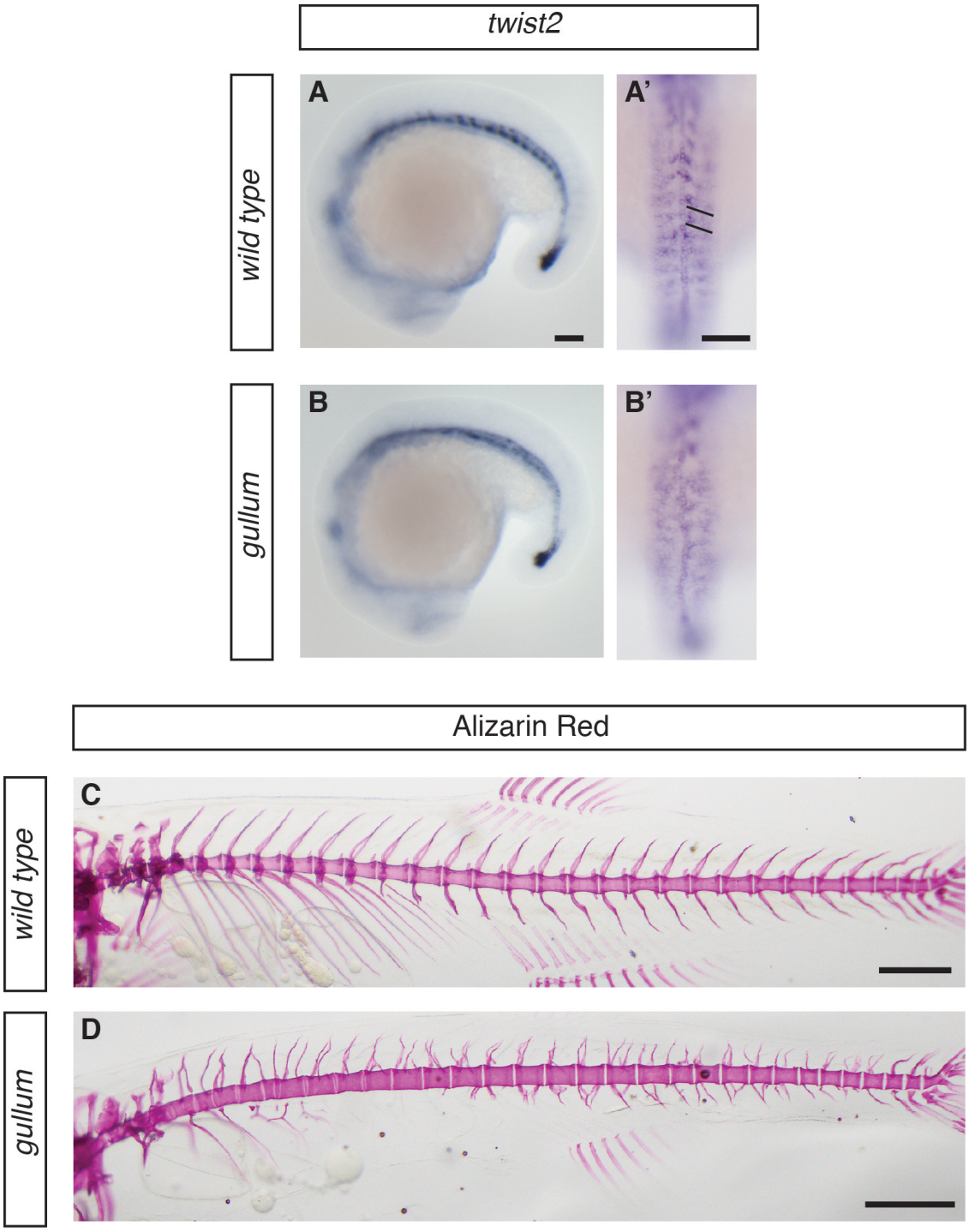

Figure 5.1 The *gullum* sclerotome lacks segmental organisation, but the vertebral column is periodic.

In situ hybridisation for sclerotome marker *twist2* in 19-somite stage wild type and *gullum* siblings **(A – B')** and alizarin red bone preparations of 21 dpf wild type and *gullum* larvae **(C, D)**. A, B are lateral views, head oriented towards the left, A; B' are dorsal views, anterior to the top. C, D are lateral views, head (not in view) towards the left.
(A, A') *twist2*+ cells are organised segmentally in wild type. Black line in B' indicates the organisation. **(B, B')** In *gullum*, these cells do not have segmental arrangement. **(C)** Wild type larvae

have periodic vertebrae in the vertebral column. **(D)** The *gullum* vertebral column also has periodic vertebrae. Scale bar 100 μm in A-D', 500 μm in C, D.

The neural and hemal arches in *gullum* showed abnormalities (Fig 5.2B – B''). In wild type adults, hemal and neural arches were present on the anterior of the vertebrae (Fig 5.2A), were always bilaterally paired and the pair fused medially. In *gullum* adults they were either 1. entirely absent 2. not consistently in pairs 3. not consistently fused 4. were ectopically present on the posterior of the centrum or 5. ectopically fused. Presence of arches on the anterior and posterior ends, on the left and right sides and on the dorsal and ventral regions of the centrum was scored. These scoring results are presented in Table 5.1.

There are 4 anterior positions and 4 posterior positions in the centrum, 2 left positions and 2 right positions, and 2 dorsal and 2 ventral positions. In wild type, arches were present on 100% of the anterior positions and on 0% of the posterior positions. Arches were present on 50% of the left positions and 50% of the right positions, and on 50% of the dorsal positions and 50% of the ventral positions. In *gullum*, arches were scored as being present on 84% of the anterior positions and 41% of the posterior positions, 65% of the left positions and 64% of the right, and on 60% of the dorsal positions and 66% of the ventral positions. These observations suggest that the precise positioning of the arches on the centra is lost. However, it is difficult to extrapolate this finding to disorder in the segmental pattern of the sclerotome as zebrafish sclerotome migration is consistent with leaky resegmentation (Morin-Kensicki et al., 2002).

Genotype	Anterior				Posterior			
	Dorsal		Ventral		Dorsal		Ventral	
	Left	Right	Left	Right	Left	Right	Left	Right
wild type	54/54	54/54	54/54	54/54	0/54	0/54	0/54	0/54
gullum	53/59	52/59	47/59	47/59	14/59	22/59	31/59	31/59

Scoring from caudal vertebrae of 4 109 dpf adults per genotype

Table 5.1 Positioning of neural and hemal arches in wild type and *gullum*

Analyses of the centra of wild type and *gullum* 21 dpf larvae revealed that although the vertebral column is periodic, it is not wild type. *gullum* has more vertebrae than wild type (30 vs. 28, Fig 5.2C, Welch corrected t (40) = 6.7, $P < 0.0001$, two-tailed). I

quantified the number of precaudal (rib-bearing) and caudal (hemal arch-bearing) vertebrae to determine if *gullum* was biased to make more of a certain type (Fig 5.2D, E). *gullum* had more precaudal (Fig 5.2D, Welch corrected t (39) = 3, $P = 0.004$, two-tailed) and caudal vertebrae (Fig 5.2E, Welch corrected t (37) = 3.8, $P = 0.0006$, two-tailed) than wild type. The lengths of the centra were also more variable in *gullum* and and fell in a wider distribution than wild type (Fig 5.2F, Mann Whitney U = 125740, $n_{wt} = 529$, $n_g = 581$, $P < 0.0001$), but on average were smaller (wild type – 0.031 ± 0.004, *gullum* – 0.0289 ± 0.006, mean ± SD normalised to notochord length, n = 21). Therefore, the vertebral column of *gullum* varies from wild type by having more centra of variable length. Additional vertebrae do not show an axial bias, as the additional centra can be either precaudal or caudal vertebrae.

Therefore, while the sclerotome does not show obvious segmental organisation, *gullum* still has a periodic vertebral column. The vertebral column however is not perfectly wild type – the positioning of the arches is erroneous and the number of vertebrae and their length varies from wild type.

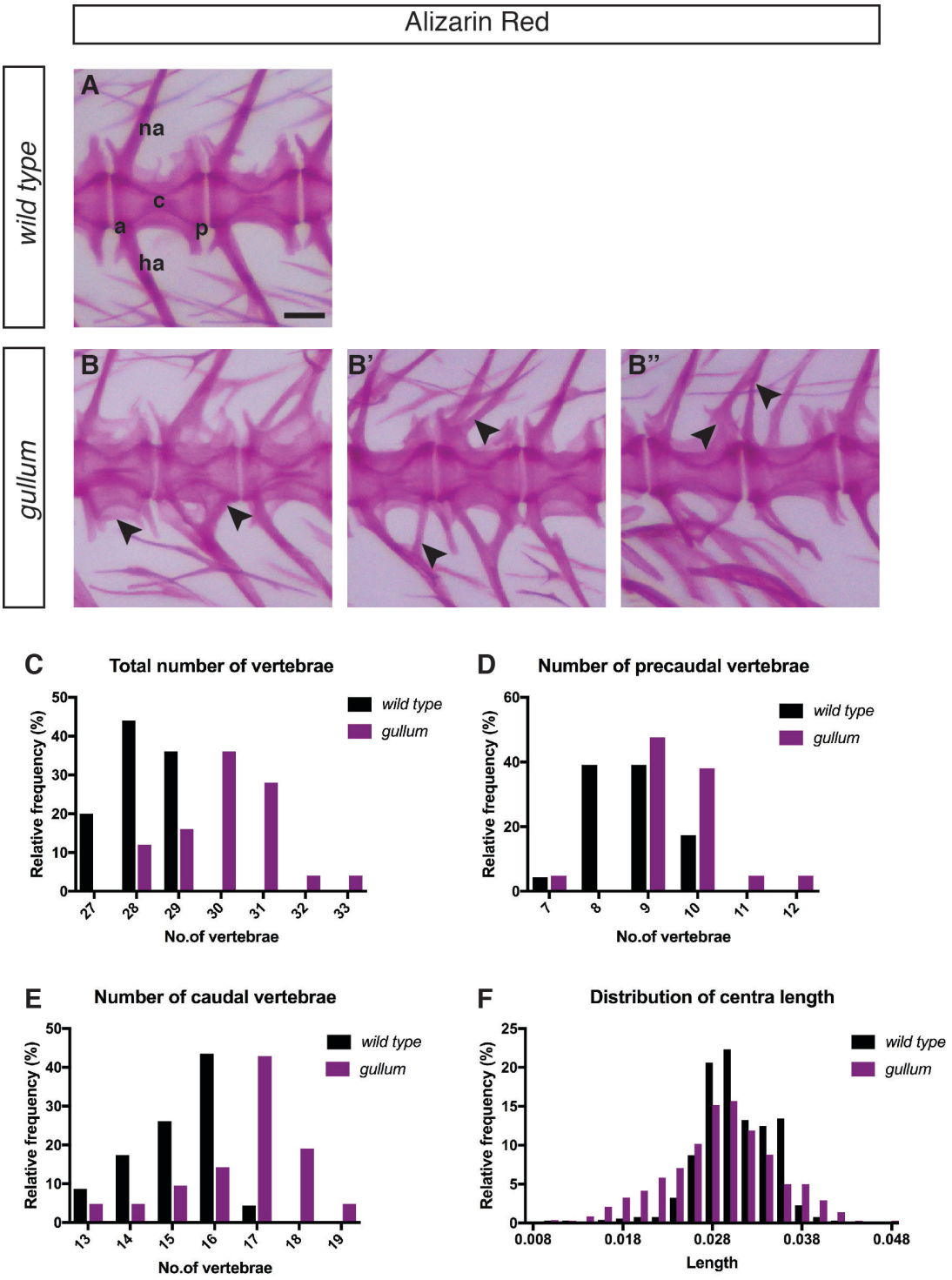

Figure 5.2 *gullum* vertebrae have abnormal and ectopic hemal and neural arches. *gullum* centra are periodic, but not wild type.

Snapshots of caudal vertebrae from alizarin red skeletal preparations of 109 dpf wildtype and *gullum* sibling adults **(A – B'')**. Distribution of total number of vertebrae **(C)**, the number of precaudal **(D)** and caudal vertebrae **(E)**, and the distribution of centrum length, normalised to notochord length **(F)** in wild type and *gullum* 6.2 – 7.4 mm standardised standard length (SSL) fry.

(A) Hemal (ha) and neural (na) arches are present on the anterior (a) end of centra (c) and never on the posterior (p) in wild type. In *gullum*, **(B)** arches can be absent, **(B')** are not strictly bilateral, (**B – B''**) can fail to fuse or fuse abnormally and can be present on the posterior end. Errors indicated with arrowheads in panels. **(C)** *gullum* have more vertebrae compared to wild type (Welch corrected t (40) = 6.7, $P < 0.0001$, two-tailed). **(D)** *gullum* have additional precaudal vertebrae (Welch corrected t (39) = 3, $P = 0.004$, two-tailed) and **(E)** additional caudal vertebrae (Welch corrected t (37) = 3.8, $P = 0.0006$, two-tailed). **(F)** Lengths of centra fall in a wider distribution in *gullum* than wild type (Mann Whitney U = 125740, $n_{wt} = 529$, $n_g = 581$, $P < 0.0001$). Measurements made in 21 larvae per genotype, pooled from 2 experiments. Scale bar 250 µm.

5.2.2 Chordacentra patterning in *gullum* is not generated by a clock-type mechanism

Having observed that the centra are periodic but not wild type, the pattern of the developing chordacentra in *gullum* was explored next. Chordacentra appear as rings of ossification around the notochord in a sequential order (Du et al., 2001). The process can be observed by means of calcein staining from 7 dpf onwards. Within each chordacentra, the calcification process is initiated laterally and then a ring is formed. This ring is then expanded anteriorly and posteriorly to form the centrum. Calcein staining was performed in 11 dpf wild type and *gullum* larvae. As body size is a more useful indicator of developmental progress than age during zebrafish postembryonic development, the system of standardised standard lengths (SSL) was adopted to stage the fry (Parichy et al., 2009). SSL was determined by measuring the standard length (the snout to tail distance) and the presence of developmental hallmarks – the onset of the ossification of fin rays and the angle of the notochord flexion in the tail. Developmental stages 4.5 mm SSL and 4.9 mm SSL were chosen for analysis.

Chordacentra development of five 4.9 mm SSL fry for wild type and *gullum* is summarised in Fig 5.3C. Wild type larvae at these stages had chordacentra in 55% (n = 12) and 65% (n = 5) of the notochord respectively. The average numbers of chordacentra present were 16 and 21 chordacentra respectively. The length of the chordacentrum varied sequentially – longer rings were present more rostrally and shorter rings more caudally. Lateral ossification initiation was seen in caudal positions of the body axis (Fig 5.3A). Chordacentra development in *gullum* was not as stereotypical as wild type. *gullum* larvae on average segmented less of their notochord (33%, n = 12 and 58%, n = 5) and had fewer chordacentra (7 and 16 respectively). The

intervertebral spaces between rings were variable. Atypically large spaces were observed between consecutive chordacentra at random positions in the *gullum* notochord (Fig 5.3B, B'). Furthermore, the sequential dependency of the length of chordacentra seemed to be lost in *gullum* – short rings and lateral ossification initiations could be seen in rostral positions, even when more caudal rings had been initiated or were forming (Fig 5.3B', B"). These short rings were interpreted to represent an earlier stage of chordacentrum development, indicating that *gullum* axial segmentation does not follow a strict head to tail schedule for segment formation. This is in contrast to the differentiation of the *gullum* paraxial mesoderm where segment defects are observed to occur sequentially (Fig 4.4). Thus, chordacentra development seems to be error-prone in *gullum* and not compatible with a clock-type mechanism.

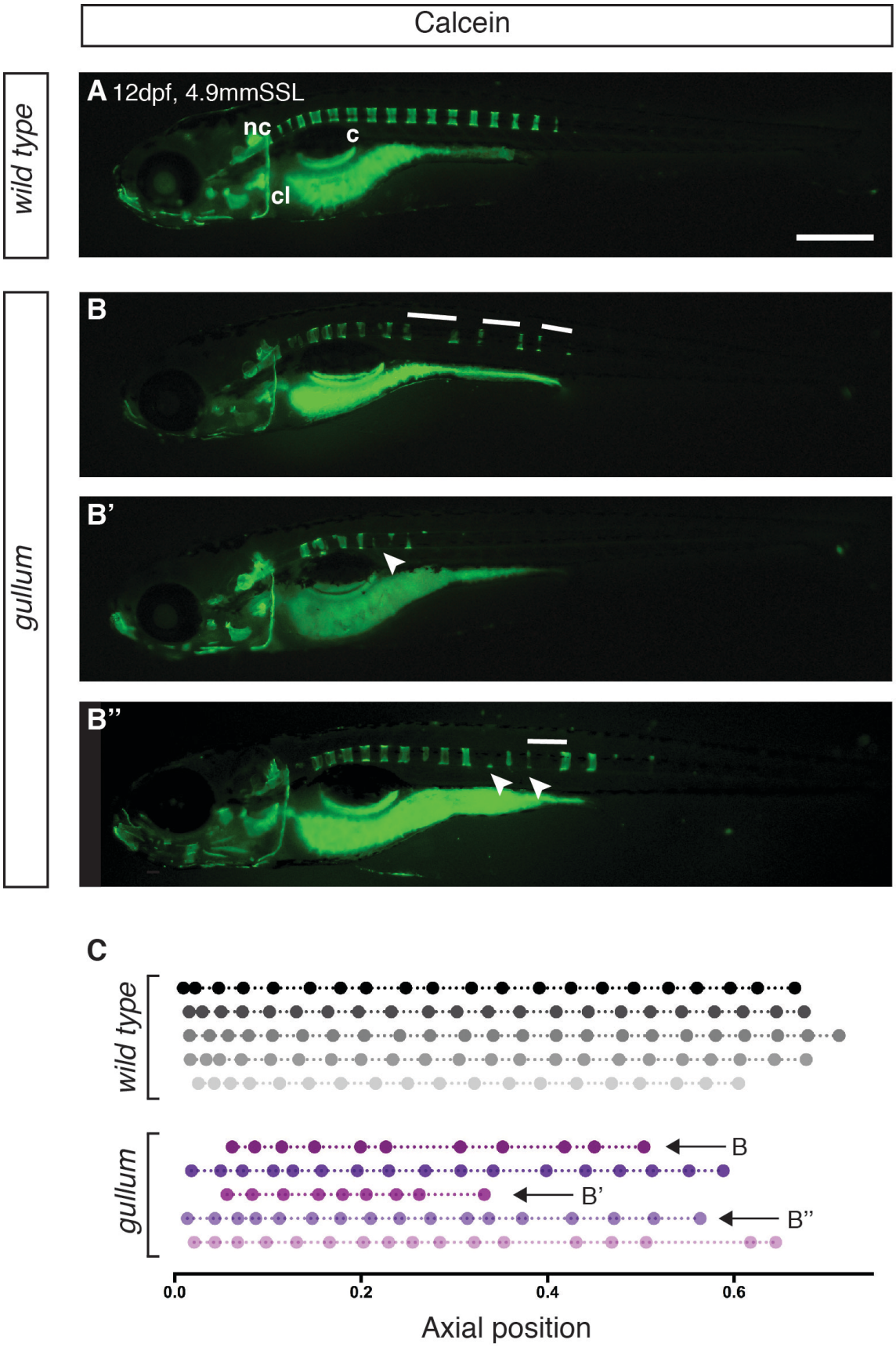
Calcein
wild type
A 12dpf, 4.9mmSSL
nc
c
cl
gullum
B
B'
B''
C
wild type
gullum
B
B'
B''
0.0
0.2
0.4
0.6
Axial position

Figure 5.3 Chordacentrum development is error-prone in *gullum*.

Chordacentra visualised by calcein staining in 4.9 mm SSL wild type and *gullum* fry **(A - B")** Lateral views, head oriented to the left. Graphical representation of chordacentrum positioning along the notochord in 5 4.9 mm SSL fish as beads on a string. Positions in the notochord were measured from the cleithrum (cl) and normalised to total notochord length **(C).**
(A) Chordacentra (c) are observed as regularly spaced rings along the notochord, thinner rings occurring in more caudal positions in wild type. **(B – B")** Irregular spacing of chordacentra is observed in *gullum* (white bars), thin rings of ossification can be observed more rostrally than seen in wild type (arrowheads). **(C)** Wild type embryos have a comparable number of chordacentra and a comparable extent of the notochord is segmented. *gullum* larvae have variable number of chordacentra that lack regular spacing and a variable extent of the notochord is segmented at the same developmental stage. Scale bar 500 µm.

5.2.3 Segmentation clock factors are not expressed in the *gullum* notochord

The observation of periodic centra and non-clock type errors in *gullum* chordacentrum patterning supports a role for the notochord in establishing the metameric vertebral column. However, this does not preclude the possibility that the segmentation clock functions directly in the notochord to establish segmental pattern. Therefore, to formally rule out this possibility the expression of clock factors in the notochord was analysed. Segmentation clock genes are not expressed in the notochord during somitogenesis (Fig 4.7, 4.8, 4.9), ruling out the early pre-patterning of the notochord by the segmentation clock. To investigate the possibility of a late function for the segmentation clock in notochord patterning, *Looping1* embryos were imaged at 5 dpf, before the onset of chordacentrum formation. *Looping1* embryos were not imaged at later stages, as time-lapse experiments on regulated animals were not included in our project license. No *her1::YFP* expression could be detected in the notochord (Fig 5.6B), suggesting that the core pace-keeping circuit of the segmentation clock is not active in the notochord at this late stage. This supports the hypothesis that a segmentation mechanism intrinsic to the notochord and distinct from the segmentation clock is responsible for the axial pattern in zebrafish. This hypothesis was explored further by analysing the axial phenotype of segmentation clock mutants *fss* and the triple mutant *fss;gullum (tbx6;her1;her7).*

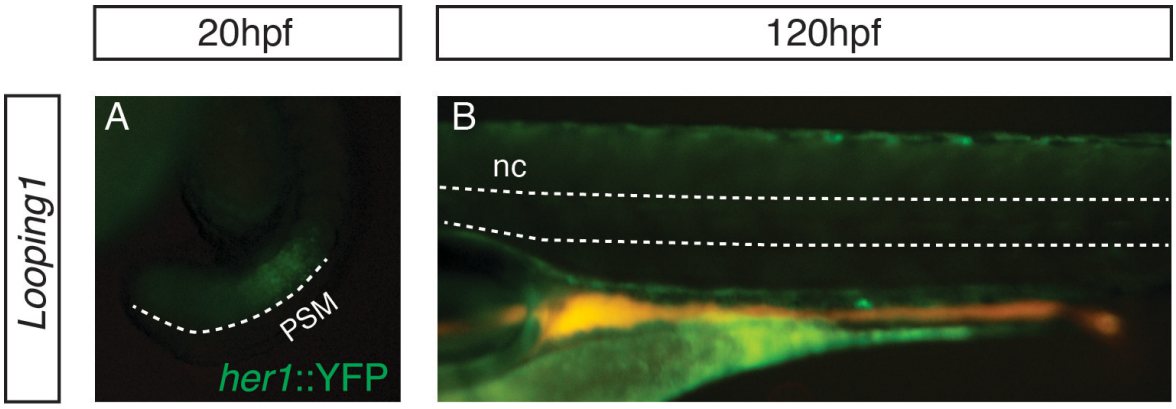

Figure 5.4 Her1-YFP is not detected in the notochord.

her1::YFP expression in a 20 hpf *Looping1* embryo **(A)** and a 120 hpf *Looping1* embryo **(B)**. Lateral views. Tailbud to the bottom left in (A), head (not shown) to the left in (B).
(A) Fluorescent signal of *her1::YFP* is seen in the PSM (white line) during somitogenesis. **(B)** No *her1::YFP* signal is detected in the notochord (nc, white lines).

5.3 Serial axial anatomy in the absence of somitogenesis

5.3.1 A functional segmentation clock in the paraxial mesoderm is not necessary for the development of periodic axial structures

gullum and fss have disrupted segmentation clocks - the former has non-dynamic cyclic gene expression in the PSM and makes disordered output in the anterior PSM while the latter has oscillating cyclic gene expression in the posterior PSM, but no segmentation output at the anterior end of the tissue. The allelic combination, *fss;gullum* was expected to have an additive phenotype. To characterize the disruption to the segmentation clock and the periodic pattern of the paraxial mesoderm in *fss* and *fss;gullum*, *in situ* hybridisations for segmentation clock markers – cyclic genes *her1* and *her7*, their downstream target *deltaC* and segmental output marker *mespb* were performed in 10-somite stage embryos and the morphology of the somite boundaries was analysed by bright field microscopy in *fss* and *fss;gullum* in 19-somite stage embryos. *fss* mutants were obtained from synchronous heterozygous *fss* pairings and the siblings that did not have a phenotype have been presented as wild type here. *fss;gullum* embryos were obtained from synchronous heterozygous *fss;gullum* matings. The Mendelian expectation of the triple mutant genotype from such a pairing was 6 in a 100. The *fss;gullum* embryos were identified by genotyping.

In keeping with published reports (Holley et al., 2000; Nikaido et al., 2002; Sawada et al., 2001; van Eeden et al., 1998), cyclic gene oscillations were observed to be restricted to the posterior PSM in *fss* (Fig 5.5B, B', E, E', H, H'**)**. *mespb* expression was not detected in the anterior PSM (Fig 5.5K). In *fss;gullum,* cyclic gene expression was detected in the posterior PSM, but was observed to lack oscillatory waves (Fig 5.5C, C', F, F', I, I') and no *mespb* (Fig 5.5L) expression was detected in the anterior PSM. Neither *fss* nor *fss;gullum* embryos had periodic somite boundaries (Fig 5.5N, O). Therefore, *fss* and *fss;gullum* have disrupted segmentation clocks, with *fss;gullum* representing the more severe disruption. However, the disruption to paraxial mesoderm pattern is similar – no somite boundaries were detected in either mutant.

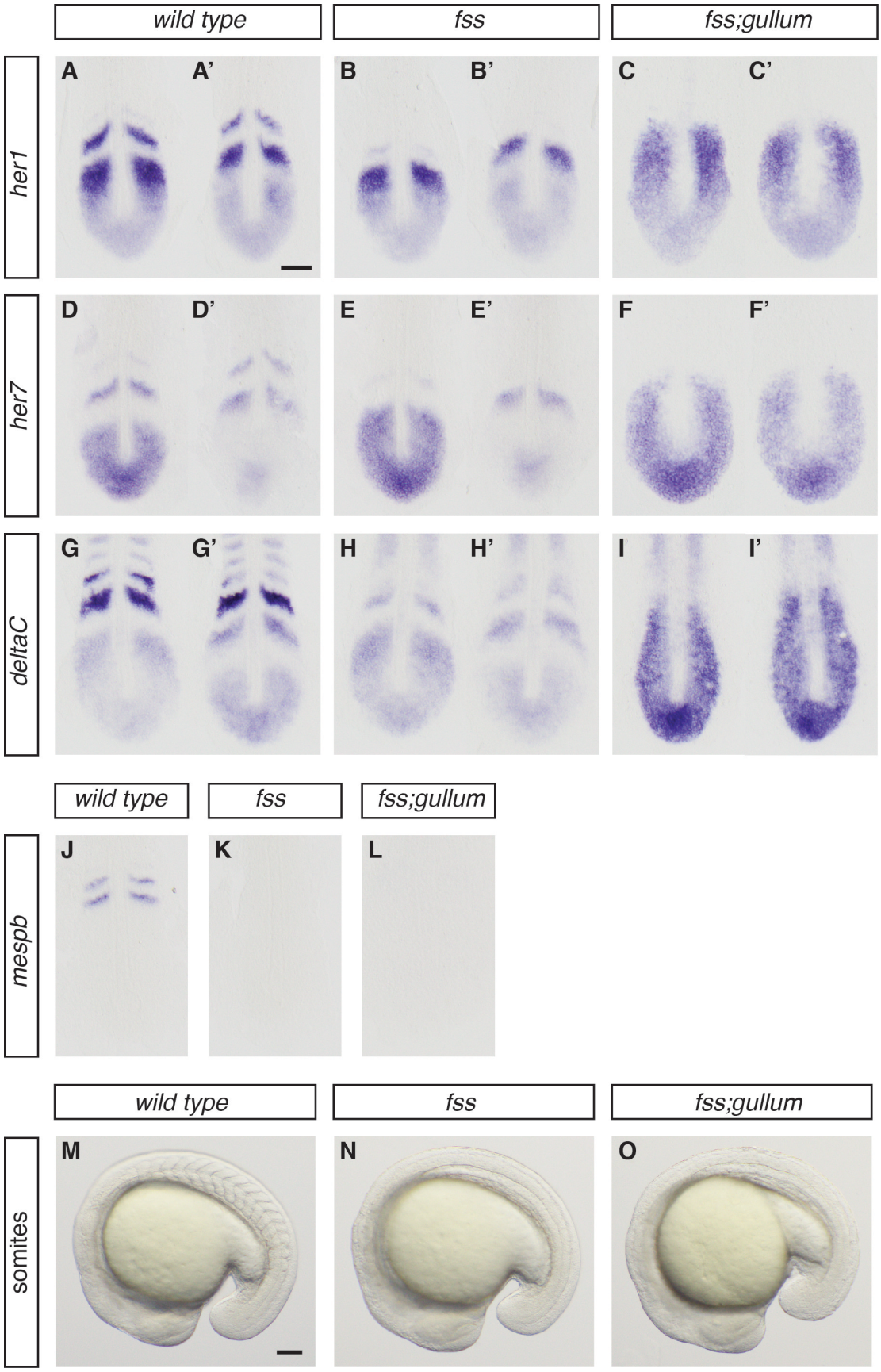
wild type
fss
fss;gullum
her1
her7
deltaC
mespb
somites
A
A'
B
B'
C
C'
D
D'
E
E'
F
F'
G
G'
H
H'
I
I'
J
K
L
M
N
O

Figure 5.5 The segmentation clock is disrupted in *fss* and *fss;gullum (fss;her1;her7) triple* mutants.

In situ hybridisations for segmentation clock markers *her1*, *her7* and *deltaC* **(A – I')** and for segmentation output marker *mespb* **(J – L)** in 10-somite stage wild type, *fss* and *fss;gullum* embryos. Dorsal views, anterior towards the top. Bright field images of 19-somite stage wild type, *fss* and *fss;gullum* embryos **(M – O)**. Lateral views, head oriented left. Genotypes are as indicated.
(A, A') Wild type *her1* wave patterns. **(B, B')** *her1* waves are restricted to the posterior PSM in *fss* (30/30). **(C, C')** *her1* expression is static and restricted to the posterior PSM in *fss;gullum* (5/5). **(D, D')** Wild type expression of *her7*. **(E, E')** Dynamic expression is restricted to *fss* posterior PSM (30/30), **(F, F')** *her7* expression is not dynamic and restricted to the posterior PSM in *fss;gullum* (5/5). **(G, G')** Dynamic expression of *deltaC* in wild type. **(H, H')** Dynamic expression is seen in the *fss posterior* PSM (30/30). **(I, I')** Static expression of *deltaC* is observed in the posterior PSM of *fss;gullum* (8/8). **(J)** Segmental stripes of *mespb* expression in wild type. **(K)** *fss* (30/30) and **(L)** *fss;gullum* lack *mespb* expression (5/5). **(M)** Somite boundaries are periodic in wild type. **(N)** *fss* (6/6) and **(O)** *fss;gullum* (3/3) lack somite boundaries. Scale bars 100 μm.

Analyses of the embryonic musculature at 36 hpf and the adult skeleton morphology were undertaken to assess the consequences of having an unsegmented paraxial mesoderm. Myotome boundary junctions were visualised by *in situ* hybridisation for *xirp2a* and bone was visualised by staining with alizarin red. All 3 somitogenesis mutants – *fss*, *gullum* and *fss;gullum* – analysed had disruptions to the myotome boundary morphology all along the body, but to differing degrees of severity (Fig 5.3E – H', graphical representation in I, 7.2). *fss* and *fss;gullum* resembled each other and had more severe disruptions to both somite boundary (Fig 5.3B, D) and myotome boundary junction morphology (Fig 5.3F, H) than *gullum* (Fig 5.3C, G). The vertebral columns of all 3 mutants, however, had periodic centra. Although defective centra were detected, the majority of the centra were well formed, being cleanly separated from neighboring centra and similar to wild type in their basic hourglass shape (Fig 5.3J – M'). These data demonstrate that periodic axial structures form despite strong disorder in the paraxial mesoderm pattern, and in the absence of a functional segmentation clock. Thus, the formation of periodic vertebrae in *fss* is not due to the presence of a dynamic segmentation clock in the posterior PSM.

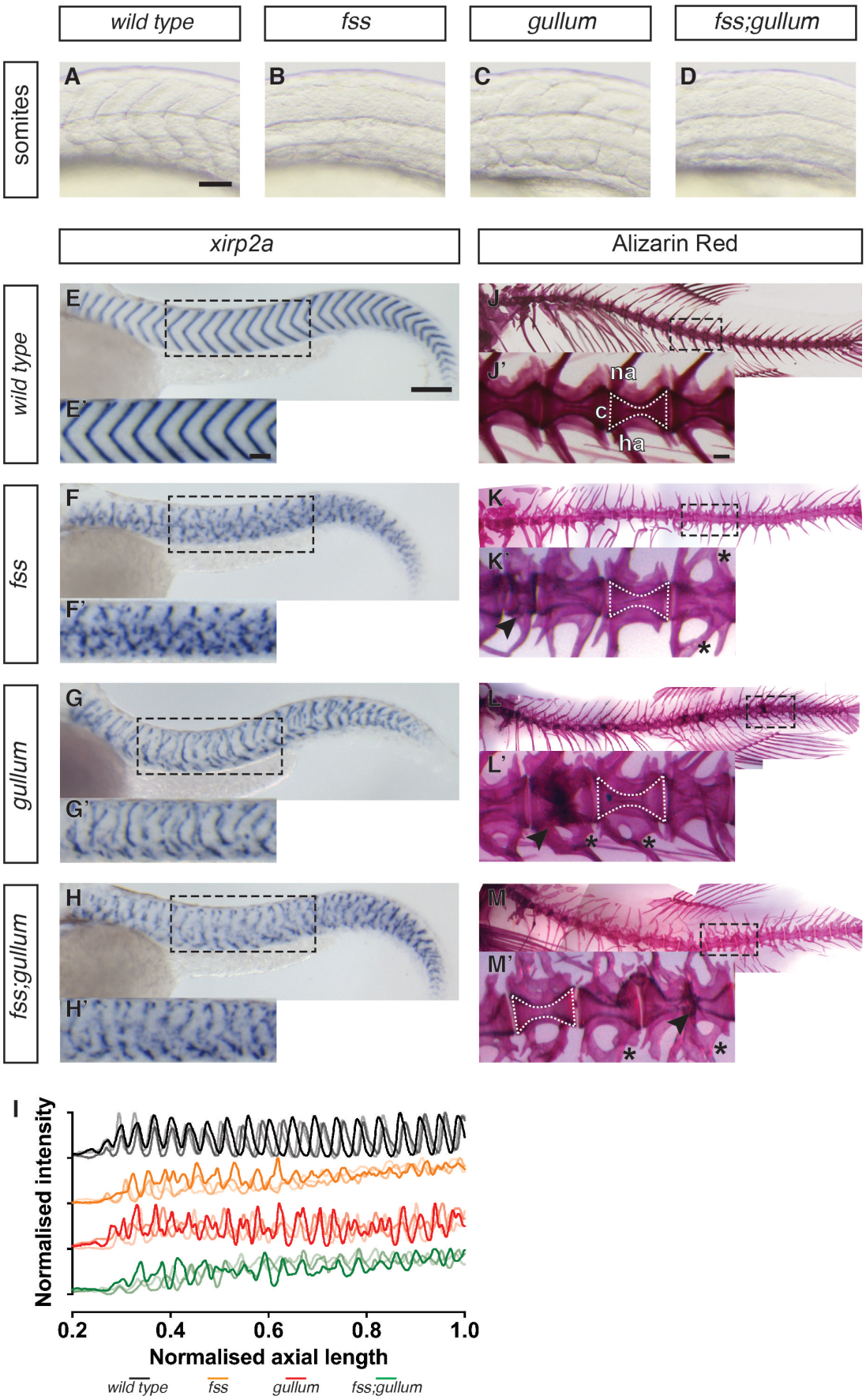
wild type
fss
gullum
fss;gullum
somites
A
B
C
D
xirp2a
Alizarin Red
wild type
E
E'
J
J'
na
c
ha
fss
F
F'
K
K'
gullum
G
G'
L
L'
fss;gullum
H
H'
M
M'
I
Normalised intensity
0.2
0.4
0.6
0.8
1.0
Normalised axial length
wild type
fss
gullum
fss;gullum

Figure 5.6 Myotome boundaries are disrupted in segmentation clock mutants but centra are still periodic.

Bright field images of boundaries in wild type*, fss, gullum* and *fss;gullum* **(A – D)**. *In situ* hybridisation for *xirp2a* in 40 hpf wild type*, fss, gullum* and *fss;gullum* embryos **(E – H')**. Graphical representation of the intensity *of xirp2a* staining along the body axis for 3 embryos per genotype **(I)**. Alizarin Red bone preparations of wild type*, fss, gullum* and *fss;gullum* 2 month – 8 month adults **(J – M')**. Lateral views, head oriented to the left.
(A) Periodic somite boundaries are observed in wild type, **(B)** no boundaries are observed in *fs*s, **(C)** boundary fragments are observed in *gullum* and **(D)** no boundaries are seen in *fss;gullum*. **(E, E')** Chevron-shaped myotome boundaries in wild type. Myotome boundaries are fragmented in **(F, F')** *fss* (12/12), **(G, G')** *gullum (*30/30*)* and **(H, H')** *fss;gullum* (7/7). **(I)** *gullum* has a milder myotome boundary phenotype compared to *fss* and *fss;gullum*. **(J, J')** Periodic centra in wild type (hour-glass shape outlined). **(K, K')** Centrum segmentation is normal in *fss*, but the neural and hemal arches are disordered (asterisk). Similarly, vertebrae of **(L, L')** *gullum* and **(M, M')** *fss;gullum* have normal centra and defective arches. Occasional defects occur in the centra, either seen as fusions of two vertebrae (arrowheads in L' and M'), or as smaller vertebrae (arrowhead in K'). na – neural arch, ha – hemal arch, c – centrum. Scale bars in A 50 µm, applies to A – D. Panels J – M' are data from Laura Lleras Forero. Scale bars in E and E' are 150 µm and 100 µm respectively and apply to E – H and E' – H' respectively. Scale bar in J' is 200 µm and applies to F' – M'.

In summary, the results presented in this chapter demonstrate that severe disruption to the segmentation clock does not result in severe disruption to the periodic pattern of the vertebral column. Centra of all 3 segmentation clock mutants analysed were distinct and the majority were well formed. This demonstrates that the segmentation clock is not required to generate the metamery of the vertebral column and the information necessary for axial pattern is provided by the notochord. Further more, the error-prone development of chordacentra in *gullum* suggests that this mechanism is not clock-type. However, the error-prone nature of gullum axial segmentation suggests that the segmentation of the paraxial mesoderm might have an influence on the axial patterning mechanism. By proposing such an interaction, the phenotype of segmentation clock mutant *hes6* that has fewer somites and correspondingly fewer vertebrae might be reconciled with the results presented in this chapter.

Work from collaborators that further demonstrators that the notochord indeed instructs vertebral column pattern is presented in the appendix (Fig 7.3 – 7.10) and a brief discussion of the work is included in the discussion of this thesis.

Chapter 6. Discussion

In the first part of this thesis I summarised preliminary results from experiments aimed to understand if RA has a role in zebrafish somitogenesis. The approaches adopted were the development of a fluorescently tagged *cyp26a1* for use as an RA signalling reporter and the evaluation of the somitogenesis of RA biosynthesis mutants. In the second part of the thesis the role of the segmentation clock in establishing segmental body pattern was evaluated. A novel segmentation clock mutant, *gullum*, was established and the segmentation clock was confirmed to be disrupted in the PSM by evaluation of the cyclic gene wave patterns by *in situ* hybridisation analyses. The myotome and sclerotome, which are segmentally patterned by the periodic activity of the segmentation clock in wild type, were also confirmed to lack overt segmental order. Despite this, the mutant had a periodic vertebral column, thus demonstrating that the segmentation clock does not instruct patterning of the centra.

The ability of the notochord to provide segmental pattern to chordacentrum development was explored together with collaborators Laura Lleras Forero, Stefan Schulte-Merker and Luis Morelli. This work forms the basis of a manuscript that has been submitted for publication. By means of a novel notochord segmentation reporter *entpd5:kaede*, the dynamics of sequential chordacentrum formation was studied in wild type and in somitogenesis mutants. The work proposes that the notochord is segmented by a reaction-diffusion mechanism that is independent of, but can be influenced by the pattern established by the segmentation clock.

I will begin this section by discussing some of the preliminary observations, and hypotheses that have been developed as a result, from the study of RA signalling in the zebrafish segmentation clock. I will then go on to discuss the segmentation of *gullum* and the clock-autonomous notochord segmentation mechanism.

6.1 The role of RA signalling in the segmentation clock

6.1.1 The transgenic *cyp26a1::venus* construct developed does not recapitulate endogenous *cyp26a1* expression

The signalling gradients of Wnt, FGF and RA are thought to be integral components of the segmentation clock, providing a positional information system for the translation of the dynamics of the clock into segmental pattern in the tissue. Understanding if RA does indeed provide this function, or any other function, in the zebrafish segmentation clock has been impeded by a lack of tools to visualise RA signalling in the PSM. Therefore, the development of a novel RA signalling reporter was undertaken. *cyp26a1* was chosen as the candidate for the RA signalling reporter on the basis of its expression in the tailbud during somitogenesis and due to it being a sensitive direct target of RA. I chose to develop a chimeric Cyp26a1 by fusing it with Venus so that in addition to visualising RA signalling events, I would also visualise the distribution and half-life of the Cyp26a1 protein. Cyp26a1 is the RA degradation enzyme and its distribution would indicate the extent of the tissue that is capable of degrading RA, therefore helping to identify the limit of the RA gradient in the PSM.

The expression of *cyp26a1* in the tailbud is thought to be established by the activity of T-box transcription factor Ta (Martin and Kimelman, 2010) and expression of *cyp26a1* in the somites is thought to be RA dependent (Dobbs-McAuliffe et al., 2004). T-box binding sequences and RA response elements (RAREs) are present in the 2.5 kb sequence upstream of the *cyp26a1* ATG site. This section was demonstrated to be sufficient to recapitulate both endogenous *cyp26a1* expression and its sensitivity to RA (Hu et al., 2008). Therefore, a transgenic Cyp26a1 that had a C-terminal Venus fusion and that was under the control of its endogenous upstream regulatory sequence was made and injected into wild type embryos. In the transgenic embryos that were identified, the endogenous expression of *cyp26a1* was not recapitulated. The transgene was not expressed in the tailbud but had ectopic expression in the somites. However, the transgene responded to exposure to exogenous RA and the upregulation of the transgene in the PSM was very similar to that of endogenous *cyp26a1*. This suggests that sequences necessary to modulate the response to RA are present in the regulatory

sequences included in the transgenic construct, while the regulatory sequences necessary to establish the basal expression of *cyp26a1* are missing from it. Therefore, contrary to the published reports, the 2.5 kb section of regulatory sequence is not sufficient for endogenous *cyp26a1* expression.

To develop a *cyp26a1* reporter, these additional regulatory sites will need to be identified. A good first strategy would be to scan for additional *t-box* sites in the vicinity of the *cyp26a1* gene. *t-box* gene *ta* is a Wnt target (Martin and Kimelman, 2008) and Wnts are expressed in the zebrafish tailbud (Thorpe et al., 2005). Therefore, it is possible that *cyp26a1* expression in the tailbud is regulated by Wnts and TCF binding sites that mediate Wnt regulation can be scanned for. If such sequences are found, these regulatory regions should be included in the transgenic molecule.

It appears that in the transgenic construct, the RA responsiveness of *cyp26a1* has been decoupled from its basal expression regulation. Therefore, an RA signalling reporter has been successfully developed. However, the fluorescence signal of the reporter in the transgenic founders identified was faint when compared to the fluorescence signal of the other transgenic lines that have been previously developed in the lab by BAC recombineering. This outcome may be linked to the potential bioactivity of the transgene – embryos that had higher copies of the transgene might have died due to insufficient RA for development. If this is the case, injecting the existing construct into *cyp26a1* mutant *gir* embryos will solve the issue of low signal to noise of the transgene. Alternatively, the construct can be redesigned such that it no longer has RA degradation ability.

If the proposed solutions do not yield a transgenic line in which RA signalling can be visualised, a new RA signalling reporter based on a different candidate will need to be developed. The expression of RA receptors *raraa* and *rarab* is RA dependent and *rarab* has been demonstrated to be RA inducible (Linville et al., 2009). *raraa* is expressed in the tailbud and *rarab* is expressed all through the paraxial mesoderm (Waxman and Yelon, 2007). Their suitability to be RA signalling reporters can be explored too.

6.1.2 RA biosynthesis mutants have somitogenesis phenotypes

Analyses of *aldh1a2* (*nof*) and *cyp26a1* (*gir*) somitogenesis show that RA has a role in the zebrafish segmentation clock. Low levels of RA in *nof* resulted in the formation of shorter somites while somitogenesis period was not affected. High levels of RA in *gir* were observed to cause the formation of longer somites and these embryos had a somitogenesis period that was slower than that of wild type (Fig 6.1D, E). This effect on somite length is, at first glance, in line with the proposed role of RA in the wavefront i.e. by perturbing the RA gradient in these mutants, the position of the threshold at which cells arrest their oscillations in the PSM is shifted causing the formation of longer or shorter somites. Less RA implies a shifting of the threshold towards the anterior of the PSM, resulting in the formation of shorter somites. Correspondingly, more RA implies the shifting of the threshold more posteriorly, resulting in the formation of longer somites. However, this simple interpretation is insufficient to explain the complex somitogenesis phenotype of these mutants – the effect on somite length is axially restricted to the somites of the rostral trunk and furthermore, *gir* appears to have a slower somitogenesis period.

Somite length is a compound parameter depending on the genetic oscillator period in the posterior PSM, the embryonic Doppler effect and the dynamic wavelength effect, in addition to the velocity of the wavefront (Jörg et al., 2015; Soroldoni et al., 2014). To begin to understand the somitogenesis phenotype of *gir*, the observables that contribute to each of the factors contributing to somite length were analyzed with the cyclic gene reporter *Looping1* in *gir*. There was no evidence to suggest that the posterior period had changed in *gir*, but the PSM shortening regime was altered and the cyclic gene wave pattern was changed. It is currently unclear whether these changes alone can explain the slower somitogenesis period and the long somite phenotype, but further experimentation to quantify these parameters might yield the answer.

6.1.3 RA and oscillator frequency

The altered phase profile observed in *gir* indicates that the oscillators are slowing their frequencies with a different profile across the tissue (Fig 6.1E). Strikingly, the oscillator

frequency begins to slow more posteriorly in the tissue than in wild type, suggesting that RA can interact with the cells of the posterior PSM, slowing their genetic oscillations. This observation provides strong support to the hypothesis that the positional information gradients of Wnt, FGF and RA bring about their opposing activity by modulating the frequency of the genetic oscillators (Aulehla and Pourquie, 2010; Aulehla et al., 2007; Sawada et al., 2001; Uriu et al., 2009). There is no current evidence to suggest that Wnt and RA signalling could directly affect the transcription of *her1* and *her7*, the core pace-keeping circuit cyclic genes. *t-box* genes, on the other hand, are possible candidate effectors of the positional information gradients –

1. *t-box* genes are expressed in overlapping domains in the PSM (Fig 6.1C). *ta* is expressed in the tailbud, *tbx16* in the tailbud and posterior PSM and *tbx6* in the anterior PSM (Fior et al., 2012). *tbx6* expression in the anterior is dependent on *tbx16* (Fior et al., 2012; Yabe and Takada, 2012), *tbx16* expression is dependent on *ta* (Garnett et al., 2009) and Wnts (Szeto and Kimelman, 2004; Thorpe et al., 2005), whose expression is regulated by *ta* (Amacher et al., 2002; Fior et al., 2012; Griffin et al., 1998; Morley et al., 2009).
2. RA can affect the expression of *t-box* gene *ta* (Fig 6.1F). The treatment of embryos with RA abolishes the *ta* expression domain and *gir* mutants have a smaller *ta* expression domain in the tailbud (Martin and Kimelman, 2010).
3. T-box binding motifs have been found in the regulatory regions of the segmentation clock genes *her1*, *her7* (Brend and Holley, 2009), *deltaC* (Jahangiri et al., 2012) and *deltaD* (Garnett et al., 2009). It is known that *her1* and *her7* are direct targets of T-box gene *tbx6* in the anterior PSM as their gene expression is lost in this region in the *tbx6* mutant *fss* (Holley et al., 2000; Nikaido et al., 2002).

Therefore, it is possible that excess RA modulates the frequency of the oscillations of *her1* and *her7* by affecting the expression of T-box gene *ta* (Fig 6.1E, F). Any effect on *ta* would also affect the expression of *tbx16* and *tbx6.* The first step to testing this hypothesis is to investigate the expression of *tbx16* and *tbx6* in the *gir* PSM and determine if their domains of expression are altered in the PSM. The expectation would be that the *tbx16* and *tbx6* expression domains have expanded posteriorly in *gir* (Fig

6.1F). Such an observation would be strong support for the hypothesis that the *t-box* genes modulate the dynamics of the segmentation clock and would motivate further experimentation along this line.

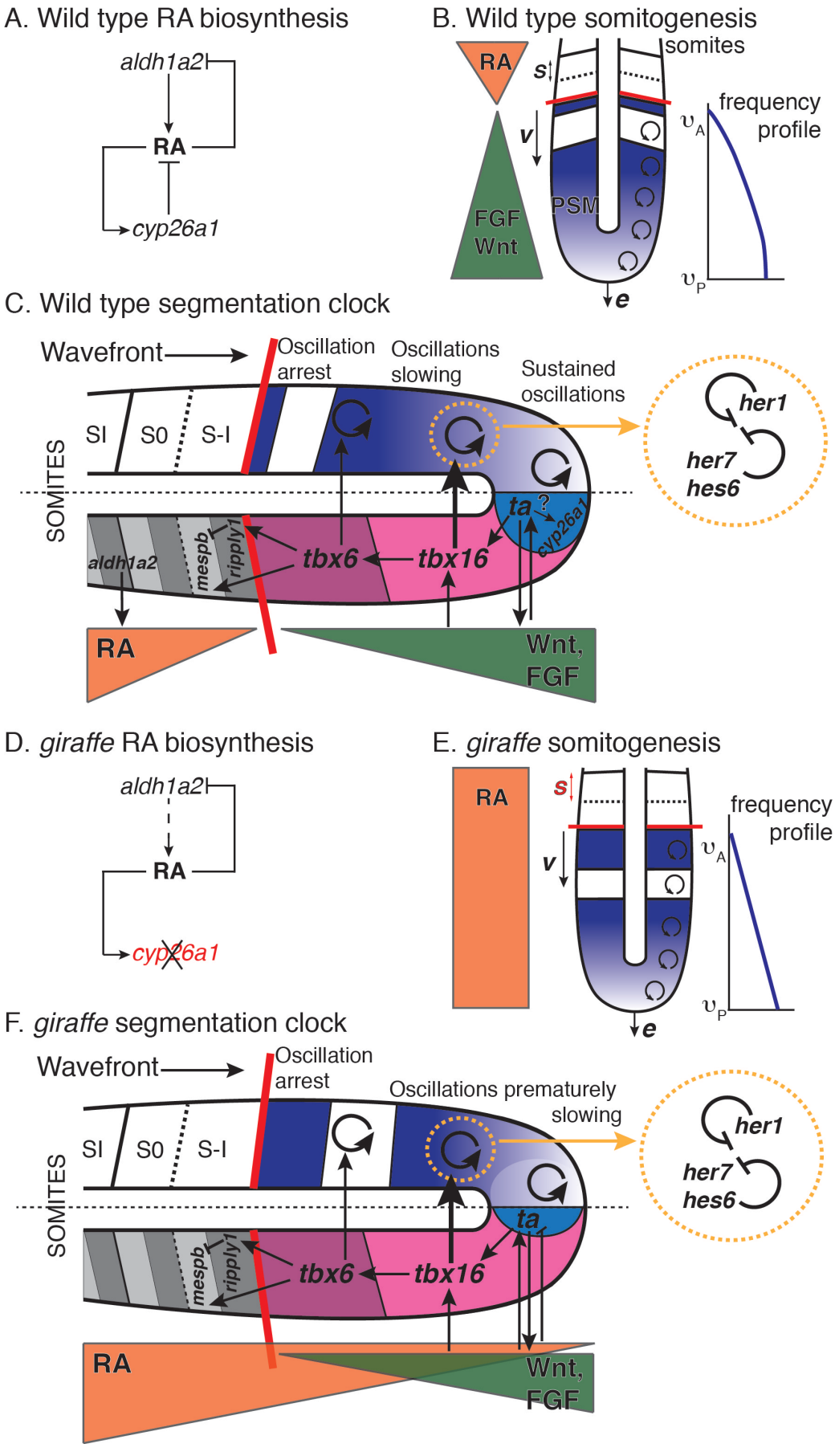
A. Wild type RA biosynthesis
aldh1a2
RA
cyp26a1
B. Wild type somitogenesis
RA
FGF
Wnt
s
v
somites
PSM
e
frequency
profile
C. Wild type segmentation clock
Wavefront
Oscillation
arrest
Oscillations
slowing
Sustained
oscillations
SI
S0
S-I
SOMITES
her1
her7
hes6
ta
cyp26a1
aldh1a2
mespb
ripply1
tbx6
tbx16
RA
Wnt,
FGF
D. giraffe RA biosynthesis
aldh1a2
RA
cyp26a1
E. giraffe somitogenesis
RA
s
v
frequency
profile
e
F. giraffe segmentation clock
Wavefront
Oscillation
arrest
Oscillations prematurely
slowing
SI
S0
S-I
SOMITES
her1
her7
hes6
ta
mespb
ripply1
tbx6
tbx16
RA
Wnt,
FGF

Figure 6.1 Proposed effect of retinoic acid on *t-box* expression to explain the somitogenesis phenotype of *giraffe.*

Schematic of retinoic acid (RA) biosynthesis in wild type **(A)**. Schematic of wild type somitogenesis and frequency profile of cellular oscillators **(B)**. Schematic of the wild type segmentation clock **(C)**. Schematic of RA biosynthesis in *giraffe* (*cyp26a1*) mutants **(D)**. Schematic of *giraffe* somitogenesis and frequency profile of cellular oscillators **(E)**. Schematic of the proposed *giraffe* segmentation clock **(F)**.
(A) RA undergoes self-enhanced degradation by upregulating the expression of RA degradation enzyme *cyp26a1* and downregulating the expression of RA biosynthesis enzyme *aldh1a2*. **(B)** The frequency of the cellular oscillators (blue) is thought to be regulated by the FGF/Wnt (green) and RA (orange) counter gradients. FGF and Wnt support oscillations and sustained oscillations occur in the posterior of the tissue. The oscillations gradually slow down as the cells traverse the tissue and arrest when they encounter RA, giving rise to the wild type kinematic wave pattern (blue). **(C)** I propose that the downstream effectors of the gradients are the *t-box* genes. *tbx6* directly regulates the core pace-keeping circuit (indicated with an arrow, gene network depicted in the yellow inset to the right of the panel). I propose that *tbx16* also has a direct effect on the circuit (indicated with the bold arrow). This thesis doesn't support the establishment of RA-independent *cyp26a1* expression in the posterior by *ta*. **(D)** In *giraffe*, the loss of *cyp26a1* leads to excessive RA which results in the downregulation of *aldh1a2* and the reduction of *de-novo* RA synthesis with the progression of somitogenesis (dashed arrow). **(E)** Excessive RA results in an altered oscillator slowing profile, where oscillator frequency begins to slow prematurely in the posterior leading to the altered *hes*/*her* kinematic wave pattern (blue). Longer somites (*S*, red) are made transiently. **(F)** Excessive RA leads to reduction of the *ta* domain (light blue). I propose that the *tbx16* domain expands in *giraffe*, leading to the premature slowing of oscillators. I hypothesise that excessive RA in *giraffe* reduces the FGF/Wnt gradients and that the antagonistic effect of RA on these is realised by its inhibition of *ta*. RA in this model modulates the frequency of the cellular oscillators. Arrows – known genetic interaction, dotted lines in PSM – forming somite boundary, red line – wavefront, *v* – wavefront velocity, *e* – axial elongation rate, υ_A – anterior frequency, υ_P – posterior frequency.

6.1.4 Axial restriction of the somite phenotype

In the FGF and Wnt perturbations that have been described so far in the vertebrate somitogenesis literature, somite lengths were altered for the duration of the perturbation. The somite phenotypes of the RA biosynthesis mutant are unexpected and unique for the following two reasons: 1. The somite length phenotype is transient even though the RA perturbation persists all through development, 2. the transient phenotype always affects the somites in the rostral trunk of the embryo. The key to understanding the activity of RA in the segmentation clock lies in understanding this phenotype.

A physical model put forward for the segmentation clock (Jörg et al., 2016) predicts that long-term perturbation of the RA gradient would not uniformly affect the length of all somites. It proposes that somites with altered length would be made initially, in response to the perturbation. The segmentation clock would then return to making

somites with wild type length. For example, if RA levels are upregulated during somitogenesis and remained upregulated, a run of longer somites would form, proceeded by the formation of wild type somites. This outcome is a result of the anterior and posterior gradients having been specified in the model as having the ability to degrade each other. Indeed, the literature does report RA and FGF to be mutually antagonistic in the vertebrate PSM (del Corral and Storey, 2004; Moreno and Kintner, 2004). Therefore, the somite phenotype of the RA biosynthesis mutants could be explained to be the result of this antagonism between the anterior RA and posterior FGF gradient. Characterization of the FGF gradient in *gir* will need to be undertaken to confirm this.

However, the model does not yet provide a complete description of *gir* somitogenesis. Firstly, it considers the situation where a long-term perturbation is applied after the onset of somitogenesis. In contrast, the *gir* mutant is likely experiencing high levels of RA before somitogenesis even begins. Secondly, it predicts that when the system returns to making wild type somite lengths, it will overshoot and make a run of shorter somites. This has not been observed in *gir* so far. It is possible that the inclusion of the additional homeostatic regulations on RA levels (Schilling et al., 2012)(Fig 6.1A) in the model, in addition to the FGF-mediated degradation already specified, might provide a more complete description of somitogenesis.

The specific position of the altered somites in the *gir* and *nof* body axes might be reflective of the dynamics of the mechanism by with the system responds to the RA perturbation – be that the mutual antagonism of the FGF and RA gradient, RA homeostasis or both. On the other hand, the specific position could be indicating that a particular subset of mesoderm progenitors is sensitive to RA signalling. There are genetic perturbations that affect the segmentation of different regions of the anterior-posterior axis. The phenotypes have been interpreted as either readout of the dynamics of the segmentation clock or as readout for a genetic hierarchy that specifies the distinct rostral, trunk and caudal somite progenitor pools. For example, the loss of the Delta-Notch pathway genes results in the disruption of somite formation from only somite 5-10 onwards. This delay has been demonstrated to represent the time required for the

cells to lose synchrony in their oscillations. It has been further demonstrated that the PSM has similar sensitivity to the loss of Delta-Notch activity at every time point in somitogenesis (Riedel-Kruse et al., 2007). On the other hand the phenotypes of the *t-box* mutants – the *ta* mutant *notail* fails to make its tail somites, the *tbx16* mutant *spadetail* fails to make all but the tail somites and the *tbx6* mutant *fss* fails to make all its somites, suggest that somites derive from distinct embryological pools that have differential requirements of T-box gene activity (Holley, 2006; Szeto and Kimelman, 2004).

Treatment of embryos with exogenous RA at different time points in somitogenesis will help differentiate between these 2 possibilities. The readout of such an RA perturbation would be the formation of longer somites. If longer somites are formed at every time point of somitogenesis investigated, this would indicate that all the cells of the PSM respond to RA with similar sensitivity and the time taken for the phenotype to manifest would represent the time needed for the system to receive the RA signal and respond to it.

Therefore, in summary, further experiments focused on understanding 1. RA homeostasis, 2. the effect of RA on the FGF gradient in the RA biosynthesis mutants and 3. the sensitivity of the PSM to RA at various time points in somitogenesis will be informative. Results from these approaches will refine the physical model and provide insights into the biological mechanism by which RA could be functioning in the segmentation clock.

6.2 The alternative mechanism of axial segmentation

6.2.1 The *her1;her7* mutant has a segmentation clock whose dynamics are perturbed

There is wide agreement that amniotes segmentally pattern their muscles and axial skeletons at the same time during development using the segmentation clock. However, this idea is controversial in zebrafish. It is also unclear how much of the axial skeleton develops from the somite-derived sclerotome. Neural and hemal arches are considered

to have a somitic origin, but it is unclear whether these cells are responsible for the ossification of the centra. Furthermore, the arches are homologous across vertebrate classes, but centra are not (Fleming et al., 2015).

It has been proposed that in zebrafish, based on the phenotype of the segmentation clock mutant *fss*, that the notochord patterns the centra. *fss* has a disordered paraxial mesoderm pattern. The axial skeleton has disordered arches but the centra are periodic. However, the segmentation clock of *fss* is still periodic, and it has been proposed that this periodicity is sufficient to generate the pattern necessary for the formation of segmented axial structures.

To differentiate between the contribution of the segmentation clock and the possible contribution of the notochord to the patterning of the axial skeleton, a novel *her1;her7* segmentation clock mutant was generated. The dynamics of the cyclic genes in the PSM, the output of the clock and the segmentation of the paraxial mesoderm of these mutants were analysed. The cyclic genes were not expressed in wild type wave patterns and the pattern of expression was not dynamic in the PSM. The segmentation clock output markers were not segmentally expressed and periodic somites did not form in the paraxial mesoderm. Myotome and sclerotome markers did not show wild type segmental expression.

A recent study in chick showed the formation of somites from non-somite mesoderm grafts (Dias et al., 2014) in the absence of a clock and the gradients that provide wavefront activity. The study proposed that somites are self-organising structures whose size and shape are determined by local cell-cell interactions rather than the interaction of a clock and wavefront. The non-somite mesoderm grafts were found to express clock genes and their gene expression varied in the time points assayed, but these variations were subtle when compared to the wave pattern in the host PSM. The grafts were observed to develop into a cluster of epithelial spheres. These spheres were found to have their apical side towards the exterior and each sphere was surrounded by a fibronectin basal lamina, like somites. Moreover, when they were grafted back into the host paraxial mesoderm, they incorporated into the tissue and contributed to the

myotome and sclerotome. Unlike somites, however, these epithelial spheres did not form sequentially in a linear array and did not have rostrocaudal polarity. Therefore, the study proposed that the role of the segmentation clock in chick is not to generate somites but to subdivide the somite into rostral and caudal halves thereby ensuring proper neuronal segmentation (Dias et al., 2014; Stern and Piatkowska, 2015).

In *gullum*, the loss of the clock genes *her1* and *her7* similarly lead to the loss of rostrocaudal polarity in the differentiated paraxial mesoderm. However, the paraxial mesoderm was not organised into somites. Fragments of boundaries that were associated with fibronectin and some cells with epithelial morphology were observed in the differentiated paraxial mesoderm instead. These results suggest that without the activity of the core pace-keeping circuit of the segmentation clock no somites form in zebrafish, unlike the self-organising somite structures of the chick. Thus, genetic waves might play a more central role in zebrafish somite formation than in chicks. However, the results in this thesis and the Dias et al. study demonstrate that a segmentation clock is not necessary for the PSM to undergo its differentiation programme – muscle and bone tissue form without the activity of a clock, and additionally in zebrafish, without a somite intermediate.

6.2.2 The vertebral column of *gullum* shows striking periodicity

Analyses of the paraxial mesoderm derivatives demonstrated that the periodic arrangement of myotomes was disrupted in *gullum*. Similarly, the *fss* and *fss;gullum* myotomes were not periodically segmented (Fig 7.2). These results suggest that somitogenesis plays an instructive role in myotome patterning. However, the *xirp2a+* boundary fragments observed in *gullum* were qualitatively different from those of *fss* and *fss;gullum*. *gullum* myotome boundary fragments were longer in length, when compared to *fss*, and occasional intact boundaries resembling the wild type chevron shape were observed. Myotome boundary fragments of the *fss;gullum* double mutant were more similar to those of *fss* than *gullum*, indicating that the additional removal of the clock output affects myotome patterning.

Somite boundary fragments in the paraxial mesoderms of *fss* and *fss;gullum* were also less distinct than those observed in *gullum*. A possibility that cannot be conclusively ruled out yet is the presence of cryptic segmental patterning information in *gullum* and that the somite and myotome boundary fragments observed might be a result of this cryptic activity. The potential sources of cryptic segmental information are explored later in this discussion (section 6.2.6). However, as a systematic characterisation of a 1:1 correspondence between somite boundaries and myotome boundaries has not been undertaken so far, it is difficult to conclude that the differences in the myotome boundary phenotype can be attributed to a cryptic patterning process that affects somite boundary formation in *gullum* mutants. The myotome boundary phenotypes of *gullum* and *fss* do not appear to be equivalent, however the method currently used to score myotome boundary defects is binary and the myotome boundary phenotype of both mutants is simply described as defective or disrupted. Without a method to measure, classify or rank segment defects with confidence, a more representative description is not possible. To redress this, I plan to undertake the development of a boundary phenotype characterisation method that will allow for more detailed descriptions than have been possible thus far.

There was no segmental organisation to the *gullum* hemal and neural arches, the structures of the vertebral column that differentiate from somite-derived sclerotome. However, a segmented vertebral column was formed, thus demonstrating that the segmentation clock does not provide the patterning information necessary for the development of the centra of the vertebral column. Furthermore, the centra were periodic in all the segmentation clock mutants analysed – *gullum* (no clock activity), *fss* (no clock output) and in *fss;gullum* (no clock activity and no clock output). This strongly suggests that the notochord and not the segmentation clock is the source of segmental patterning information for the development of the centra. However, when compared to wild type, *gullum* had more centra. The centra also showed high variability in length compared to wild type. Therefore, while there is periodicity to the *gullum* centra, they are not wild type, suggesting that while the segmentation clock doesn't determine axial pattern, it might be capable of influencing it.

6.2.3 Source of the periodicity for the periodic pattern of centra

The hypothesis that the notochord provides the patterning information for the formation of centra was explored in detail in collaboration with the Schulte-Merker lab and Luis Morelli by means of a novel transgenic reporter for enzyme ectonucleoside triphosphate/diphosphohydrolase 5 (Entpd5). It has been previously described as essential for ossification in zebrafish (Huitema et al., 2012). *entpd5* mutants, *nobone*, are characterized by a complete absence of bone due to their failure to mineralize osteoid. *entpd5* is co-expressed with the osteoblast marker *osterix* (*osx*) in all osteoblasts of the bony structures of the head (Fig 7.4). We discovered that *entpd5* is also expressed in notochord cells and starting at 4 dpf, the expression in the axial mesoderm became restricted to segmentally organized rings in the notochord sheath (Fig 7.3). These rings were added sequentially in the anterior to posterior direction. *osx* is not expressed at these early stages in the notochord sheath, nor do *osx* mutants have an axial mineralization phenotype in zebrafish (Fig 7.4) or medaka (Yu et al., 2017). These results suggest that the cells that are functionally important for chordacentrum formation in zebrafish are the notochord sheath cells themselves. This is in contrast with medaka where sclerotome-derived osteoblasts are thought to provide the initial enzymatic activity for the mineralization of the chordacentra (Inohaya et al., 2007; Renn et al., 2013). Thus *osx*-, *entpd5*+ sheath cells are responsible for the initial chordacentra formation and segmental patterning of the notochord is established by 4 dpf in these cells, making *entpd5* the earliest known marker of the segmental pattern of the notochord. Thus, it allows for the evaluation of the segmentation clock's input in the establishment of the segmented notochord.

6.2.4 Autonomy of the notochord segmentation mechanism

gullum chordacentra did not develop like wild type where new chordacentra were added sequentially. Interestingly in *gullum*, it appeared that this strict schedule was broken. Notochord segmentation observed with the *entpd5* reporter in *gullum*, *fss* and *fss;gullum* was also similarly error-prone (Fig 7.5). Sequential generation of periodic *entpd5* expression rings was lost, leaving variable inter-segmental spaces (Fig 7.5, 7.6), which were later repaired by intercalation of a new ring of *entpd5* expression when they were

longer than the corresponding space in wild type (Fig 7.6). The new ring would either develop as a small centra or fuse to one of its neighbours.

The loss of strict sequentiality in the formation of *entpd5* rings and the subsequent intercalation, argues against their generation by a clock-type mechanism, like the segmentation clock of the paraxial mesoderm, which would prescribe a strict sequential order to ring formation. Furthermore, *her1, her7* and *tbx6* are not expressed in the notochord during somitogenesis and no *her1::YFP* reporter expression could be detected the notochord of *Looping1* at 5 dpf, a developmental stage at which a few rings of *entpd5* expression are already visible. Therefore, it appears highly unlikely that segmentation clock activity in the notochord, early or late, is responsible for the segmentation of the notochord. The ability of the notochord to segment in the absence of a functional segmentation clock strongly supports the existence of a second segmentation mechanism intrinsic to the notochord sheath cells. However, the segmentation clock mutant *hes6* that has a slower segmentation clock period leading to the formation of fewer somites has correspondingly fewer centra. Using the *entpd5* transgene, it was confirmed that the *hes6* mutant also made fewer chordacentra, thus suggesting that there is a mechanism of communication between the paraxial and axial tissues.

6.2.5 Physical model for notochord segmentation and influence of the PSM on the process

Based on experimental observations, collaborator Luis Morelli developed a physical model which describes the intrinsic patterning mechanism operating in the notochord sheath cells as a reaction-diffusion system with two components, an activator and an inhibitor (Green and Sharpe, 2015; Murray, 2011). The cues provided by the paraxial mesoderm pattern are implemented as a distribution of sinks for the inhibitor (Fig 7.7). Although other descriptions are possible, this simple theory successfully accounted for the sequential formation of regular segments in the presence of sinks, as observed in wild type (Fig 7.8). It also remains agnostic to the nature of the molecules that might be involved in the biological process. The theory conjectures that the paraxial mesoderm defects of the mutants do not affect the intrinsic notochord patterning mechanism, but

can change the features of the sink distribution (Fig 7.8). Thus the model describes a dynamic notochord segmentation mechanism that is sensitive to information from the paraxial mesoderm, most likely provided by the myotome structure, which can bias the position of a ring to enable the development of the later-forming skeleton in biomechanical register with the early-developing myotome in wild type.

The influence of the paraxial mesoderm on axial segmentation maybe reflected in the differences observed between the distributions of *entpd5* defects – smaller vertebrae and vertebral fusions, in the somitogenesis mutants (Fig 7.9, 7.10). *gullum* had the strongest axial phenotype and possessed prominent myotome boundary fragments in the paraxial mesoderm, whereas *fss* and *fss;gullum* had weaker axial phenotypes, which were preceded by a greater reduction of myotome boundary fragments. This is consistent with a dominant interfering effect of paraxial structures on notochord segmentation. The similarities between the paraxial and axial phenotypes of *fss* and *fss;gullum* can be explained by proposing that the effect of the disrupted segmentation clock is removed by the loss of *tbx6* in the anterior PSM, which leads to the absence of patterning output.

The proposed transfer of information from the segmentation clock-derived segmental pattern of the musculature to an autonomous but plastic mechanism in the notochord resolves the apparent discrepancy between the *fss* and *hes6* mutant phenotypes. It also explains how the animal coordinates the development of segmented muscles and axial skeleton in biomechanical register, despite the fact that they develop days to weeks apart in time. Another possible interpretation is that the notochord's intrinsic segmentation mechanism is highly noisy and the paraxial mesoderm has no influence on it. However, it is also plausible that errors due to molecular stochasticity are low in the notochord as the rate of *entpd5* ring formation is about 20 times slower than somitogenesis, a timescale that is long enough to allow for the synthesis of a sufficiently large number of molecules that could ensure a low error rate.

The genetic basis of the proposed autonomous notochord mechanism and signal from myotome to notochord is not yet understood. The model proposed does not assume any specifics with regard to molecular identities. Understanding the control of *entpd5*

expression in the notochord sheath cells may hold the key to understanding the molecular regulation of the proposed notochord segmentation mechanism.

6.2.6 Sources of pattern that might be remnant in the *gullum* body

gullum and the other somitogenesis mutants we have used to interfere with the segmentation clock and its output leave the PSM without any overt signs of segmental pattern. However, it remains a possibility that some pattern might remain in the paraxial mesoderm of the somitogenesis mutants analysed here. This does not affect the argument made for the intrinsic segmentation mechanism of the notochord, as what pattern might remain in the *gullum* paraxial mesoderm cannot explain the development of the highly ordered axial structures observed. In this section, the possible sources of pattern remaining in the mutant paraxial mesoderms are explored.

1. Cryptic oscillations in the segmentation clock

Although no coordinated dynamic oscillations were detected on the tissue level, it is possible that the core pace-keeping circuit still oscillates in the single cells. Mutant *her1* and *her7* mRNA can still be detected in the tissue and recent reports suggest that genome editing can lead to altered mRNA processing (Anderson et al., 2017), thereby rescuing some dynamic behaviour. This can be investigated by firstly, assessing if the mutant mRNA has some functionality by injection into wild type embryos. Overexpression of cyclic gene mRNA dominantly interferes with the segmentation clock, causing defective somitogenesis (Campos-Ortega, 1999; Shankaran et al., 2007). Therefore, if the mutant mRNA injection were associated with a somite phenotype, it would indicate that the protein product is still capable of generating some oscillatory behaviour. The second approach is to visualise oscillations in single cells directly. *Looping1* is unsuitable for this purpose, but a *her7::YFP* reporter *Lector2* (Daniele Soroldoni, unpublished) could be used for this experiment in *gullum;hes6* (*her1;her7;hes6*) triple mutants, without restoring any functionality to the core pace-keeping circuit.

Possible alternative sources of dynamic activity in the segmentation clock are the 9 additional cyclic genes expressed in the PSM (Gajewski et al., 2006; Krol et al., 2011;

Shankaran et al., 2007; Sieger et al., 2004). Their contribution to the segmentation clock has not been clearly established yet as their loss does not affect somitogenesis. However, the overexpression of these genes does interfere with segmentation clock activity (Shankaran et al., 2007). The preliminary assessment of the expression of these genes suggests that they do not oscillate in the *gullum* PSM (Fig 7.11, 7.12). Whatever the contribution of these genes, it seems that it is small in the absence of *her1* and *her7*.

2. Cell sorting driven self-organization

The paraxial mesoderm lacks overt segmentation; however, boundary fragments still form in the tissue. The formation of boundary fragments might be due to the *gullum* paraxial mesoderm having both anterior and posterior identity. This is in contrast to *fss,* where only posterior identity is specified and no somite boundaries form (Barrios et al., 2003; Oates et al., 2005b; van Eeden et al., 1998). The length of the boundaries fragments formed in *gullum* could be a function of the anterior-posterior interface that develops in the tissue. Cells of the anterior and posterior compartments of the somite have been hypothesized to have differential adhesion and an affinity to aggregate with the cells of similar identity (Horikawa, 1999). It is possible that in the *gullum* paraxial mesoderm, cells expressing identity markers also behave like cells from the respective somite compartment and have differential adhesion. Homophily could lead to self-organization of a pattern that will improve with time, which would be read out as the formation of longer somite boundary fragments with time.

3. Elongation of slow muscle precursors

A final source of pattern to consider is the imposition of a spatial length scale in the tissue by the developing musculature. Muscle fibres, by virtue of their rod-shaped morphology, could be capable of generating nematic order in the tissue. This phenomenon has been observed in dense colonies of *E. coli* due to their cell growth (Volfson et al., 2008). Indeed, in line with the expectation of this kind of order, muscle fibres are orientated with their long axes parallel.

The sequential differentiation of the adaxial cells into the elongating slow muscle precursors has been proposed to be the agent of muscle imposed ordering of the PSM

(van Eeden et al., 1998). The loss of these Hedgehog induced precursors in *fss;yot* double mutants that lack Hedgehog signalling has been reported to cause the loss of all muscle boundary fragments, which was interpreted as a complete loss of order in the *fss* paraxial mesoderm. Inhibiting slow muscle induction with Hedgehog inhibitor cyclopamine (Chen et al., 2002) in Delta – Notch mutants that fail to segment the body posterior to ~somite 7 was also found to prevent the formation of myotome boundary fragments in the trunk and caudal regions of the body axis (Henry et al., 2005). A similar Hedgehog signalling abrogation approach was attempted in *gullum* with cyclopamine. The preliminary data indicate that Hedgehog signalling inhibition cannot affect the rostral myotome boundary fragments of *gullum*, but has a strong effect on the caudal myotome fragments (Fig 7.13). This suggests that the slow muscle precursors can impose order on the PSM, but further experimentation is necessary to detemine their exact contribution to segmental body pattern.

Chapter 7. Appendix

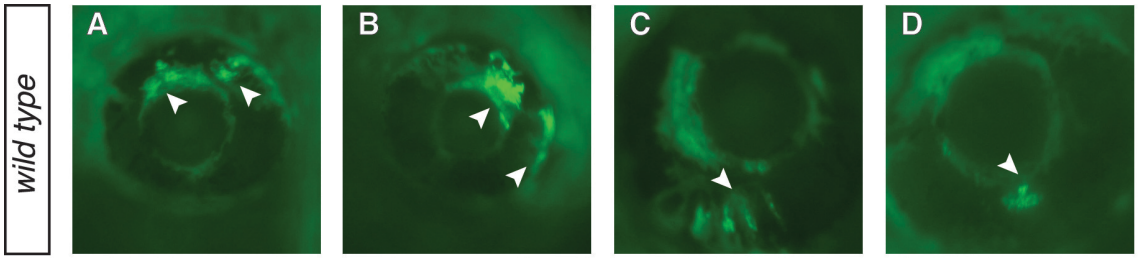

E Visual scoring

CLUTCH	GFP +ve at 72 hpf
1	6%
2	4%
3	8%
4	4%
5	4%
6	2%
7	8%
8	4%
9	4%
10	6%
11	6%
12	2%
13	6%
14	6%

F PCR analysis for fluorescent contaminants in fish strains

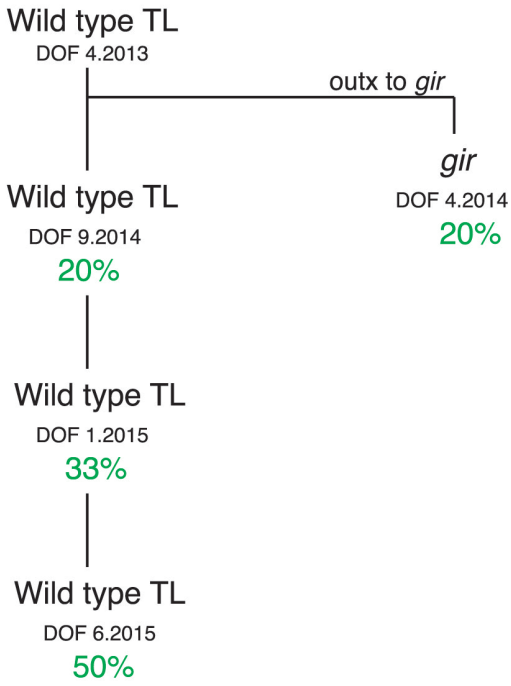

Figure 7.1 Unknown transgenic contaminants in wild type fish strains.

GFP expression of an unknown transgenic contaminant (arrowheads) in the eyes of wild type TL embryos at 72 hpf (hours post fertilization) **(A – D)**. The frequency of the observation in clutches from pairwise wild type matings (50 embryos per clutch were scored) **(E)**. Frequency of GFP and RFP contamination (green) in 3 generations of wild type TL fish and one generation of heterozygous *gir* fish as detected by PCR from genomic DNA extracted from adult fins (10 adults tested per generation of the fish strains). DOF (date of fertilization) given as month and year **(F)**.

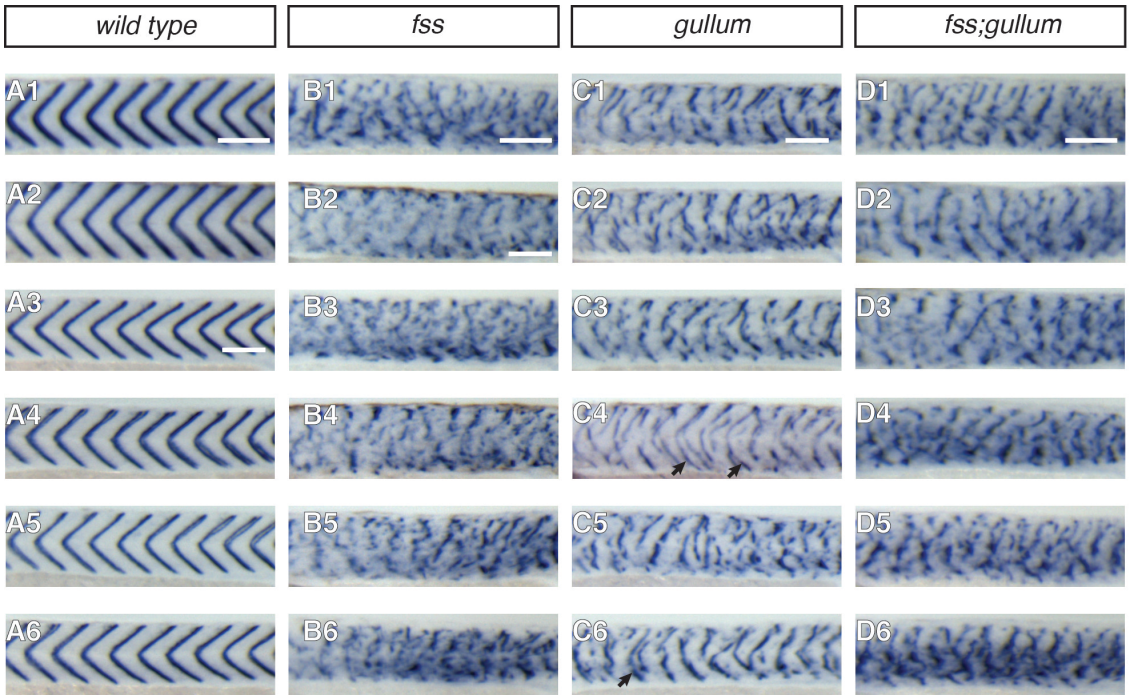

Figure 7.2 Severity of myotome boundary disruptions in the segmentation clock mutants differs according to genotype.

In situ hybridisation for *xirp2a* in 36 – 41 hpf wild type, *fss*, *gullum* and *fss*;*gullum* embryos **(A1 – D6)**. Insets are taken from the trunk abutting the yolk extension, corresponding to segments 7 to 17 in wild type.
(B1 – B6) *fss* myotome boundaries are either fragmented or indistinct and *xirp2a* staining is visible in most of the trunk. **(C1 – C6)** *gullum* myotome boundaries are fragmented and scattered in the trunk. Occasional chevron-shaped boundaries can be observed (arrows in C4 and C6). **(D1 – D6)** Myotome boundary disorder of *fss*;*gullum* mutants resembles the *fss* myotome boundary phenotype. Scale bars are 100 µm. Scale bar in A1 applies to A1 – A2, in A3 applies to A3 – A6, in B2 applies to B2 – B6, in C1 to C1 – C6 and in D1 to D1 – D6.

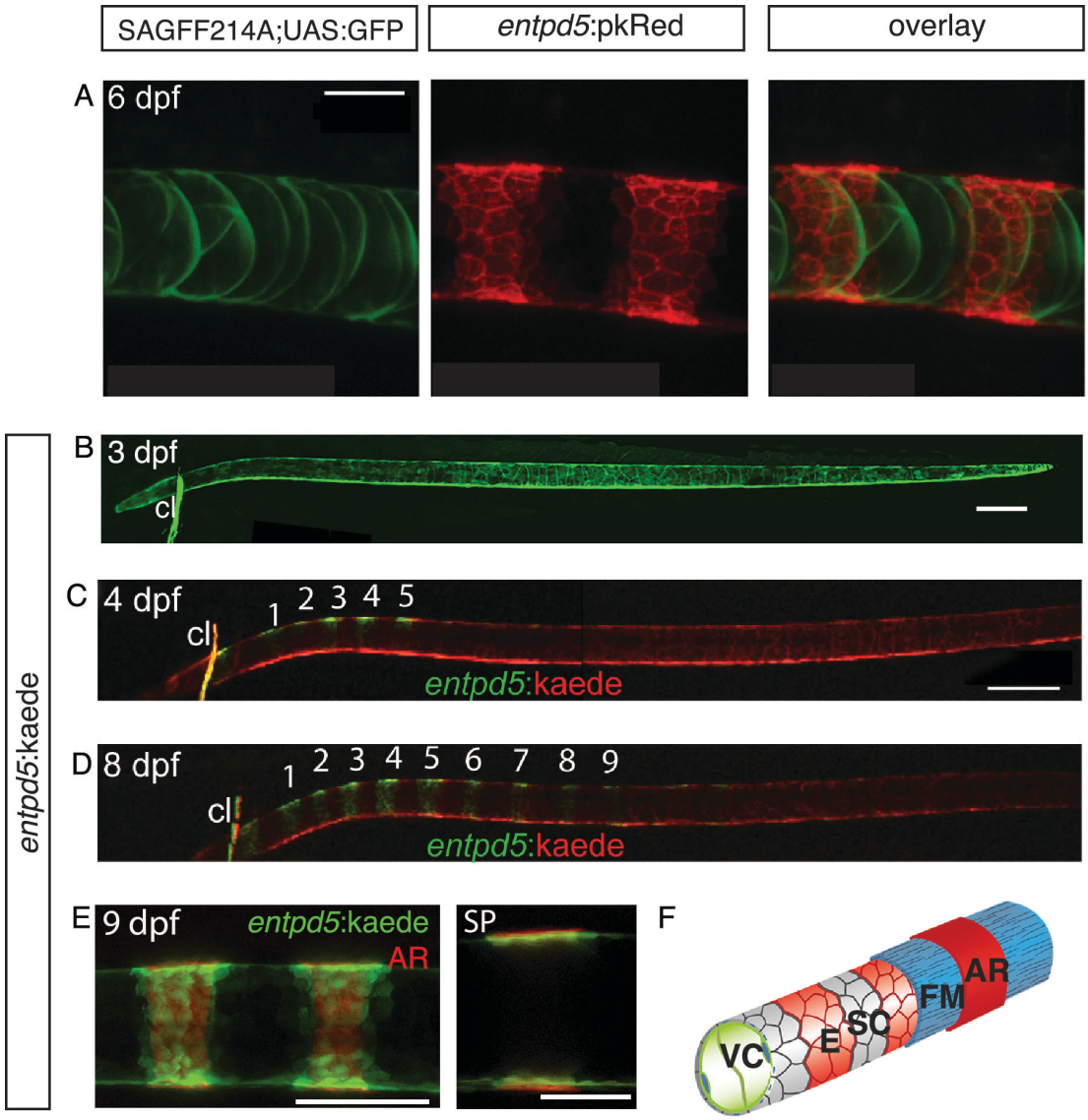

Figure 7.3 Segmental e*ntpd5* expression in notochord sheath cells marks the sites of chordacentrum mineralization.

Live confocal images of transgenes of *entpd5* in the notochord of zebrafish larvae **(A – D)** and confocal image of *entpd5* in larvae stained with alizarin red **(E)**. Schematic illustrating *entpd5* expression in the notochord **(F)**. Lateral views, head towards the left.
(A) *entpd5* is expressed only by the notochord sheath cells and not by the vacuolated notochord cells (labelled by SAGFF214A;UAS:GFP). **(B)** At 3 dpf *entpd5* is expressed in the whole notochord and does not display a segmented pattern. **(C)** After photo-conversion of *entpd5*:Kaede, new axial expression domains (green) restricted to a segmental pattern within the axis and the cleithrum (cl) is observed at 4 dpf and **(D)** at 8 dpf. **(E)** *entpd5*+ domains (green) overlap with areas of mineralization (stained with alizarin red). They localize proximal to the site of mineralization of the future chordacentra (left – lateral view and SP – sagittal view). **(F)** *entpd5* is expressed in the notochord sheath cells that are external to the notochord. Alternating *entpd5*+ (red) and *entpd5*- (grey) rings in the sheath cells (SC) are depicted. The sheath cells are surrounded by a fibrous matrix (FM), which in turn become mineralized in *entpd5*+ segments. AR – alizarin red, SC – sheath cells, FM – fibrous matrix, SC – sheath cells, VC – vacuolated cells. Scale bar in A and E 40 µm, scale bar in B and C 150 µm. Data from Leonie Huitema and Laura Lleras Forero.

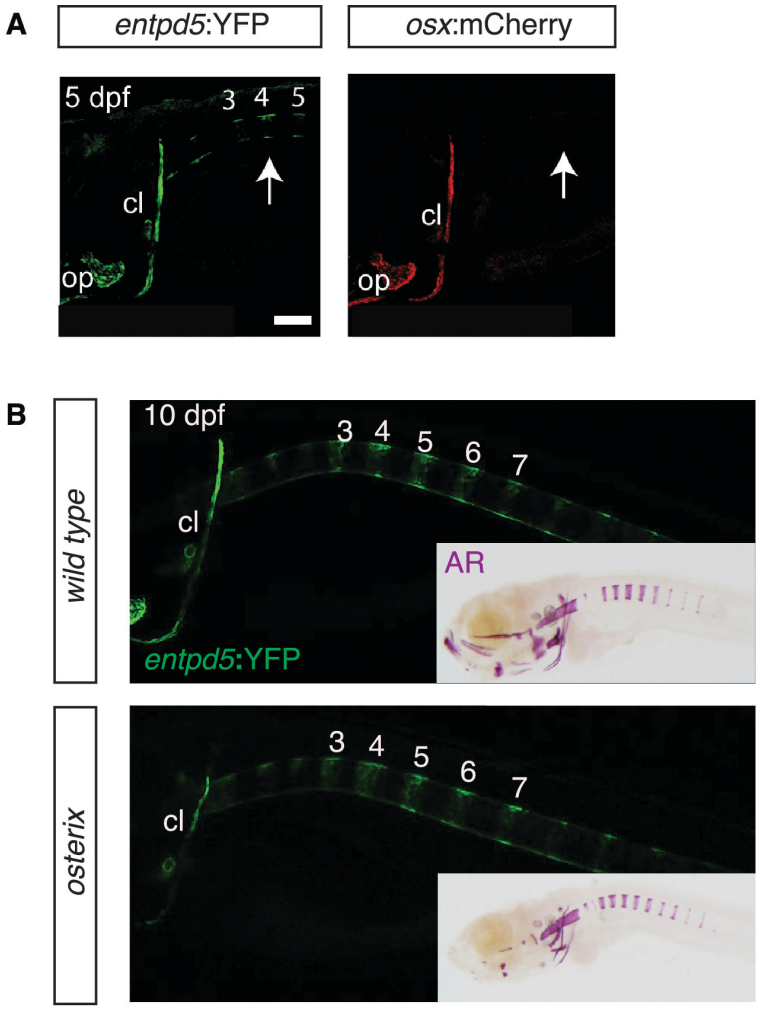

Figure 7.4 *Osterix* is not required for the segmentation of the axial skeleton.

Live confocal images of *entpd5*:*YFP* and *osx*:*mCherry* reporter expression in the head and notochord of 5 dpf (days post fertilization) embryos **(A)**. Confocal images of *entpd5:*YFP expression (main panel) and photomicrographs of alizarin red (AR) preparations (inset) of sibling wild type and *osterix* mutant 10 dpf larve **(B)**. Lateral views, head to the left.
(A) *entpd5*:YFP expressing cells are present at positions where mineralization of the vertebral centra are predicted to occur (arrows; numbers – position of prospective vertebrae 3 – 5). *osx*:mCherry expressing cells are not observed at these positions. **(B)** Reduction of *entpd5* expression (main panel) and mineralization (inset) in the craniofacial bones of the *osx* mutant compared with the sibling. The segmental pattern in the notochord shows no changes either by *entpd5* reporter expression (main panel) or by alizarin red staining (inset). cl – cleithrum, op – operculum. Scale bars are 100 µm. Data from Leonie Huitema and Laura Lleras Forero.

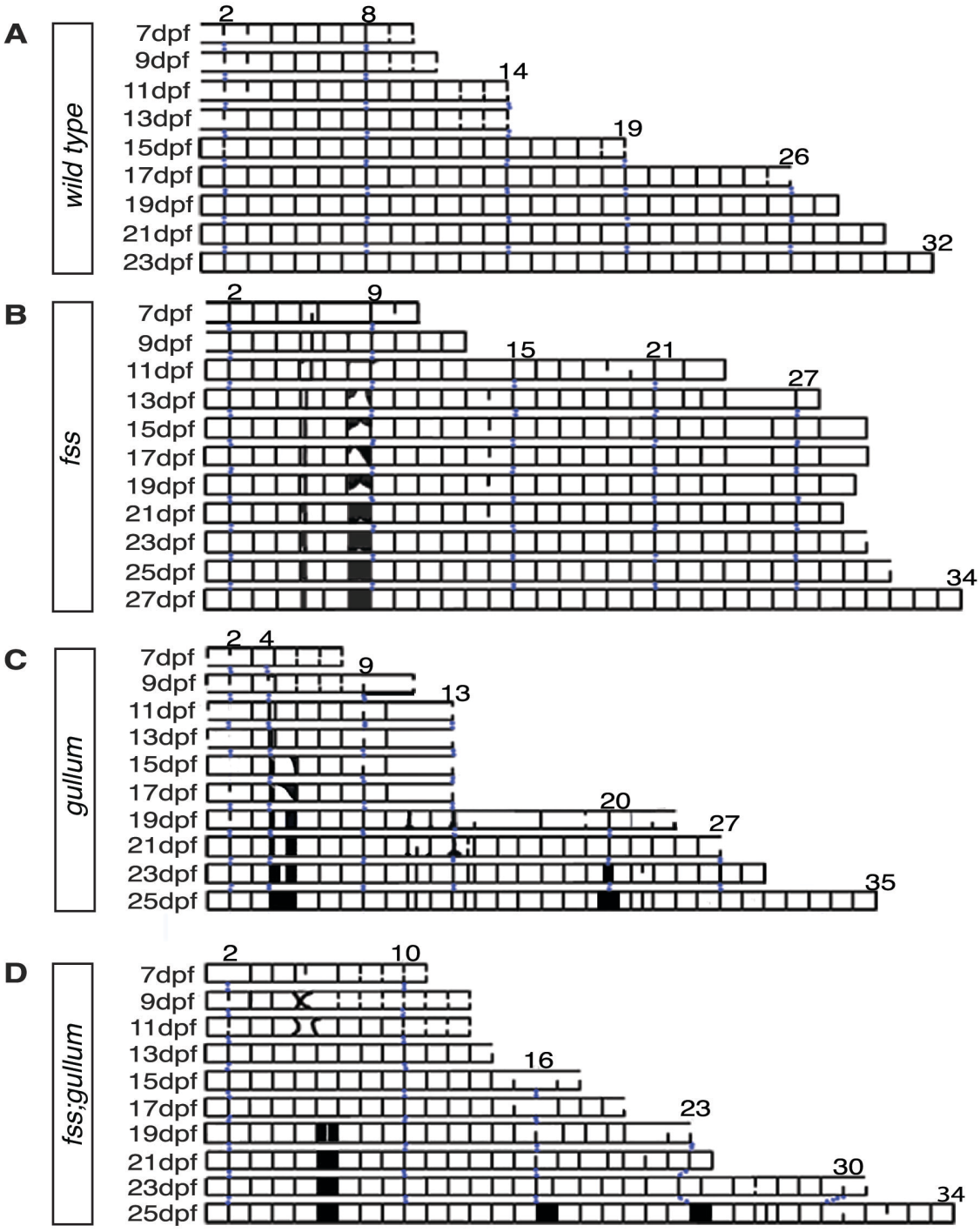

Figure 7.5 Segmentation clock mutants still segment the notochord sequentially.

Kymograph representations of virtual time-lapses of *entpd5* expression in wild type, *fss*, *gullum* and *fss;gullum* larvae from 7 dpf onwards. Chordacentra are represented as black lines **(A – D)**.
(A) In wild type (n = 16), *entpd5*+ segments are added sequentially from anterior to posterior. **(B)** *fss* mutants (n = 4), **(C)** *gullum* mutants (n = 4) and **(D)** *fss;gullum* mutants (n=4) also form chordacentra in an anterior to posterior order, but segmentation errors such as atypically large intervertebral spaces and fusions of chordacentra (black boxes) can be seen at random positions along the axis. Data from Laura Lleras Forero.

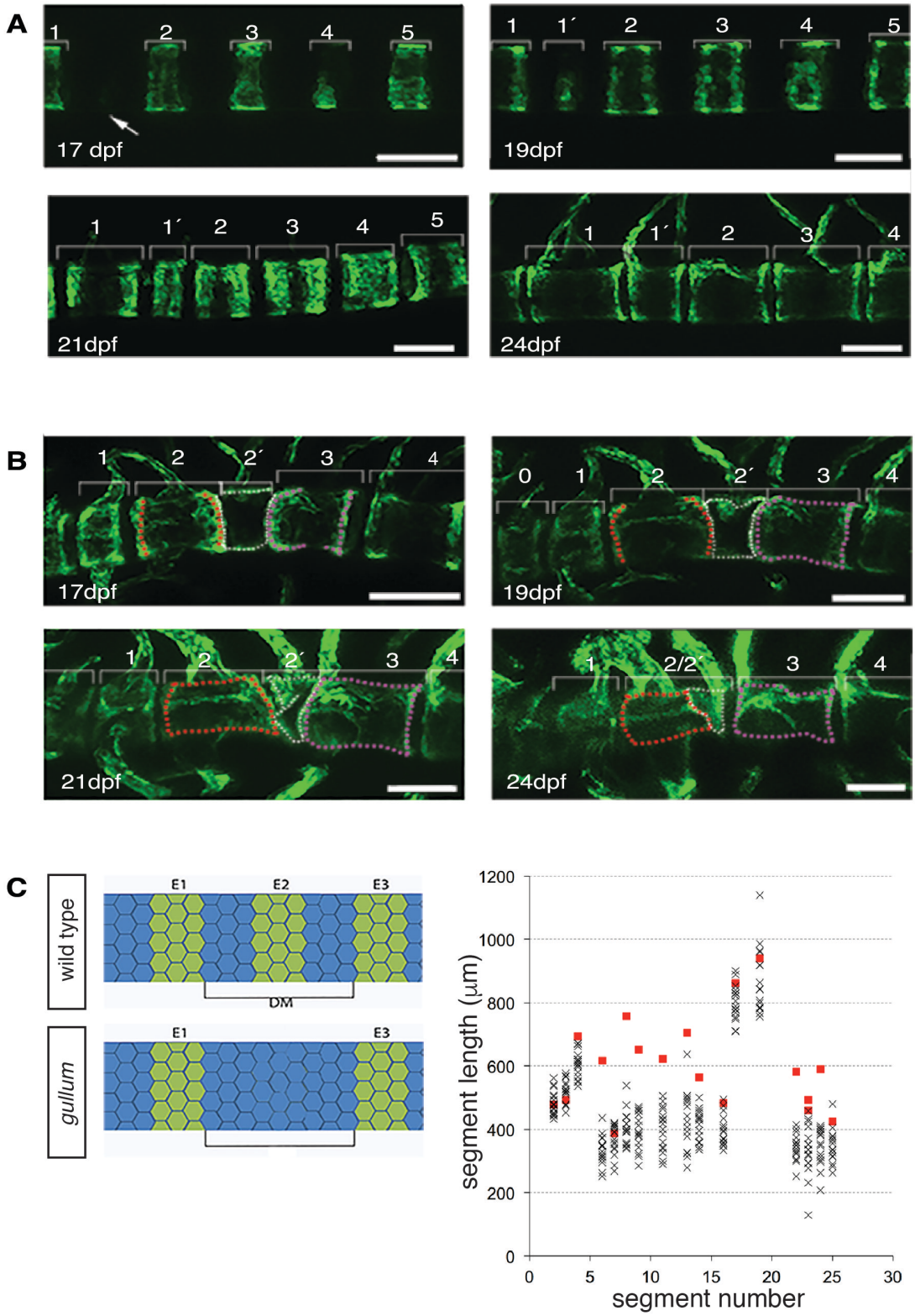

Figure 7.6 Atypically large spaces between *entpd5* segments are associated with erroneous chordacentrum formation.

Images of *entpd5* segments at progressing time points in their maturation (time points indicated in dpf) **(A, B)**. Schematic and quantification of segment length at positions of intercalation in *gullum* **(C)**.

(A) An atypically large intervertebral spaces (arrow) develops a smaller *entpd5* segment (segment 1'). **(B)** The additional smaller segments sometime fuse to the adjacent vertebra (segment 2' fuses to segment 2). **(C)** Segment length at positions of intercalation in *gullum* (18 intercalations, n = 4, red dots) are the same or larger than the equivalent distance between *entpd5* rings at the same axial position in wild type (288 segments, n=16, black crosses). DM – distance measured; E – *entpd5* segment. Scale bars are 100 μm. Data from Laura Lleras-Forero and Andrew Oates.

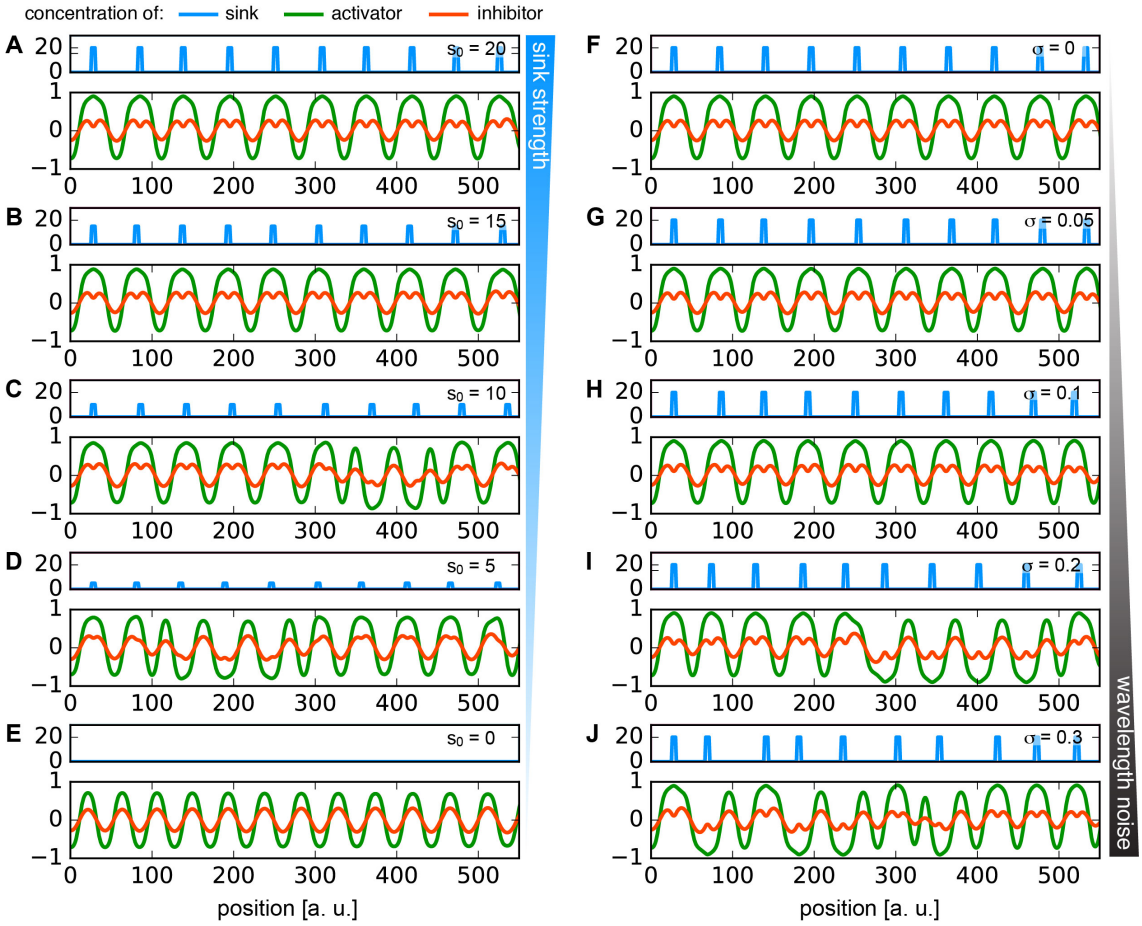

Figure 7.7 Theoretical effects of sink strength and sink wavelength noise on the notochord patterning mechanism.

Effect of sink strength on activator and inhibitor concentrations **(A – E)** and effect of sink position (wavelength) on activator and inhibitor concentration **(F – J)** in the reaction-diffusion mechanism. The sink profile (blue) describes cues from myotomes that bias the positions of segments. The Entpd5 pattern is given by the concentration of an activator (green) that is regulated by an inhibitor (red).
(A – E) As sink strength S_0 is decreased the reaction-diffusion mechanism fails to match some sink positions, giving rise to shorter segments in the activator pattern. **(E)** For vanishing sinks, $S_0 = 0$, the patterning mechanism is free from external perturbations and progresses without noise in a deterministic way, giving rise to regular, shorter segments. **(F – J)** As noise in sink positions σ is increased, the distance between sinks in the sink profile can be either too short or too large for the intrinsic reaction-diffusion system to cope with, giving rise to sink skipping and intercalations in the activator pattern. Model by Luis Morelli.

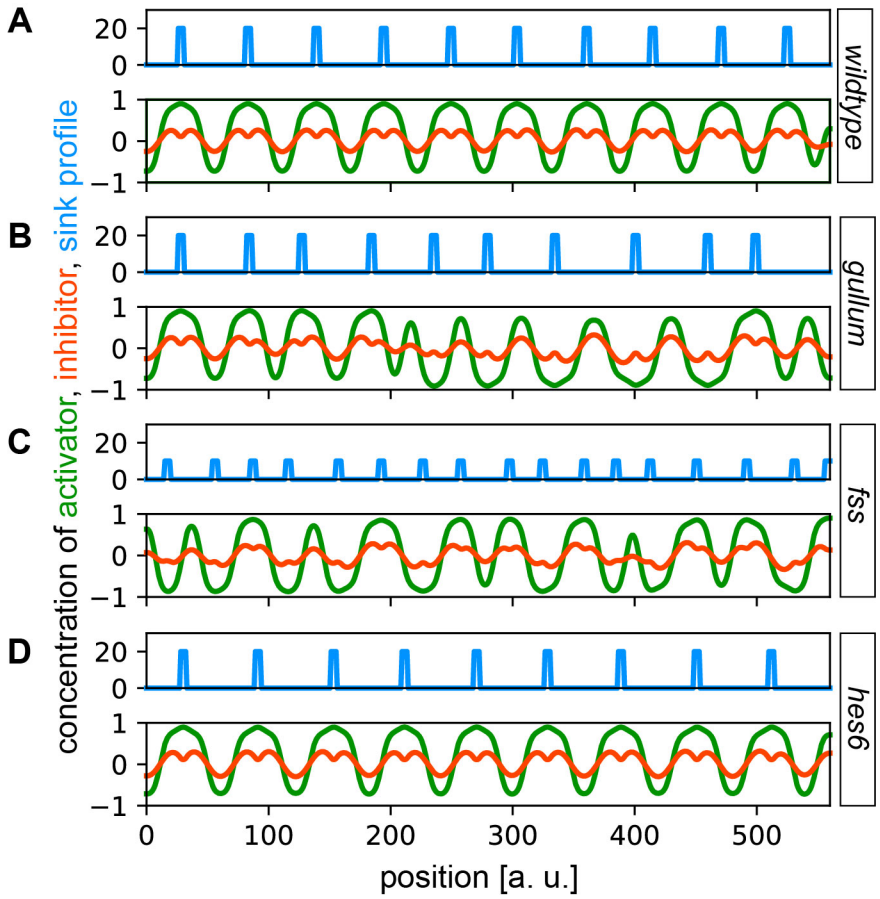

Figure 7.8 The reaction-diffusion theory accounts for both sequential patterning of the notochord and the defects of the pattern observed in the somitogenesis mutants.

Sink profiles (blue), describing cues from myotome boundary fragments, and the corresponding Entpd5 pattern, given by the concentration of an activator (green) that is regulated by an inhibitor (red) in wild type **(A)**, *gullum* **(B)**, *fss* and *fss;gullum* **(C)** and *hes6* **(D)**.
(A) The wild type condition is described by regularly placed strong sinks, according to the output of a functioning segmentation clock. **(B)** In *gullum*, strong sinks are misplaced due to a malfunctioning segmentation clock, resulting in the formation of defective myotome boundary junctions. **(C)** *fss* (and *fss;gullum)* mutants are characterized by weaker sinks with a shorter wavelength due to the fragmented myotome boundaries observed. **(D)** *hes6* is characterized by a sink profile wavelength that is 6% larger than wild type. Parameters: $a = 10^{-3}$, $b = 10^{-2}$, $\tau = 0.1$, $d = 0.5$. Sink profile parameters: (A) $S_0 = 20$, $\lambda = 0.57$, $\sigma = 0.05$, (B) $S_0 = 20$, $\lambda = 0.57$, $\sigma = 0.30$, (C) $S_0 = 10$, $\lambda = 0.35$, $\sigma = 0.25$ and (D) $S_0 = 20$, $\lambda = 0.60$, $\sigma = 0.05$. Model by Luis Morelli.

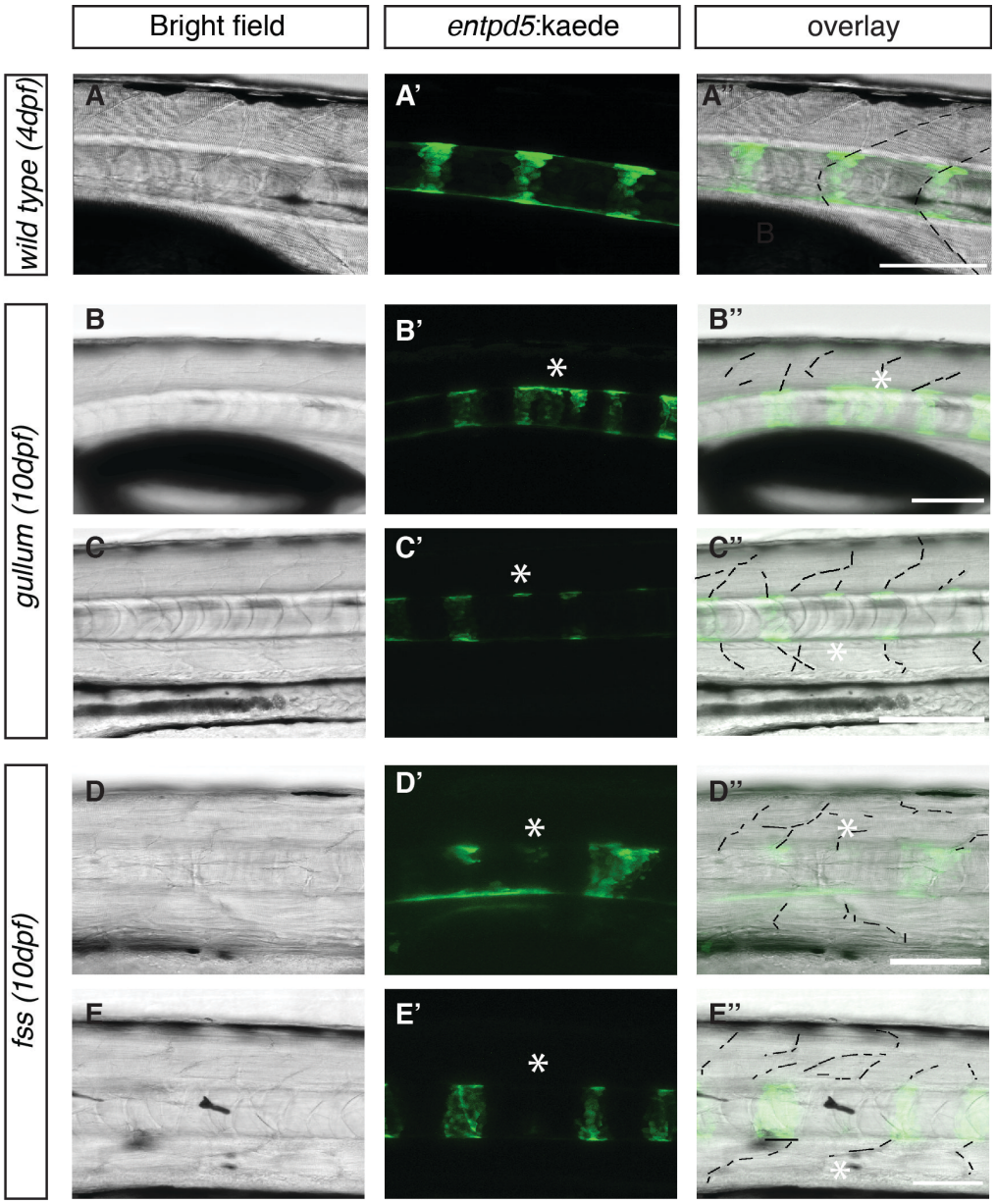

Figure 7.9 Chordacentra align with the myotome boundaries in wild type larvae, but not in *fss* and *gullum* mutants.

Live confocal images of *entpd5:kaede* expression in wild type **(A – A'')**, *gullum* **(B – C")** and *fss* **(D – E")** embryos and larvae. Genotypes and developmental ages are as indicated.
(A – A") *entpd5*:*kaede*+ segments are in register with the myotome boundary junctions in wild type. In **(B – C")** *gullum* and **(D – E")** *fss* mutants, *entpd5:kaede* segments are not in register with myotome boundary fragments. Asterisks- defective *entpd5:kaede* segments. Scale bars 100 µm. Data from Laura Lleras Forero.

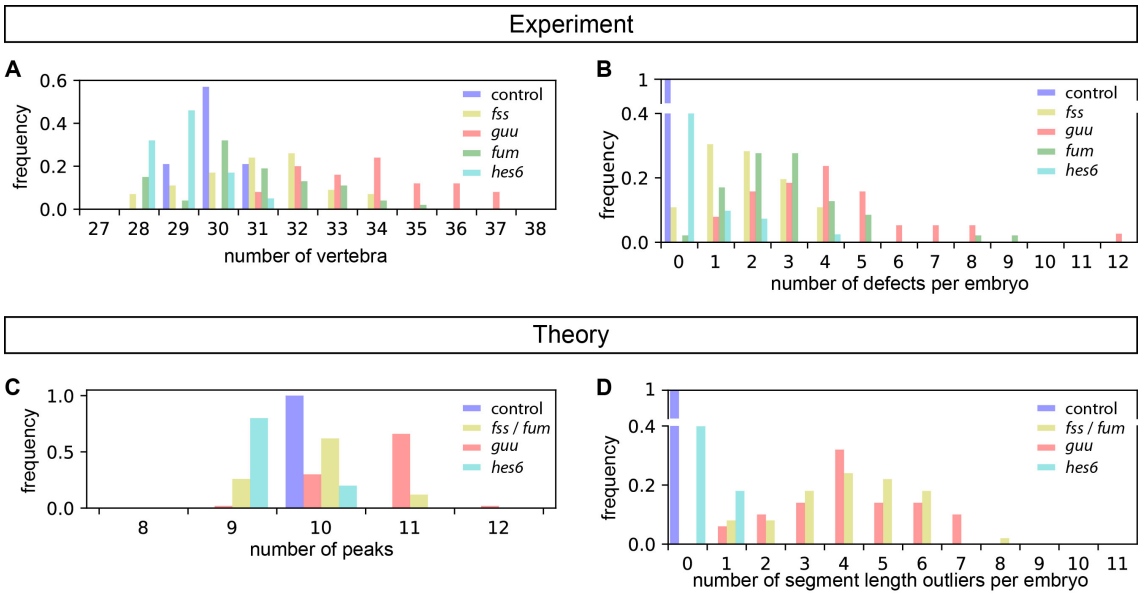

Figure 7.10 Quantification of mutant phenotype observables and theoretical description.

Distribution of the number of *entpd5* segments at 28 dpf **(A)** and of the number of defects – smaller vertebrae and vertebral fusions – per embryo **(B)**. Histograms of the number of peaks in the activator pattern **(C)** and number of segment length outliers **(D)**, for mutant conditions from the theory with the parameters defined in Fig 7.8.
(A, B) The number of vertebrae and the number of defects are higher in the mutants than wild type. **(B)** *gullum (guu)* mutants have the highest number of segmentation defects and it is partially recovered to *fss* levels in *fss;gullum (fum)*. **(C, D)** The theory captures the trends observed in experiments. Histograms in the theory computed over 50 realizations. Data from Laura Lleras-Forero, Andrew Oates and Luis Morelli.

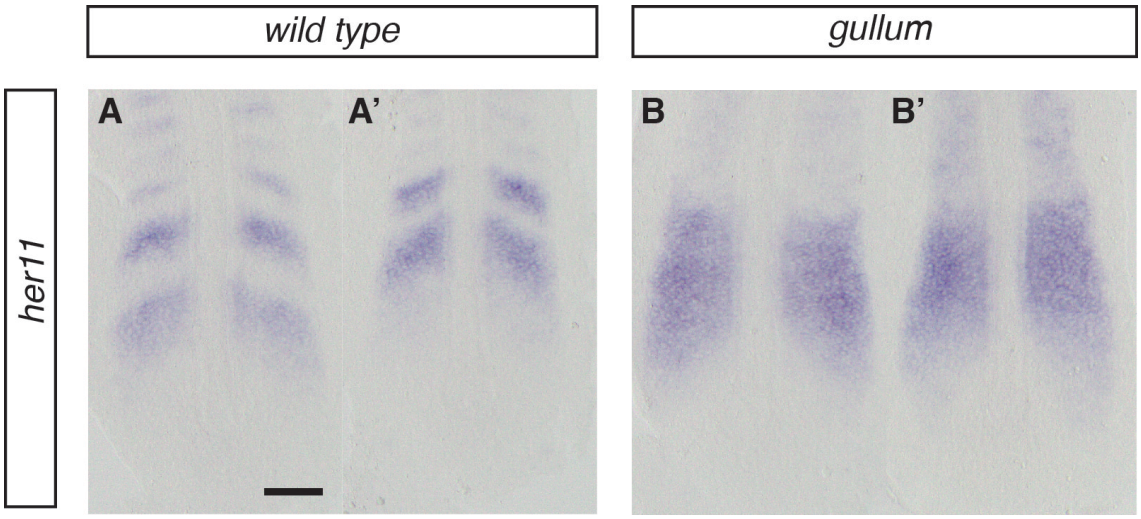

Figure 7.11 *her11* does not oscillate in the *gullum* PSM.

In situ hybridisation for *her11* in 10-somite stage wild type **(A, A')** and *gullum* siblings **(B, B')**. Genotypes are as indicated, anterior to the top.
(A, A') Kinematic waves of *her11* restricted to the anterior PSM are seen in wild type. **(B. B')** Static expression in the anterior PSM is seen in *gullum*. Scale bar 100 µm.

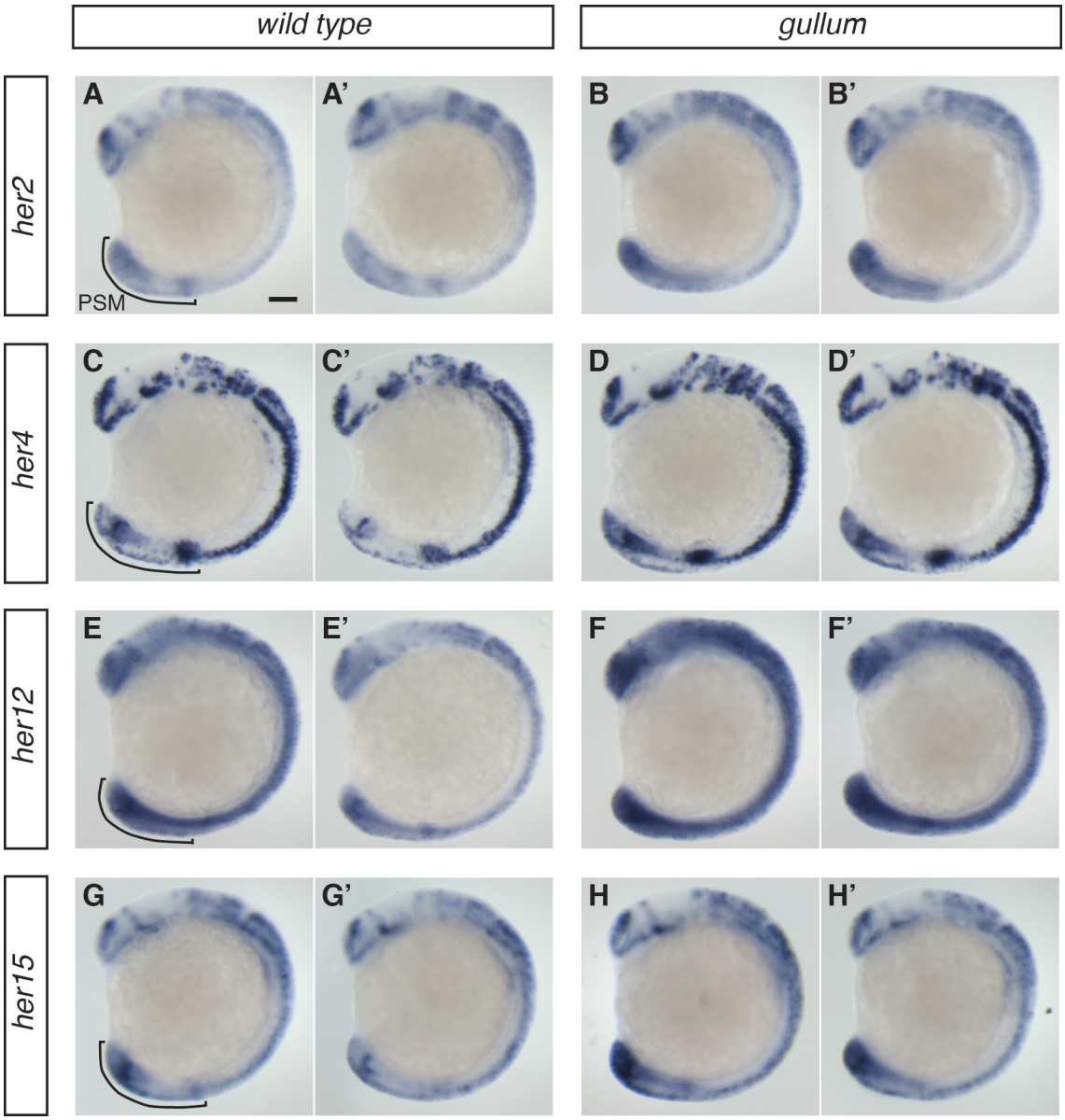

Figure 7.12 Zebrafish homologs of the mouse *Hes5* gene do not oscillate in the *gullum* PSM.

In situ hybridisations for *her2* **(A – B')**, *her4* (**C – D'**), *her12* **(E – E'**) and *her15* **(G – G')** in 12-somite stage wild type and *gullum* sibling embryos. Genotypes are as indicated. Lateral views, PSM to the bottom left (indicated by the black line in A, C, E and G).
Cyclic expression is observed in the wild type PSM for **(A, A')** *her2*, **(C, C')** *her4*, **(E, E')** *her12* and **(G, G')** *her15*. Static expression patterns are observed in the *gullum* PSM for **(B, B')** *her2*, **(D, D')** *her4*, **(F, F')** *her12* and **(H, H')** *her 15*. Scale bar 100 µm.

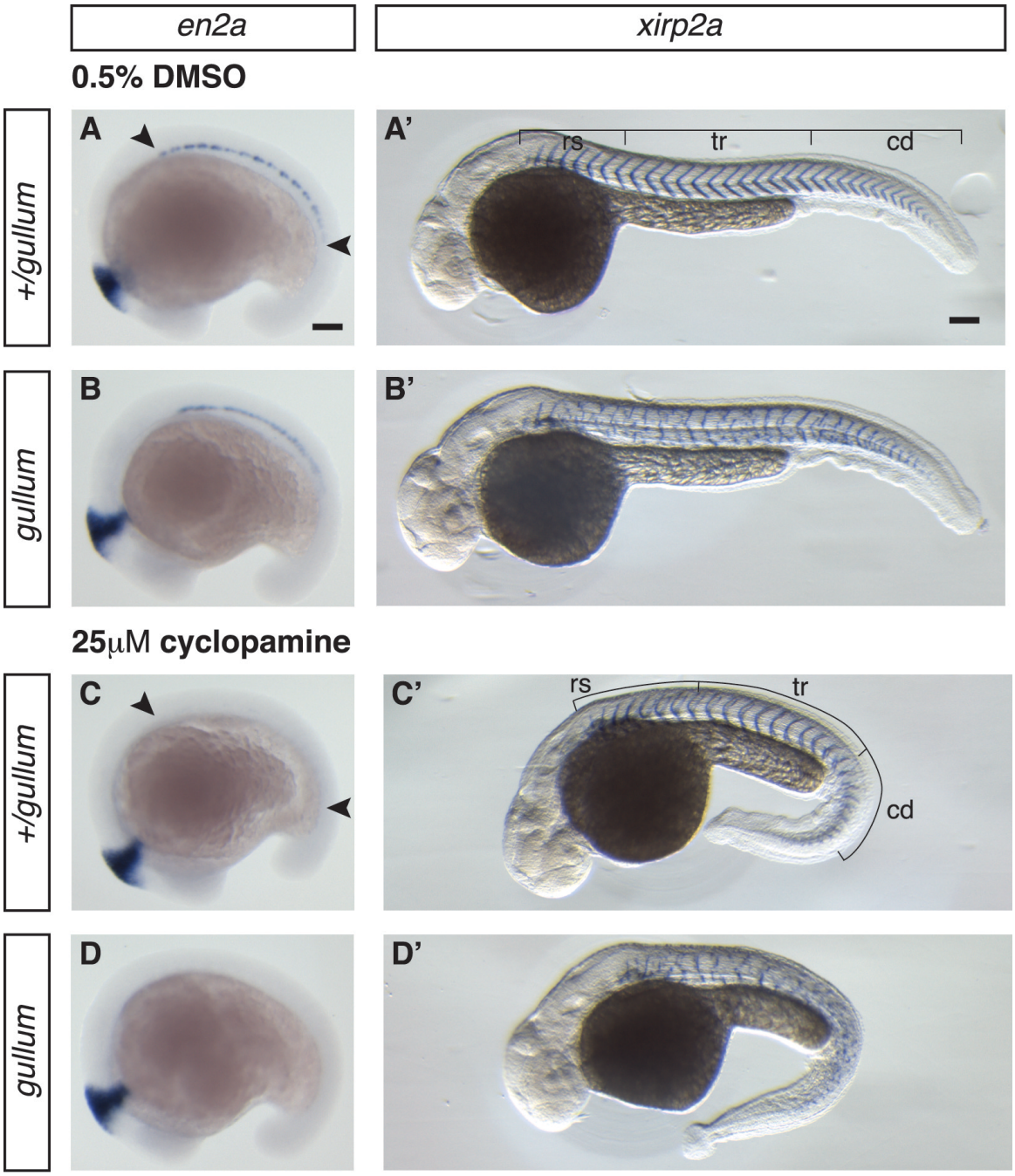

Figure 7.13 Loss of muscle pioneers in *gullum* affects the caudal myotome boundaries.

Sibling embryos treated with 0.5% DMSO (control) **(A – B')** and with 25 μM Hedgehog signalling inhibitor cyclopamine **(C – D')**. *In situ* hybridisation for *en2a* to visualise muscle pioneers in 18-somite stage embryos and for *xirp2a* to visualise myotome boundaries in 36 hpf (hours post fertilization) embryos. Lateral views, head oriented to the left, genotypes are as indicated.
Control embryos: Muscle pioneers are stained with *en2a* (area between the arrowheads) **(A)** in wild type and **(B)** *gullum* embryos. *xirp2a* to visualise **(A')** chevron-shaped myotome boundaries in 36 hpf (hours post fertilization) wild type and **(B')** myotome boundary fragments in *gullum* embryos.
Cyclopamine treated embryos: Muscle pioneers are absent **(C)** in wild type and **(D)** *gullum*. **(C')** Boundaries are U shaped in wild type. **(D')** Boundaries fragments have a more severe disruption in the caudal body in *gullum*. rs – rostral, tr- trunk, cd – caudal. Scale bar 100 μm.

Reference List

Amacher, S.L., Draper, B.W., Summers, B.R., and Kimmel, C.B. (2002). The zebrafish T-box genes no tail and spadetail are required for development of trunk and tail mesoderm and medial floor plate. Development *129*, 3311–3323.

Anderson, J.L., Mulligan, T.S., Shen, M.-C., Wang, H., Scahill, C.M., Tan, F.J., Du, S.J., Busch-Nentwich, E.M., and Farber, S.A. (2017). mRNA processing in mutant zebrafish lines generated by chemical and CRISPR-mediated mutagenesis produces unexpected transcripts that escape nonsense-mediated decay. PLoS Genet *13*, e1007105.

Aoyama, H., and Asamoto, K. (1988). Determination of somite cells: independence of cell differentiation and morphogenesis. Development *104*, 15–28.

Aoyama, H., and Asamoto, K. (2000). The developmental fate of the rostral/caudal half of a somite for vertebra and rib formation: experimental confirmation of the resegmentation theory using chick-quail chimeras. Mechanisms of Development *99*, 71–82.

Ares, S., Morelli, L.G., Jörg, D.J., Oates, A.C., and Jülicher, F. (2012). Collective modes of coupled phase oscillators with delayed coupling. Phys. Rev. Lett. *108*, 204101.

Aulehla, A., and Pourquie, O. (2010). Signaling Gradients during Paraxial Mesoderm Development. Cold Spring Harbor Perspectives in Biology *2*, a000869–a000869.

Aulehla, A., Wiegraebe, W., Baubet, V., Wahl, M.B., Deng, C., Taketo, M., Lewandoski, M., and Pourquié, O. (2007). A β-catenin gradient links the clock and wavefront systems in mouse embryo segmentation. Nat Cell Biol *10*, 186–193.

Bajard, L., Morelli, L.G., Ares, S., Pecreaux, J., Julicher, F., and Oates, A.C. (2014). Wnt-regulated dynamics of positional information in zebrafish somitogenesis. Development *141*, 1381–1391.

Barresi, M.J., D'Angelo, J.A., Hernández, L.P., and Devoto, S.H. (2001). Distinct mechanisms regulate slow-muscle development. Curbio *11*, 1432–1438.

Barrios, A., Poole, R.J., Durbin, L., Brennan, C., Holder, N., and Wilson, S.W. (2003). Eph/Ephrin signaling regulates the mesenchymal-to-epithelial transition of the paraxial mesoderm during somite morphogenesis. Curbio *13*, 1571–1582.

Begemann, G., Marx, M., Mebus, K., Meyer, A., and Bastmeyer, M. (2004). Beyond the neckless phenotype: influence of reduced retinoic acid signaling on motor neuron development in the zebrafish hindbrain. Developmental Biology *271*, 119–129.

Begemann, G., Schilling, T.F., Rauch, G.J., Geisler, R., and Ingham, P.W. (2001). The zebrafish neckless mutation reveals a requirement for raldh2 in mesodermal signals that

pattern the hindbrain. Development *128*, 3081–3094.

Bessho, Y., Sakata, R., Komatsu, S., Shiota, K., Yamada, S., and Kageyama, R. (2001). Dynamic expression and essential functions of Hes7 in somite segmentation. Genes & Development *15*, 2642–2647.

Bessho, Y., Hirata, H., Masamizu, Y., and Kageyama, R. (2003). Periodic repression by the bHLH factor Hes7 is an essential mechanism for the somite segmentation clock. Genes & Development *17*, 1451–1456.

Bird, N.C., and Mabee, P.M. (2003). Developmental Morphology of the Axial Skeleton of the Zebrafish, Danio rerio (Ostariophysi: Cyprinidae). Dev. Dyn. *228*, 337–357.

Brend, T., and Holley, S.A. (2009). Expression of the oscillating gene her1 is directly regulated by Hairy/Enhancer of Split, T-box, and Suppressor of Hairless proteins in the zebrafish segmentation clock. Dev. Dyn. *238*, 2745–2759.

Bryson-Richardson, R.J., and Currie, P.D. (2008). The genetics of vertebrate myogenesis. Nature Reviews Genetics *9*, 632–646.

Campos-Ortega, C.T.A.J.A. (1999). her1, a zebrafish pair-rule like gene, acts downstream of notch signalling to control somite development. 1–10.

Charvet, B., Malbouyres, M., Pagnon-Minot, A., Ruggiero, F., and Le Guellec, D. (2011). Development of the zebrafish myoseptum with emphasis on the myotendinous junction. Cell Tissue Res *346*, 439–449.

Chen, J.K., Taipale, J., Cooper, M.K., and Beachy, P.A. (2002). Inhibition of Hedgehog signaling by direct binding of cyclopamine to Smoothened. Genes & Development *16*, 2743–2748.

Choe, C.P., and Brown, S.J. (2007). Evolutionary flexibility of pair-rule patterning revealed by functional analysis of secondary pair-rule genes, paired and sloppy-paired in the short-germ insect, Tribolium castaneum. Developmental Biology *302*, 281–294.

Choe, C.P., Miller, S.C., and Brown, S.J. (2006). A pair-rule gene circuit defines segments sequentially in the short-germ insect Tribolium castaneum. Proc. Natl. Acad. Sci. U.S.a. *103*, 6560–6564.

Choorapoikayil, S., Willems, B., Ströhle, P., and Gajewski, M. (2012). Analysis of her1 and her7 mutants reveals a spatio temporal separation of the somite clock module. PLoS ONE *7*, e39073.

Cooke, J., and Zeeman, E.C. (1976). A clock and wavefront model for control of the number of repeated structures during animal morphogenesis. Journal of Theoretical Biology *58*, 455–476.

Crawford, B.D., Henry, C.A., Clason, T.A., Becker, A.L., and Hille, M.B. (2003). Activity and distribution of paxillin, focal adhesion kinase, and cadherin indicate cooperative roles during zebrafish morphogenesis. Mol. Biol. Cell *14*, 3065–3081.

Daggett, D.F., Domingo, C.R., Currie, P.D., and Amacher, S.L. (2007). Control of morphogenetic cell movements in the early zebrafish myotome. Developmental Biology *309*, 169–179.

Dahlem, T.J., Hoshijima, K., Jurynec, M.J., Gunther, D., Starker, C.G., Locke, A.S., Weis, A.M., Voytas, D.F., and Grunwald, D.J. (2012). Simple methods for generating and detecting locus-specific mutations induced with TALENs in the zebrafish genome. PLoS Genet *8*, e1002861.

Dahmann, C., Oates, A.C., and Brand, M. (2011). Boundary formation and maintenance in tissue development. Nature Reviews Genetics *12*, 43–55.

De Robertis, E.M., and Sasai, Y. (1996). A common plan for dorsoventral patterning in Bilateria. Nature *380*.

del Corral, R.D., and Storey, K.G. (2004). Opposing FGF and retinoid pathways: a signalling switch that controls differentiation and patterning onset in the extending vertebrate body axis. Bioessays *26*, 857–869.

Delaune, E.A., François, P., Shih, N.P., and Amacher, S.L. (2012). Single-cell-resolution imaging of the impact of Notch signaling and mitosis on segmentation clock dynamics. Dev. Cell *23*, 995–1005.

Deniziak, M., Thisse, C., Rederstorff, M., Hindelang, C., Thisse, B., and Lescure, A. (2007). Loss of selenoprotein N function causes disruption of muscle architecture in the zebrafish embryo. Exp. Cell Res. *313*, 156–167.

Devoto, S.H., Melançon, E., Eisen, J.S., and Westerfield, M. (1996). Identification of separate slow and fast muscle precursor cells in vivo, prior to somite formation. Development *122*, 3371–3380.

Dias, A.S., de Almeida, I., Belmonte, J.M., Glazier, J.A., and Stern, C.D. (2014). Somites Without a Clock. Science *343*, 791–795.

Diez del Corral, R., Breitkreuz, D.N., and Storey, K.G. (2002). Onset of neuronal differentiation is regulated by paraxial mesoderm and requires attenuation of FGF signalling. Development *129*, 1681–1691.

Diez del Corral, R., Olivera-Martinez, I., Goriely, A., Gale, E., Maden, M., and Storey, K. (2003). Opposing FGF and retinoid pathways control ventral neural pattern, neuronal differentiation, and segmentation during body axis extension. Neuron *40*, 65–79.

Dobbs-McAuliffe, B., Zhao, Q., and Linney, E. (2004). Feedback mechanisms regulate retinoic acid production and degradation in the zebrafish embryo. Mechanisms of Development *121*, 339–350.

Du, S.J., Frenkel, V., Kindschi, G., and Zohar, Y. (2001). Visualizing Normal and Defective Bone Development in Zebrafish Embryos Using the Fluorescent Chromophore Calcein. Developmental Biology *238*, 239–246.

Dubrulle, J., McGrew, M.J., and Pourquie, O. (2001). FGF signaling controls somite boundary position and regulates segmentation clock control of spatiotemporal Hox gene activation. Cell *106*, 219–232.

Durbin, L., Sordino, P., Barrios, A., Gering, M., Thisse, C., Thisse, B., Brennan, C., Green, A., Wilson, S., and Holder, N. (2000). Anteroposterior patterning is required within segments for somite boundary formation in developing zebrafish. Development *127*, 1703–1713.

El-Sherif, E., Zhu, X., Fu, J., and Brown, S.J. (2014). Caudal regulates the spatiotemporal dynamics of pair-rule waves in Tribolium. PLoS Genet *10*, e1004677.

Emoto, Y., Wada, H., Okamoto, H., Kudo, A., and Imai, Y. (2005). Retinoic acid-metabolizing enzyme Cyp26a1 is essential for determining territories of hindbrain and spinal cord in zebrafish. Developmental Biology *278*, 415–427.

Erickson, T., Scholpp, S., Brand, M., Moens, C.B., and Jan Waskiewicz, A. (2007). Pbx proteins cooperate with Engrailed to pattern the midbrain–hindbrain and diencephalic–mesencephalic boundaries. Developmental Biology *301*, 504–517.

Felsenfeld, A.L., Curry, M., and Kimmel, C.B. (1991). The fub-1 mutation blocks initial myofibril formation in zebrafish muscle pioneer cells. Developmental Biology *148*, 23–30.

Fior, R., Maxwell, A.A., Ma, T.P., Vezzaro, A., Moens, C.B., Amacher, S.L., Lewis, J., and Saude, L. (2012). The differentiation and movement of presomitic mesoderm progenitor cells are controlled by Mesogenin 1. Development *139*, 4656–4665.

Fleming, A., Kishida, M.G., Kimmel, C.B., and Keynes, R.J. (2015). Building the backbone: the development and evolution of vertebral patterning. Development *142*, 1733–1744.

Fleming, A., Keynes, R., and Tannahill, D. (2004). A central role for the notochord in vertebral patterning. Development *131*, 873–880.

Gajewski, M. (2003). Anterior and posterior waves of cyclic her1 gene expression are differentially regulated in the presomitic mesoderm of zebrafish. Development *130*, 4269–4278.

Gajewski, M., Elmasri, H., Girschick, M., Sieger, D., and Winkler, C. (2006). Comparative analysis of her genes during fish somitogenesis suggests a mouse/chick-like mode of oscillation in medaka. Dev Genes Evol *216*, 315–332.

Garnett, A.T., Han, T.M., Gilchrist, M.J., Smith, J.C., Eisen, M.B., Wardle, F.C., and Amacher, S.L. (2009). Identification of direct T-box target genes in the developing zebrafish mesoderm. Development *136*, 749–760.

Germanguz, I., Lev, D., Waisman, T., Kim, C.-H., and Gitelman, I. (2007). Four twistgenes in zebrafish, four expression patterns. Dev. Dyn. *236*, 2615–2626.

Gilbert, S.F., and Raunio, A.M. (1997). Embryology (Sinauer Associates Incorporated).

Giudicelli, F., Özbudak, E.M., Wright, G.J., and Lewis, J. (2007). Setting the tempo in development: an investigation of the zebrafish somite clock mechanism. Plos Biol *5*, e150.

Gomez, C., Özbudak, E.M., Wunderlich, J., Baumann, D., Lewis, J., and Pourquié, O. (2008). Control of segment number in vertebrate embryos. Nature *454*, 335–339.

Grandel, H., Lun, K., Rauch, G.-J., Rhinn, M., Piotrowski, T., Houart, C., Sordino, P., Küchler, A.M., Schulte-Merker, S., Geisler, R., et al. (2002). Retinoic acid signalling in the zebrafish embryo is necessary during pre-segmentation stages to pattern the anterior-posterior axis of the CNS and to induce a pectoral fin bud. Development *129*, 2851–2865.

Green, J.B.A., and Sharpe, J. (2015). Positional information and reaction-diffusion: two big ideas in developmental biology combine. Development *142*, 1203–1211.

Griffin, K.J., Amacher, S.L., Kimmel, C.B., and Kimelman, D. (1998). Molecular identification of spadetail: regulation of zebrafish trunk and tail mesoderm formation by T-box genes. Development *125*, 3379–3388.

Grotmol, S., Kryvi, H., Nordvik, K., and Totland, G.K. (2003). Notochord segmentation may lay down the pathway for the development of the vertebral bodies in the Atlantic salmon. Anat. Embryol. *207*, 263–272.

Hanisch, A., Holder, M.V., Choorapoikayil, S., Gajewski, M., Özbudak, E.M., and Lewis, J. (2013). The elongation rate of RNA polymerase II in zebrafish and its significance in the somite segmentation clock. Development *140*, 444–453.

Harima, Y., Takashima, Y., Ueda, Y., and Ohtsuka, T. (2013). Accelerating the Tempo of the Segmentation Clock by Reducing the Number of Introns in the Hes7 Gene. Cell Reports.

Hatta, K., Bremiller, R., Westerfield, M., and Kimmel, C.B. (1991). Diversity of expression of engrailed-like antigens in zebrafish. Development *112*, 821–832.

Hauptmann, G., and Gerster, T. (1994). Two-color whole-mount in situ hybridization to vertebrate and Drosophila embryos. Trends in Genetics *10*, 266.

Henry, C.A., Hall, L.A., Burr Hille, M., Solnica-Krezel, L., and Cooper, M.S. (2000). Somites in zebrafish doubly mutant for knypek and trilobite form without internal mesenchymal cells or compaction. Curbio *10*, 1063–1066.

Henry, C.A., and Amacher, S.L. (2004). Zebrafish slow muscle cell migration induces a wave of fast muscle morphogenesis. Dev. Cell *7*, 917–923.

Henry, C.A., McNulty, I.M., Durst, W.A., Munchel, S.E., and Amacher, S.L. (2005). Interactions between muscle fibers and segment boundaries in zebrafish. Developmental Biology *287*, 346–360.

Henry, C.A., Urban, M.K., Dill, K.K., Merlie, J.P., Page, M.F., Kimmel, C.B., and Amacher, S.L. (2002). Two linked hairy/Enhancer of split-related zebrafish genes, her1 and her7, function together to refine alternating somite boundaries. Development *129*, 3693–3704.

Herrgen, L., Ares, S., Morelli, L.G., Schröter, C., Jülicher, F., and Oates, A.C. (2010). Intercellular Coupling Regulatesthe Period of the Segmentation Clock. Curbio *20*, 1244–1253.

Holley, S.A. (2006). Anterior-posterior differences in vertebrate segments: specification of trunk and tail somites in the zebrafish blastula. Genes & Development *20*, 1831–1837.

Holley, S.A., Geisler, R., and Nüsslein-Volhard, C. (2000). Control of her1 expression during zebrafish somitogenesis by a delta-dependent oscillator and an independent wave-front activity. Genes & Development *14*, 1678–1690.

Holley, S.A., Jülich, D., Rauch, G.-J., Geisler, R., and Nusslein-Volhard, C. (2002). her1 and the notch pathway function within the oscillator mechanism that regulates zebrafish somitogenesis. Development *129*, 1175–1183.

Horikawa, K.E.A. (1999). Adhesive Subdivisions Intrinsic to the Epithelial Somites. 1–8.

Hu, P., Tian, M., Bao, J., Xing, G., Gu, X., Gao, X., Linney, E., and Zhao, Q. (2008). Retinoid regulation of the zebrafish cyp26a1 promoter. Dev. Dyn. *237*, 3798–3808.

Huitema, L.F.A., Apschner, A., Logister, I., Spoorendonk, K.M., Bussmann, J., Hammond, C.L., and Schulte-Merker, S. (2012). Entpd5 is essential for skeletal mineralization and regulates phosphate homeostasis in zebrafish. Proc. Natl. Acad. Sci. U.S.a. *109*, 21372–21377.

Huppert, S.S., Ilagan, M.X.G., De Strooper, B., and Kopan, R. (2005). Analysis of Notch function in presomitic mesoderm suggests a gamma-secretase-independent role for presenilins in somite differentiation. Dev. Cell *8*, 677–688.

Inohaya, K., Takano, Y., and Kudo, A. (2007). The teleost intervertebral region acts as a growth center of the centrum: In vivo visualization of osteoblasts and their progenitors in transgenic fish. Dev. Dyn. *236*, 3031–3046.

Itoh, M., Kim, C.-H., Palardy, G., Oda, T., Jiang, Y.-J., Maust, D., Yeo, S.-Y., Lorick, K., Wright, G.J., Ariza-McNaughton, L., et al. (2003). Mind bomb is a ubiquitin ligase that is essential for efficient activation of Notch signaling by Delta. Dev. Cell *4*, 67–82.

Jackson, H.E., and Ingham, P.W. (2013). Control of muscle fibre-type diversity during embryonic development: The zebrafish paradigm. Mechanisms of Development *130*, 447–457.

Jahangiri, L., Nelson, A.C., and Wardle, F.C. (2012). Developmental Biology. Developmental Biology *371*, 110–120.

Jiang, Y.J., Aerne, B.L., Smithers, L., Haddon, C., Ish-Horowicz, D., and Lewis, J. (2000). Notch signalling and the synchronization of the somite segmentation clock. Nature *408*, 475–479.

Jörg, D.J., Morelli, L.G., Soroldoni, D., Oates, A.C., and Jülicher, F. (2015). Continuum theory of gene expression waves during vertebrate segmentation. New J. Phys. *17*, 093042.

Jörg, D.J., Oates, A.C., and Jülicher, F. (2016). Sequential pattern formation governed by signaling gradients. Physical Biology *0*, 1–8.

Jülich, D., Geisler, R., Holley, S.A., Tübingen 2000 Screen Consortium (2005a). Integrinalpha5 and delta/notch signaling have complementary spatiotemporal requirements during zebrafish somitogenesis. Dev. Cell *8*, 575–586.

Jülich, D., Hwee Lim, C., Round, J., Nicolaije, C., Schroeder, J., Davies, A., Geisler, R., Lewis, J., Jiang, Y.-J., Holley, S.A., et al. (2005b). beamter/deltaC and the role of Notch ligands in the zebrafish somite segmentation, hindbrain neurogenesis and hypochord differentiation. Developmental Biology *286*, 391–404.

Jülich, D., Mould, A.P., Koper, E., and Holley, S.A. (2009). Control of extracellular matrix assembly along tissue boundaries via Integrin and Eph/Ephrin signaling. Development *136*, 2913–2921.

Kageyama, R., Ohtsuka, T., and Kobayashi, T. (2007). The Hes gene family: repressors and oscillators that orchestrate embryogenesis. Development *134*, 1243–1251.

Kawamura, A., Koshida, S., Hijikata, H., Ohbayashi, A., Kondoh, H., and Takada, S. (2005a). Groucho-associated transcriptional repressor ripply1 is required for proper transition from the presomitic mesoderm to somites. Dev. Cell *9*, 735–744.

Kawamura, A., Koshida, S., Hijikata, H., Sakaguchi, T., Kondoh, H., and Takada, S. (2005b). Zebrafish hairy/enhancer of split protein links FGF signaling to cyclic gene expression in the periodic segmentation of somites. Genes & Development *19*, 1156–1161.

Kim, S.H., Jen, W.C., De Robertis, E.M., and Kintner, C. (2000). The protocadherin PAPC establishes segmental boundaries during somitogenesis in xenopus embryos. Curbio *10*, 821–830.

Kimmel, C.B., Ballard, W.W., Kimmel, S.R., Ullmann, B., and Schilling, T.F. (1995). Stages of embryonic development of the zebrafish. Dev. Dyn. *203*, 253–310.

Koshida, S., Kishimoto, Y., Ustumi, H., Shimizu, T., Furutani-Seiki, M., Kondoh, H., and Takada, S. (2005). Integrinα5-Dependent Fibronectin Accumulation for Maintenance of Somite Boundaries in Zebrafish Embryos. Dev. Cell *8*, 587–598.

Krol, A.J., Roellig, D., Dequeant, M.L., Tassy, O., Glynn, E., Hattem, G., Mushegian, A., Oates, A.C., and Pourquie, O. (2011). Evolutionary plasticity of segmentation clock networks. Development *138*, 2783–2792.

Leimeister, C., Dale, K., Fischer, A., Klamt, B., Hrabe de Angelis, M., Radtke, F., McGrew, M.J., Pourquié, O., and Gessler, M. (2000). Oscillating Expression of c-Hey2 in the Presomitic Mesoderm Suggests That the Segmentation Clock May Use Combinatorial Signaling through Multiple Interacting bHLH Factors. Developmental Biology *227*, 91–103.

Lewis, J. (2003). Autoinhibition with transcriptional delay: a simple mechanism for the zebrafish somitogenesis oscillator. Curbio *13*, 1398–1408.

Liao, B.-K., and Oates, A.C. (2017). Delta-Notch signalling in segmentation. Arthropod Structure and Development *46*, 1451–1456.

Liao, B.-K., rg, D.J.J.O., and Oates, A.C. (2016). Faster embryonic segmentation through elevated Delta-Notch signalling. Nature Communications *7*, 1–12.

Linville, A., Radtke, K., Waxman, J.S., Yelon, D., and Schilling, T.F. (2009). Combinatorial roles for zebrafish retinoic acid receptors in the hindbrain, limbs and pharyngeal arches. Developmental Biology *325*, 60–70.

Long, J.H., Adcock, B., and Root, R.G. (2002). Force transmission via axial tendons in undulating fish: a dynamic analysis. Comparative Biochemistry and Physiology Part a: Molecular & Integrative Physiology *133*, 911–929.

Maden, M., Graham, A., Zile, M., and Gale, E. (2000). Abnormalities of somite development in the absence of retinoic acid. Int. J. Dev. Biol. *44*, 151–159.

Mandal, A., Rydeen, A., Anderson, J., Sorrell, M.R.J., Zygmunt, T., Torres-Vázquez, J., and Waxman, J.S. (2013). Transgenic retinoic acid sensor lines in zebrafish indicate regions of available embryonic retinoic acid. Dev. Dyn. *242*, 989–1000.

Maroto, M., Dale, J.K., Dequéant, M.-L., Petit, A.-C., and Pourquié, O. (2005). Synchronised cycling gene oscillations in presomitic mesoderm cells require cell-cell contact. Int. J. Dev. Biol. *49*, 309–315.

Martin, B.L., and Kimelman, D. (2008). Regulation of canonical Wnt signaling by Brachyury is essential for posterior mesoderm formation. Dev. Cell *15*, 121–133.

Martin, B.L., and Kimelman, D. (2010). Brachyury establishes the embryonic mesodermal progenitor niche. Genes & Development *24*, 2778–2783.

Masamizu, Y., Ohtsuka, T., Takashima, Y., Nagahara, H., Takenaka, Y., Yoshikawa, K., Okamura, H., and Kageyama, R. (2006). Real-time imaging of the somite segmentation clock: revelation of unstable oscillators in the individual presomitic mesoderm cells. Proc. Natl. Acad. Sci. U.S.a. *103*, 1313–1318.

McGregor, A.P., Pechmann, M., Schwager, E.E., and Damen, W.G. (2009). An ancestral regulatory network for posterior development in arthropods. Commun Integr Biol *2*, 174–176.

Meeker, N., Hutchinson, S., Ho, L., and Trede, N. (2007). Method for isolation of PCR-

ready genomic DNA from zebrafish tissues. Biotech. *43*, 610–614.

Morelli, L.G., Ares, S., Herrgen, L., Schröter, C., Jülicher, F., and Oates, A.C. (2009). Delayed coupling theory of vertebrate segmentation. HFSP Journal *3*, 55–66.

Moreno, T.A., and Kintner, C. (2004). Regulation of segmental patterning by retinoic acid signaling during Xenopus somitogenesis. Dev. Cell *6*, 205–218.

Morin-Kensicki, E.M., and Eisen, J.S. (1997). Sclerotome development and peripheral nervous system segmentation in embryonic zebrafish. Development *124*, 159–167.

Morin-Kensicki, E.M., Melancon, E., and Eisen, J.S. (2002). Segmental relationship between somites and vertebral column in zebrafish. Development *129*, 3851–3860.

Morley, R.H., Lachani, K., Keefe, D., Gilchrist, M.J., Flicek, P., Smith, J.C., and Wardle, F.C. (2009). A gene regulatory network directed by zebrafish No tail accounts for its roles in mesoderm formation. Proc. Natl. Acad. Sci. U.S.a. *106*, 3829–3834.

Murray, J.D. (2011). Mathematical Biology (Springer Science & Business Media).

Müller, M., Weizsäcker, von, E., and Campos-Ortega, J.A. (1996). Expression domains of a zebrafish homologue of the Drosophila pair-rule gene hairy correspond to primordia of alternating somites. Development *122*, 2071–2078.

Nguyen-Chi, M.E., Bryson-Richardson, R., Sonntag, C., Hall, T.E., Gibson, A., Sztal, T., Chua, W., Schilling, T.F., and Currie, P.D. (2012). Morphogenesis and Cell Fate Determination within the Adaxial Cell Equivalence Group of the Zebrafish Myotome. PLoS Genet *8*, e1003014.

Niederreither, K., Subbarayan, V., Dolle, P., and Chambon, P. (1999). Embryonic retinoic acid synthesis is essential for early mouse post-implantation development. Nat. Genet. *21*, 444–448.

Nikaido, M., Kawakami, A., Sawada, A., Furutani-Seiki, M., Takeda, H., and Araki, K. (2002). Tbx24, encoding a T-box protein, is mutated in the zebrafish somite-segmentation mutant fused somites. Nat. Genet. *31*, 195–199.

Nusslein-Volhard, C., and Dahm, R. (2002). Zebrafish (Oxford University Press).

Oates, A.C., Morelli, L.G., and Ares, S. (2012). Patterning embryos with oscillations: structure, function and dynamics of the vertebrate segmentation clock. Development *139*, 625–639.

Oates, A.C., and Ho, R.K. (2002). Hairy/E(spl)-related (Her) genes are central components of the segmentation oscillator and display redundancy with the Delta/Notch signaling pathway in the formation of anterior segmental boundaries in the zebrafish. Development *129*, 2929–2946.

Oates, A.C., Mueller, C., and Ho, R.K. (2005a). Cooperative function of deltaC and her7 in anterior segment formation. Developmental Biology *280*, 133–149.

Oates, A.C., Rohde, L.A., and Ho, R.K. (2005b). Generation of segment polarity in the paraxial mesoderm of the zebrafish through a T-box-dependent inductive event. Developmental Biology *283*, 204–214.

Otten, C., van der Ven, P.F., Lewrenz, I., Paul, S., Steinhagen, A., Busch-Nentwich, E., Eichhorst, J., Wiesner, B., Stemple, D., Strähle, U., et al. (2012). Xirp Proteins Mark Injured Skeletal Muscle in Zebrafish. PLoS ONE *7*, e31041.

Pais-de-Azevedo, T., Magno, R., Duarte, I., and Palmeirim, I. (2018). Recent advances in understanding vertebrate segmentation. F1000Res *7*, 97.

Palmeirim, I., Henrique, D., Ish-Horowicz, D., and Pourquie, O. (1997). Avian hairy gene expression identifies a molecular clock linked to vertebrate segmentation and somitogenesis. Cell *91*, 639–648.

Parichy, D.M., Elizondo, M.R., Mills, M.G., Gordon, T.N., and Engeszer, R.E. (2009). Normal table of postembryonic zebrafish development: staging by externally visible anatomy of the living fish. Dev. Dyn. *238*, 2975–3015.

Perz-Edwards, A., Hardison, N.L., and Linney, E. (2001). Retinoic Acid-Mediated Gene Expression in Transgenic Reporter Zebrafish. Developmental Biology *229*, 89–101.

Pourquie, O., and Tam, P.P. (2001). A nomenclature for prospective somites and phases of cyclic gene expression in the presomitic mesoderm. Dev. Cell *1*, 619–620.

Pourquié, O. (2009). The Skeletal System.

Renn, J., Büttner, A., To, T.T., Chan, S.J.H., and Winkler, C. (2013). Developmental Biology. Developmental Biology *381*, 134–143.

Richmond, D.L., and Oates, A.C. (2012). The segmentation clock: inherited trait or universal design principle? Current Opinion in Genetics & Development *22*, 600–606.

Richter, S. (2017). A small molecule screen targeting zebrafish somitogenesis. 1–118.

Richter, S., Schulze, U., Tomançak, P., and Oates, A.C. (2017). Small molecule screen in embryonic zebrafish using modular variations to target segmentation. Nature Communications 1–14.

Riedel-Kruse, I.H., Muller, C., and Oates, A.C. (2007). Synchrony Dynamics During Initiation, Failure, and Rescue of the Segmentation Clock. Science *317*, 1911–1915.

Rost, F., Eugster, C., Schroter, C., Oates, A.C., and Brusch, L. (2014). Chevron formation of the zebrafish muscle segments. Journal of Experimental Biology *217*, 3870–3882.

Ruvinsky, I., Silver, L.M., and Ho, R.K. (1998). Characterization of the zebrafish tbx16 gene and evolution of the vertebrate T-box family. Dev Genes Evol *208*, 94–99.

Saga, Y., Hata, N., Koseki, H., and Taketo, M.M. (1997). Mesp2: a novel mouse gene expressed in the presegmented mesoderm and essential for segmentation initiation. Genes & Development *11*, 1827–1839.

Sakai, Y., Meno, C., Fujii, H., Nishino, J., Shiratori, H., Saijoh, Y., Rossant, J., and Hamada, H. (2001). The retinoic acid-inactivating enzyme CYP26 is essential for establishing an uneven distribution of retinoic acid along the anterio-posterior axis within the mouse embryo. Genes & Development *15*, 213–225.

Sarov, M., Schneider, S., Pozniakovski, A., Roguev, A., Ernst, S., Zhang, Y., Hyman, A.A., and Stewart, A.F. (2006). A recombineering pipeline for functional genomics applied to Caenorhabditis elegans. Nat Meth *3*, 839–844.

Sarrazin, A.F., Peel, A.D., and Averof, M. (2012). A Segmentation Clock with Two-Segment Periodicity in Insects. Science *336*, 338–341.

Sasai, Y., Kageyama, R., Tagawa, Y., Shigemoto, R., and Nakanishi, S. (1992). Two mammalian helix-loop-helix factors structurally related to Drosophila hairy and Enhancer of split. Genes & Development *6*, 2620–2634.

Sawada, A., Fritz, A., Jiang, Y.J., Yamamoto, A., Yamasu, K., Kuroiwa, A., Saga, Y., and Takeda, H. (2000). Zebrafish Mesp family genes, mesp-a and mesp-b are segmentally expressed in the presomitic mesoderm, and Mesp-b confers the anterior identity to the developing somites. Development *127*, 1691–1702.

Sawada, A., Shinya, M., Jiang, Y.J., Kawakami, A., Kuroiwa, A., and Takeda, H. (2001). Fgf/MAPK signalling is a crucial positional cue in somite boundary formation. Development *128*, 4873–4880.

Schilling, T.F., Nie, Q., and Lander, A.D. (2012). Dynamics and precision in retinoic acid morphogen gradients. Current Opinion in Genetics & Development *22*, 562–569.

Schröter, C., and Oates, A.C. (2010). Segment Number and Axial Identityin a Segmentation Clock Period Mutant. Curbio *20*, 1254–1258.

Schröter, C., Ares, S., Morelli, L.G., Isakova, A., Hens, K., Soroldoni, D., Gajewski, M., Jülicher, F., Maerkl, S.J., Deplancke, B., et al. (2012). Topology and Dynamics of the Zebrafish Segmentation Clock Core Circuit. Plos Biol *10*, e1001364.

Schröter, C., Herrgen, L., Cardona, A., Brouhard, G.J., Feldman, B., and Oates, A.C. (2008). Dynamics of zebrafish somitogenesis. Dev. Dyn. *237*, 545–553.

Schulte-Merker, S., van Eeden, F.J., Halpern, M.E., Kimmel, C.B., and Nüsslein-Volhard, C. (1994). no tail (ntl) is the zebrafish homologue of the mouse T (Brachyury) gene. Development *120*, 1009–1015.

Schwendinger-Schreck, J., Kang, Y., and Holley, S.A. (2014). Modeling the Zebrafish Segmentation Clock's Gene Regulatory Network Constrained by Expression Data Suggests Evolutionary Transitions Between Oscillating and Non-Oscillating Transcription. Genetics.

Shankaran, S.S., Sieger, D., Schröter, C., Czepe, C., Pauly, M.-C., Laplante, M.A., Becker, T.S., Oates, A.C., and Gajewski, M. (2007). Completing the set of h/E(spl) cyclic genes in zebrafish: her12 and her15 reveal novel modes of expression and contribute to the segmentation clock. Developmental Biology *304*, 615–632.

Shih, N.P., François, P., Delaune, E.A., and Amacher, S.L. (2015). Dynamics of the slowing segmentation clock reveal alternating two-segment periodicity. Development *142*, 1785–1793.

Shimizu, T., Bae, Y.-K., and Hibi, M. (2006). Cdx-Hox code controls competence for responding to Fgfs and retinoic acid in zebrafish neural tissue. Development *133*, 4709–4719.

Shimoda, N., Knapik, E.W., Ziniti, J., Sim, C., Yamada, E., Kaplan, S., Jackson, D., de Sauvage, F., Jacob, H., and Fishman, M.C. (1999). Zebrafish genetic map with 2000 microsatellite markers. Genomics *58*, 219–232.

Shimozono, S., Iimura, T., Kitaguchi, T., Higashijima, S.-I., and Miyawaki, A. (2013). Visualization of an endogenous retinoic acid gradient across embryonic development. Nature *496*, 363–366.

Sieger, D., Tautz, D., and Gajewski, M. (2004). her11 is involved in the somitogenesis clock in zebrafish. Dev Genes Evol *214*.

Soroldoni, D., Hogan, B.M., and Oates, A.C. (2009). Simple and Efficient Transgenesis with Meganuclease Constructs in Zebrafish. In Methods in Molecular Biology, (Totowa, NJ: Humana Press), pp. 117–130.

Soroldoni, D., Jörg, D.J., Morelli, L.G., Richmond, D.L., Schindelin, J., Jülicher, F., and Oates, A.C. (2014). Genetic oscillations. A Doppler effect in embryonic pattern formation. Science *345*, 222–225.

Spoorendonk, K.M., Peterson-Maduro, J., Renn, J., Trowe, T., Kranenbarg, S., Winkler, C., and Schulte-Merker, S. (2008). Retinoic acid and Cyp26b1 are critical regulators of osteogenesis in the axial skeleton. Development *135*, 3765–3774.

Stellabotte, F., Dobbs-McAuliffe, B., Fernandez, D.A., Feng, X., and Devoto, S.H. (2007). Dynamic somite cell rearrangements lead to distinct waves of myotome growth. Development *134*, 1253–1257.

Stellabotte, F., and Devoto, S.H. (2007). The teleost dermomyotome. Dev. Dyn. *236*, 2432–2443.

Stern, C.D., and Keynes, R.J. (1987). Interactions between somite cells: the formation and maintenance of segment boundaries in the chick embryo. Development *99*, 261–272.

Stern, C.D., and Piatkowska, A.M. (2015). Seminars in Cell & Developmental Biology. Seminars in Cell and Developmental Biology *42*, 134–139.

Stickney, H.L., Barresi, M.J., and Devoto, S.H. (2000). Somite development in zebrafish. Dev. Dyn. *219*, 287–303.

Stollewerk, A., Schoppmeier, M., and Damen, W.G.M. (2003). Involvement of Notch and Delta genes in spider segmentation. Nature *423*, 863–865.

Szeto, D.P., and Kimelman, D. (2004). Combinatorial gene regulation by Bmp and Wnt in zebrafish posterior mesoderm formation. Development *131*, 3751–3760.

Thermes, V., Grabher, C., Ristoratore, F., Bourrat, F., Choulika, A., Wittbrodt, J., and Joly, J.-S. (2002). I-SceI meganuclease mediates highly efficient transgenesis in fish. Mechanisms of Development *118*, 91–98.

Thisse, C., Thisse, B., Schilling, T.F., and Postlethwait, J.H. (1993). Structure of the zebrafish snail1 gene and its expression in wild type, spadetail and no tail mutant embryos. Development *119*, 1203–1215.

Thomas, A.G., and Henry, J.J. (2014). Developmental Biology. Developmental Biology *386*, 291–301.

Thorpe, C.J., Weidinger, G., and Moon, R.T. (2005). Wnt/beta-catenin regulation of the Sp1-related transcription factor sp5l promotes tail development in zebrafish. Development *132*, 1763–1772.

Trofka, A., Schwendinger-Schreck, J., Brend, T., Pontius, W., Emonet, T., and Holley, S.A. (2012). The Her7 node modulates the network topology of the zebrafish segmentation clock via sequestration of the Hes6 hub. Development *139*, 940–947.

Tsiairis, C.D., and Aulehla, A. (2016). Self-Organization of Embryonic Genetic Oscillators into Spatiotemporal Wave Patterns. Cell *164*, 656–667.

Uriu, K., Morishita, Y., and Iwasa, Y. (2009). Traveling wave formation in vertebrate segmentation. Journal of Theoretical Biology *257*, 385–396.

van Eeden, F.J., Granato, M., Schach, U., Brand, M., Furutani-Seiki, M., Haffter, P., Hammerschmidt, M., Heisenberg, C.P., Jiang, Y.J., Kane, D.A., et al. (1996). Mutations affecting somite formation and patterning in the zebrafish, Danio rerio. Development *123*, 153–164.

van Eeden, F.J., Holley, S.A., Haffter, P., and Nüsslein-Volhard, C. (1998). Zebrafish segmentation and pair-rule patterning. Dev. Genet. *23*, 65–76.

Vermot, J. (2005). Retinoic Acid Controls the Bilateral Symmetry of Somite Formation in the Mouse Embryo. Science *308*, 563–566.

Volfson, D., Cookson, S., Hasty, J., and Tsimring, L.S. (2008). Biomechanical ordering of dense cell populations. Proc. Natl. Acad. Sci. U.S.a. *105*, 15346–15351.

Walker, M.B., and Kimmel, C.B. (2007). A two-color acid-free cartilage and bone stain for zebrafish larvae. Biotech Histochem *82*, 23–28.

Wang, S., Kryvi, H., Grotmol, S., Wargelius, A., Krossøy, C., Epple, M., Neues, F., Furmanek, T., and Totland, G.K. (2013). Mineralization of the vertebral bodies in Atlantic salmon (Salmo salar L.) is initiated segmentally in the form of hydroxyapatite crystal accretions in the notochord sheath. J. Anat. *223*, 159–170.

Wanglar, C., Takahashi, J., Yabe, T., and Takada, S. (2014). Tbx protein level critical for clock-mediated somite positioning is regulated through interaction between Tbx and Ripply. PLoS ONE *9*, e107928.

Waxman, J.S., and Yelon, D. (2007). Comparison of the expression patterns of newly identified zebrafish retinoic acid and retinoid X receptors. Dev. Dyn. *236*, 587–595.

Webb, A.B., Lengyel, I.M., Jörg, D.J., Valentin, G., Jülicher, F., Morelli, L.G., and Oates, A.C. (2016). Persistence, period and precision of autonomous cellular oscillators from the zebrafish segmentation clock. eLife *5*.

Weinberg, E.S., Allende, M.L., Kelly, C.S., Abdelhamid, A., Murakami, T., Andermann, P., Doerre, O.G., Grunwald, D.J., and Riggleman, B. (1996). Developmental regulation of zebrafish MyoD in wild type, no tail and spadetail embryos. Development *122*, 271–280.

Weisblat, D.A., and Kuo, D.-H. (2014). Developmental biology of the leech Helobdella. Int. J. Dev. Biol. *58*, 429–443.

Wilson, V., Olivera-Martinez, I., and Storey, K.G. (2009). Stem cells, signals and vertebrate body axis extension. Development *136*, 2133–2133.

Windner, S.E., Doris, R.A., Ferguson, C.M., Nelson, A.C., Valentin, G., Tan, H., Oates, A.C., Wardle, F.C., and Devoto, S.H. (2015). Tbx6, Mesp-b and Ripply1 regulate the onset of skeletal myogenesis in zebrafish. Development *142*, 1159–1168.

Wolpert, L., Wolpert, E.P.O.B.L., Tickle, C., and Arias, A.M. (2015). Principles of Development (Oxford University Press, USA).

Yabe, T., and Takada, S. (2012). Mesogenin causes embryonic mesoderm progenitors to differentiate during development of zebrafish tail somites. Developmental Biology *370*, 213–222.

Yabe, T., Hoshijima, K., Yamamoto, T., and Takada, S. (2016). Quadruple zebrafish mutant reveals different roles of Mesp genes in somite segmentation between mouse and zebrafish. Development *143*, 2842–2852.

Yamamoto, A., Amacher, S.L., Kim, S.H., Geissert, D., Kimmel, C.B., and De Robertis, E.M. (1998a). Zebrafish paraxial protocadherin is a downstream target of spadetail involved in morphogenesis of gastrula mesoderm. Development *125*, 3389–3397.

Yamamoto, A., Amacher, S.L., Kim, S.H., Geissert, D., Kimmel, C.B., and De Robertis, E.M. (1998b). Zebrafish paraxial protocadherin is a downstream target of spadetail involved in morphogenesis of gastrula mesoderm. Development *125*, 3389–

3397.

Yasutake, J., Inohaya, K., and Kudo, A. (2004). Twist functions in vertebral column formation in medaka, Oryzias latipes. Mechanisms of Development *121*, 883–894.

Yu, T., Graf, M., Renn, J., Schartl, M., Larionova, D., Huysseune, A., Witten, P.E., and Winkler, C. (2017). A vertebrate-specific and essential role for osterix in osteogenesis revealed by gene knockout in the teleost medaka. Development *144*, 265–271.